

NATIONAL HIGHWAY TRAFFIC SAFETY ADMINISTRATION
WASHINGTON, D C

CONTRACTOR FINAL REPORT

TEST #

75

75 AF 2

DOT HS-801 081

FRONTAL AND SIDE IMPACT CRASHWORTHINESS-COMPACT CARS

Contract No. DOT-HS-257-2-461

March 1974

Final Report

PREPARED FOR

U S DEPARTMENT OF TRANSPORTATION
NATIONAL HIGHWAY TRAFFIC SAFETY ADMINISTRATION
WASHINGTON, D C. 20590

Document is available to the public through
the National Technical Information Service,
Springfield, Virginia 22151

This document is disseminated under the sponsorship of the Department of Transportation in the interest of information exchange. The United States Government assumes no liability for its contents or use thereof.

Technical Report Documentation Page

1. Report No DOT HS-801 081	2. Government Accession No	3. Recipient's Catalog No	
4. Title and Subtitle Frontal and Side Impact Crashworthiness - Compact Cars		5. Report Date March 1974	6. Performing Organization Code
		8. Performing Organization Report No	
7. Author(s) William J. Wingenbach & Roger E. Lagerquist		10. Work Unit No. (TRAIS)	11. Contract / Grant No DOT-HS-257-2-461
9. Performing Organization Name and Address AMF Incorporated Advanced Systems Laboratory 495 South Fairview Avenue Goleta, California 93017		13. Type of Report and Period Covered Final Report June 1972-Dec. 1973	
		14. Sponsoring Agency Code	
12. Sponsoring Agency Name and Address U.S. Department of Transportation National Highway Traffic Safety Administration, 400 Seventh Street, S.W. Washington, D.C. 20590		15. Supplementary Notes	
16. Abstract A study was conducted to develop techniques for the improvement of front and side vehicle crashworthiness. These techniques were applied to a production compact vehicle, the 1973 AMC Hornet. General vehicle configuration was maintained as was production feasibility. Total weight increase for all modifications was 104 lbs. Five baseline, three subsystem and fifteen system vehicle crash tests were conducted. Modified vehicles demonstrated substantial improvement over baseline vehicle performance. Mathematical models for estimating dynamic response characteristics of vehicles involved in a wide variety of crash conditions including flat barrier, oblique barrier, pole and vehicle-to-vehicle impacts were developed. Computer simulations were conducted and results of simulations compared with crash test results.			
17. Key Words Crashworthiness, computer simulations, compact car.		18. Distribution Statement Unlimited available through the National Technical Information Service, Springfield, Virginia 22151	
19. Security Classif. (of this report) Unclassified	20. Security Classif. (of this page) Unclassified	21. No. of Pages 211	22. Price

Form DOT F 1700.7 (8-72)

TABLE OF CONTENTS

<u>Section</u>	<u>Title</u>	<u>Page</u>
1	INTRODUCTION	1-1
2	PROGRAM OBJECTIVES	2-1
3	BASIC ELEMENTS OF THE PROGRAM	3-1
4	VARIABLE MODIFICATIONS	4-1
	System Design	4-1
	Control Functions	4-3
	Control Programs	4-7
5	DEVELOPMENT OF THE PROGRAM	5-1
	Control Elements	5-1
	Subsystem Test	5-11
	Test Results	5-21
6	SYSTEM TEST PROGRAM	6-1
	Description of the Test Results	6-1
	System Test No. 1	6-6
	System Test No. 2	6-10
	System Test No. 3	6-14
	System Test No. 4	6-18
	System Test No. 5	6-22
	System Test No. 6	6-29
	System Test No. 7	6-34
	System Test No. 8	6-40
	System Test No. 9	6-45
	System Test No. 10	6-49
	System Test No. 11	6-55
	System Test No. 12	6-58

TABLE OF CONTENTS (Continued)

<u>Section</u>	<u>Title</u>	<u>Page</u>
	System Test No. 13	6-62
	System Test No. 14	6-64
	System Test No. 15	6-69
7	EVALUATION OF SYSTEM PERFORMANCE	7-1
	Front End System Crashworthiness	7-1
	Front End System Aggressivity	7-6
	Front End Components	7-9
	Side Crashworthiness	7-12
	Side Components	7-13
8	MATHEMATICAL MODELS	8-1
	Dynamic Response Models	8-1
	Models	8-8
	Frontal Flat Barrier - Normal Impact	8-8
	Frontal Flat Barrier - Angular Impact	8-21
	Frontal Pole	8-29
	Side Pole	8-35
	Front-to-Front Aligned	8-37
	Front-to-Front Offset	8-47
	Front-Side	8-55
	Computer Programs	8-61
	Other Models	8-62
	Second-Stage Bumper and Intrusion-Resistant Door Panel	8-65
	Plastic Hinge in Rear Sill	8-68
	Non-Deforming Elements	8-71
9	CONCLUSIONS	9-1
10	RECOMMENDATIONS	10-1

LIST OF FIGURES

<u>Number</u>	<u>Title</u>	<u>Page</u>
2-1	Program Logic	2-2
3-1	Baseline Test No. I	3-3
3-2	Baseline Test No. II	3-5
3-3	Baseline Test No. III	3-6
3-4	Baseline Test No. IV	3-8
3-5	Baseline Test No. V.	3-9
4-1	Front End Structure - System Test Vehicle.	4-2
4-2	Revised Lock Post	4-3
4-3	Door Beam and Attachment Hardware	4-4
5-1	Plastic Hinge Tests	5-9
5-2	Effect of Foam Filler Density in Plastic Hinge Tests . . .	5-10
6-1	Test No. 1. Deformation of Front End Components. . . .	6-8
6-2	Test No. 1. Longitudinal Crash Pulse - Vehicle #1 . . .	6-9
6-3	Test No. 2. Deformation of Front End Components. . . .	6-11
6-4	Test No. 2. Longitudinal Crash Pulse - Vehicle #5 . . .	6-13
6-5	Test No. 3. Sill Deformation	6-15
6-6	Test No. 3. Front End Configuration 52 msec After Contact	6-16
6-7	Test No. 3. Front End Configuration 68 msec After Contact	6-17
6-8	Test No. 3. Longitudinal Crash Pulse - Vehicle #2 . . .	6-19
6-9	Test No. 3. Lateral Crash Pulse - Vehicle #2.	6-20
6-10	Test No. 4. Deformation	6-23
6-11	Test No. 4. Lateral Crash Pulse - Vehicle #12	6-24
6-12	Test No. 5. Condition of Vehicles After Collision	6-26
6-13	Test No. 5. Longitudinal Crash Pulse - Vehicle #10 . .	6-27
6-14	Test No. 5. Longitudinal Crash Pulse - Vehicle #11 . .	6-28
6-15	Test No. 6. Interaction of Vehicles After Contact	6-31

LIST OF FIGURES (Continued)

<u>Number</u>	<u>Title</u>	<u>Page</u>
6-16	Test No. 6. Longitudinal Crash Pulse - Vehicle #3 . . .	6-32
6-17	Test No. 6. Longitudinal Crash Pulse - Vehicle #4 . . .	6-33
6-18	Test No. 7. Condition of Vehicles After Collision . . .	6-36
6-19	Test No. 7. Longitudinal Crash Pulse - Vehicle #6 . . .	6-37
6-20	Test No. 7. Longitudinal Crash Pulse - Vehicle #14 . .	6-38
6-21	Test No. 8. Position of Vehicles at Time of Contact . .	6-41
6-22	Test No. 8. Configuration of Vehicles After Contact . .	6-42
6-23	Test No. 8. Longitudinal Crash Pulse - Vehicle #8 . . .	6-43
6-24	Test No. 8. Longitudinal Crash Pulse - Vehicle #16 . .	6-44
6-25	Test No. 9. Interaction of Vehicles After Contact	6-47
6-26	Test No. 9. Longitudinal Crash Pulse - Vehicle #7 . . .	6-48
6-27	Test No. 9. Longitudinal Crash Pulse - Vehicle #17. . .	6-50
6-28	Test No. 9. Displacements Obtained from Motion Picture Films	6-51
6-29	Test No. 10. Position of Vehicles at Time of Impact . .	6-52
6-30	Test No. 10. Lateral Crash Pulse - Vehicle #13	6-54
6-31	Test No. 11. Position of Vehicles at Time of Contact .	6-56
6-32	Test No. 11. Post-Crash Condition	6-57
6-33	Test No. 11. Lateral Crash Pulse - Vehicle #13	6-59
6-34	Test No. 12. Lateral Crash Pulse - Vehicle #15	6-61
6-35	Test No. 13. Post-Crash Condition	6-63
6-36	Test No. 13. Lateral Crash Pulse - Vehicle #16	6-65
6-37	Test No. 14. Condition of Vehicles After Contact	6-67
6-38	Test No. 14. Lateral Crash Pulse - Vehicle #12	6-68
6-39	Test No. 15. Damage Resulting from Impact	6-70
6-40	Test No. 15. Lateral Crash Pulse - Vehicle #4	6-71

LIST OF FIGURES (Continued)

<u>Number</u>	<u>Title</u>	<u>Page</u>
7-1	Comparison of Frontal Impacts	7-2
7-2	Comparison of Oblique Impacts	7-5
7-3	Comparison of Side Impacts	7-7
8-1	Load-Deflection Characteristics of Modified Vehicle Used in System Test Series	8-11
8-2	Frontal Normal Barrier Impact Model	8-16
8-3	Logic Diagram for Frontal Normal Barrier Impact Model	8-18
8-4	Front Normal Barrier Simulation (50 mph)	8-20
8-5	Angular Frontal Barrier Model	8-22
8-6	Logic Diagram for Frontal Angular Impact Model	8-26
8-7	Front Angular Barrier Simulation (50 mph)	8-28
8-8	Frontal Pole Impact Model	8-30
8-9	Logic Diagram for Front Pole Impact Model	8-32
8-10	Front Pole Simulation (40 mph)	8-34
8-11	Side Pole Impact Model	8-36
8-12	Logic Diagram for Side Pole Impact Model	8-38
8-13	Side Pole Simulation (10 mph)	8-40
8-14	Front/Front Aligned Impact Model	8-41
8-15	Logic Diagram for Front/Front Aligned Impact Model	8-44
8-16	Front to Front Aligned Simulation (75 mph)	8-46
8-17	Front/Front Offset Impact Model	8-48
8-18	Logic Diagram for Front/Front Offset Impact Model	8-52
8-19	Front to Front Offset Simulation (75 mph)	8-54
8-20	Front/Side Normal Impact Model	8-56
8-21	Logic Diagram for Front/Side Normal Impact Model	8-58
8-22	Front to Side Simulation (25 mph)	8-60
8-23	Structural Hysteresis Loop	8-63

LIST OF FIGURES (Continued)

<u>Number</u>	<u>Title</u>	<u>Page</u>
8-24	Crushable Beam Membrane Structure	8-66
8-25	Rear Sill Plastic Hinge Structure	8-70
8-26	Frontal Structural Model Compact Car Stress Model . . .	8-72
8-27	Side Structure Model Compact Car Stress Model	8-73

LIST OF TABLES

<u>Number</u>	<u>Title</u>	<u>Page</u>
1-1	Performance Goals	1-2
4-1	Weight Evaluation System Test Vehicle	4-5
5-1	Square Tube Compression Tests	5-3
5-2	Ripple Panel Subassembly Compression Tests	5-6
6-1	System Test Program Summary	6-2
6-2	Results of System Test 1 and Baseline Test I	6-10
6-3	Results of System Test 2 and Baseline Test II	6-12
6-4	Results of System Test 3	6-18
6-5	Results of System Test 4 and Baseline Test III	6-22
6-6	Results of System Test 5 and Baseline Test IV	6-29
6-7	Results of System Test 6	6-34
6-8	Results of System Test 7	6-39
6-9	Results of System Test 8	6-45
6-10	Results of System Test 9	6-46
6-11	Results of System Test 10 and Baseline Test V	6-55
6-12	Results of System Test 11	6-58
6-13	Results of System Test 12	6-60
6-14	Results of System Test 13	6-64
6-15	Results of System Test 14	6-66
6-16	Results of System Test 15	6-72
8-1	Blocks Used in DYSIM	8-3
8-2	Structural Elements Used in Dynamic Response Models	8-7
8-3	Load-Deflection Characteristics of Modified Vehicle Structural Elements	8-9
8-4	Frontal Normal Barrier Test Case	8-19
8-5	Frontal Angular Barrier Test Case	8-27
8-6	Front Pole Test Case	8-33

LIST OF TABLES (Continued)

<u>Number</u>	<u>Title</u>	<u>Page</u>
8-7	Side Pole Test Case	8-39
8-8	Front to Front Aligned Test Case	8-45
8-9	Front to Front Offset Test Case	8-53
8-10	Front to Side Test Case	8-59
8-11	Second-Stage Bumper Simulation	8-67
8-12	Honeycomb Sandwich Door Beam Simulation	8-69

SECTION 1 INTRODUCTION

This report describes the work accomplished under DOT Contract DOT-HS-257-2-461 entitled, "Frontal and Side Impact Crashworthiness - Compact Cars." The contract, which was for an eighteen month period, had as its objective the improvement in crashworthiness of a production compact car. The DOT Contract Technical Monitor was Mr. S. Craig Keifer. The contract was performed at the Advanced Systems Laboratory of AMF Incorporated under the program management of Mr. William J. Wingenbach. The major subcontractor was American Motors Corporation, who supplied the production vehicles used in the project, performed vehicle design for the incorporation of energy absorption concepts, and studied the production feasibility of the various vehicle modifications. The AMC effort was managed by Mr. Kenneth Schang of the Vehicle Safety Department. Other subcontractors were Aero Spacelines Inc. who performed all modification to production vehicles; Dynamic Science who conducted a series of baseline and subsystem vehicle impact tests; and Calspan Corporation who conducted a series of system vehicle impact tests. All mathematical modeling, concept generation, analyses and component development testing were performed at the AMF/ASL facility.

The vehicle selected for use in the program was the 1973 AMC Hornet. The 2-door sedan with 6-cylinder engine and automatic transmission was specified because that model was most representative of 1973 Hornets in use. Constraints on modifications to the vehicle included retention of the engine in its current configuration. Increases in length, width, weight and cost were limited to levels which would not change the character and public acceptability of the vehicle. An additional constraint adopted during the project was control of the aggressivity of the modified vehicle front end. That is, the modified front end should not cause a great deal more damage to another vehicle than an unmodified vehicle under similar crash conditions.

Energy absorption concepts and the methods used for designing them were selected on the basis of their adaptability to a wide variety of production vehicles. Performance goals sought were derived from consideration of occupant acceleration and vehicle intrusion limits which had been specified on past DOT projects. These are summarized in Table 1-1. Maximum impact velocity at which these performance goals could be realized were estimated by consideration of vehicle geometry and crush space.

Table 1-1. Performance Goals

Type of Impact	Maximum Acceleration	Maximum Intrusion
Frontal Barrier	40 g	5 inches
Frontal Pole	40 g	5 inches
Side Pole	20 g	3.5 inches

For example, the maximum frontal crush space available in the standard Hornet is 15 inches. The maximum the vehicle could be lengthened without violation of previously-mentioned constraints is about 3 inches. This provides a maximum of 18 inches of crush space in the modified vehicle. The range of total weight of vehicles in service can be estimated as follows:

	<u>Weight (lbs)</u>
<u>Low Limit</u>	
Baseline curb weight	2837
One Occupant	150
Design modifications	<u>150</u>
	3137
<u>High Limit</u>	
Baseline curb weight	2837
Two occupants	300
Accessories	300
Cargo	175
Design modifications	<u>150</u>
	3762

The maximum crush efficiency likely to be attainable with any structural system is estimated to be about 80 percent.

The heavy vehicle will experience greater intrusion while the light vehicle will experience higher acceleration.

The heavy vehicle will experience an average acceleration of $.8 \times 40 \text{ g} \times 3137 \text{ lbs}/3762 \text{ lbs}$ or 26.5 g .

Under these assumptions and constraints, the maximum frontal impact velocity can be estimated by:

$$V = \sqrt{\frac{b \times a}{.4}}$$

where

a = average acceleration in g = 26.5

b = maximum crush in inches = $18 + 5 = 23$

V = impact velocity in mph

$$V = \sqrt{\frac{26.5 \times 23}{.4}} \approx 40 \text{ mph}$$

That is the estimate of maximum barrier impact velocity at which the goals of 40 g maximum acceleration and 5 inches maximum intrusion are attainable is 40 mph. A similar consideration of side impact geometry and structural efficiency led to the belief that the practical limit for side barrier impact velocity is 10 mph. Actual test velocities selected were:

50 mph - frontal barrier

40 mph - frontal pole

10 mph - side pole

75 mph - relative velocity, vehicle front to vehicle front

25 mph - relative velocity, vehicle front to vehicle side

The sequence in which the various tasks were undertaken to achieve performance goals is described in Section 2.

SECTION 2 PROGRAM LOGIC

The program logic for the Compact Car Front and Side Impact Crashworthiness program is outlined in Figure 2-1. The program involved both hardware and software development. Hardware development included the following studies:

- Front end component level
- Side component level
- Front end subsystem level
- Side subsystem level
- Integrated system level

Paralleling hardware development and interrelating with it was a continuing mathematical model development effort.

The program began with an examination of the production vehicle which had been selected for modification. This included studies of various components of the vehicles as well as a comprehensive set of crash tests of the unmodified vehicle. These studies led to the identification of vehicle structures which would require modification.

Mathematical modeling of vehicles in various crash configurations was undertaken and the results of the baseline vehicle test program used to verify the validity of the modeling techniques.

In parallel efforts, various energy absorbing concepts were developed for front and side structures. The development effort involved component concept generation, analyses, and evaluation. Laboratory versions of promising concepts were fabricated, tested and further evaluated.

Since the selection of component concepts for fabrication and test was based on a performance evaluation in a system context, the second development cycle (subsystem level) overlapped the first cycle. Preliminary

PROGRAM LOGIC

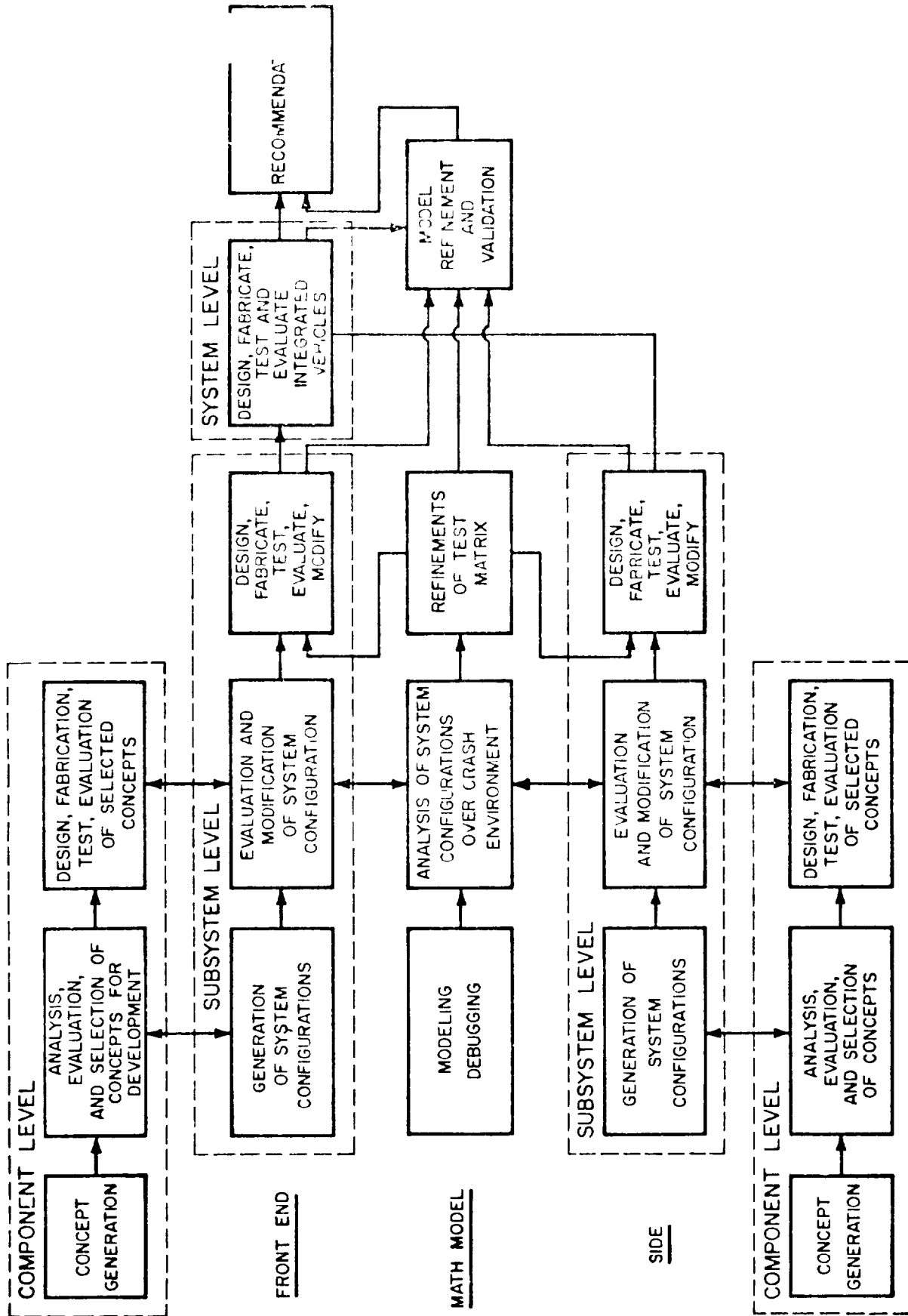


Figure 2-1

selection of front end and side structural configurations accompanied component selections.

At the completion of component testing, one front and one side structural configuration was selected for development. This started with a design program at the American Motors facility. Continuous manufacturing feasibility evaluation was performed as the designs emerged. The front end and side structural modifications were incorporated into a series of vehicles and a second cycle of testing performed. These tests were designed to explore the behavior of either the front end or side subsystem only, and not the entire vehicle. Therefore, the vehicle structure away from the subsystem under study was strongly reinforced so that deformation was concentrated in the area of interest. The subsystem test program consisting of a front barrier, a front pole and a side pole test provided a second opportunity for comparing math model simulations with crash test results.

The last cycle (system level) was directed toward improving the front end and side structure as indicated by subsystem tests and incorporating these refined structures into an integrated design with the basic vehicle structure. This was accompanied by a continuing effort to minimize weight and to maintain production feasibility.

A comprehensive series of tests was conducted with systems level modified vehicles. The series of fifteen tests explored the behavior of the modified vehicle in a wide variety of crash situations. It included a study of the effects of vehicle aggressiveness since the series involved both modified and unmodified vehicles in identical crash situations. Also studied was the behavior of the modified vehicle in encounters with full-sized 4200 lb vehicles.

The results of this test series were evaluated leading to a series of conclusions and recommendations. The system level test series results provided an additional opportunity for checking and verifying the results of the mathematical simulations of crash events.

SECTION 3
BASELINE VEHICLE TEST PROGRAM

A series of tests involving unmodified American Motors Hornets was conducted at the Phoenix, Arizona test facility of Ultrasystems Inc., Dynamic Science Division, in January of 1973.

The 1973 Hornet was selected to serve as the basis for the Compact Car Crashworthiness project. The objective of the baseline test program was to determine the crash performance of the production vehicle. The test results were used to guide the design of vehicle modifications and to serve as a basis for evaluating the effectiveness of vehicle modifications.

The test series which was conducted per AMF Test Directive #3-52 involved the following tests:

- Frontal barrier - 50 mph
- Frontal pole - 40 mph
- Side pole - 10 mph
- Vehicle front to vehicle front - 75 mph
- Vehicle front to vehicle side - 25 mph

Each of the seven vehicles involved was a 2-door sedan, with 6-cyl. engine, and automatic transmission, and had a test weight of approximately 2800 lbs. Curb weight of the vehicle was approximately 2830 lbs. The as-tested vehicles had liquids, hood and rear deck removed and instrumentation added. Results presented are taken from rear trunk-mounted accelerometers for frontal impacts and front floor-mounted accelerometers on the side opposite the impact for side impacts. All intrusions and displacements are from post-crash static measurements unless otherwise stated. All acceleration data has been filtered per SAE J211.

Test results are as follows:

Baseline Test I, 49.71 mph, 0° Frontal Flat Barrier

The front of the vehicle was crushed a maximum of 33 inches. Maximum deceleration occurred as the engine was contacted and pushed rearward into the firewall. The engine was displaced a total of 19 inches causing 17.4 inches intrusion in the forward center floor pan area (transmission hump). Intrusion in the forward left and right floor pan areas were 10.5 inches and 10.8 inches respectively. Floor buckling extended rearward to a position slightly forward of the rear seat location. The right side of the front seat separated from its guide rail due to floor pan buckling. The steering wheel was displaced rearward approximately 4 inches.

The sills collapsed early in the impact by buckling at a point approximately 12 inches aft of their forward ends. Buckling occurred abruptly and without discernible crush. The "A" pillar and "B" pillar roof attachment points showed signs of metal failure. Both doors were jammed against the "B" posts. The left-hand door could not be opened without excessive force. The right-hand door opened approximately 2 feet without difficulty.

The crush pulse, shown in Figure 3-1, rose to an average level of 32 g by 12 milliseconds after initial contact and remained at this level for 18 milliseconds. Acceleration then increased to an average level of 35 g for the remainder of the crash.

While the maximum acceleration was not excessive, the maximum levels were reached relatively late in the crash. The amount of intrusion is the primary concern in this crash.

Baseline Test II, 39.61 mph, Frontal Pole, Centered

Maximum static crush of the vehicle was 39.5 inches. The engine was pushed rearward into the firewall, causing 7.8 inches intrusion into the passenger compartment. Floor buckling occurred throughout the passenger compartment to a location just aft of the front seat. The steering wheel was displaced rearward 4 inches. The accelerator pedal was displaced rearward about 10 inches.

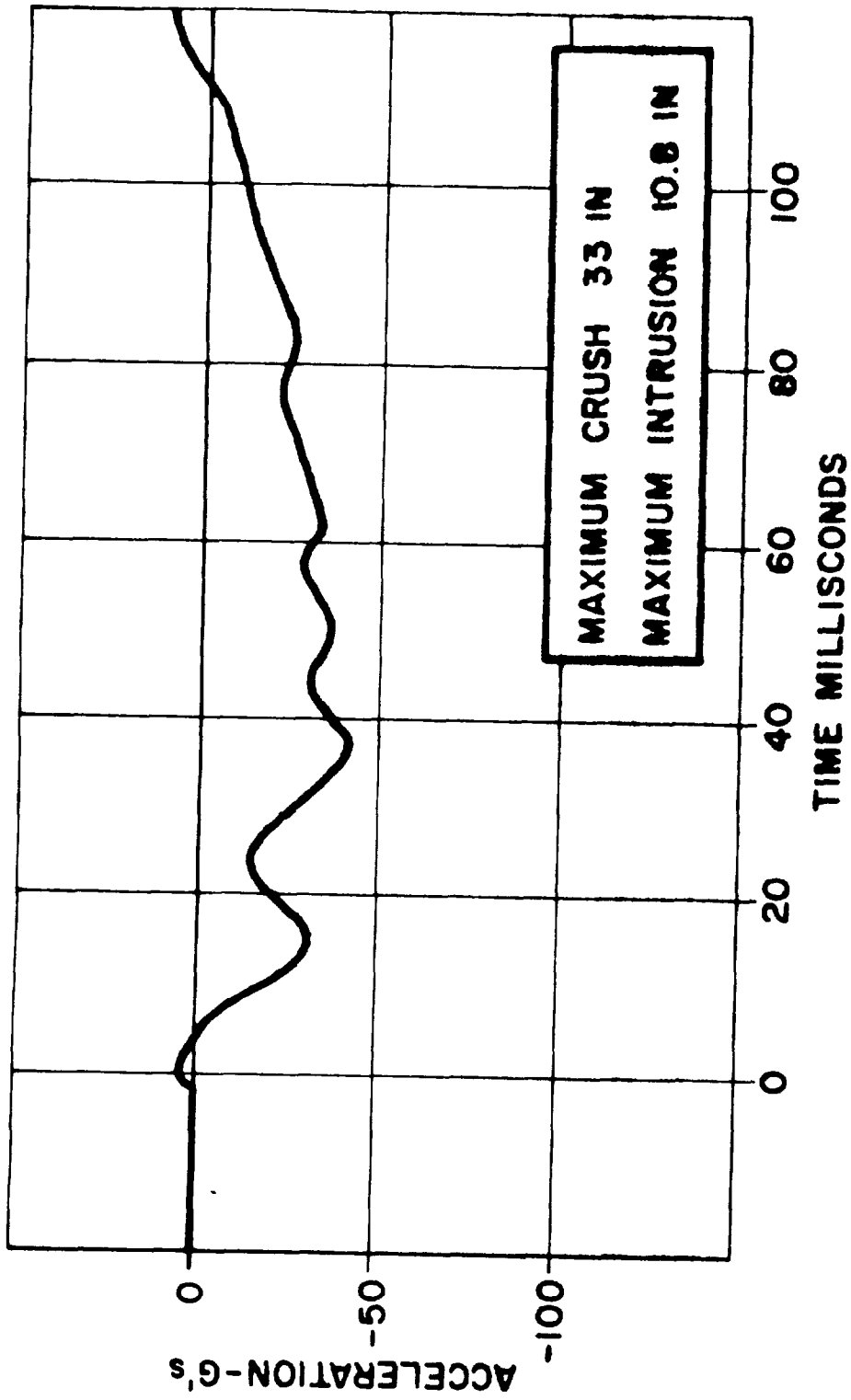


Figure 3-1. Baseline Test No. I 49.71 mph 0° Frontal Barrier

The front frame crossmember was torn from the left-hand sill early in the impact, providing little retardation to the vehicle. The pole contacted the engine slightly off-center, deflecting it to the right and upward, and causing the left front engine mount to tear apart.

Acceleration during the first 40 milliseconds of the crash averaged 8 g. By 45 milliseconds, acceleration reached 25 g and remained at this level for another 35 milliseconds. Then acceleration diminished, finally reaching zero about 120 milliseconds after initial contact. The long and relatively low-level crash pulse, shown in Figure 3-2, was a consequence of the large front end crush that occurred. Although relatively lightweight components were crushed, the intrusion and floor deformation indicate that the force levels were too high for the load paths that were available. If the engine had been impacted more squarely, even greater firewall intrusion could have been expected along with an earlier and higher level crash pulse.

Baseline Test III, 9.57 mph Side Pole Impact, 90^o,
Impact Point at Door Centerline

Impact of the vehicle occurred approximately 5 inches forward of the intended aim point. Damage to the vehicle structure was confined to the right door and the right side of the rocker panel. A slight dent was made in the roof due to contact with pole. Intrusion was approximately 6 inches with the inside of the right door pushing about an inch into the right edge of the front seat. The crash pulse is shown in Figure 3-3.

Baseline Test IV, 37.89 mph Vehicle to Vehicle (75.78 mph
Relative Velocity), Frontal 0^o,
Centerlines Colinear

Maximum intrusion in the vehicles was 5.6 and 6.0 inches. Maximum static crush was 25.0 and 27.0 inches. Both engines were displaced rearward 11 inches, resulting in 7 inches deformation of the center floor pan (transmission

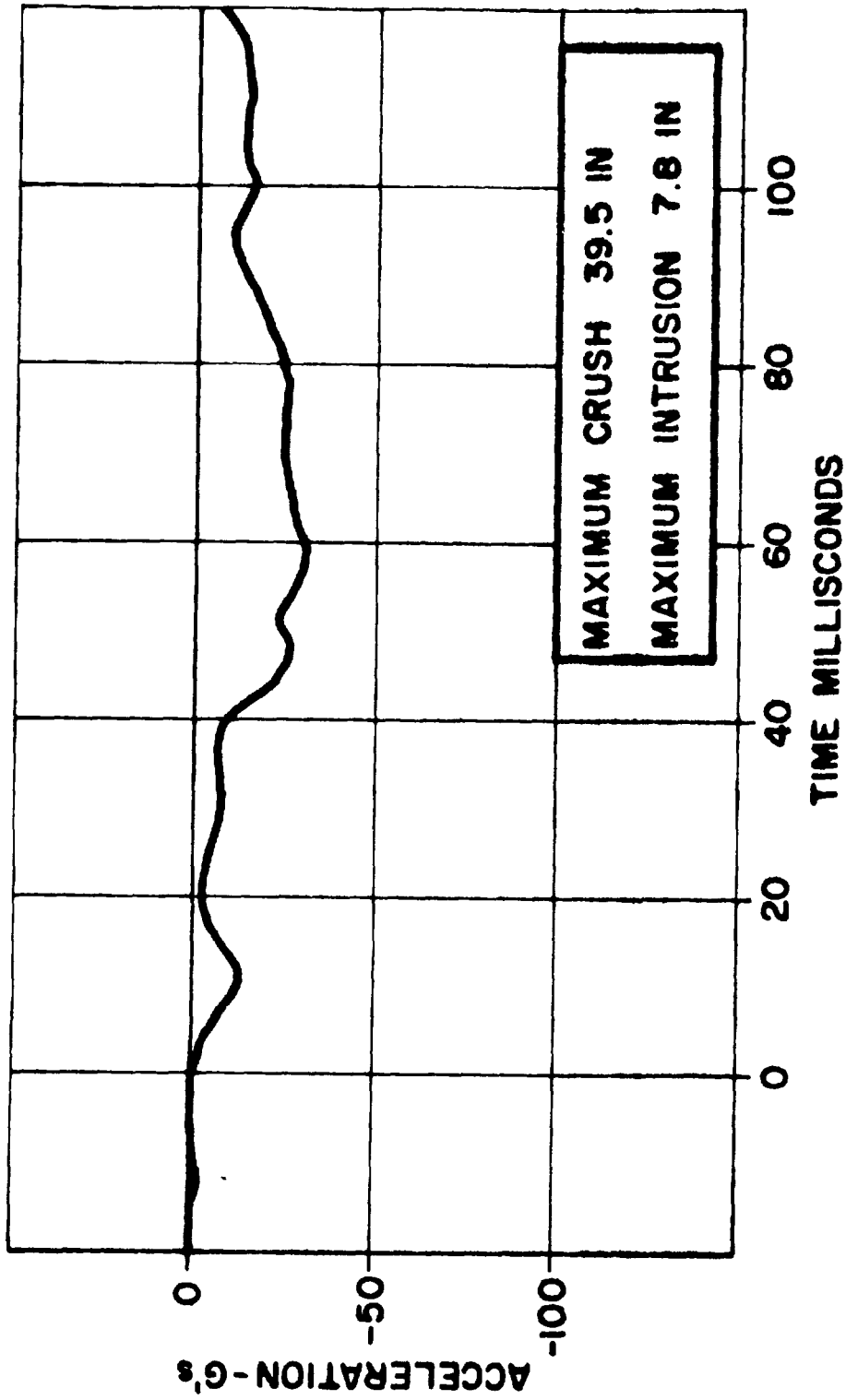


Figure 3-2. Baseline Test No. II 39.61 mph Frontal Pole Centered

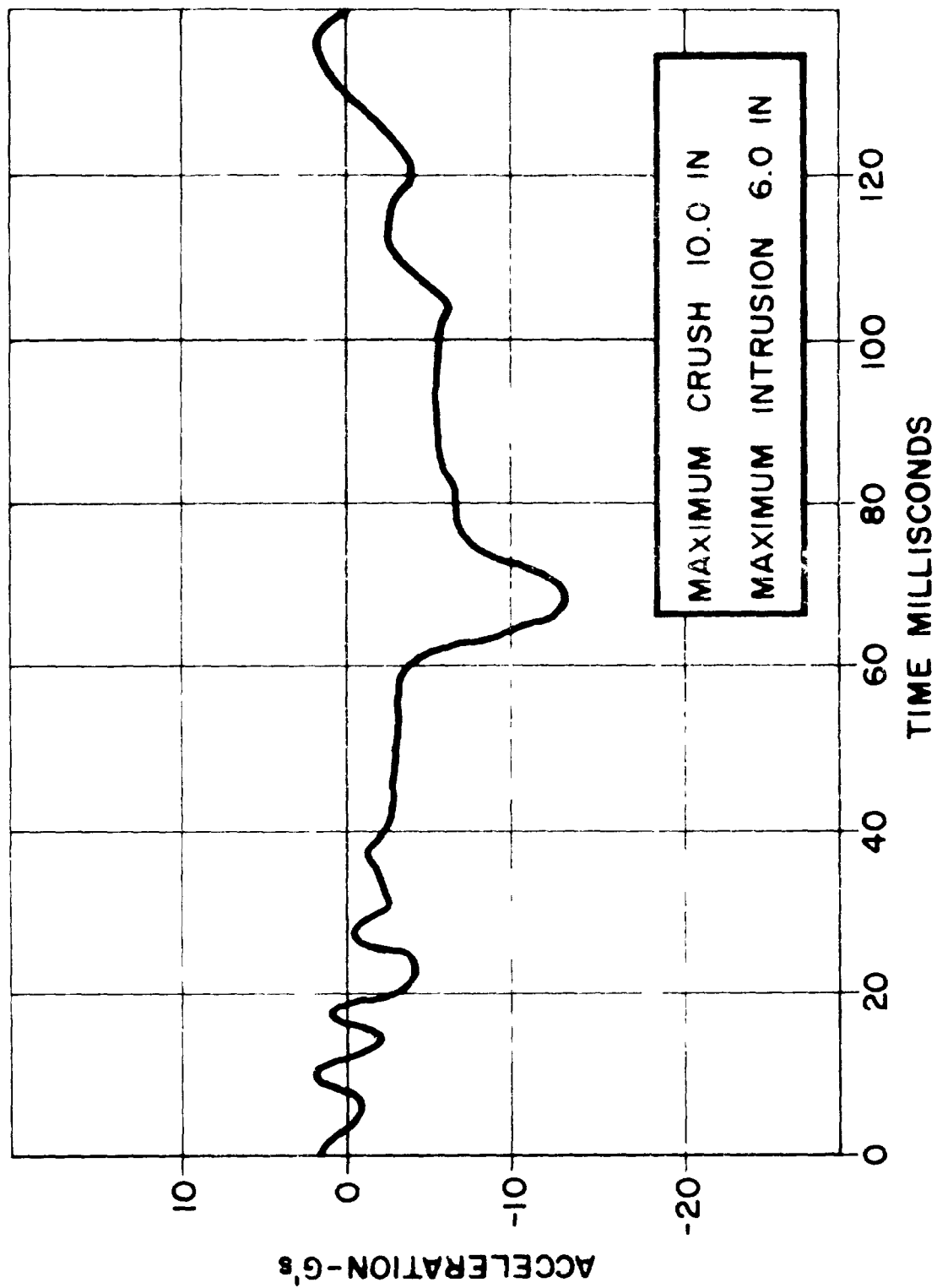


Figure 3-3. Bas line Test No. III 9.57 mph Side Pol

hump) in each vehicle. All four doors could be opened after impact, although some force was required to open three of them.

The crash pulse, shown in Figure 3-4, built up to a maximum level of 32 g, 25 milliseconds after initial contact. A level of 12 to 30 g acceleration was maintained throughout the 90 millisecond duration of the impact.

Baseline Test V, 24.78 mph Vehicle-to-Vehicle Side Impact,
90° Impact at Door Centerline

The door and "A" post were severely deformed and the "B" post was torn loose from the rocker panel. Dynamic crush at the "B" post reached 19 inches, resulting in static crush of 13.5 inches. Static crush at the door centerline was 13.0 inches. Maximum intrusion was 9.5 inches at the "B" post. Intrusion at the door centerline was 7.0 inches. The crash pulse, shown in Figure 3-5, has three distinct peaks of sinusoidal form and 11 to 14 g amplitude, occurring 16, 35 and 66 milliseconds after impact. Overall duration of the crash pulse is 80 msec.

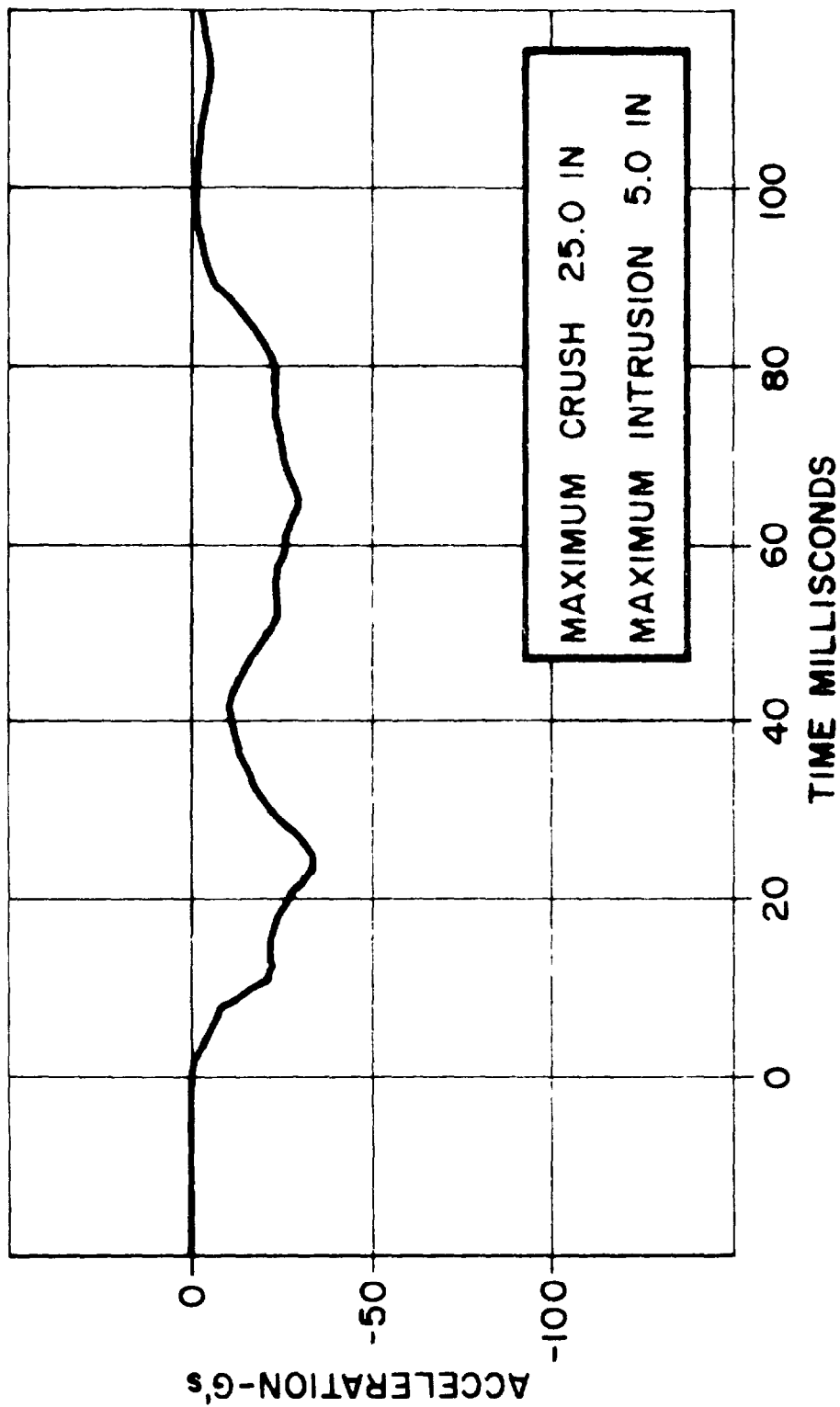


Figure 3-4. Baseline Test No. IV 37.89mph (75.78mph Relative Velocity)
 From to Front Aligned

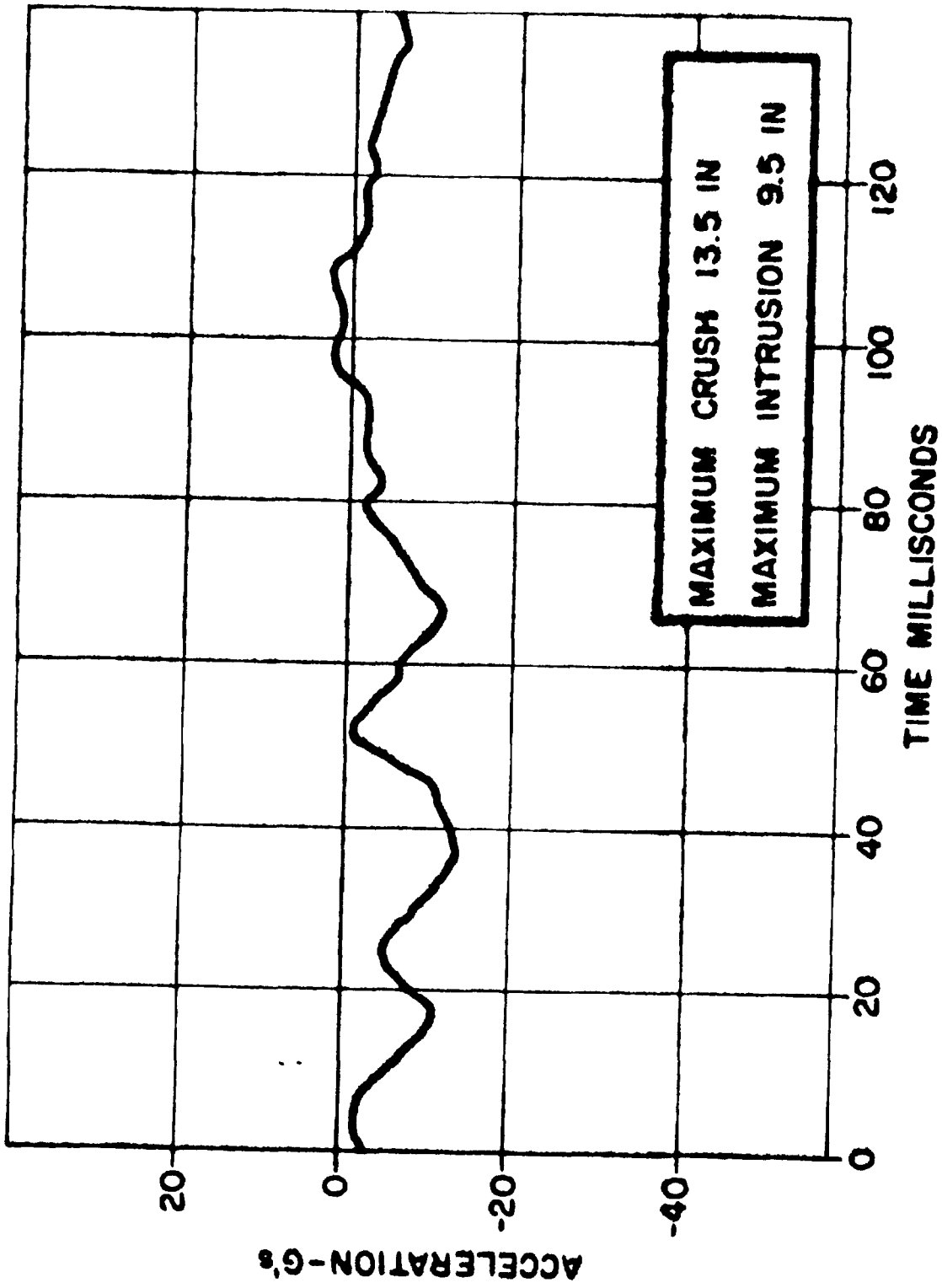


Figure 3-5. Baseline Test No. V 24.78 mph Front to Side

SECTION 4

VEHICLE MODIFICATIONS

The vehicle modifications discussed in this section refer to final design configurations. Some of the component and subsystem development work involved proposed modifications which may be slightly different than those discussed here; however, the general intent of the concepts remained constant throughout the program.

SYSTEM DESIGN

In designing for frontal impacts, the approach taken was to collect concentrated loads and to distribute them to energy absorbing components. The primary energy absorbing components include the crushable forward sills, the plastic hinge rear sills and the ripple panels. The second-stage bumper absorbs energy when large concentrated loads are applied to it. The energy absorbing components are backed up by non-deforming components that carry loads into the passenger compartment. The reinforced "A" post structure, door beam and "B" post provide a major path for longitudinal loads. The upper "A" pillar and roof form a secondary load path, with hinging expected in the roof over the "B" pillar. The vehicle was lengthened 3.5 inches to provide front end crush space. The engine mounts were modified to simulate an interlocking type mount. The complete front end modification is shown in Figure 4-1.

In side impacts, the "A" post, "B" post and door beam were designed to work together in reducing intrusion and providing an earlier crash pulse. The lateral braces between the sills and rocker panels also contributed. The revised "B" or lock post is shown in Figure 4-2, and the door beam and attachment hardware are shown in Figure 4-3.

All of the vehicle modifications were accomplished with a net weight increase of 104.3 pounds. This does not include any secondary weight effects, such as a possible need of a modified front suspension. A detailed breakdown of the weight changes is given in Table 4-1. With the exception of the door beam, all components were fabricated from carbon steel.

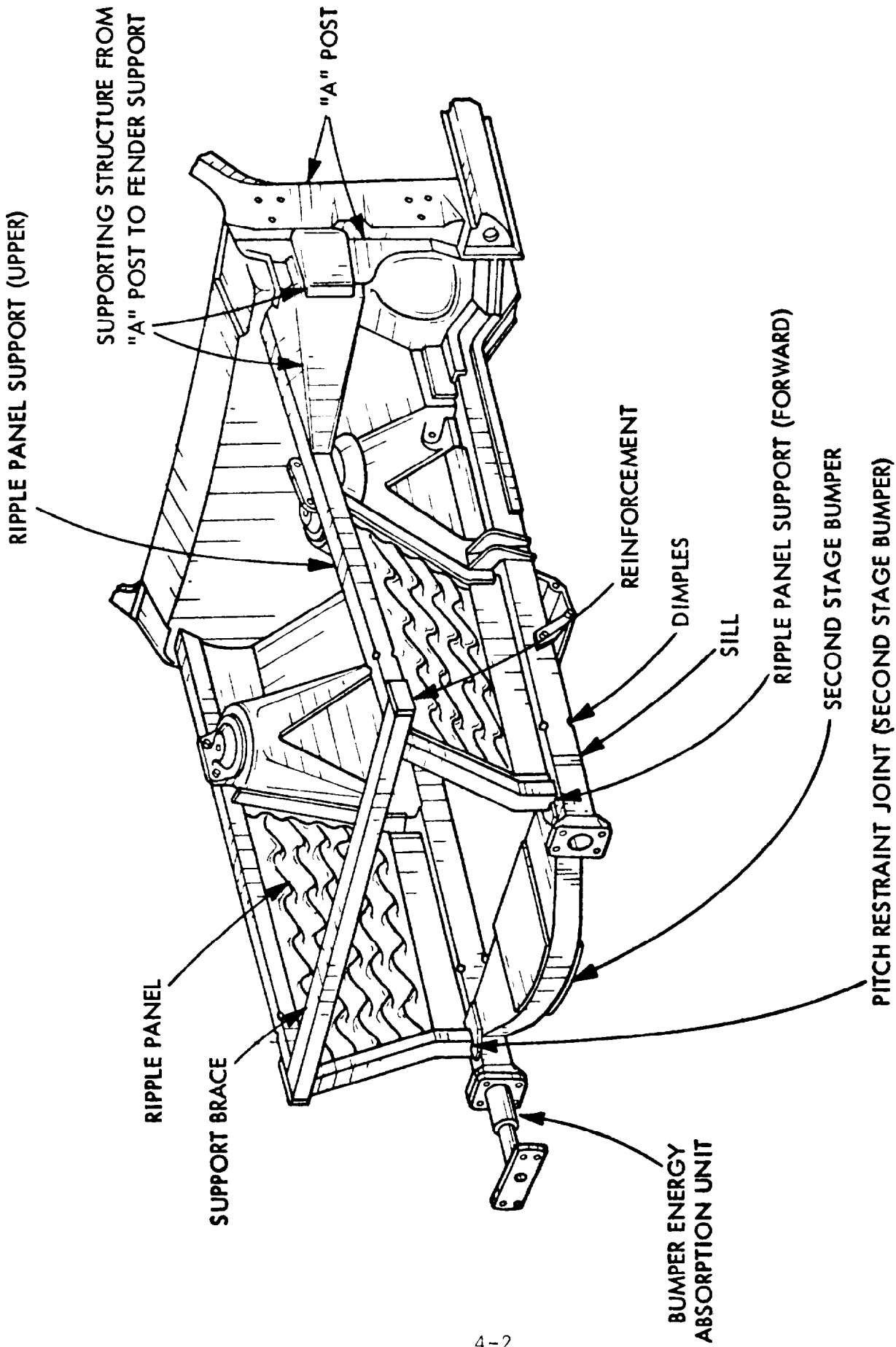


Figure 4-1. Front End Structure - System Test Vehicle

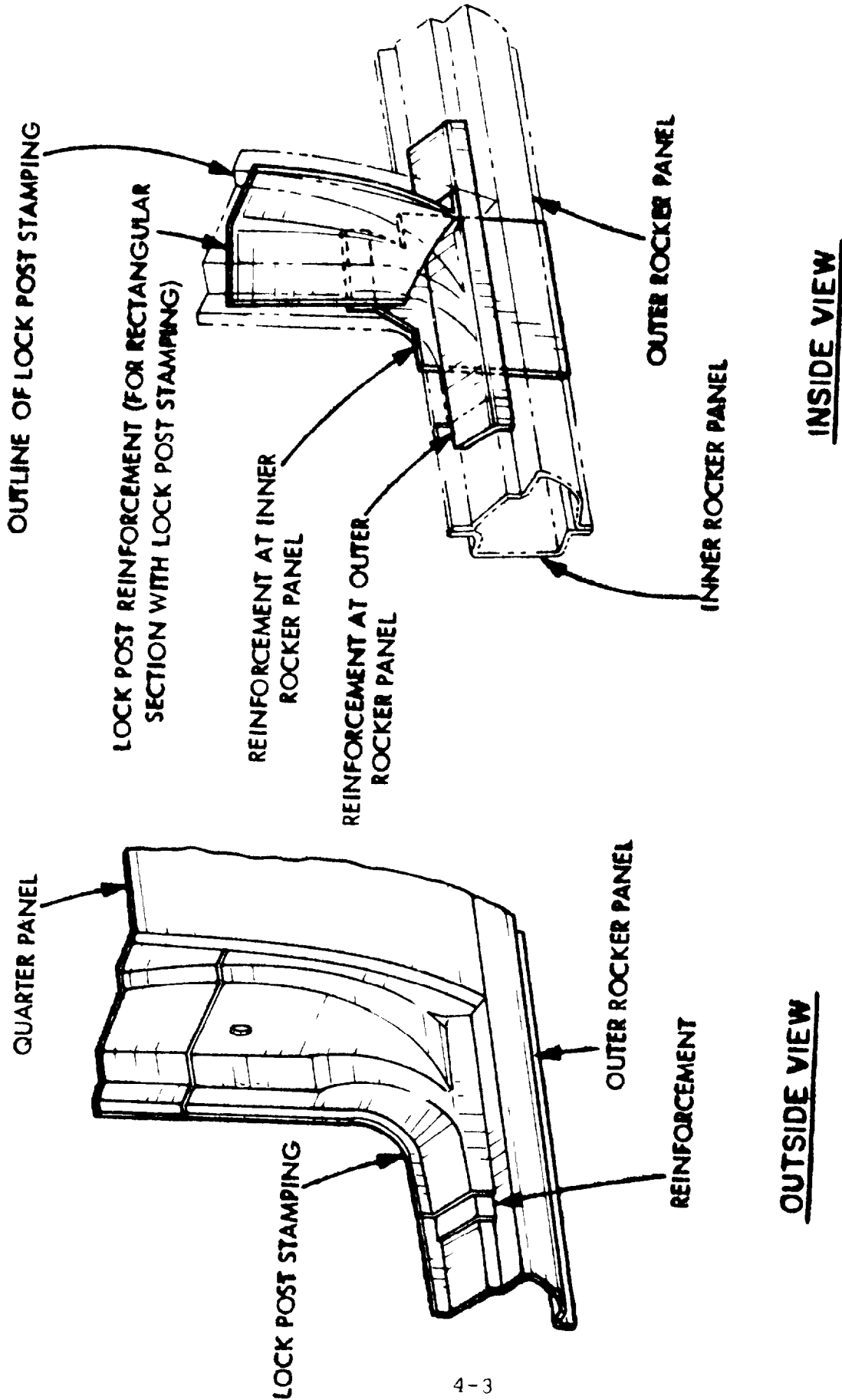


Figure 4-2. Revised Lock Post

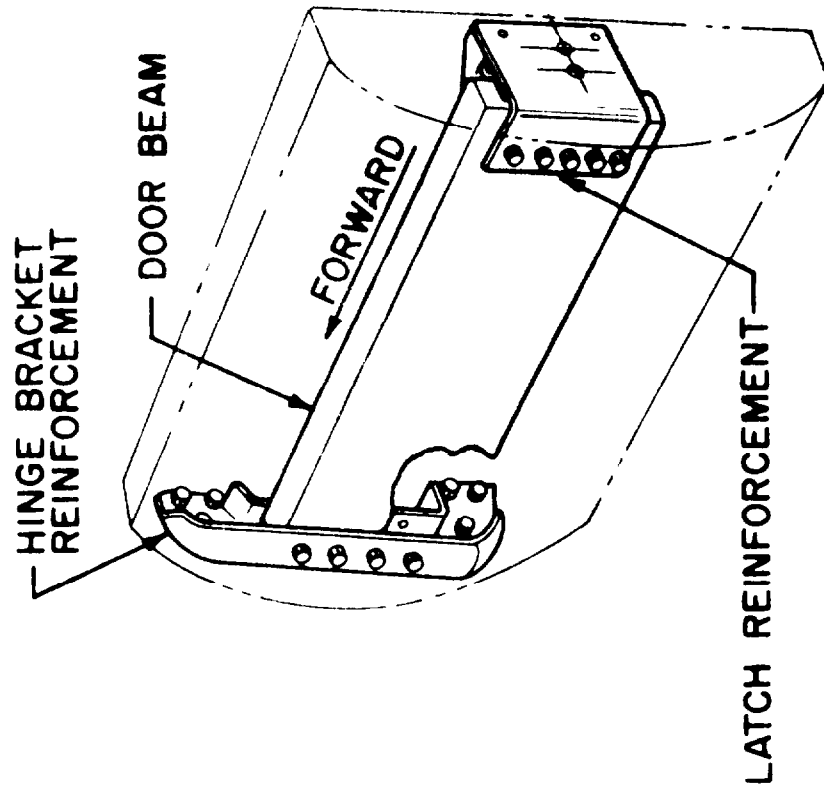


Figure 4-3. Door Beam and Attachment Hardware

Table 4-1. Weight Evaluation System Test Vehicle

COMPONENT	WEIGHT ADDED lbs.	WEIGHT REMOVED lbs.	NET CHANGE lbs.
SILLS, GUTTERS, PANELS & MISC.	146.8	122.5	24.3
LATERAL BRACES	18.6		18.6
2nd STAGE BUMPER	26.0	8.0	18.0
"A" POST	28.6	5.0	23.6
"B" POST	31.0	4.0	27.0
DOOR BEAM ASSY.	26.4	33.6	-7.2
TOTAL	277.4	173.1	104.3

COMPONENT FUNCTIONS

Low-Speed Impacts. The conventional vehicle bumper and its hydraulic energy absorbing units were retained for low-speed impacts. The energy absorbing units were modified to enable them to function at impact speeds up to 50 mph without bursting. In impacts above 5 mph, the bumper strokes rearward and seats against a second-stage bumper that is mounted behind it.

Second-Stage Bumper. The second-stage bumper resists concentrated loads such as those imposed by a fixed pole barrier or the engine block of an impacting vehicle. The second-stage bumper transfers loads into the sills, which are primary energy absorbing members. The second-stage bumper also absorbs energy directly by deforming in a severe impact. The second-stage bumper ties the forward ends of the sills together. In an oblique or off-center impact, the second-stage bumper transmits forces from the impacted side of the vehicle to the non-impacted side.

Sills. The sills are major energy absorbing components. The forward ends of the sills are designed to collapse or crush over a long stroke without buckling. The aft portions of the sills are designed to function as plastic hinges, sustaining large plastic deformations without crippling. The square tubular sections are filled with plastic foam to provide support against crippling. The foam-filled sills can resist bending moments equivalent to the ultimate strength of the steel without undergoing crippling.

Ripple Panels. The inner fender panels of the vehicle were replaced by rippled sheet metal panels whose forward and upper edges were reinforced by square tubes. The rear edges of the ripple panels were supported by sheet metal strips that were welded to the spring towers. The lower edges of the ripple panels were welded to the sills. The ripple panels acted as shear panels in helping to hold the sills parallel to the vehicle longitudinal centerline. They also helped to support the sills against buckling. In

addition to this, the ripple panels are crushable energy absorbing components. The ripples provide structural stability enabling progressive crush to take place without buckling.

Compressive loads are carried to the "A" post through the sills and through structures that acquire loads from the ripple panel upper supports. From the "A" posts, compressive loads are carried through the "A" pillar to the roof. They are carried through the rocker panel and through the door beam to the "B" pillar and the quarter panel. Force is transmitted to the floor pan by the sills and rocker panel.

The "A" post and "B" post are reinforced to provide direct resistance to side impacts and also to support the door beam. The door beam is designed to transmit concentrated loads to the "A" post and "B" post. The door beam is made with aluminum honeycomb sandwich construction. Crushability of the core and stretching of face sheets provide energy absorption capacity. The ends of the door beam are provided with reinforcement members that transmit forces from the door to the "A" post and to the "B" post.

Compressive loads are carried by lateral and diagonal braces from the rocker panel to the sills. These braces are sheet metal hat sections acting as short columns.

COMPONENT DESIGNS

Energy Absorption Units. A 5/8 inch diameter hole was drilled through the piston of the hydraulic energy absorbing units to prevent them from bursting in a high-speed impact.

Second-Stage Bumper. The second-stage bumper spans the 27.8 inch distance between the sills. The second-stage bumper is a hollow beam weldment made up of components formed from .125 inch thick 1010 hot rolled steel. Depth of the beam is a maximum of 8.5 inches at the center of the span. Width of the beam (vertical dimension, since the beam is horizontal) is a nominal 3.25 inches. Doubler plates in the central 10 inches of the

span increase the width of the beam to 3.50 inches. The calculated load-carrying capacity for loads applied at the center of the second-stage bumper is 75,000 lbs.

Ripple Panels. The ripple panels were die-formed from .033 inch (21 gauge) 1010 hot rolled steel sheet. Viewed from inside the engine compartment, the formed pattern consists of three raised zig-zag ridges aligned parallel to the vehicle centerline. The height of the ridges is 1.0 inches. They are spaced at 3.0 inches apart and the peak-to-peak pitch of the ripples is 3.0 inches.

The ripple panels replaced the original fender inner panels which were formed from .042 inch (19 gauge) sheet steel. The ripple panels weigh less than the components they replaced.

Ripple Panel Supports. The forward and upper edges of the panels were reinforced with 2" x 2" x .065" 1018 steel tubing. Creases were formed in the four corners of the ripple panel upper supports near the forward end to induce crushing. The upper forward corners of the ripple panels were tied together by a support brace also formed of 2" x 2" x .065" 1018 steel tubing. The rear edges of the ripple panels were reinforced by 4.25" x 3" x 16" stripes of 1020 steel plate. These strips also reinforced the spring tower. The lower edges of the ripple panel were welded to the sills.

Sills. The sills were fabricated from 3" x 3" x .095" steel tubing. Creases or dimples were formed in the four corners of the tube near the forward end to initiate crushing without an initial load spike (drilled holes were substituted for the dimples in the component level tests).

Steel doublers reinforced the upper and lower surfaces of the sills from the spring towers to the "A" posts. In the firewall kick-up region, the hollow section of the sills was filled with 20 lb per cubic foot density polyurethane foam. This insured maximum plastic hinge resistance by preventing crippling of the section.

Supporting Structure from "A" Post to Fender Support. The supporting structure was fabricated by forming and welding .090 inch thick 1020 steel sheet. The structure was welded to the "A" post and to the ripple panel upper support aft of the spring tower.

"A" Post and "B" Post Modifications. The "A" post was reinforced by adding a doubler to the lower two-thirds of the existing .042 inch (19 gauge) formed section. A .135 inch (10 gauge) inner panel was welded to the reinforced member forming a closed section with greatly improved strength and rigidity.

The "B" post was reinforced in similar fashion to the "A" post. The lower portion of the outer skin was replaced with a stamping of the same shape but with thickness increased to .125 inches. The inside of the post was strengthened with a .125 inch plate which completed a closed section for good bending and torsional rigidity. A plate was inserted in the post and extended down into the rocker panel, providing a rigid lower post connection.

Lateral Sill - Rocker Panel Supports. The sills are connected to the rocker panel by three hat sections formed from .063 inch steel sheet. These act as short columns to carry compressive loads from the rocker panel to the sill in a side impact.

Door Beam. The door beam has an overall span of 48.5 inches within the door. The width of the beam is 8.0 inches and the depth is 1.33 inches. The beam is constructed entirely of aluminum. The core was fabricated from .002 inch thick 5056 aluminum honeycomb with 3/8 inch cell size. Both face sheets were fabricated from .040 inch thick 7075-T6 aluminum. The door beam was fabricated with end pieces made of solid 7075-T6 aluminum. The components of the door beam were assembled by adhesive bonding. The door beam was attached to the hinges and to the lock mechanism by means of fittings formed from .13 inch thick steel sheet.

SECTION 5

DEVELOPMENT TEST PROGRAM

The development effort associated with the Compact Vehicle Crash-worthiness program involved extensive analysis and a companion development test program. This section discusses both the component and subsystem test programs.

COMPONENT TESTS

The objective of the component test program was to:

- Verify design calculations
- Determine the effects of parametric variations
- Determine failure modes
- Determine performance limits
- Establish proportions and sizing of components

Design calculations provided approximations to the force levels and crush distances available from components. The component level tests verified the accuracy of these calculations.

Parametric variations were studied to determine the effects of loading from various crash conditions and to help select optimally-designed component configurations. Parametric variations included load level and direction, loading rate, restraints, material size, shape and properties.

The component level tests determined the failure patterns that occurred in components. Any tendency of a component to fail prematurely was identified and corrected.

Off-axis loading and dynamic loading were used to determine some of the performance limits of components. Maximum stroke and energy absorption capacity were determined for various components.

The component tests were used most extensively in proportioning and sizing components, to achieve a balance between compressive strength energy absorbing capacity, elastic stability, cost and weight. The geometric properties of components were arranged so that local failure could occur without incurring gross collapse. The means were devised to support components against gross failure without over-constraining them and preventing localized failure.

Square Tube Tests. Twenty-one static and dynamic compression tests were performed on square tube specimens to assist in front sill design. The results of these tests are summarized in Table 5-1. The onset force shown in the first column is the force required to cause initial compressive failure of the tube. The mean force shown in the next column represents the resistance of the tube to crushing after the initial excursion has occurred. It is desirable that the onset force not greatly exceed the steady state mean force. Minimum variation in the steady state force (Column 3) is desirable. Stress raisers can be provided to reduce the onset force and bring it more into line with the mean force. The use of stress raisers is indicated in Column 4.

In the first four tests shown, the specimens were 3" square tubes with .120" wall thickness. Three of the tubes had indentations spaced 3" apart along two opposite sides. These were intended to induce uniform folding of the tube as it collapsed (Type I Stress Raisers). Type II stress raisers were used in two of the tubes including that which had no indentations. Type II stress raisers consist of four half-inch holes drilled through the corners of a tube 2" from one end.

Test 2B demonstrated that indentations are not necessary to induce uniform folding of a specimen. The first four tests also demonstrated that Type II stress raisers adequately diminish the onset force. The first four tests established the 3" square tube with .120" wall thickness as a reliable component with a 35,000 to 40,000 lb mean crush force.

Table 5-1. Square Tube Compression Tests

Test	Onset Force X1000 lb.	Steady State		Stress ⁽¹⁾ Raisers	Type of Test
		Mean Force X1000 lb.	Force Variation		
3' x 3' x .120' Specimen ⁽²⁾ (4.70 lb/ft) - Axial Loading					
1	73	40	± 18%	I	Static
2A	79	38	± 18%	I	Dynamic
2B	66	40	± 26%	II	Dynamic
7	62	35	± 34%	I & II	Static
4' x 4' x .120' Specimen ⁽²⁾ (6.33 lb/ft) - Axial Loading					
3	92	26	± 34%	None	Static
4	98	31	± 31%	II	Dynamic
4' x 3' x .120' Specimen (4.07 lb/ft) - Axial Loading					
5	60	15	± 67%	None	Static
6	67	21	± 29%	None	Dynamic
3' x 3' x .095' Specimen ⁽³⁾ (3.75 lb/ft) - Axial Loading					
8	41	23	± 15%	II	Static
9	48	11	± 33%	II	Static
10	47	18	± 44%	II	Dynamic
11	56	18	± 45%	II	Dynamic
22	44	18	± 45%	II	Dynamic
3' x 3' x .095' Specimen (3.75 lb/ft) - 3° Offset Loading					
14	30	15	± 33%	II	Dynamic
15	47	15	± 33%	II	Dynamic
3' x 3' x .095' Specimen (3.75 lb/ft) - 5° Offset Loading					
16	27	21	± 24%	II	Static
17	43	23	± 17%	II	Dynamic
2' x 2' x .065' Specimen (1.711 lb/ft) - Axial Loading					
18	17	5.5	± 64%	II	Static
19	18	7.0	± 43%	II	Static
20	24	12	± 17%	II	Dynamic
21	23	18 ⁽⁴⁾	± 44%	II	Dynamic
<p>(1) Types of Stress Raisers I - Indentations formed in two opposite sides of tube. 3" spacing on centers. II - 1/2" dia. holes drilled through corners of tube 2' from one end.</p> <p>(2) All specimens initially 20" long.</p> <p>(3) The specimens for Tests 8 and 9 were cut from a single length of tubing to minimize the effect of material variations. The same applies to specimens for Tests 10, 11 and 22.</p> <p>(4) Specimen became skewed in fixture after initial crush occurred. Subsequent crush occurred at the opposite end of the tube.</p>					

In Tests #3 and 4, the four-inch square by .120" wall thickness tubes were shown to be less satisfactory than the 3" tubes due to the greater difference between the onset force and the mean force. The 4" tubes had a lower mean force than the 3" tubes which weigh less per foot.

In Tests #5 and 6, the 4" x 3" tubes exhibited a much lower mean force than the 3" square tubes.

The 3" square by .095" tubes are representative of the material that was used in fabricating the sills of the modified vehicles. The behavior of this material under axial loading was examined in Tests #8, 9, 10, 11 and 12. The specimens repeatedly yielded an 18,000 lb mean force with $\pm 45\%$ variation under axial dynamic loading. Under 3% offset dynamic loading, similar specimens repeatedly developed a 15,000 lb mean force with $\pm 33\%$ variation (Tests 14 and 15). Under 5% offset dynamic loading, a similar specimen developed a 23,000 lb mean force with $\pm 17\%$ variation.

The 2" square by .065" specimens are representative of material that was used to make the ripple panel upper supports. This material produced a 12,000 lb mean force with $\pm 17\%$ variation under dynamic axial loading (Test 20). Test #21 was to have been a repetition of Test #20, but after 4" of normal stroke, an offset loading condition developed. Crushing ceased at the end of the tube having stress raisers and it began on the opposite end. As a result, the applied force reached a level of 25,000 lbs.

Ripple Panel Compression Tests. The ripple panels used in the system test vehicles were different from those used in the subsystem test vehicles and in the component tests. The peak to peak pitch of the sinusoidal ripples in the panels used on the system test vehicles was 3.0 inches. The pitch used in the panels on the component tests and subsystem tests was 6.0 inches. In all panels, the distance between adjacent ripples was the same as the pitch of the ripples; that is, 6" in the component and system test panels and 3" in the system test panels. The depth of the ripples in all panels was 1.00 inches.

Ripple panel specimens measuring 20 x 21-1/2" were prepared. Compressive loads were applied parallel to the axis of the ripples. Several tests were run using specimens made from .036" material. They failed by buckling at a load of approximately 5,000 lbs, before significant crush had taken place. This failure mode is an off-design condition since the edges of the panels are normally supported by the sills and upper ripple panel supports. In subsequent tests, square tubes were welded to the free edges of the ripple panels to simulate a sill and upper ripple panel support. One tube was 3" square by .095" wall thickness and the other was 2" square by .065" wall thickness. Holes were drilled in the corners of the tubes near one end to simulate the stress raisers used in actual components. Static and dynamic compression tests were performed on panels fabricated from .047" and .030" thick carbon steel. The results of these tests are shown in Table 5-2. In order to isolate the contribution of the ripple panels, the force contributed by the square tubes was subtracted from the ripple panel mean force. Dynamic test values were used to approximate the force contributed by the semi-constrained square tubes.

The cross head of the testing machine was driven by two hydraulic cylinders so that equal force could be applied to both sides of the test article. In all tests, crushing was initiated in the vicinity of the stress raisers in the square tubes.

In Test #1 (static test of a .047" panel), the subassembly buckled after approximately 7" of crush occurred. Buckling was initiated in the 2" square tube.

In Test #2 (dynamic test of a .047" panel), the subassembly was crushed uniformly throughout a stroke of 7 inches, at which point buckling of the two inch tube began. In both tests of the .047" subassembly, deformation alternated from one edge of the panel to the other. In both tests, total deformation of the 3" tube was approximately equal to that of the 2" tube when buckling occurred.

Table 5-2. Ripple Panel Subassembly⁽¹⁾ Compression Tests

Test	Onset Force X1000 lb.	Steady State			Type of Test
		Mean Force X1000 lb.	Force Variation	Net Ripple ⁽²⁾ Panel Force X1000 lb.	
.047" Ripple Panel Subassembly					
1	45	38	± 6%	8	Static
2	72	39	± 22%	9	Dynamic
.030" Ripple Panel Subassembly					
3	62	37	± 22%	7	Static
4	84	62 ⁽³⁾	± 11%	32	Dynamic

(1) The ripple panel subassembly is composed of a ripple panel welded to a simulated sill (3" x 3" x .095" tube) and to a simulated ripple panel upper support (2" x 2" x .065" tube). Overall dimensions of sub-assembly are 20" wide x 21.5" long.

(2) Net ripple panel force was derived by subtracting the force contributed by the square tubes: a value of 18,000 lbs was used for the 3" tube and 12,000 lbs was used for the 2" tube.

(3) Load data unreliable - derived from applied hydraulic pressure. Fixture wracking introduced a high and unknown friction component.

In Test #3 (static test of a .030" ripple panel subassembly), crushing began simultaneously in the 3" and 2" tubes. The 3" tube crushed at a faster rate than the 2" tube, resulting in 4" more deflection at one edge of the panel than at the other. No buckling of the tubes occurred. Some tearing of the metal took place, primarily at the weld joint of the 3" tube.

In Test #4 (dynamic test of a .030" ripple panel subassembly), both tubes buckled after approximately 2" of crush occurred. The nature of buckling disrupted the force-measuring equipment. Data for both tests of the .030" subassemblies were derived from the applied hydraulic pressure rather than from load cell readings. Large and variable errors are probably present due to friction.

The tests of the ripple panel subassemblies indicated that a better match could be obtained between the collapse mode of the square tubes and the ripple panels if the ripples were more closely spaced. This change could not be implemented in the subsystem test vehicles, but was introduced in the system test vehicles. In the system tests, the collapse mode of panels having 3" pitch ripples proved to be compatible with the collapse mode of the sills. The folding that took place in the ripple panels was matched by the folding that took place in the sill. There was a minimum of distortion and tearing at the interface.

Plastic Hinge Tests. The front end energy management system includes plastic hinges at the kick-up of the sills around the dash. The design approach that was adopted was to fill the tubular sills with plastic foam material. This prevents collapse of the section when it is subjected to plastic deformation. Maximum energy absorption is achieved when the material in the sills is worked to its ultimate strength.

As the tubing deforms, the compressive strength of the plastic foam also contributes to the hinge resistance of the component. Despite the low modulus of elasticity of the foam ($\approx 20,000$ psi) and its low compressive strength (≈ 900 psi), the contribution is significant. Deformations are relatively large and the cross-sectional area of the foam is large compared to that of the steel.

The purpose of the plastic hinge tests was to determine the optimum density of foam to be used in the sills. Polyurethane foam was selected over more expensive syntactic foams, which had proven effective in previous tests.

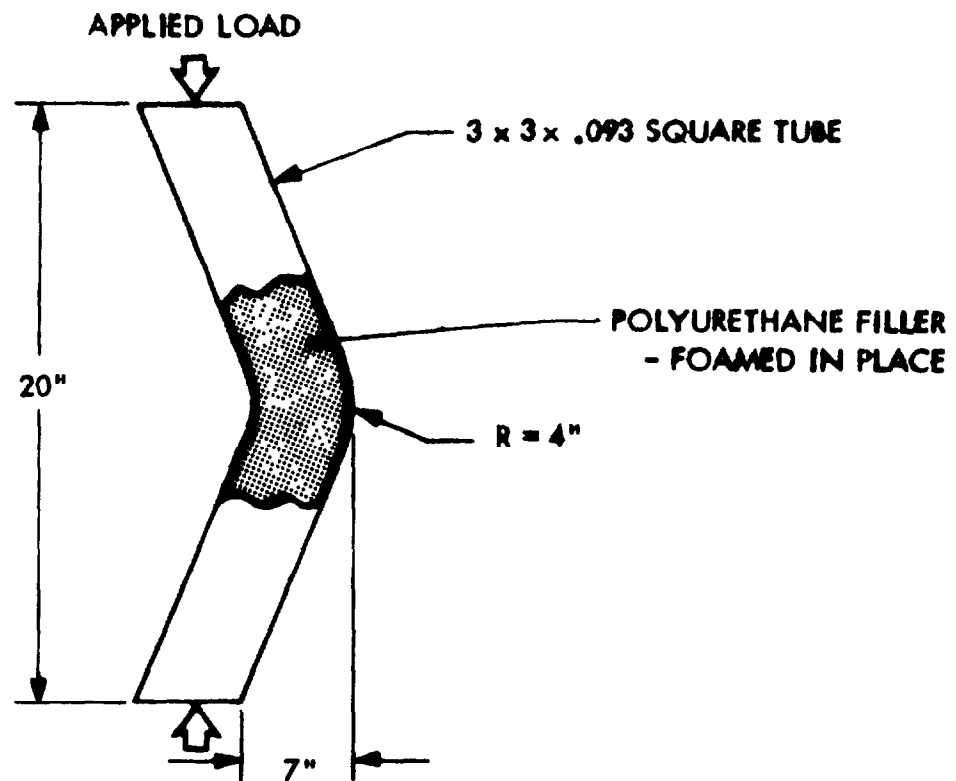
Five tests were run using foam fillers with densities ranging from 6 lbs/cu ft to 25 lbs/cu ft. The test specimens were columns formed from 3" square by .093" wall thickness tubing. The mid section of each column was bent through an angle of 43° . This resulted in 20" high columns having a 4" offset at the mid point. The test setup for applying compressive loads to the plastic hinge specimens is shown in Figure 5-1.

The energy absorption capacity and load capacity of the test specimens as a function of foam density are shown in Figure 5-2. The specimen having 6 lb/cu ft density filler carried a maximum load of 8750 lbs. This corresponds to the maximum theoretical moment for the tubing used. Maximum load capacity increased linearly as foam density was increased. Energy absorption capacity increased more rapidly than load capacity because higher loads were maintained over longer strokes as the foam density was increased. Improvements in energy absorption capacity did not continue beyond 20 lb/cu ft foam density. The high forces that were developed caused failure in the tubing which shortened the effective stroke.

The foam material used in the sills of the system test vehicles had a density of 20 lb/cu ft. This gave the sills the maximum energy absorption capacity that can be obtained from the gage and size of carbon steel tubing that was used.

Honeycomb Door Beam Test. The primary function of the honeycomb door beam is to resist concentrated side loads such as those that occur in a pole impact. An effective door beam increases the energy absorbing capacity of the door structure. This is accomplished within a limited stroke distance by developing higher force levels in the earlier stages of deflection. The goals of door beam development were to provide the best intrusion resistance and force-deflection characteristics within constraints imposed by weight, cost and size.

TEST	MAXIMUM COMPRESSIVE LOAD APPLIED x 1000 lbs.	MAXIMUM MOMENT DEVELOPED IN - KIPS	TOTAL ENERGY ABSORBED IN - LBS	DENSITY OF POLYURETHANE FOAM FILLING lbs./ft ³
1	8.75	35.0	41,550	6
2	10.30	41.2	49,700	10
3	11.50	46.0	58,250	15
4	13.10	52.4	71,200	20
5	14.50	58.0	69,900	25*



* INCORRECT PROPORTIONS OF FOAM COSTITUENTS USED.
EXACT FILLER DENSITY NOT KNOWN IN TEST #5

Figure 5-1. Plastic Hinge Tests

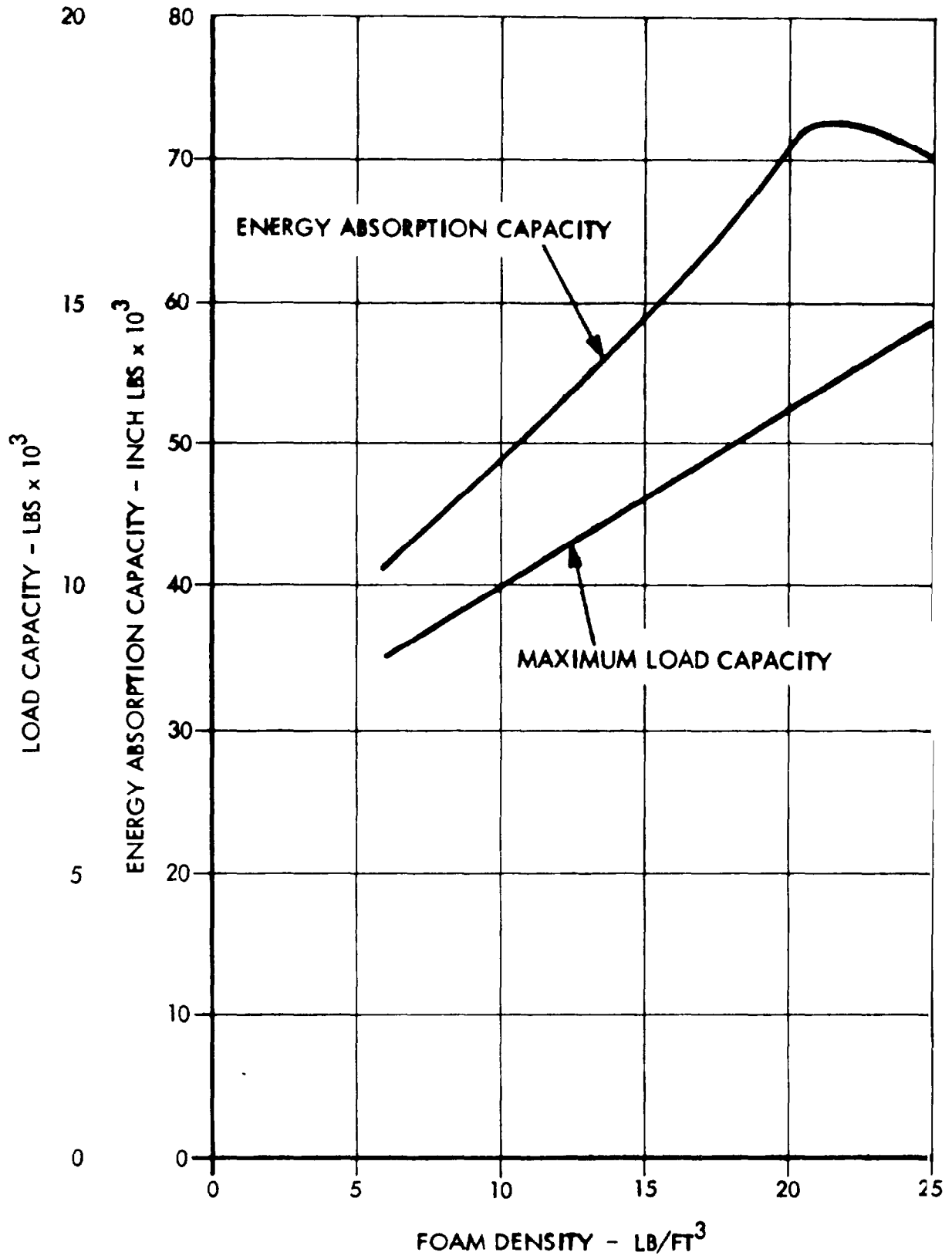


Figure 5-2. Effect of Foam Filler Density in Plastic Hinge Tests

A dynamic test was performed on a door beam having the configuration later used in test vehicles. As the ends of the door beam were supported, a load was applied at the center by a simulated 14" diameter pole.

During the dynamic test, the door beam initially resisted the applied load as a simple beam. Then the honeycomb began to crush at the pole contact area resulting in increased deflection. Both of the honeycomb face sheets were placed in tension and the door beam resisted the applied load as a simple membrane. When deflection reached 5.25 inches, the joint between the door hinge and the test fixture failed.

No adhesive failure occurred during the test. Post-test inspection revealed two areas in which tensile failure of the honeycomb core had occurred. Indications are that this took place after failure of the test fixture. The honeycomb in the contact area of the ram was crushed to about 75% of its initial thickness. There was some indication of necking down of the face sheets due to tensile forces that occurred during the time the beam was acting as a membrane.

Performance of the door beam was as had been intended with the beam action being followed by crushing and by membrane action. Initial yielding of the beam took place at a load of 15,500 lbs with a deflection of 0.15 inches. The load dropped to 6,000 lbs at 0.60" deflection and then rose steadily as membrane action developed. The ultimate load was 27,200 lbs at a deflection of 5.25".

SUBSYSTEM TESTS

A series of tests involving partially modified 1973 Hornets was conducted at the Phoenix, Arizona facility of Dynamic Science. The vehicles were three of the same vehicles employed in the baseline test series. They were partially modified to permit study of the behavior of specific energy absorption systems without involving the total vehicle. Tests were conducted per AMF Test Directive #3-12. All acceleration data has been filtered per SAE J211.

Tests conducted in this series were:

- Frontal barrier - 50 mph
- Frontal pole - 40 mph
- Side pole - 10 mph

The tests demonstrated general agreement between the mathematical model predictions and observed performance. However, numerous design deficiencies were observed.

In the frontal pole impact, the second-stage bumper rotated about its pitch axis, exposing its weaker side to the pole. As a result, the crash pulse deviated from the predicted curve.

The desired crushing load of the sills was demonstrated in the frontal barrier crash. Both ripple panels were deformed and distorted to some extent. As a result of component tests, it had been decided to use ripple panels with a finer ripple pattern in the system test vehicles. Results of the subsystem tests supported this decision.

A number of design improvements were made as a result of the subsystem tests. A jog that existed in the ripple panel upper support near the spring tower was eliminated to reduce a tendency of the component to buckle. The ripple panel forward supports were added to help stabilize the second-stage bumper and prevent it from rotating about its pitch axis. The door striker bolt was relocated to a position nearer the load path of the door beam. The door beam mounting bracket attached to the hinge was redesigned to withstand higher twisting moments.

TEST RESULTS

Test #1, 49.20 mph Frontal Barrier Test

Sills: The sills collapsed in the desired folding mode up to the steering brackets. The right sill buckled laterally aft of the steering bracket. The plastic hinges formed at the kick-up as desired and were sufficiently stable to cause tension failure of the metal.

Second-Stage Bumper: The bumper crushed against the engine with approximately 2 inches crush as desired.

Ripple Panel: The ripple panels showed extensive structural deformations. Some of the crush was ripple action and some was panel buckling.

Ripple Panel Upper Support: Some folding action started at the forward end, then the component buckled at the spring tower.

Static engine displacement - 9.0 inches. Total static crush - 25.0 inches. Maximum longitudinal acceleration (trunk floor) - 45 g. Maximum residual intrusion - 9.0 inches.

Test #2, 40.27 mph Frontal Pole Test

Sills: The sills bent upwards 90⁰ just aft of the bumper energy absorption units. The failure started at the weakened section where the sill corners were notched. There was extensive tearing of the sill material.

Second-Stage Bumper: The twisting of the sills placed the bumper in its weak axis and it crushed completely against the engine. Connections to the sills tore loose.

Ripple Panels: Some structural deformation occurred at the forward edges of the panels, particularly the right side.

Static engine displacement - 9.5 inches. Total static crush - 31.5 inches. Maximum longitudinal acceleration (L.R. passenger compartment) - 42 g. Maximum residual intrusion - 7.5 inches.

Test #3, 9.75 mph Side Pole Test

Door Beam: The door beam deflected 6 inches at the center, but the honeycomb did not crush. The beam apparently did not develop membrane action.

Door Beam Attach Brackets: The brackets showed no internal yielding, but the bracket at the "B" post rotated due to bending of the striker bolt.

The roof was barely contacted by the pole. Minor localized floor buckling occurred near the contact area.

Maximum static crush - 7.5 inches.

Maximum lateral acceleration - 9.0 g.

Maximum residual intrusion - 3.2 inches.

SECTION 6 SYSTEM TEST PROGRAM

Fifteen full-scale vehicle crash tests were conducted at the Calspan Corporation facility in Buffalo, New York, in October and November of 1973. These tests were the culmination of a development process whose purpose was to demonstrate methods for improving the front and side crashworthiness of compact vehicles.

The test series was conducted per AMF Test Directive #3-14, and involved the following vehicles:

- Four front and side modified 1973 AMC Hornets
- Seven front modified 1973 AMC Hornets
- Two side modified 1973 AMC Hornets
- Three unmodified 1973 AMC Hornets
- Two unmodified 1970 Ford Galaxies

A front modification included the complete modification as shown in Figure 4-1, including the "A" post strengthening. Rear sill modification was carried out to the rear of the dash panel kick-up. Side modification included "A" post strengthening, "B" post modification as shown in Figure 4-2, underbody strengthening, replacement of the door beam as shown in Figure 4-3, rear sill strengthening extending forward of the dash panel kick-up and replacement of door retention hardware with higher-strength components.

Vehicles having only front modifications or side modifications were used in tests where their performance would be equivalent to that of a vehicle having both front and side modifications. Several vehicles were used in more than one test when the damage from the previous test would not interfere with the subsequent test. A summary of the system test program giving a description of the impact geometry and a description of the vehicles involved are given in Table 6-1.

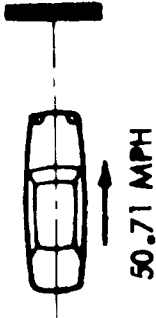
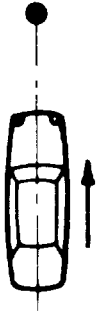
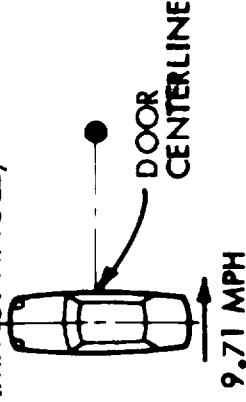
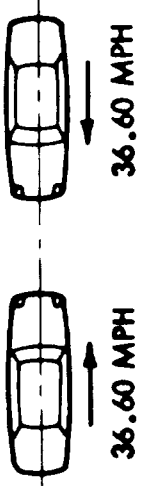
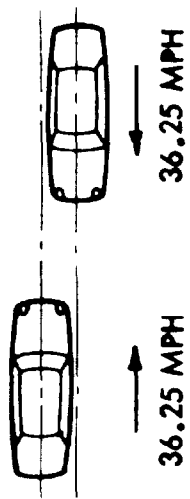
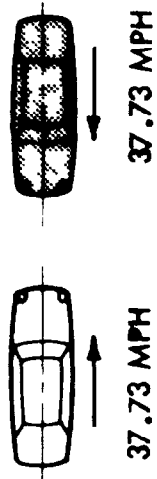
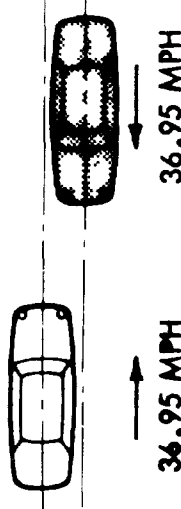
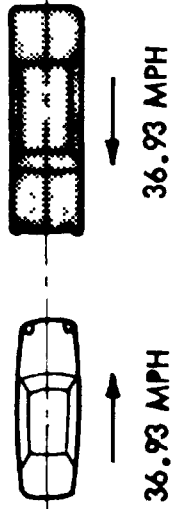
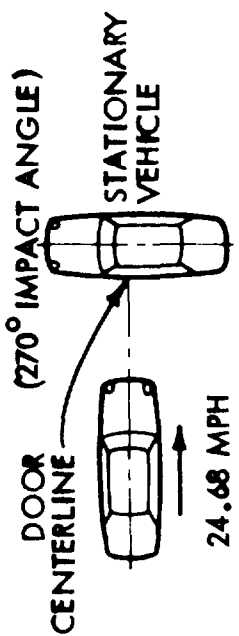
TEST #	IMPACTING VEHICLE	IMPACTED VEHICLE	IMPACT GEOMETRY
1.	#1 FRONT AND SIDE MODIFIED HORNET 2940 LB	FLAT BARRIER	 50.71 MPH (Comparable to Baseline Test I)
2.	#5 FRONT MODIFIED HORNET 2940 LB	POLE	 40.23 MPH (Comparable to Baseline Test II)
3.	#2 FRONT AND SIDE MODIFIED HORNET 2930 LB	FLAT BARRIER	 50.0 MPH
4.	#12 SIDE MODIFIED HORNET 2930 LB	POLE	 9.71 MPH (90° IMPACT ANGLE) (Comparable to Baseline Test III)
5.	#10 FRONT MODIFIED HORNET 2930 LB	#11 FRONT MODIFIED HORNET 2910 LB	 36.60 MPH (Comparable to Baseline Test IV)

Table 6-1. System Test Program Summary

TEST #	IMPACTING VEHICLE	IMPACTED VEHICLE	IMPACT GEOMETRY
6.	#3 FRONT AND SIDE MODIFIED HORNET 2930 LB	#4 FRONT AND SIDE MODIFIED HORNET 2930 LB	
7.	#6 FRONT MODIFIED HORNET 2930 LB	#14 UNMODIFIED HORNET 2830 LB	
8.	#8 FRONT MODIFIED HORNET 2930 LB	#16 UNMODIFIED HORNET 2830 LB	
9.	#7 FRONT MODIFIED HORNET 2930 LB	#17 UNMODIFIED FORD CUSTOM 4170 LB	
10.	#8 FRONT MODIFIED HORNET 2920 LB	#13 SIDE MODIFIED HORNET 2930 LB	

(Comparable to Baseline Test V)

Note: Shading indicates unmodified vehicle.

Table 6-1. System Test Program Summary (C ntinued)

TEST #	IMPACTING VEHICLE	IMPACTED VEHICLE	IMPACT GEOMETRY
11.	# 9 FRONT MODIFIED HORNET 2920 LB	# 13 SIDE MODIFIED HORNET 2930 LB	<p>DOOR CENTERLINE 24.33 MPH 60° STATIONARY VEHICLE</p>
12.	# 8 FRONT MODIFIED HORNET 2920 LB	# 15 UNMODIFIED HORNET 2920 LB	<p>DOOR CENTERLINE 25.45 MPH 90° IMPACT ANGLE STATIONARY VEHICLE</p>
13.	# 9 FRONT MODIFIED HORNET 2920 LB	# 16 UNMODIFIED HORNET 2830 LB	<p>DOOR CENTERLINE 24.95 MPH 60° 300° IMPACT ANGLE STATIONARY VEHICLE</p>
14.	# 18 UNMODIFIED FORD CUSTOM 4170 LB	# 12 SIDE MODIFIED HORNET 2930 LB	<p>DOOR CENTERLINE 24.08 MPH 270° IMPACT ANGLE STATIONARY VEHICLE</p>
15.	# 4 FRONT AND SIDE MODIFIED HORNET 2930 LB	POLF	<p>DOOR CENTERLINE 20.62 MPH 5 INCHES 270° IMPACT ANGLE</p>

Note: Shading indicates unmodified vehicle.

Table 6-1. System Test Program Summary (Continued)

The unmodified vehicles are indicated in Table 6-1 by shading. All of the flat fixed barrier and pole crashes (Tests 1, 2, 3, 4, and 15) involved modified vehicles. The head-on collisions with centerlines colinear (Tests 5, 7 and 9) measured the performance of a modified Hornet, in impacts with another modified Hornet, an unmodified Hornet, and an unmodified 4,170 lb vehicle. The head-on tests with vehicle centerlines offset (Tests 6 and 8) include an impact between two modified Hornets and an impact between a modified Hornet and an unmodified Hornet. The side impacts (Tests 10, 12 and 14) involve various combinations of modified and unmodified vehicles. In the oblique impacts (Tests 11 and 13), a modified Hornet and an unmodified Hornet were impacted by a modified Hornet.

DESCRIPTIONS OF CRASH TEST RESULTS

The descriptions of the crash tests that follow were derived from high-speed motion pictures of the crashes, recordings from accelerometers at several locations within the vehicles, and pre-crash and post-crash observations, measurements and still photographs. Barrier force recordings from the single-vehicle crashes were utilized.

Deformations of the various components were observed in films taken from different angles. These were correlated with respect to time and related to the crash pulse recordings. In some cases, dynamic deflections were plotted by scaling successive frames of the film.

In the more severe impacts, resonant oscillations were induced in the floor pan and driveshaft tunnel, obscuring acceleration data recorded at these locations. While data recorded at all locations were analyzed, only that from a single location is reproduced in this report. In frontal impacts, the rear trunk recording is used. In side and oblique impacts, the recordings from the front passenger location on the non-impacted side of the vehicle is used, unless otherwise noted. All acceleration data has been filtered per SAE J211.

Timing of the crashes is reckoned from the moment at which the bumper of an impacting vehicle first contacts the barrier or another vehicle.

The terms "after impact" and "after initial contact" are used interchangeably in referring to the interval between the first bumper contact and other events. The term "at 27 msec" implies "27 milliseconds after initial bumper contact".

One of the objectives of this program was to achieve an early onset of the acceleration pulse in order to conserve available stroking distance. By reaching maximum acceleration levels early in the crash, the vehicle crush distance and passenger compartment intrusion can be reduced. Restraint systems that are designed to function with a "square wave" crash pulse can then limit the accelerations experienced by the passenger. Depending on the filtering action of a particular restraint system, the passenger will be isolated from high vehicle accelerations if they are of short enough duration. The average acceleration over a longer period then becomes important to the passenger. In evaluating the acceleration data in this test program, an attempt has been made to identify accelerations that have the most significance in terms of restraint system performance. Effectiveness of the energy management system is measured in terms of reduced passenger compartment intrusion along with an early crash pulse and an absence of sustained accelerations above levels established in the design criteria.

System Test No. 1 - 50.71 mph, Flat Barrier, Frontal 0⁰,
Front and Side Modified Vehicle

The second-stage bumper was halted by the barrier 6 msec after impact. This caused the sills to start collapsing forward of the dimpled sections. Regular convolutions were formed, resembling those observed in component level tests. The second-stage bumper absorbed the engine's kinetic energy. The engine struck the rear of the second-stage bumper at 16 msec and crushed it against the barrier, coming to rest at 27 msec.

The forward edges of the ripple panels contacted the barrier 15 msec after impact and the panels began to crush. Compressive loads were carried through the doors, causing diagonal creases to appear in the rear

quarter panels. Loads carried through the upper "A" posts pushed the forward corners of the roof upward between 20 msec and 50 msec after impact, causing extensive roof deformation. The ripple panels continued to crush progressively until 25 msec after impact. Then the ripple panels buckled inward at their mid point causing the spring towers to swing inward about plastic hinges located at the firewall. Bending and deformation of the ripple panels and the sills continued until 50 msec after impact.

The lower right hand corner door hinge failed 38 msec after impact, allowing the front right side of the passenger compartment to pitch downward. Since this occurred relatively late in the crash, it did not result in appreciable vertical acceleration. In the last 20 milliseconds of the crash, the rear of the vehicle moved upward and forward an additional 4 inches. This was accompanied by forward thrusting and deformation of the roof and by narrowing of the right hand door opening (following hinge failure). The post-crash condition of the vehicle is shown in Figure 6-1.

The crash pulse, shown in Figure 6-2, had a rise time of 5 msec and maintained an average level of 20 to 40 g's until 70 msec after impact. Several peaks with a maximum amplitude of 50 g's occurred.

Maximum dynamic crush of the vehicle was approximately 30 inches. This is in agreement with the post-crash measurement of 30.5 inches. The vehicle did not rebound from the barrier.

System Test No. 1 may be compared with Baseline Test I. The crash pulse for the modified vehicle had a higher onset rate than that observed in the baseline test. A substantially greater share of the vehicle acceleration occurred in the first 30 milliseconds of the crash with proportionately less acceleration occurring after 60 milliseconds.

Failure of the right hand door hinge interrupted the load path through the door beam to the "B" pillar and quarter panel. This resulted in greater intrusion occurring at the dash panel on the right hand side than on the left. The generalized floor buckling that was observed in Baseline Test I was not present in System Test #1. Minor localized floor deformation occurred.

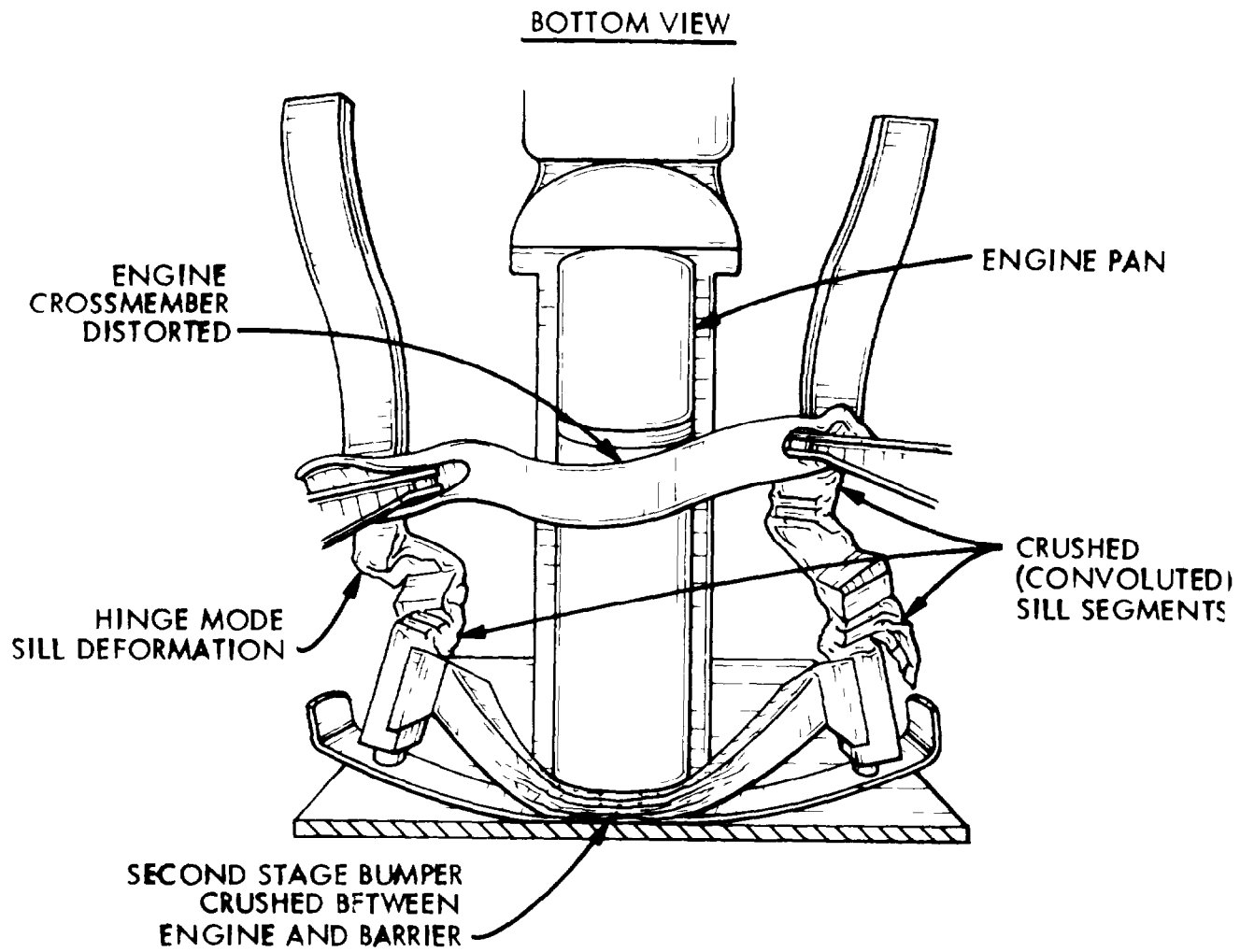


Figure 6-1. Test No. 1. Deformation of Front End Components (Post-Crash Condition). Vehicle No. 1 Front Modified Hornet 50.71 mph 0° Flat Barrier Impact

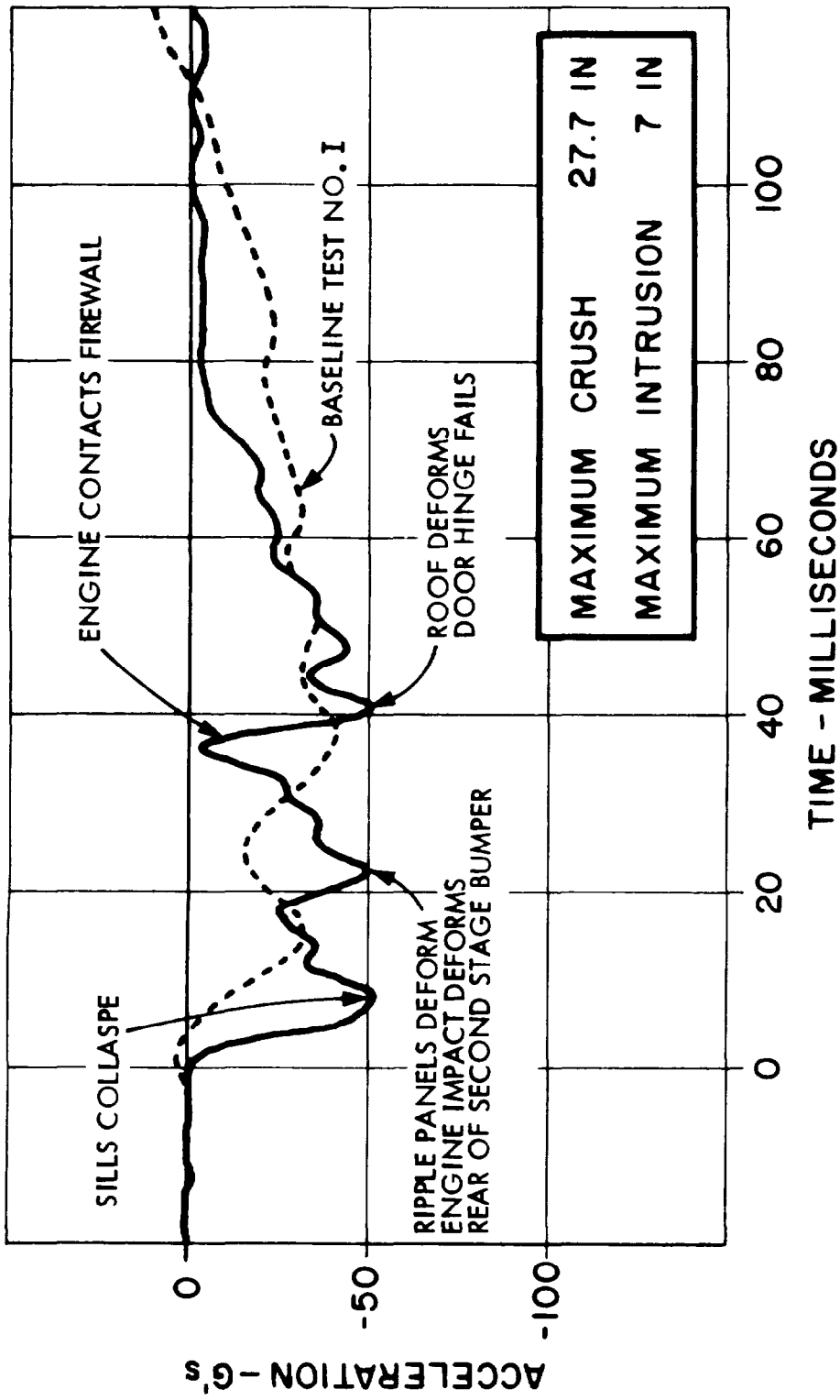


Figure 6-2. Test No. 1. 50.0 mph Flat Barrier Frontal 0° Front Modified Hornet
LONGITUDINAL CRASH PULSE - VEHICLE NO. 1

Results of System Test #1 and Baseline Test I are summarized in Table 6-2.

Table 6-2

	System Test 1	Baseline Test I
Maximum vehicle crush	27.7"	33"
Maximum intrusion at dash center	9.6"	17.4"
Occupant area intrusion		
Left side	5"	10.5"
Right side	7"	10.8"
Maximum compartment acceleration	50 g	40 g

System Test No. 2 - 40.2 mph, Frontal Pole, Centered,
Front Modified Vehicle

The bumper was bent into a U shape, compressing the second-stage bumper between the radiator and the front of the engine. The second-stage bumper maintained its orientation in the path of the pole throughout the test and was severely deformed. The engine and transmission moved 7 inches rearward underneath the floor pan with minimal disturbance of the passenger compartment. The support brace was bent into a V shape and pushed the radiator against the upper portion of the engine. The sills were bent inward at their forward ends due to deformation of the second-stage bumper. The ripple panel forward supports followed the motion of the sills and support brace, crushing the first two to three convolutions of the ripple panels. The post-crash condition of the vehicle is shown in Figure 6-3.

Deformation of the second-stage bumper by the pole began at 13 msec and was accompanied by the onset of sill crushing. The crushing and hinging of the sills continued until 45 msec after impact. Gaps appeared between the tops of the doors and the roof due to compressive loads in the windshield and "A" pillars. As the forward portion of the roof moved upward,

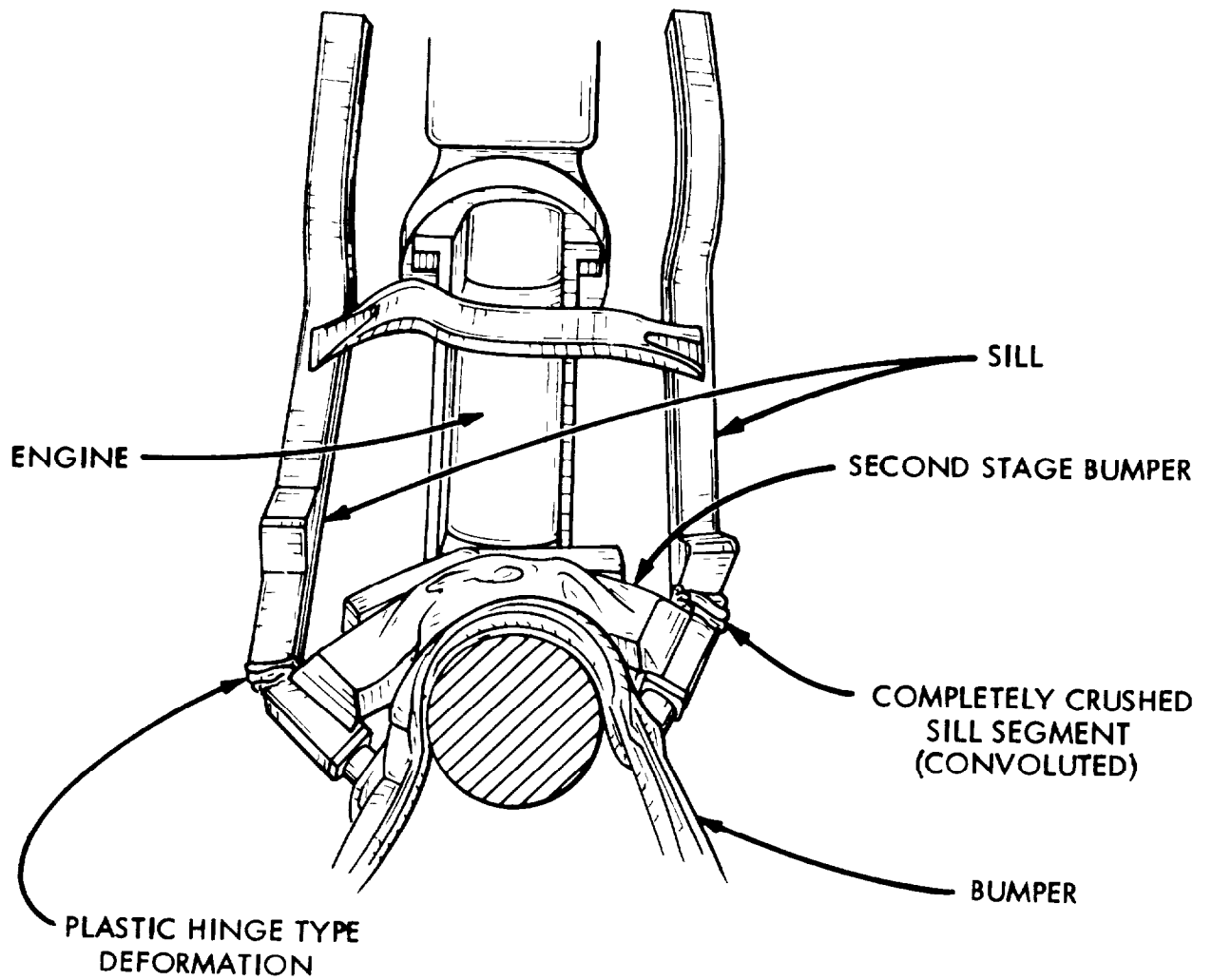


Figure 6-3. Test No. 2. Deformation of Front End Components (Post Crash Condition)
 Vehicle No. 5 Front Modified Hornet 40.2 mph 0° Frontal Pole Impact

indentations formed above the "B" pillars as the "B" pillars restrained the center portion of the roof against upward movement. All of the windows in the vehicle remained intact.

The engine compressed the radiator against the second-stage bumper at 33 msec. At the same time, diagonal creases formed in the rear quarter panels indicating the presence of high compressive loads. The engine moved rearward with respect to the passenger compartment until 58 msec after impact. Movement of the engine and deformation of the engine crossmember and transmission crossmember coincide with a period of 45 g acceleration.

Distortion of the passenger compartment was minimal. Minor distortion occurred in the doors, quarter panels and roof.

The crash pulse, shown in Figure 6-4, had an average amplitude of 20 to 25 g's during the first 45 msec after impact. This was followed by a 25 msec period in which acceleration was 45 g's.

The crash pulse took place in 45 milliseconds less time relative to pole contact, than was observed in Baseline Test II. The entire crash pulse in the modified vehicle was concluded within 75 milliseconds, while that of the baseline vehicle persisted for 120 milliseconds. The earlier crash pulse in the modified vehicle enabled a significant reduction in passenger compartment intrusion without incurring unreasonable acceleration levels.

Results of System Test #2 and Baseline Test II are summarized in Table 6-3.

Table 6-3

	System Test 2	Baseline Test II
Maximum vehicle crush	27.9"	39.5"
Maximum intrusion at dash center	5.6"	12.1"
Occupant area intrusion		
Left side	1.7"	6.0"
Right side	2.3"	7.8"
Maximum compartment acceleration	50 g	30 g

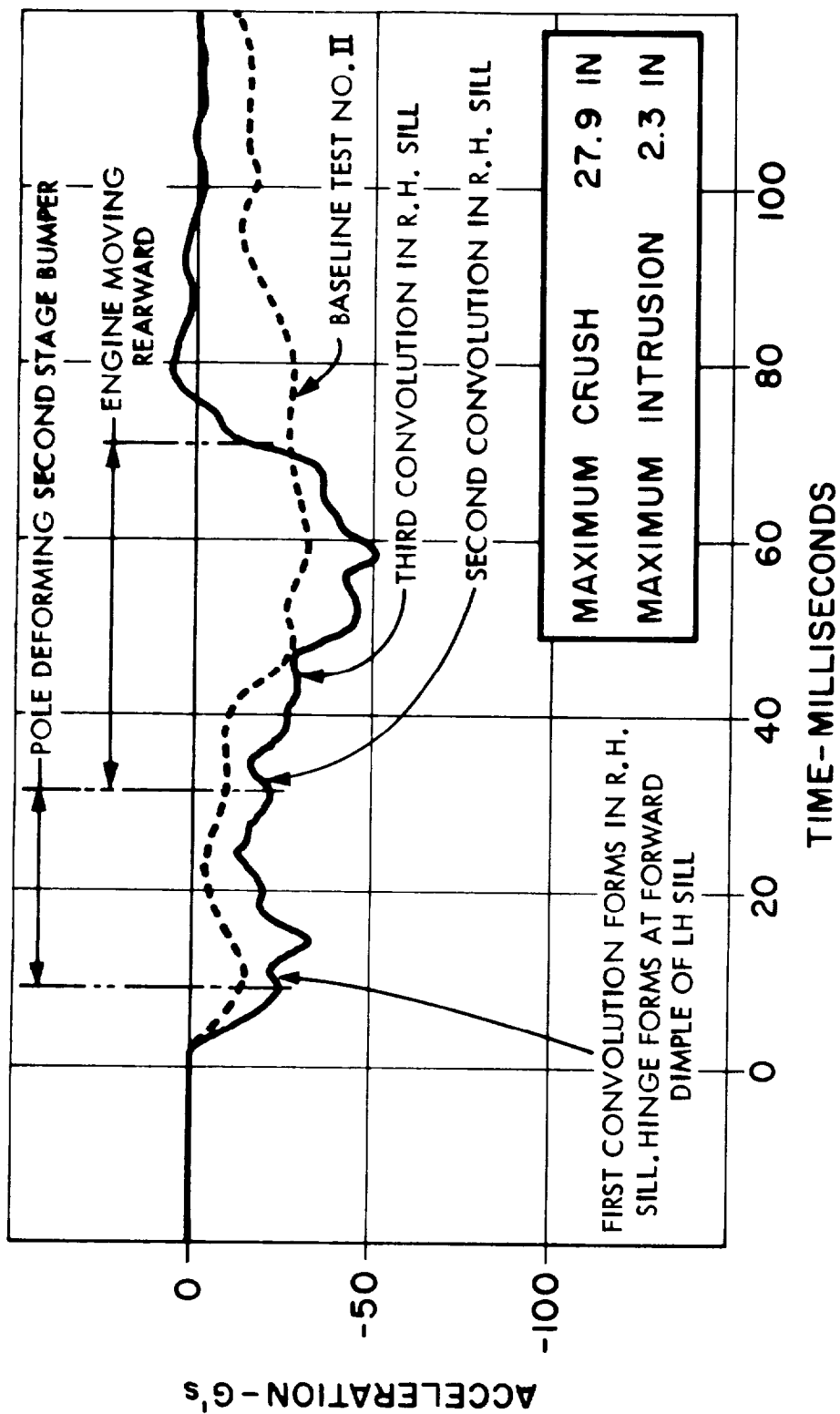


Figure 6-4. Test No. 2. 40.2 Frontal Pole - Centered. Front Modified Hornet
LONGITUDINAL CRASH PULSE - VEHICLE NO. 5

System Test No. 3 - 50.0 mph, Flat Barrier Frontal 30^o,
Front and Side Modified Vehicle

Although the angle of incidence was 30^o, the vehicle was deflected away from the barrier during impact. The front end structural components behaved as relatively rigid members of parallelogram linkages during the impact. As the left hand (impacted) rippled panel deflected to the right, the upper support and the secondary bumper transmitted this motion to the right hand rippled panel causing it also to deflect to the right. The impacted side of the front end structure deflected upward while the opposite side deflected downward.

During the first 15 msec of impact, the bumper and the left hand energy absorbing unit were deformed. By 20 msec after impact, the sills and rippled sheet metal panels began to deflect. The engine was contacted 35 msec after impact and was pushed sideways and rearward. The left front wheel (impacted side) was deformed by the barrier 35 msec after impact. The tire and wheel were crushed against the "A" post from 50 to 80 msec after impact. Deformation of the front end terminated by 70 msec after impact. Behavior of the front end components during this time interval are shown in Figures 6-5, 6-6 and 6-7. Deformation of the roof began at this time with a maximum separation of two inches between the driver's door and the roof occurring 80 msec after impact.

Rotation of the passenger compartment started about 50 msec after impact as the bumper slid across the face of the barrier. The vehicle reached a maximum angular velocity of 6.6 radians per second (63 rpm) 140 msec after impact. This rotation accounts for 35% of the pre-impact kinetic energy. Rotational energy was dissipated through friction and a gentle impact between the rear fender and the barrier 360 msec after initial impact. The vehicle departed approximately parallel to the barrier with a velocity of 27.5 ft per second (18.8 mph). This is equivalent to 14% of the kinetic energy that was present prior to impact.

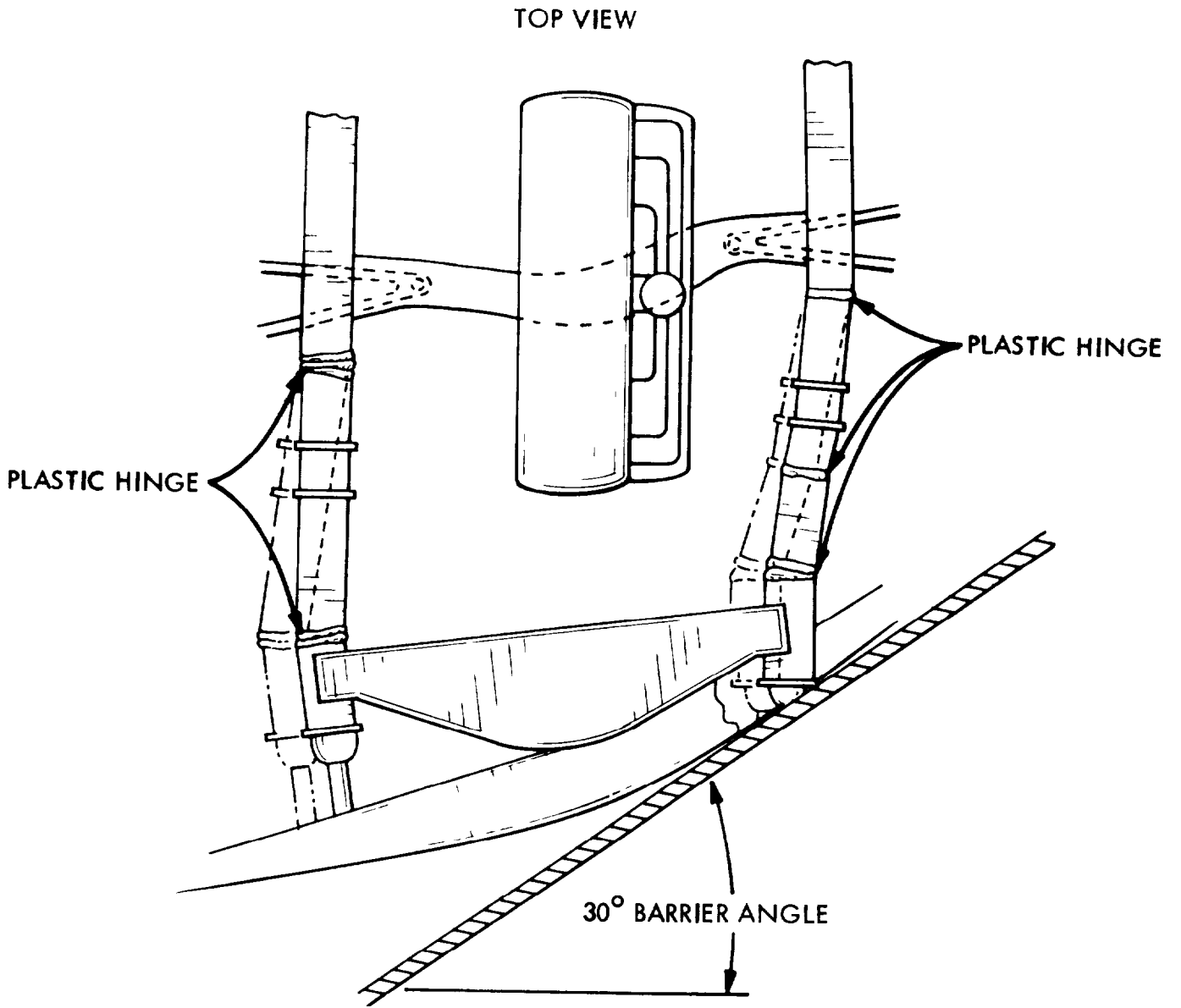


Figure 6-5. Test No. 3. Sill Deformation 22 Msec After Initial Barrier Contact

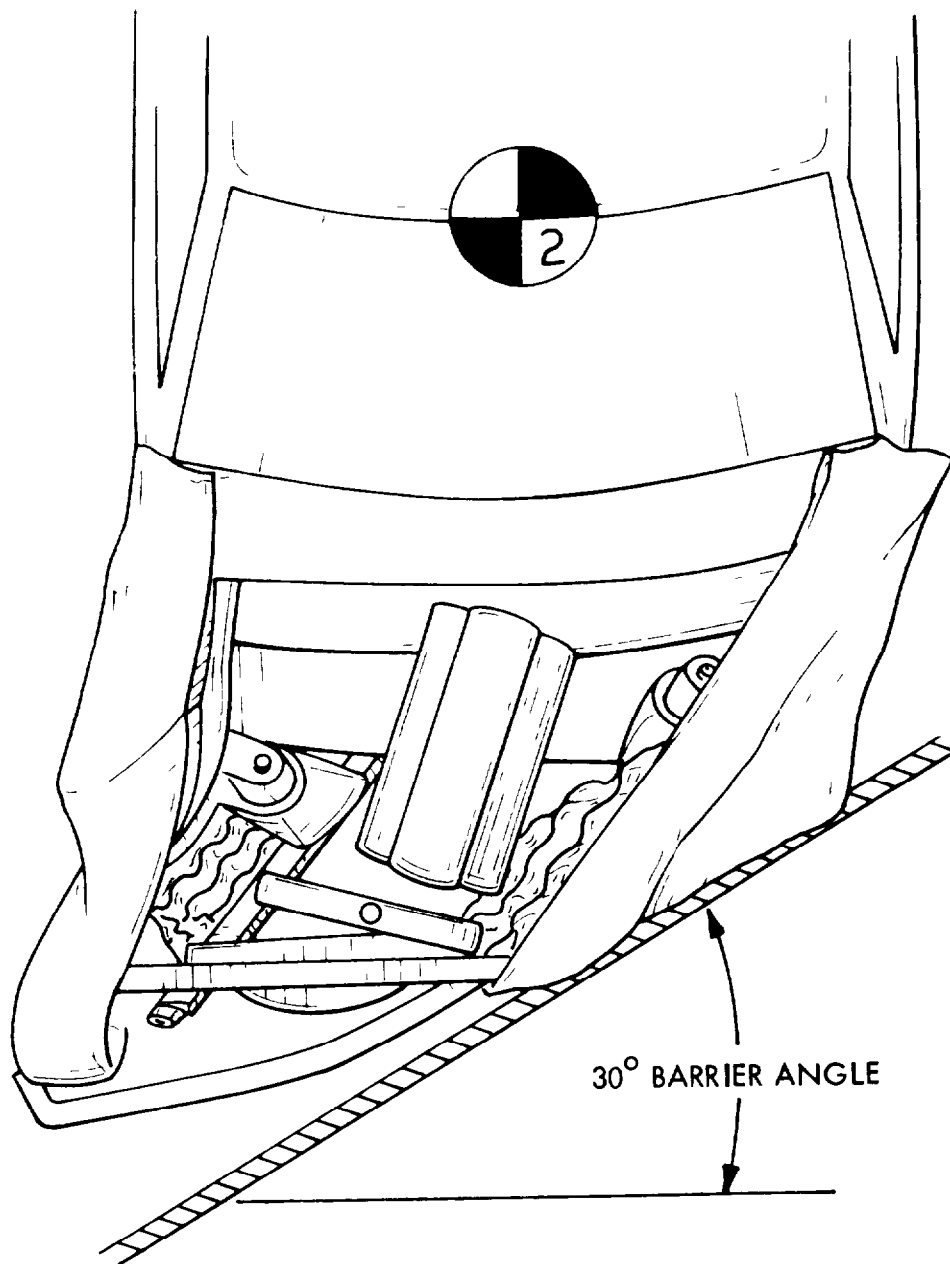


Figure 6-6. Test No. 3. Front End Configuration 52 Msec After Contact

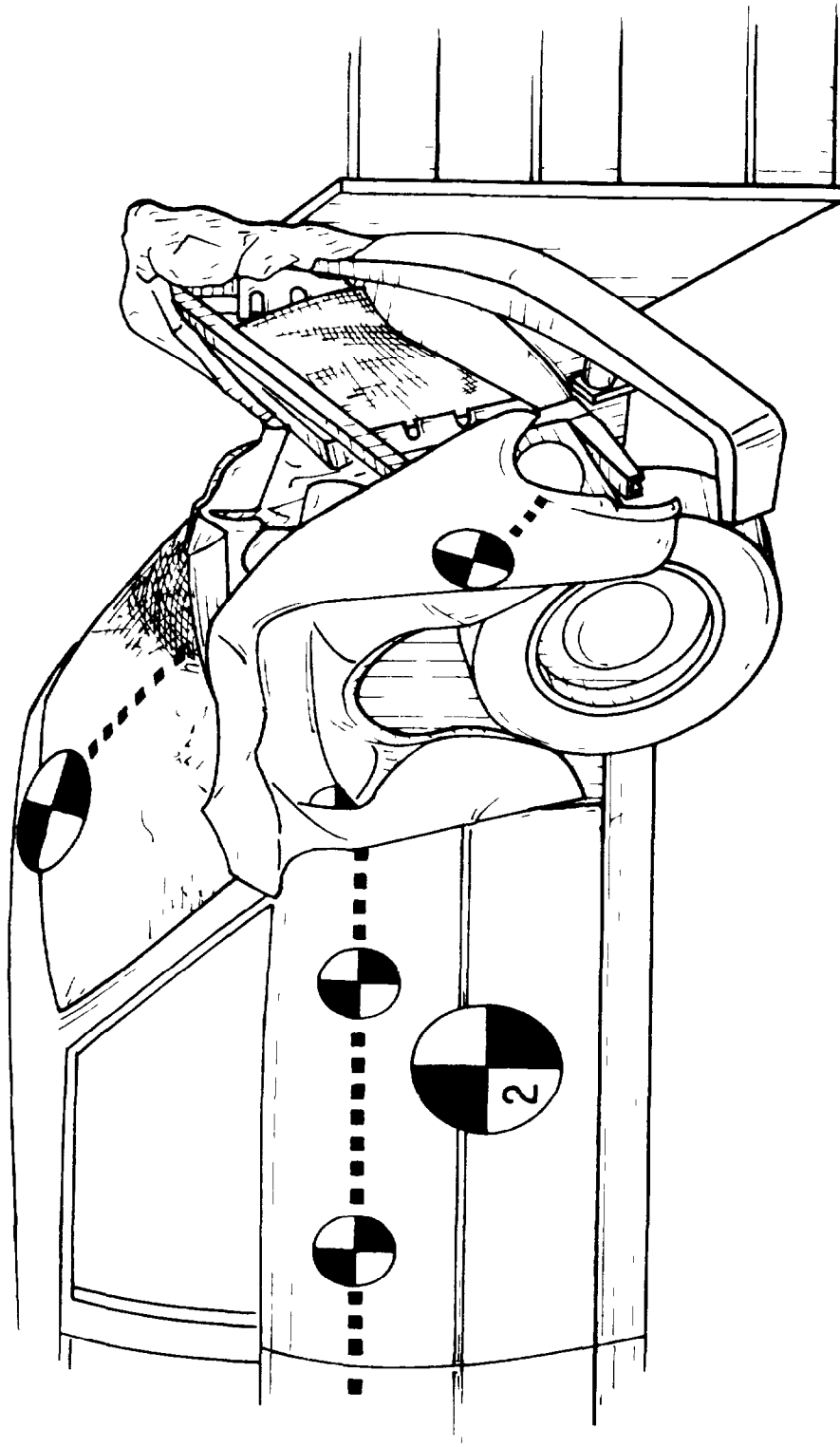


Figure 6-7. Test No. 3. Front End Configuration of Vehicle 68 Msec After Contacting 30
Barrier at 50.0 mph. (Vehicle No. 2 Front and Side Modified Hornet).

Results of System Test #3 are summarized in Table 6-4.

Table 6-4

	System Test 3
Maximum vehicle crush	30"
Maximum intrusion at dash center	8.1"
Occupant area intrusion	
Left side	6.7"
Right side	2.3"
Maximum compartment acceleration	35 g

A moderate crash pulse, shown in Figure 6-8, was recorded in the longitudinal direction. Peak amplitude was 35 g. Average acceleration fluctuated between 12 g and 30 g throughout the 85 milliseconds of the crash. Average lateral acceleration of 20 g was recorded at the left front passenger compartment location (impacted side). Lateral accelerations of slightly lower magnitude and in the opposite direction were recorded at the rear of the passenger compartment. These lateral accelerations, shown in Figure 6-9, are associated with the rotation of the passenger compartment.

There is no baseline test that is directly comparable to System Test #3. The energy management system performed satisfactorily in this test. It served more to deflect the vehicle from the barrier than to arrest its motion and absorb the kinetic energy that was present. The resulting crash pulse and intrusion satisfy the design criteria.

System Test No. 4 - 9.71 mph Side Pole Impact, 90° Impact Point at Door Centerline, Side Modified Vehicle

The pole deformed the door and rocker panel and made contact with the roof rail causing 1.5 inches deformation of the roof rail. Maximum static intrusion of the door interior panel was 3-1/2 inches. The honeycomb

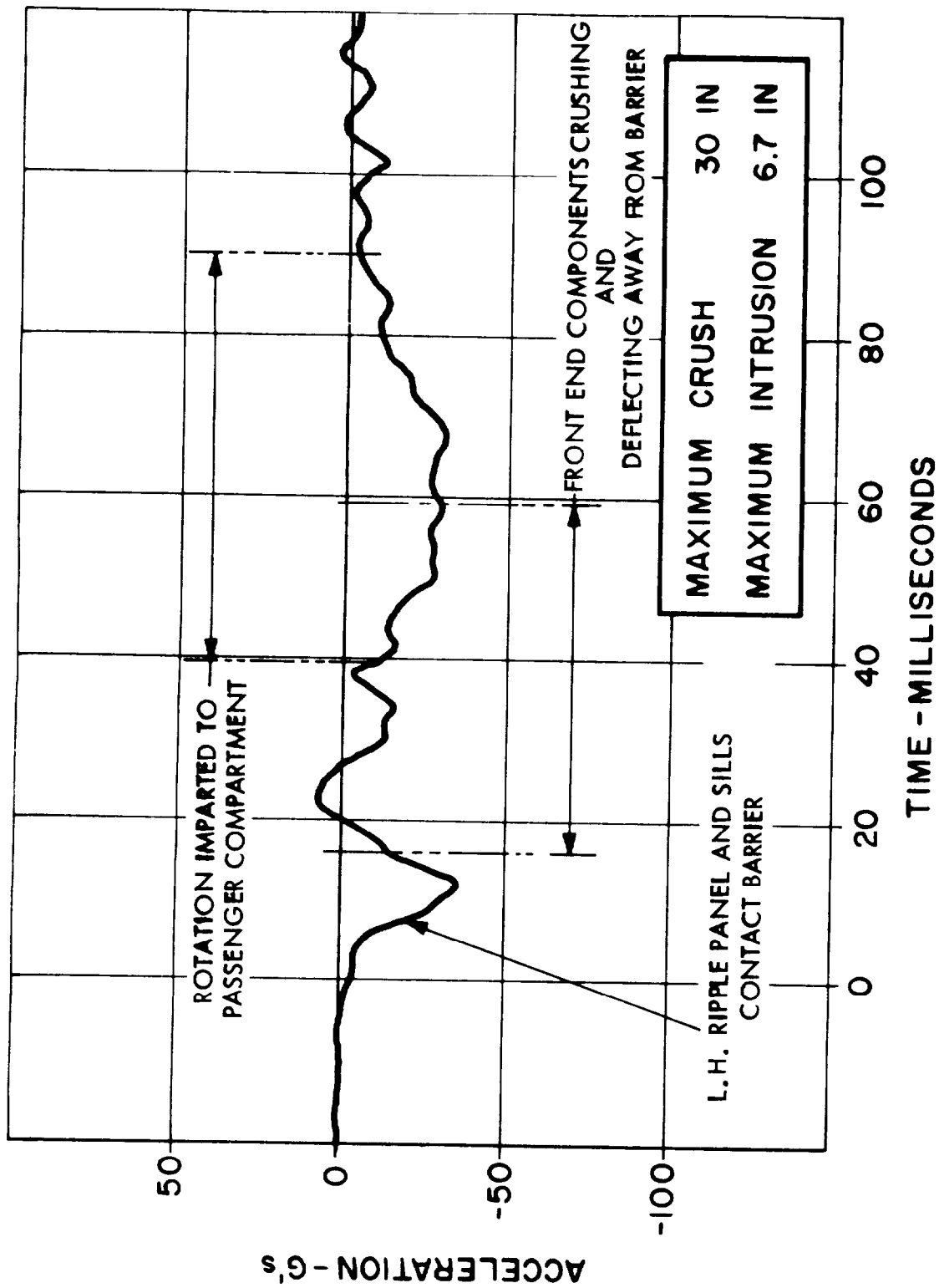


Figure 6-8. Test No. 3 50.0 mph Flat Barrier Frontal 30° Front and Side Modified Hornet LONGITUDINAL CRASH PULSE - VEHICLE NO. 2

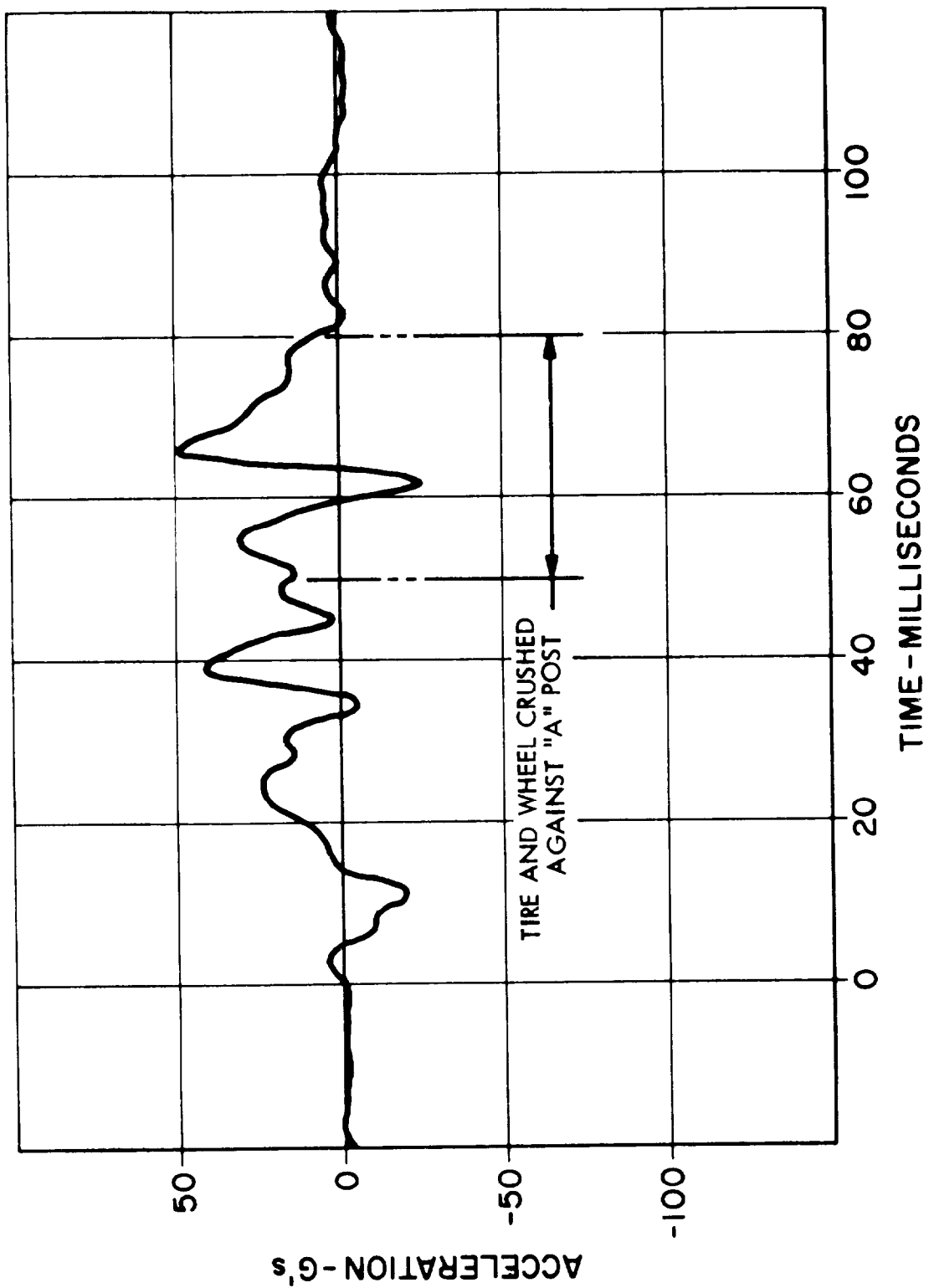


Figure 6-9. Test No. 3. 50.0 mph Flat Barrier Frontal 30°. Front and Sid Modified Hornet Left Front Position (Impacted Side) LATERAL CRASH PULSE - VEHICLE NO. 2

door beam remained attached at both ends. The face sheet on the impacted side of the honeycomb door beam became delaminated on both sides of the impact point. Only minimal crush occurred in the honeycomb core material.

The pole contacted the right hand door of the vehicle in line with the left front accelerometer location. Except for spikes occurring at 50 and 58 msec, the peak Y accelerations recorded by the left front accelerometer were approximately 6 g's. The peaks at 50 and 58 msec were of short duration and coincided with high loads that occurred as the pole contacted the floor and roof of the vehicle. Similar crash pulses were recorded at the tunnel, at the rear deck, and other locations. A pulse at 50 msec due to floor loading is observable in most of the traces. Lateral compression of the tunnel increased from 0.5 inches at 50 msec to 1.5 inches at 70 msec, confirming the presence of high compressive loads in the floor structure during this time period. Accelerations recorded on the engine did not exceed 6 g's at any time. Decoupling between the chassis and the engine prevented spikes at 50 and 58 msec from appearing. Similar decoupling would be expected between the chassis and a restrained passenger. An accelerometer placed within the right hand door recorded low levels of acceleration except for peaks occurring at 20, 50 and 58 msec. The brief 22 g peak occurring at 20 msec coincides approximately with the time at which the pole contacted the honeycomb door beam. The later peaks again correspond to contact of the pole with the floor and roof structures.

The impact caused 7 inches of permanent deformation in the outer panel of the right hand door. Maximum deformation during the impact was 11.5 inches. The maximum static intrusion at the "B" post was 4.1 inches. The rocker panel was crushed 6.3 inches, the roof rail was crushed 1.5 inches. The door hinges and latch remained intact. The door beam appears to have carried substantial membrane loads. The face sheet of the honeycomb door beam on the compression (impacted) side became delaminated. Damage elsewhere in the vehicle was minimal.

The post-crash condition of the vehicle is shown in Figure 6-10 and the crash pulse in Figure 6-11.

System Test #4 is directly comparable to Baseline Test III. Damage to the vehicle is similar in appearance. Intrusion in the modified vehicle was reduced to 3.5 inches from 6.0 inches in the unmodified vehicle. At the same time, maximum acceleration was reduced from 13.5 g's to 8.0 g's. The crash pulses are similar in form, except for the larger peak amplitude recorded in the unmodified vehicle.

The results of System Test #4 and Baseline Test III are given in Table 6-5.

Table 6-5

	System Test 4	Baseline Test III
Maximum vehicle crush	7"	10"
Maximum intrusion at rocker panel	5.1"	
Occupant area intrusion	3.5"	6"
Maximum compartment acceleration	8 g	13 g

System Test No. 5 - 36.6 mph, Vehicle-to-Vehicle (73.2 mph Relative Velocity), Frontal 0° Aligned, Both Vehicles
 Front Modified

The crushable front end structures of the vehicles absorbed nearly all of the energy of the crash. The passenger compartments remained virtually intact. There was slight deformation of the door openings and buckling of the doors in both vehicles. There was minor deformation of the firewall of vehicle #10. The extent of the damage was minimal.

The bumper of vehicle #11 rode over the bumper and second-stage bumper of vehicle #10. Almost all of the rippled sheet metal of vehicle #10 was crushed uniformly. About 1/3 of the rippled sheet metal in vehicle #11 was crushed. Energy absorbing convolutions formed in the sills of both vehicles. The second-stage bumper of vehicle #11 remained in position and

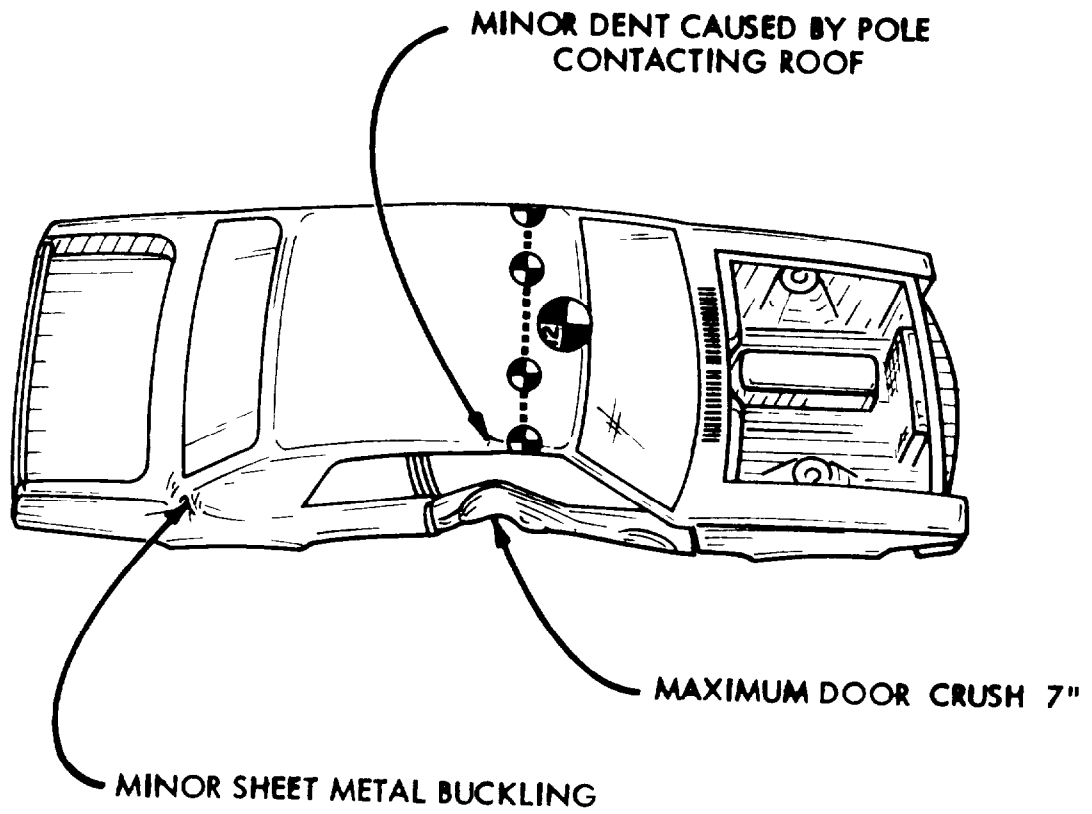


Figure 6-10. Test No. 4. Deformation Due to 9.71 mph Side Pole Impact.
Vehicle No. 12 Side Modified Hornet

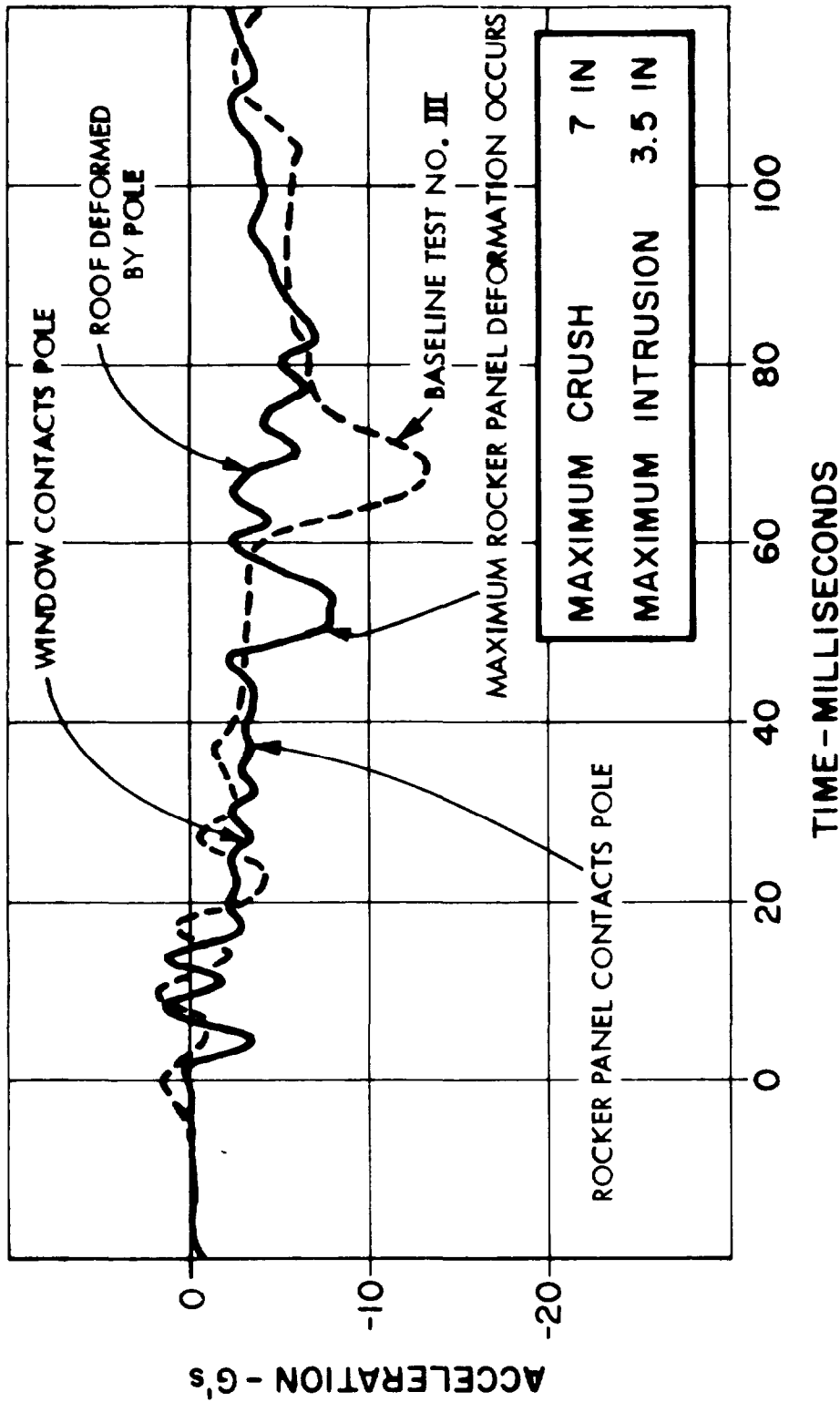


Figure 6-11. Test No. 4. 9.71 mph Side Pole Impact - 90° Side Modified Homed LATERAL CRASH PULSE - VEHICLE NO. 12

was deformed against the engine of vehicle #10. The second-stage bumper of vehicle #10 rotated into a nearly vertical position after receiving slight deformation. The post-crash condition of the vehicles is shown in Figure 6-12.

The crash pulses, shown in Figures 6-13 and 6-14, are most clearly discernible in the rear deck acceleration records. The crash pulses for both vehicles reached the 40 g level with a rise time of 5 msec. Then as the bumper of vehicle #11 overrode the bumper of vehicle #10, 15 msec after impact, the crash pulses fell abruptly and remained below 20 g's until 26 msec after initial impact. Forces transmitted to the passenger compartments were limited by the crush characteristics of the ripple panels and collapsible sills.

A 100 g acceleration was recorded on each engine, lasting from 24 msec to 38 msec after impact. This corresponds to the time at which the engines were contacted by the overriding/underriding second-stage bumpers.

System Test #5 may be compared with Baseline Test IV. Modified vehicles showed improvement in performance over the baseline vehicles. The crash pulse, passenger compartment intrusion and especially, the engine displacement were more favorable in the modified vehicles. Part of the reason that the improvement was not as dramatic as in other tests is that the unmodified vehicles performed well in the baseline tests. Although both baseline vehicles received large amounts of crush and engine deflection, these did not result in excessive intrusion.

Maximum intrusion in a modified vehicle was 2.3 inches, compared to a maximum of 6.0 inches in one of the baseline vehicles. An earlier onset of acceleration was achieved in the modified vehicles. However, when one second-stage bumper overrode the other, it caused a drop-off in acceleration for a period of 10 to 12 msec. Still, the duration of the crash pulse was reduced from 90 msec to 70 msec. Tougher joints between the second-stage bumper and the ripple panel forward supports would have

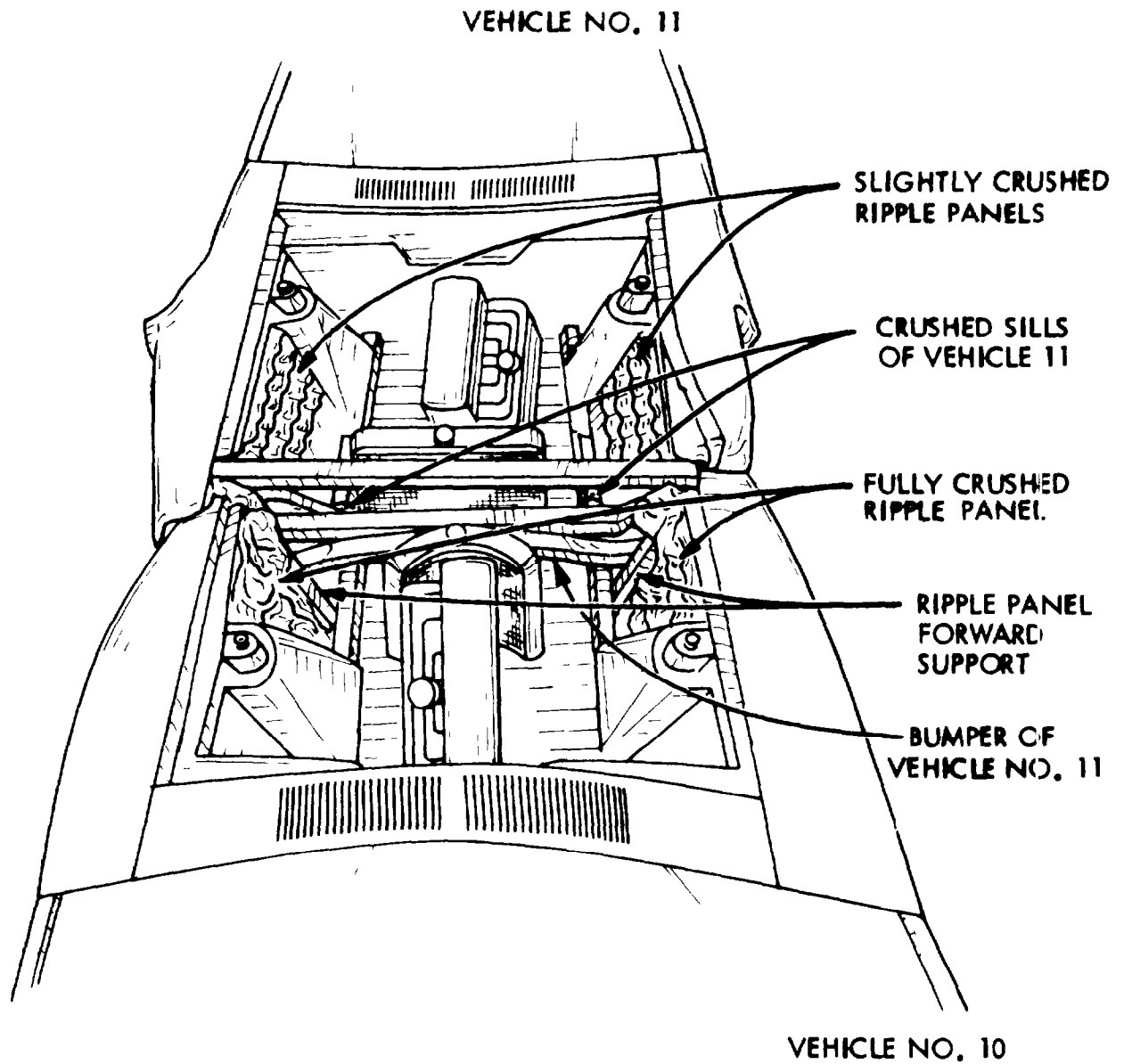


Figure 6-12. Test No. 5. Condition of Vehicles After Collision in Which Each Was Traveling 36.6 mph. Both Vehicles are Front Modified Hornets

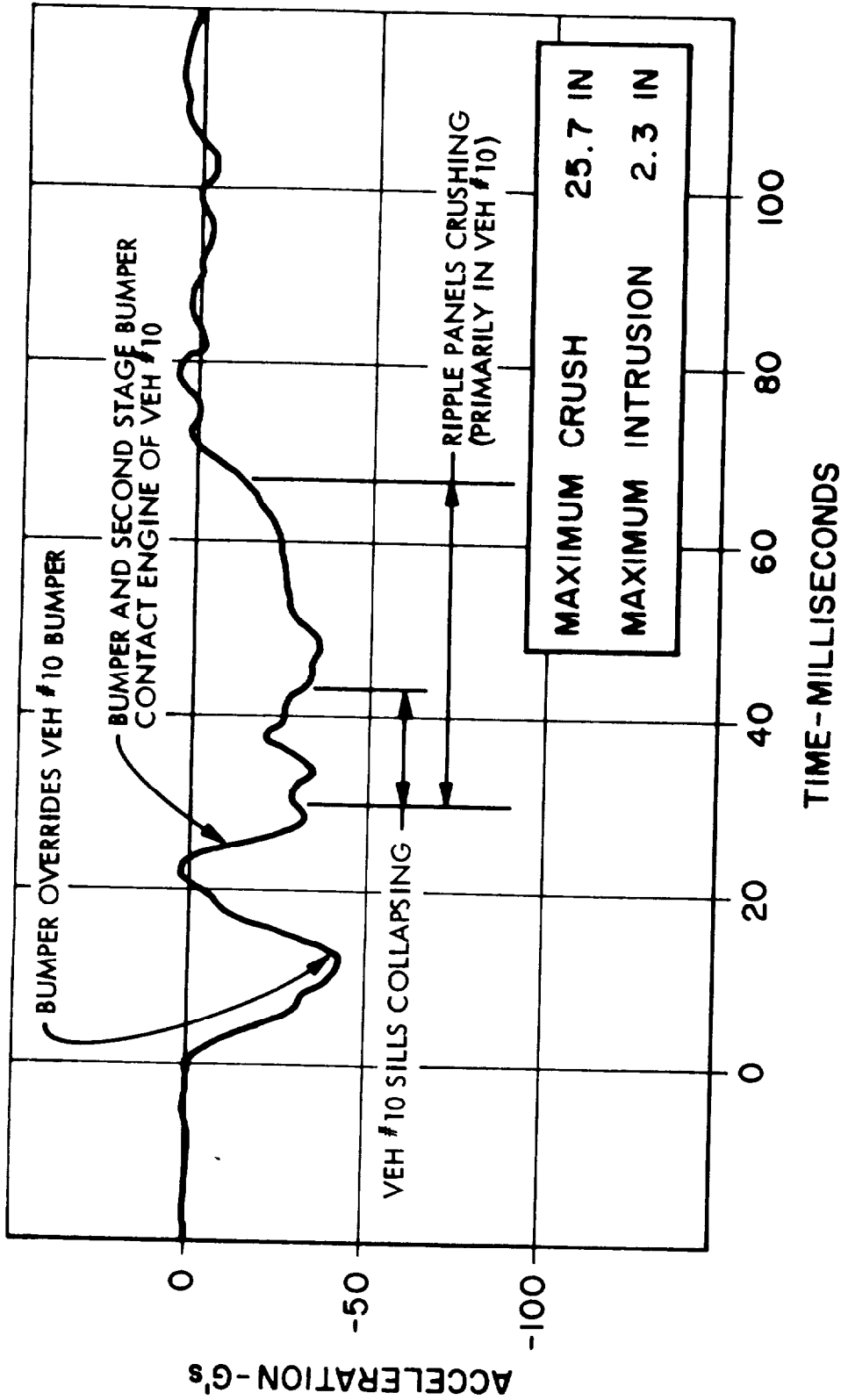


Figure 6-13. Test No. 5. 36.6 mph Vehicle-to-Vehicle (73.2 mph Relative Velocity) Frontal 0° Aligned. Vehicle No. 10 Front-Modified Hornet and Vehicle No. 11 Front Modified Hornet
 LONGITUDINAL CRASH PULSE - VEHICLE NO. 10 (Modified)

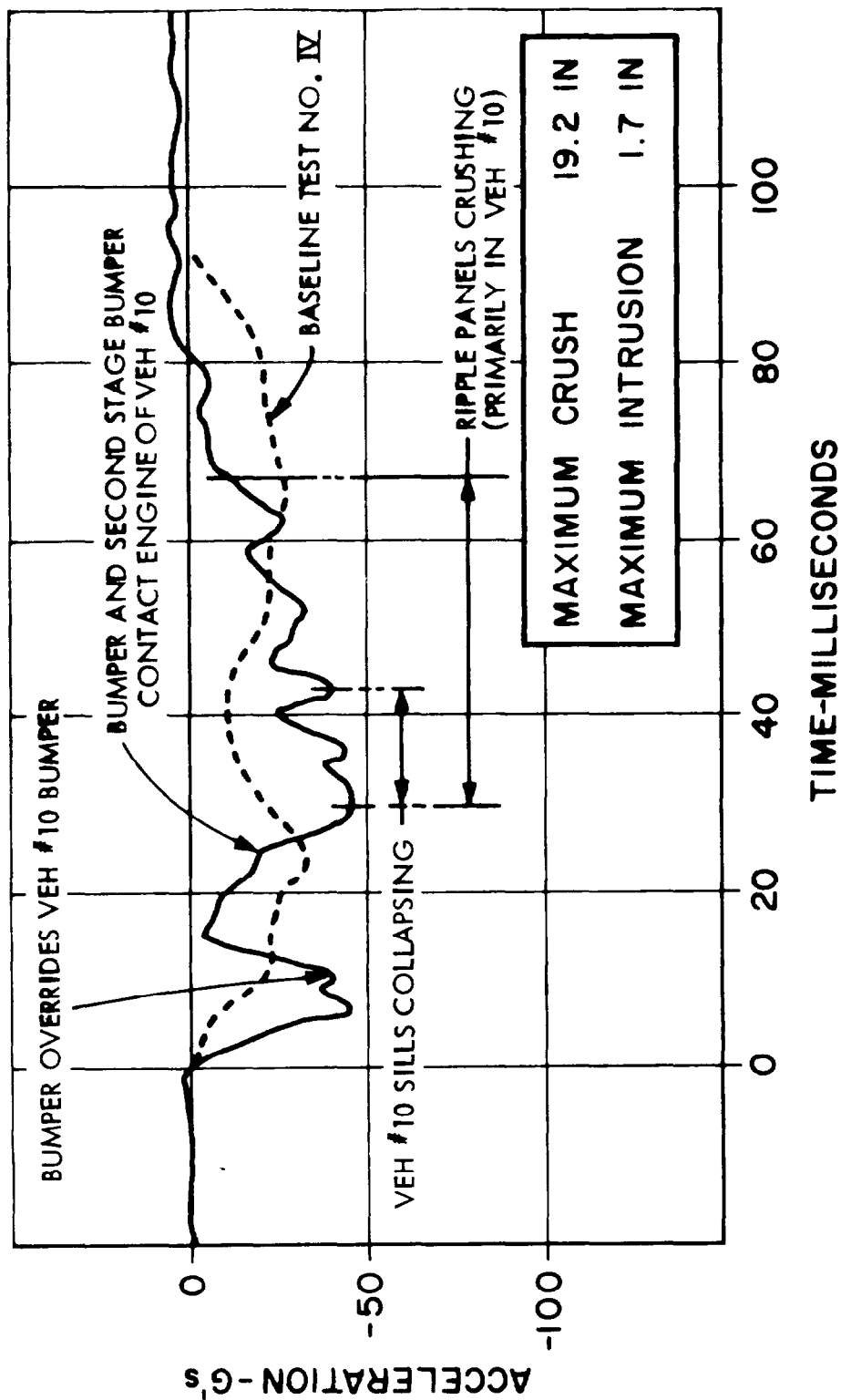


Figure 6-14. Test No. 5. 36.6 mph Vehicle-to-Vehicle (73.2 mph Relative Velocity)
 Frontal 0° Aligned. Vehicle No. 10 Front-Modified Hornet and
 Vehicle No. 11 Front-Modified Hornet
 LONGITUDINAL CRASH PULSE - VEHICLE NO. 11 (Modified)

enabled the second-stage bumper of vehicle #10 to more effectively resist overriding by vehicle #11. The ripple panels provided an energy absorbing backup once overriding had occurred. Engine deflection was limited to 2 inches and 4 inches in the modified vehicles, compared to 11 inches in each of the baseline vehicles.

Results of system Test #5 and Baseline Test IV are summarized in Table 6-6.

Table 6-6

	System Test 5		Baseline Test IV	
	Car 10	Car 11	Car A	Car B
Maximum vehicle crush	25.7"	19.2"	25"	27"
Dash center intrusion	3.9"	.6"	5.6"	
Maximum occupant area intrusion	2.3"	1.7"	5.0"	
Maximum acceleration	46 g	48 g	33 g	

System Test No. 6 - 36.25 mph, Vehicle-to-Vehicle (72.5 mph Relative Velocity), Frontal 0° Offset 1/2 Vehicle Width, Both Vehicles Front Modified and Side Modified

Most of the energy of the crash was absorbed within the right hand structures of the vehicles. The forward portion of the right hand sill of vehicle #3 was uniformly collapsed. The bumper of vehicle #3 reached the "A" post region and leading edge of the door of vehicle #14. The bumper of vehicle #4 stopped short of the "A" post of vehicle #3.

Damage to the passenger compartments of the vehicles was minimal. The engines were deflected aside and were not pushed back into the firewalls.

The main interaction during the crash occurred between the ripple panels on the impacted side of the vehicles. The ripple panels overlapped during the impact. The front end structures of the two vehicles interlocked in such a way that the ripple panels were constrained, forming a column

between the two vehicles. The first few convolutions of each ripple panel were crushed. Additional stroke was realized at both ends of the column composed of the ripple panels as plastic hinges formed at the firewall and at the spring tower on the impacted side of each vehicle.

The interaction of the vehicles is shown in Figure 6-15.

The crash pulses recorded for the two vehicles are very similar. These are shown in Figures 6-16 and 6-17. An initial peak of 32 g to 35 g was reached within 13 milliseconds after initial contact. By 15 milliseconds, the accelerations for both vehicles had returned to 15 g. Acceleration remained at the 15 g level for the duration of the crash.

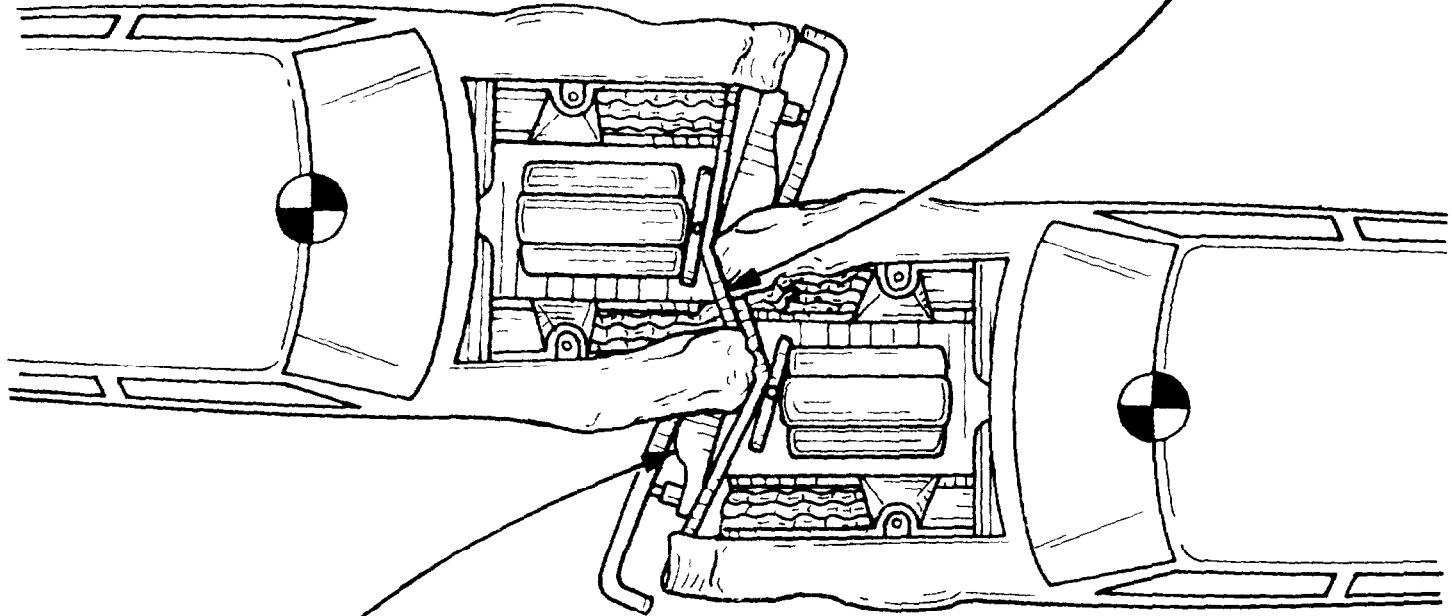
The initial acceleration peak was caused by momentary interaction of the sills on the impact side of the vehicles. As the sills were crushed, the second-stage bumpers rotated about a vertical axis. Within a few milliseconds, the bumpers rotated sufficiently to allow the sills to slide past each other. A reduced acceleration level resulted as the ripple panels were crushed and deformed and slid past each other.

The weld joint between the support brace and the ripple panel forward support failed on the non-impacted side of both vehicles 55 milliseconds after initial impact. This had no adverse effect since the ripple panels remained interlocked after the joints failed. Strengthened joints might prove to be of some benefit in more severe impacts.

No baseline test is directly comparable to System Test #6. The crash was highly symmetrical, with almost identical damage occurring to both vehicles. Maximum crush was 33.6 inches and 34.8 inches, resulting in almost total overlap of the engine compartments. Intrusion was limited to the immediate vicinity of the impact side "A" post and was 5.5 inches and 4.8 inches in the two vehicles.

A summary of the results of System Test #6 is given in Table 6-7.

FRONT ENDS OF VEHICLES BECOMING INTERLOCKED
AND CAPTURING RIPPLE PANELS



SECOND STAGE BUMPERS HAVE ROTATED ABOUT A VERTICAL
AXIS, ALLOWING SILLS TO SLIP PAST EACH OTHER

Figure 6-15. Test No. 6. Interaction of Vehicles 32 Msec After Contact
(Midway Through the Crash). Both Vehicles Front and Side Modified
Hornets. Both Vehicles Travelling 36.25 mph Prior to Impact

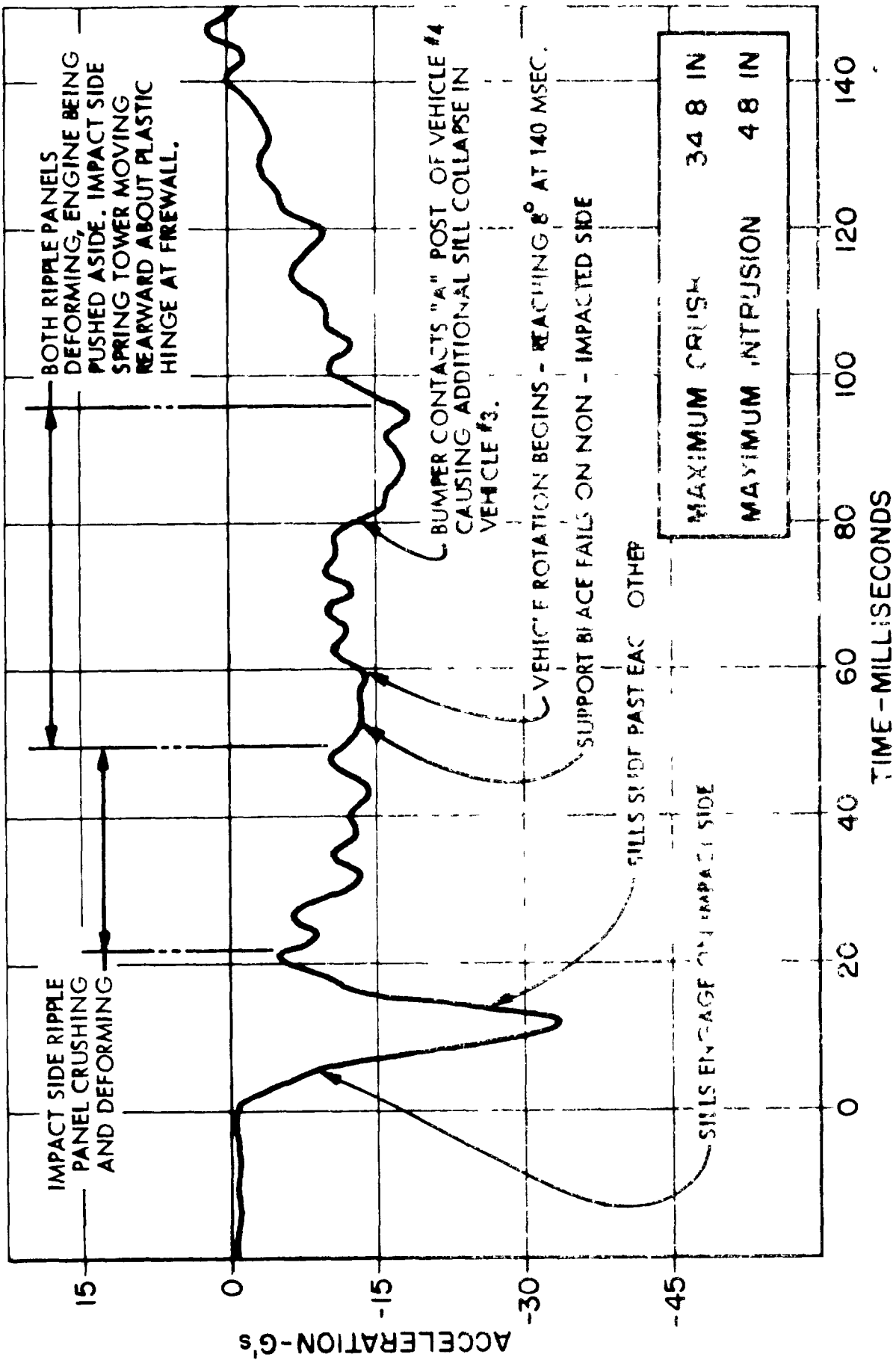


Figure 6-1A. Test No. 6. 36.25 mph Vehicle -to-Vehicle (75.50 mph Relative Velocity) Frontal 0° Off-set 1/2 Vehicle Width. Both Vehicles Front Modified and Side Modified LONGITUDINAL CRASH PULSE VEHICLE NO. 3

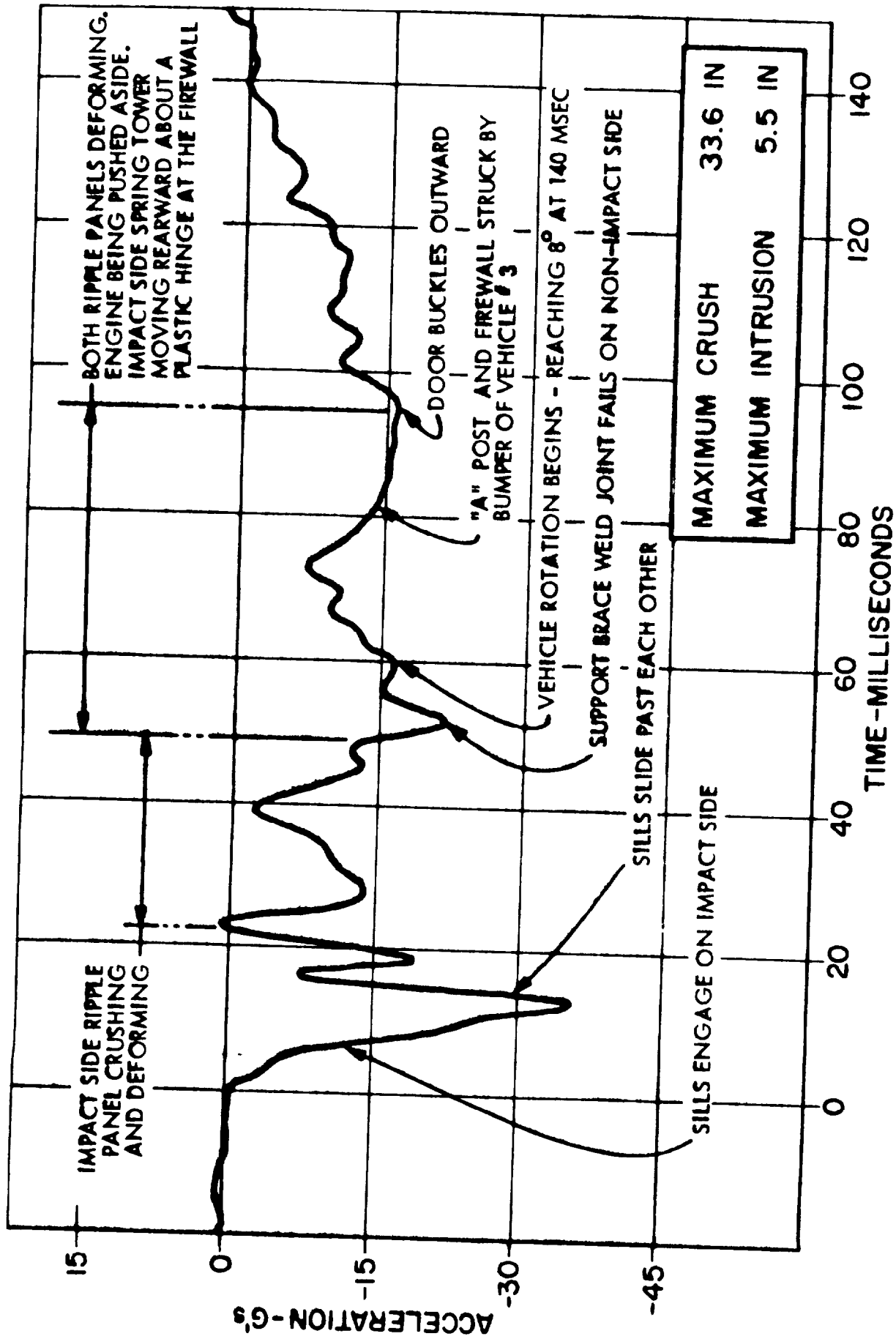


Figure 6-17. Test No. 6. 36.25 mph Vehicle-to-Vehicle (72.50 mph Relative Velocity) Frontal 0° Off-set 1/2 V hicl Width. Both Vehicles Front Modified and Side Modified LONGITUDINAL CRASH PULSE - VEHICLE NO. 4

Table 6-7

	System Test #6	
	Car 3	Car 4
Maximum vehicle crush	34.8"	33.6"
Dash center intrusion	1.5"	2.5"
Maximum occupant area intrusion	4.8"	5.5"
Maximum acceleration	35 g	35 g

System Test No. 7 - 37.73 mph, Two Vehicle (75.46 mph Relative Velocity Front/Front 0° Impact, Vehicle Centerlines Colinear, Vehicle #6 Front Modified Hornet and #14 Unmodified Hornet

The front modified vehicle rode upward slightly on the unmodified vehicle causing the front wheels of the modified vehicle to leave the ground. The passenger compartment of the modified vehicle remained approximately horizontal while the passenger compartment of the unmodified vehicle pitched downward to ground level. The engine of the unmodified vehicle was pushed rearward, deforming the firewall. The engine of the modified vehicle did not move appreciably. The steering column of the unmodified vehicle rotated downward lowering the rim of the steering wheel 3 inches. The passenger compartments of both vehicles remained intact. No glass was broken in either vehicle with the exception of the windshield in the unmodified vehicle. This glass was cracked, but remained in place. Slight compression occurred in the ripple panels of the modified vehicle.

The fenders of the two vehicles came together 12 msec after impact. The bumper of vehicle #6 seated against the second-stage bumper 14 msec after impact and began to override the bumper of the unmodified vehicle. The sills of the modified vehicle began to crush 20 msec after impact as the bumper and second-stage bumper pushed against the engine of the unmodified vehicle. Crushing of the sills continued until 38 msec after impact at which

time the rearward movement of the engine in vehicle #14 ceased. The engine then began to tilt downward at the rear. The firewall and cowl of vehicle #14 were distorted by the engine between 35 and 40 msec after impact. The side panels and spring tower of vehicle #14 were pushed inward at this time adding to distortion of the firewall. Evidence of high roof loads appeared in vehicle #6 starting 50 msec after impact and in vehicle #14, 55 msec after impact. Maximum roof loads persisted until relative motion of the vehicles stopped at about 70 msec after impact.

Vehicle #6 began to pitch upward and vehicle #14 began to pitch downward 30 msec after impact. Maximum pitch angles of about 6 degrees were reached 75 msec after impact. In the modified vehicle, a crash pulse with an average amplitude of 35 g's was recorded between 6 msec and 50 msec after impact. Distortion of the floor structure produced spurious "y" and "z" acceleration signals at several locations. No lateral or vertical acceleration was sustained for a significant length of time. The post-crash conditions of the vehicles is shown in Figure 6-18.

The crash pulse for the unmodified vehicle was of slightly smaller magnitude and longer duration than that for the modified vehicle. The crash pulse averaged 25 g's from 2 msec after impact to 60 msec after impact.

The crash pulses for both vehicles, shown in Figures 6-19 and 6-20, were reasonable approximations of square waves. Although the unmodified vehicle was damaged more extensively than the modified vehicle, damage was confined primarily to the front end structure and the firewall.

System Test #7 (one modified Hornet and one unmodified Hornet) may be compared to Baseline Test IV (two unmodified Hornets) and to System Test #5 (two modified Hornets).

The crash pulse for the modified vehicle in Test #7 resembles the crash pulses for the modified vehicles in Test #5. In fact, it is more favorable since the 10 to 12 msec drop-off in the crash pulse that took place in Test #5 was not present in Test #7. In Test #7, the second-stage bumper in the modified vehicle maintained its horizontal orientation and pushed steadily against the opposing vehicle structure.

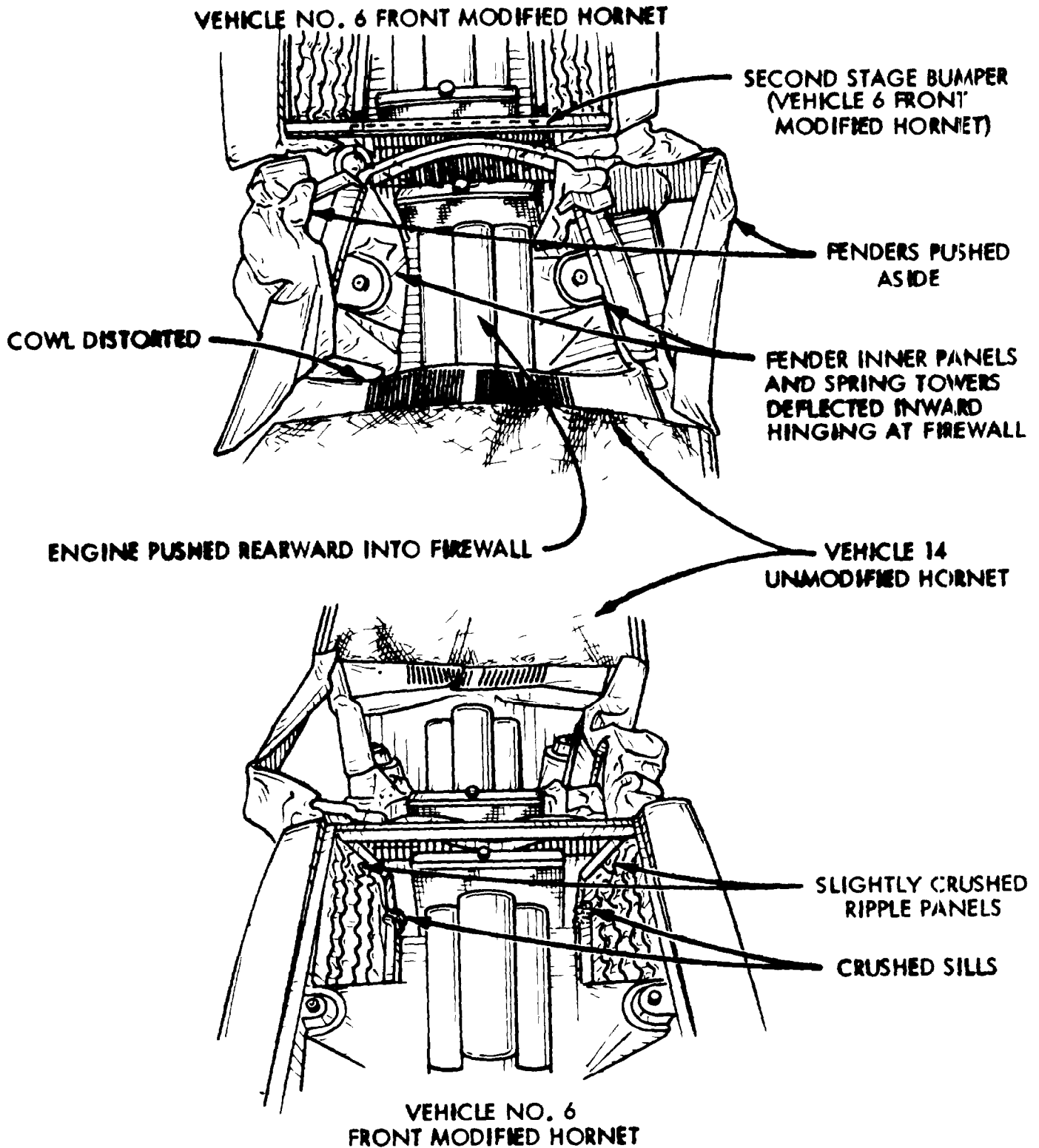


Figure 6-18. Test No. 7. Condition of Vehicles After Collision in Which Both Were Travelling 37.73 mph. Front Modified Hornet Vs Unmodified Hornet (Two Views of Damaged Vehicles Taken From Opposite Directions)

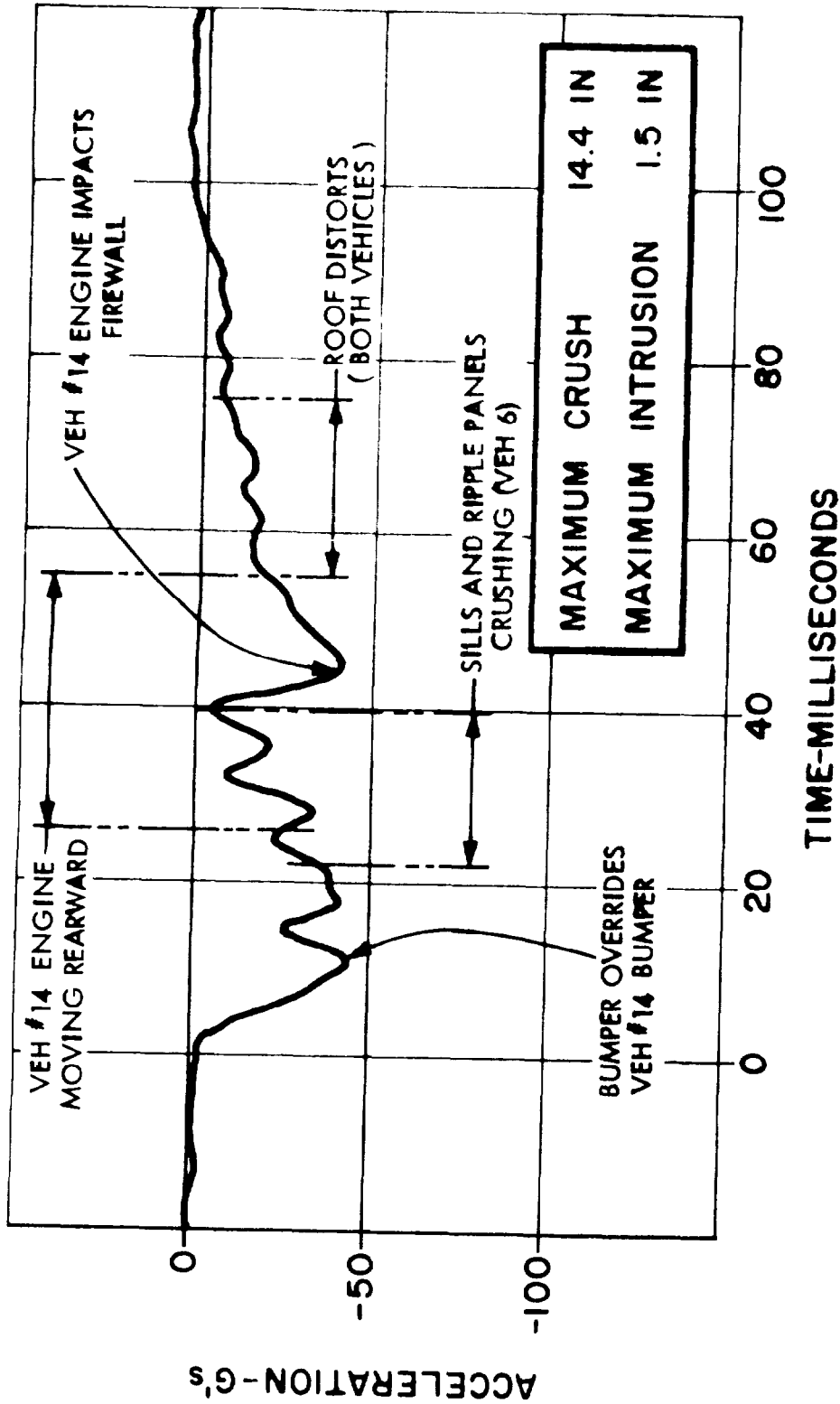


Figure 6-19. Test No. 7. 37.73 Vehicle-to-Vehicle (75.46 mph Relative Velocity) Frontal 0° Aligned. Vehicle No. 6 (Front Modified Hornet) and Vehicle No. 14 (Unmodified Hornet) LONGITUDINAL CRASH PULSE - VEHICLE NO. 6 (Modified)

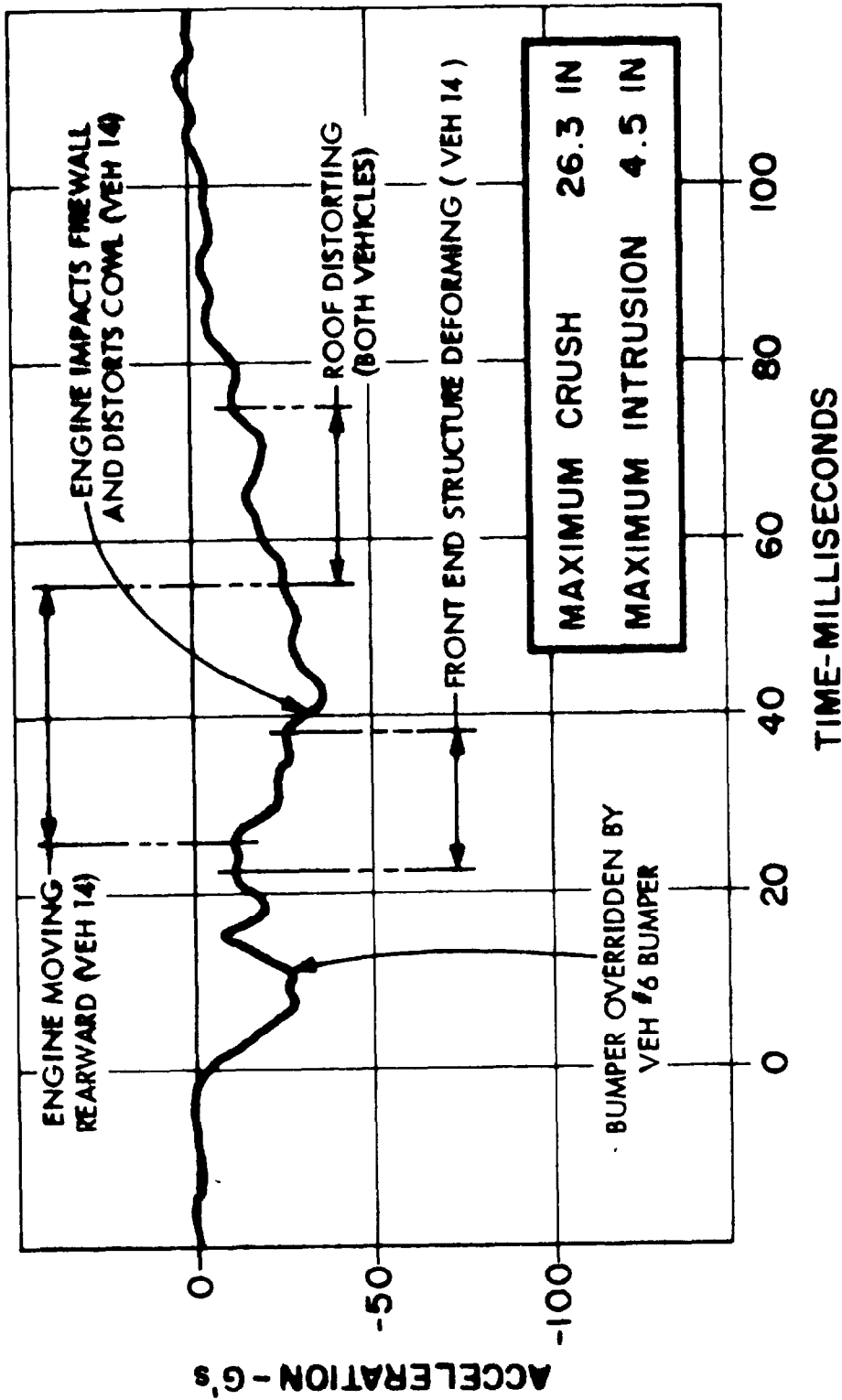


Figure 6-20. Test No. 7. 37.73 mph Vehicle-to-Vehicle (75.46 mph Relative Velocity) Frontal 0° Aligned. Vehicle No. 6 (Front Modified Hornet) and Vehicle No. 14 (Unmodified Hornet) LONGITUDINAL CRASH PULSE - VEHICLE NO. 14 (Unmodified)

The crash pulse for the unmodified vehicle in Test #7 shows some improvement over the baseline crash pulse. The onset is faster and the overall duration of the pulse is shorter. The unmodified vehicle's crash pulse benefited from the energy management system of the modified vehicle.

Intrusion in the modified vehicle was slightly less than in either modified vehicle in Test #5. Intrusion in the unmodified vehicle was about the same (4.5 inches) as the maximum intrusion in the baseline test (5.0 inches).

Total crush of the modified vehicle was 14.4 inches, compared to 26.3 inches in the unmodified vehicle. Maximum crush in the impact between two modified vehicles (Test #5) was 25.7 inches. Although the modified vehicle is more aggressive than the unmodified, it is not unreasonably aggressive in an absolute sense. The total crush (sum of both vehicles) in Test #7 was 40.7 inches. This is more favorable than the 44.9 inches of Test #5 and the 47.0 inches in Baseline Test IV. The lower values of total crush go along with the favorable crash pulses obtained with modified vehicles.

A summary of results of System Test #7 is given in Table 6-8.

Table 6-8

	System Test 7	
	Car 6	Car 14
Maximum vehicle crush	14.4"	26.3"
Dash center intrusion	1.3"	10.0"
Occupant area intrusion	1.5"	4.5"
Maximum acceleration	45 g	37 g

System Test No. 8 - Vehicle-to-Vehicle 35.95 mph (71.90 mph Relative Velocity), Front/Front 0° Offset 1/2 Vehicle Width, Impacting Vehicle #8 Front Modified Hornet, and Vehicle #16 Unmodified Hornet

Deflection of the energy absorbing components of the modified vehicle was very slight. The geometry of the engine compartment and front end of the modified vehicle were not appreciably altered. The modified vehicle pushed the bumper and engine of the unmodified vehicle aside and intruded through the engine compartment, contacting the "A" post and firewall. The passenger compartment of the unmodified vehicle was badly distorted on the impact side (an earlier test had damaged the non-impacted side). The door on the impacted side was severely buckled, the roof, firewall and cowl were deformed.

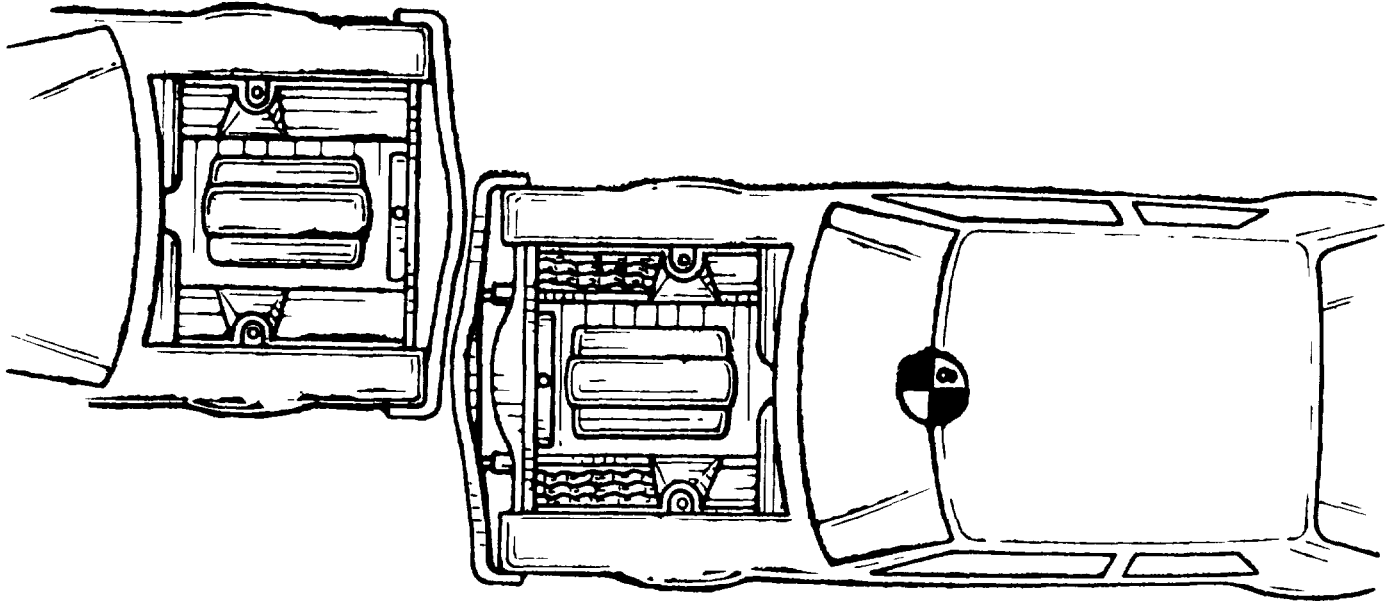
Similar crash pulses were recorded for both vehicles. Throughout most of the crash, acceleration was below 20 g's. A 24 g pulse was recorded in the modified vehicle between 62 and 72 msec after impact as it reached the firewall and "A" pillar of the opposing vehicle. By 110 msec after impact, both crash pulses had fallen below 15 g's and reached zero by 140 msec after impact. The nature of the crash pulse was determined almost entirely by the crush characteristics of the unmodified vehicle. Most of the energy of the crash was dissipated in deformation of lightweight sheet metal components.

The pre-crash position of the vehicles is shown in Figure 6-21 and the maximum deformation condition is shown in Figure 6-22. Vehicle acceleration pulses are shown in Figures 6-23 and 6-24.

No baseline test is directly comparable to System Test #8. System Test #6, involving two modified vehicles, may be used for reference. The main area of concern in Test #8 is the aggressivity of the modified vehicle.

Maximum crush of the unmodified vehicle was 56.0 inches, with maximum intrusion of 6.0 inches. The intrusion involved the right hand "A" post, the dash panel and the transmission hump. Maximum crush in the modified vehicle was 24.6 inches and maximum intrusion was 3.1 inches at the dash panel.

**VEHICLE NO. 18 UNMODIFIED
HORNET**



VEHICLE NO. 8 FRONT-MODIFIED HORNET

**Figure 6-21. Test No. 8. Position of Vehicles At Time of Initial Contact.
Both Vehicles Traveling 35.95 mph.**

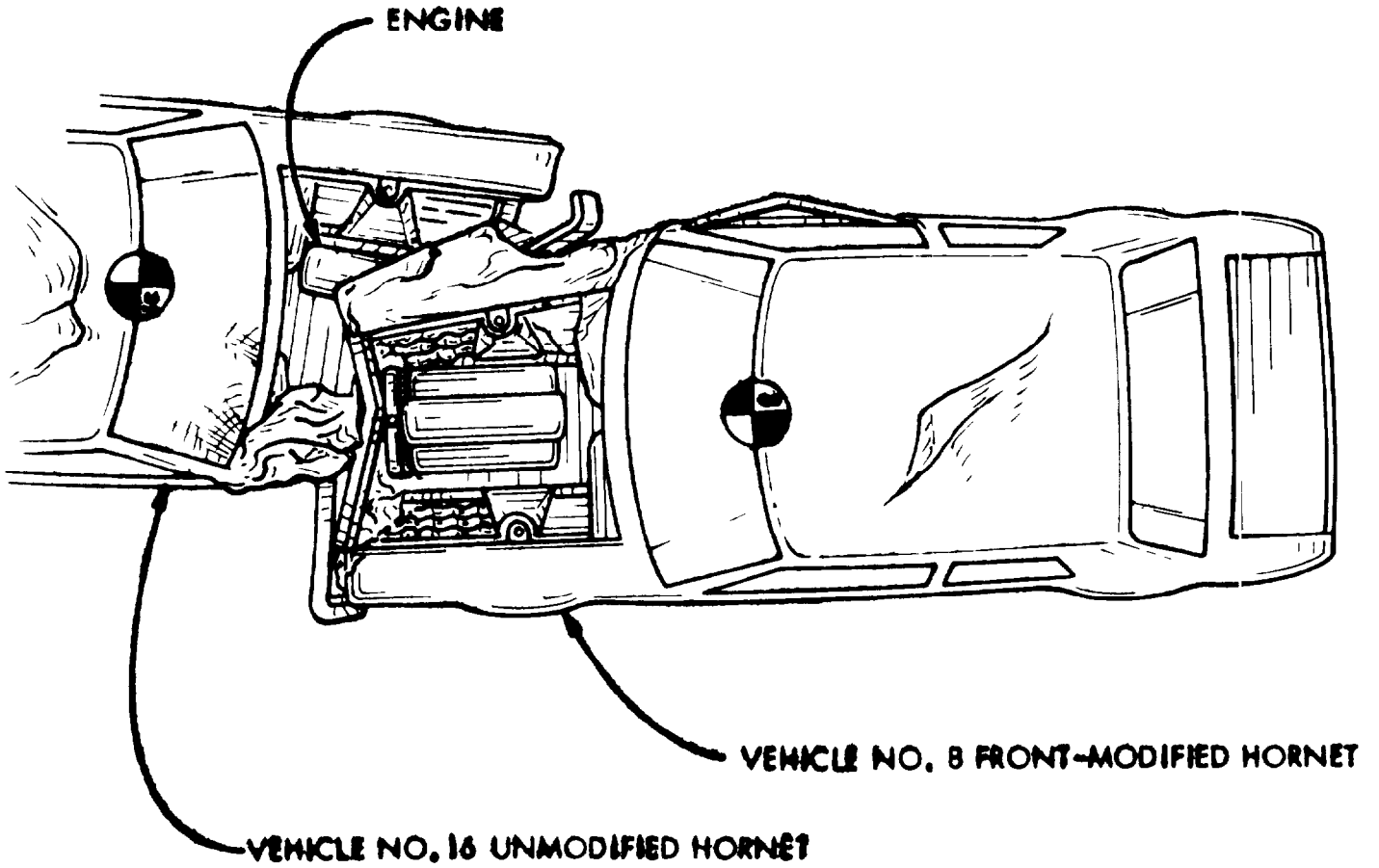


Figure 6-22. Test No. 8. Configuration of Vehicles 112 Mass After Contact (Maximum Deformation).

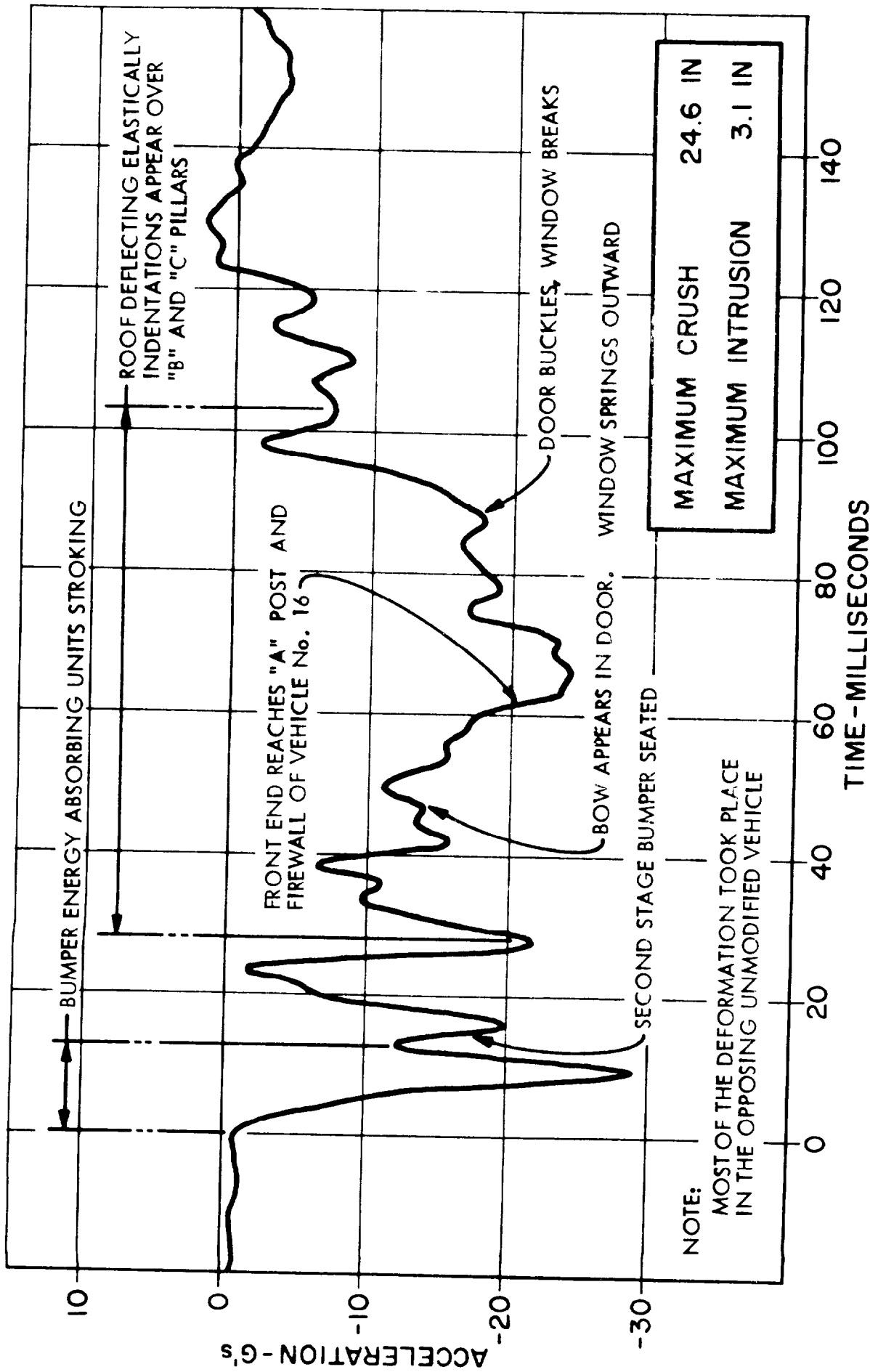


Figure 6-23. Test No. 8 35.95 mph V hicl -t -V hicl (71.90 mph R lativ V locity)
 Front 0° Off-set 1/2 Vehicl Width Vehicle No. 8 Front Modified Hornet And
 V hicl No. 16 Unmodified Hornet
 LONGITUDINAL CRASH PULSE - VEHICLE NO. 8 (Modified)

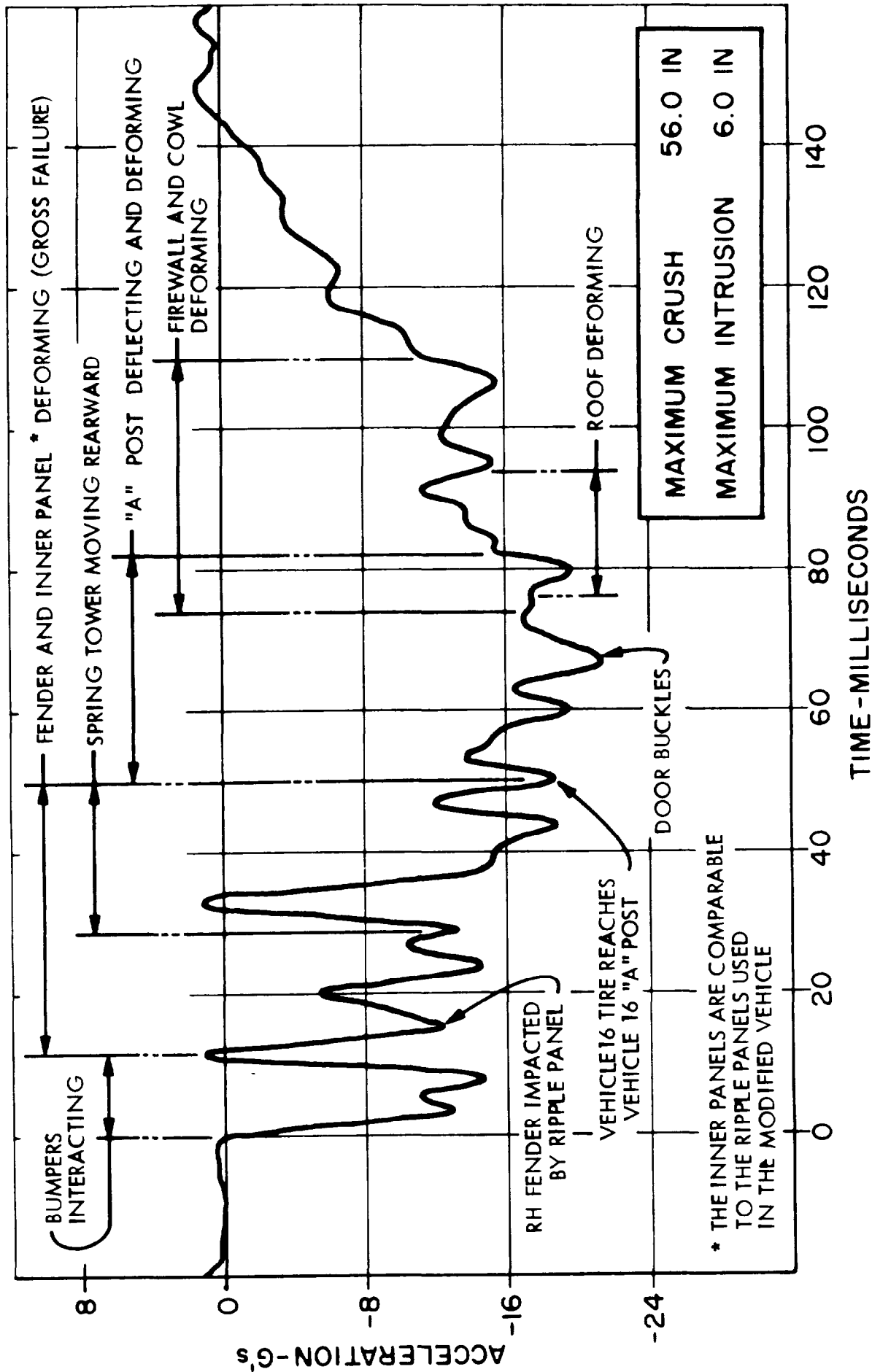


Figure 6-24. Test No. 8 35.95 mph Vehicle-to-Vehicle (71.90 mph Relative Velocity) Frontal 0° Off-axis 1/2 Vehicle Width Vehicle No. 8 Front-Modified Horn t and Vehicle No. 16 Unmodified Horn t LONGITUDINAL CRASH PULSE - VEHICLE No. 16 (Unmodified)

The large total crush (20.6 inches) is responsible for the very moderate crash pulse recorded in each vehicle.

The results of System Test #8 are summarized in Table 6-9.

Table 6-9

	System Test 8	
	Car 14	Car 16
Maximum crush	24.6"	56.0" Corner
Dash center intrusion	2.6"	4.1"
Maximum occupant area intrusion	3.1"	6.0"
Maximum acceleration	24 g	21.5 g

System Test No. 9 - Two Vehicles, 36.93 mph (73.86 mph Relative Velocity), Front/Front 0°, Vehicle Centerlines Colinear, Vehicle #7 Front Modified Hornet and Vehicle #17 Unmodified 4170 lb Ford Custom

The Hornet rode over the bumper and between the widely spaced fenders of the Ford. Little resistance was encountered until the bumper and second-stage bumper contacted the Ford engine. The Ford engine was pushed rearward 21 inches, causing 6.0 inches intrusion at the transmission hump. The Hornet engine caused 2.3 inches intrusion. Aside from transmission hump distortion, the passenger compartments of both vehicles remained intact. Considerable elastic deformation took place in the doors and roof of the modified vehicle. The passenger compartment of the standard vehicle was not deflected or deformed appreciably. No glass was broken in either vehicle.

Sheet metal components of the two vehicles made contact 10 msec after the bumpers first touched. The bumper of the Hornet was seated against the second-stage bumper 13 msec after impact. The onset of loading became apparent in the Hornet 23 msec after impact as a shock passed through the ripple panel and roof distortion caused a gap to form between the roof and forward edge of the door. At 25 msec, the bumper of the Hornet contacted the

engine of the Ford. The engine was pushed rearward a total of 21 inches coming to rest 80 msec after impact. Convolutions began to form in the sills of the Hornet 30 msec after impact. The sills and lower portion of the ripple sheet metal panels collapsed a maximum of 8 inches. The upper support and upper portions of the rippled panels were deformed less than one inch as a result of having ridden over the Ford front end. The Hornet engine was deflected rearward 6 inches between 35 msec and 60 msec after initial impact. Maximum deformation of the vehicles occurred 75 msec after impact. Figure 6-25 illustrates the appearance of the vehicles at that time.

Maximum crush of the front modified Hornet was 22.3 inches in the fender-sill region. Crush of the upper components was less extensive since the front end of the Hornet rode up over the Ford front end. The right hand door of the Hornet buckled outward approximately 5 inches. The front edge of the roof was permanently displaced upward 1 inch accompanied by large indentations above the "B" pillars. The rocker panels were distorted upward about 2 inches at the front end.

The results of the test are summarized in Table 6-10.

Table 6-10

	System Test 9	
	Car 7	Car 17
Maximum vehicle crush	22.3"	34.4"
Dash center intrusion	2.3"	1.6"
Occupant area intrusion	1.8"	2.5"
Maximum acceleration	50 g	50 g

The crash pulse for the front modified Hornet, shown in Figure 6-26, had a fast rise time. It reached an average level of 40 g's within 10 msec after impact, dwelled for 15 msec, then diminished to 20 g's for the next 18

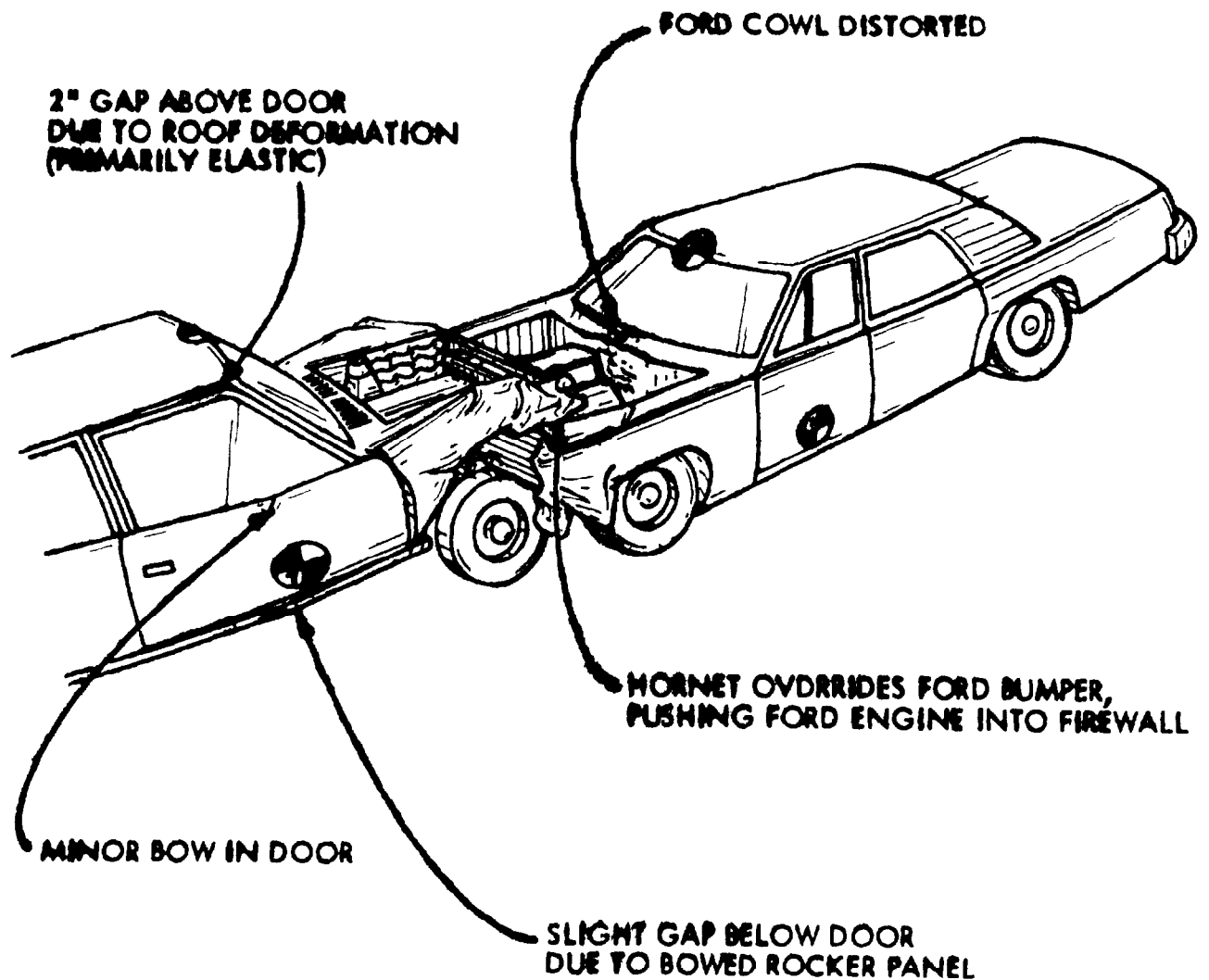


**Figure 6-25. Interaction of Vehicles 75 msec After Initial Contact (Midway Through the Crash)
 Vehicle No. 7 Front Modified Hornet Impacting 4170 lb Unmodified Ford Custom
 (Vehicle 17) Both Vehicles Travelled 26.93 mph Prior to Impact**

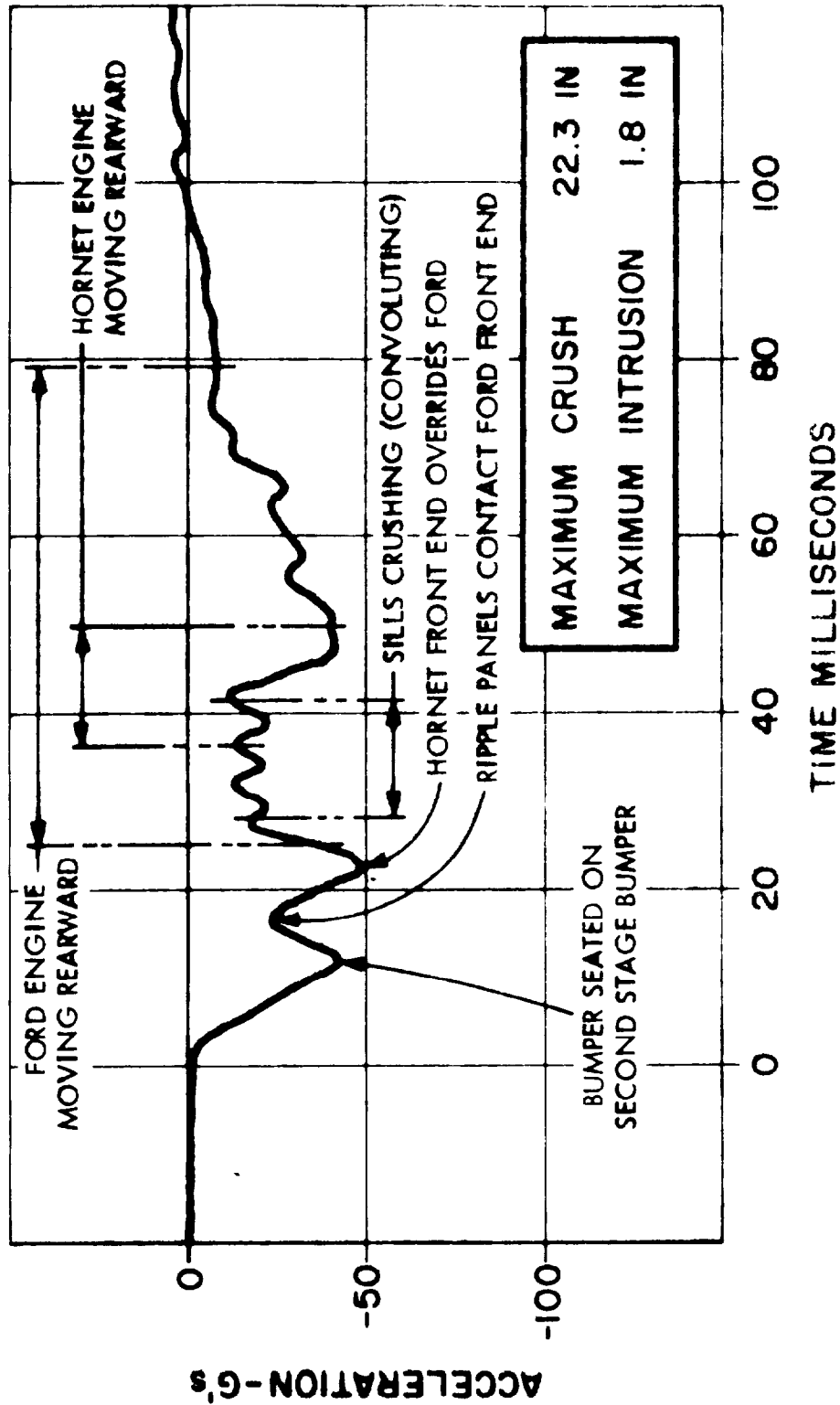


Figure 6-26. Test No. 9. 36.93 mph Vehicle-to-Vehicle (73.86 mph Relative Velocity) Frontal 0° Aligned. Vehicle No. 7 (Front Modified Hornet) and Vehicle No. 17 (4170 lb LB Ford) LONGITUDINAL CRASH PULSE - VEHICLE NO. 7 (Modified)

msec. Acceleration returned briefly to 40 g, then diminished linearly to zero 90 msec after initial impact.

The crash pulse for the impacting 4170 lb Ford, shown in Figure 6-27, had a long rise time. Acceleration remained at 15 g's for the first 30 msec of the crash. Then, as the engine began to be pushed rearward, the level rose to 30 g's. It remained between 20 and 30 g during the remainder of the crash. Engine acceleration averaged 75 g between 18 and 40 msec after impact. This agrees with the observed motion of the Ford engine. The Ford was crushed a maximum of 34.4 inches in an area 33 inches wide, symmetrical with the vehicle centerline. The crush diminished farther from the centerline with only a few inches occurring at the fenders.

Total deformation of vehicles and displacement of engines as a function of time are shown in Figure 6-28.

No baseline test is directly comparable with System Test #9. System Test #5 (two modified Hornets) and System Test #7 (one unmodified Hornet and one modified Hornet) may be used for reference.

This collision with a heavier vehicle was to determine the effectiveness of the energy management system in protecting the occupants in the lighter vehicle. A secondary consideration was the aggressivity of the modified vehicle against a heavier unmodified vehicle.

The energy management system of the modified vehicle performed very well in System Test #9. The crash pulse for the modified vehicle had a reasonably fast rise time despite the apparent "soft nose" of the heavier vehicle. Intrusion in the heavier unmodified vehicle was not excessive and resulted primarily from rearward movement of the engine.

System Test No. 10 - 24.68 mph Vehicle-to-Vehicle, Front/Side 270°,
Impact Location Door Centerline, Impacting Vehicle #8
Front Modified Hornet, Impacted Vehicle #13, Side
Modified Hornet

The relative position of the vehicles prior to impact is shown in Figure 6-29. The major structural components of the impacting front modified vehicle were not deformed. The bumper energy absorbing units traveled full

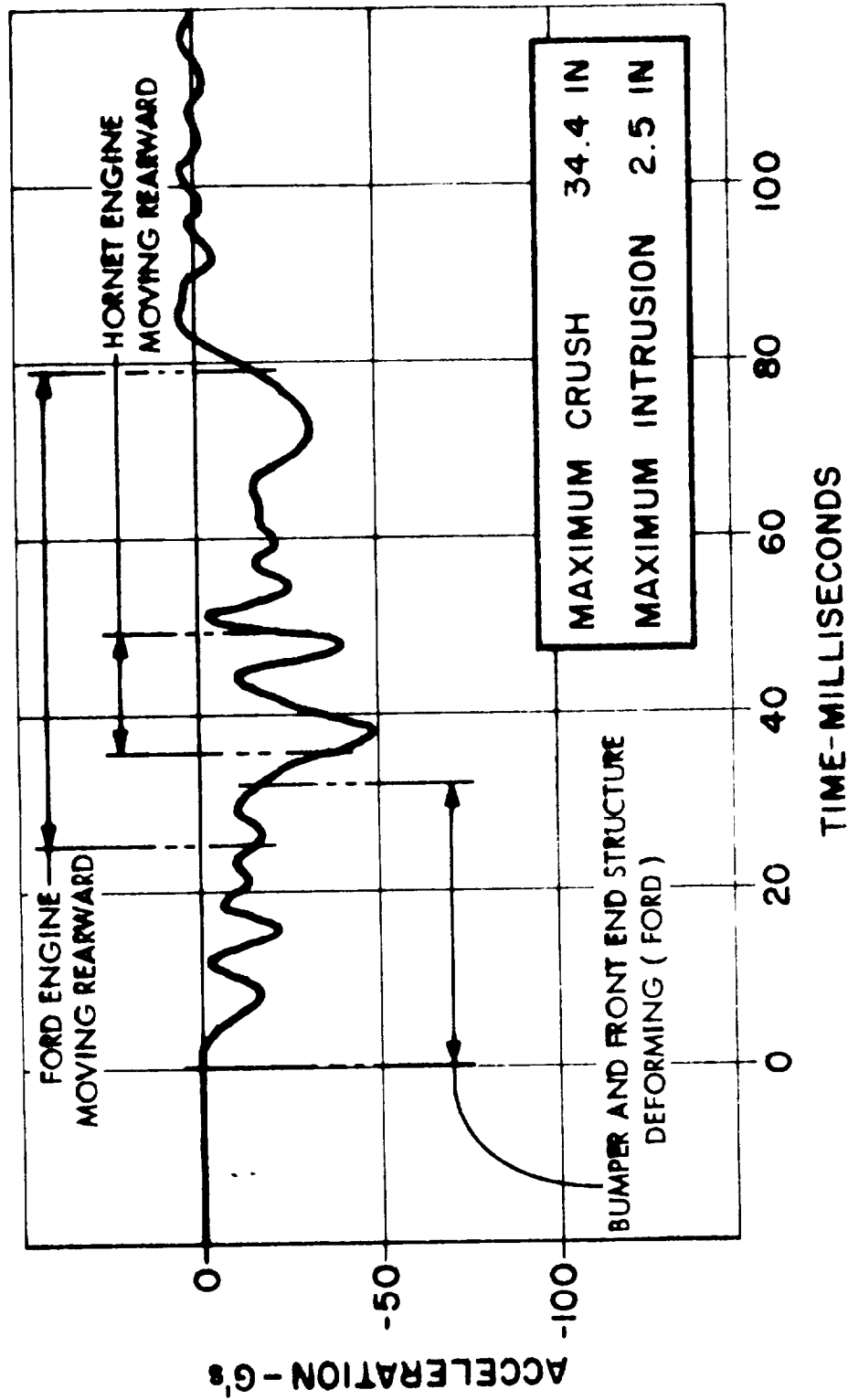


Figure 6-27. Test No. 9. 36.93 mph Vehicle-to-Vehicle (73.86 mph Relative Velocity) Frontal 0° Aligned. Vehicle No. 7 (Front Modified Hornet) and Vehicle No. 17 (4170 lb Ford) LB LONGITUDINAL CRASH PULSE - VEHICLE NO. 17 (4170 lb. Unmodified)

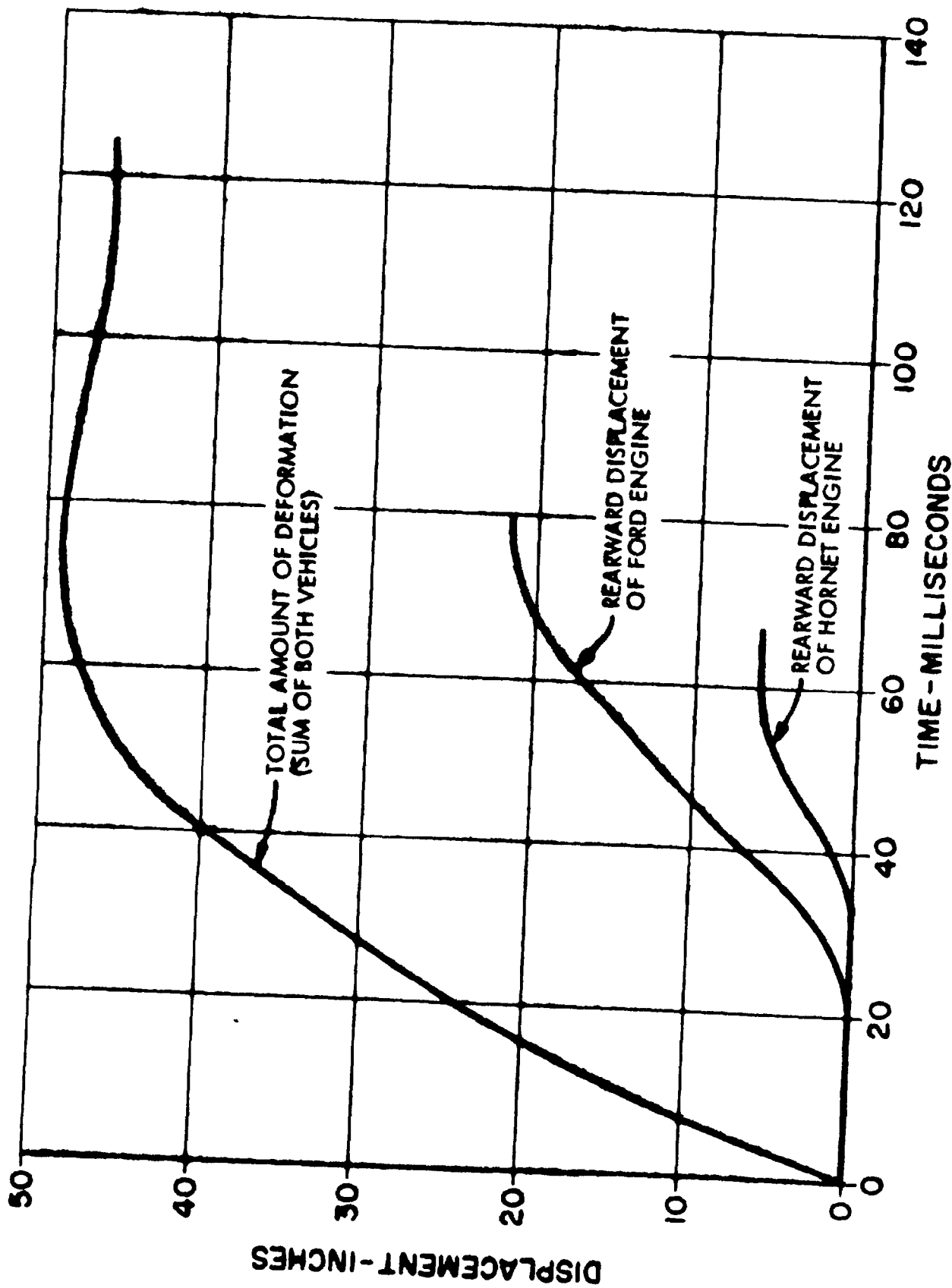
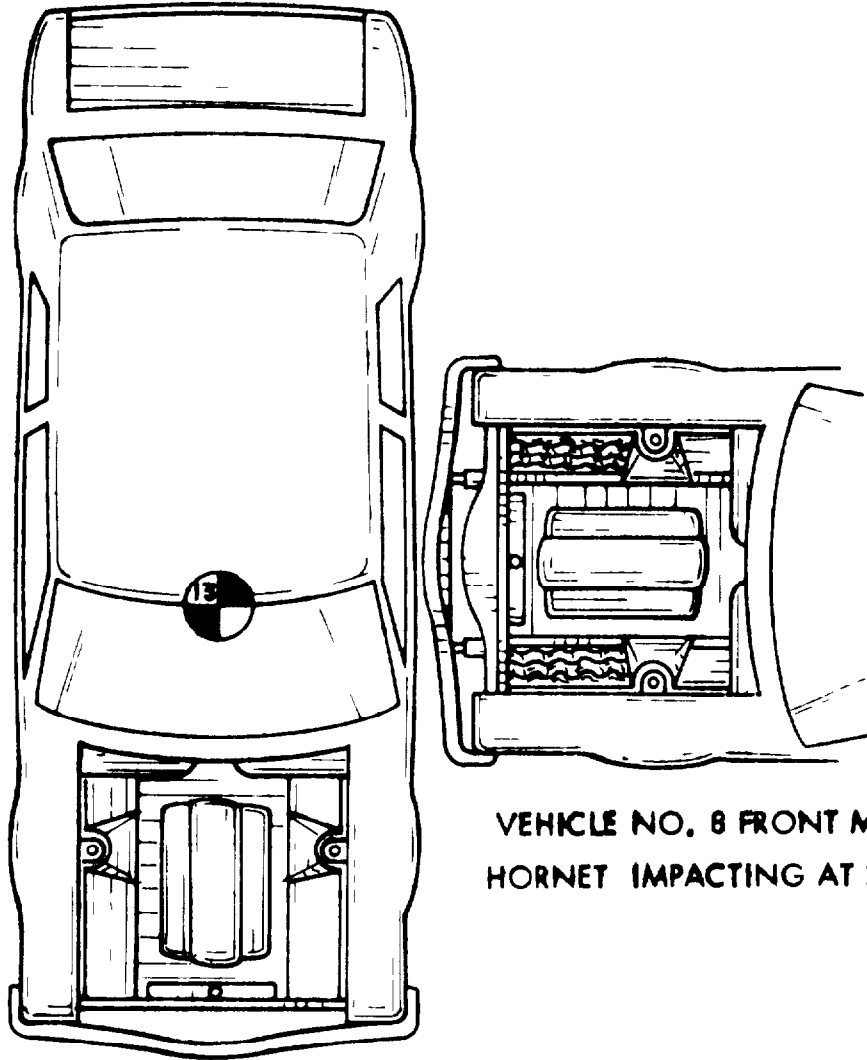


Figure 6-28. Test No. 9 Head-on Impact - Front Modified Hornet and Unmodified Ford Custom
 Both Vehicles were Travelling 36.93 mph at Impact
 DISPLACEMENTS OBTAINED FROM MOTION PICTURE FILMS



VEHICLE NO. 8 FRONT MODIFIED
HORNET IMPACTING AT 24.68 mph

VEHICLE NO. 13 SIDE MODIFIED HORNET (STATIONARY)

Figure 6-29. Test No. 10. 24.68 mph Side Impact of Side Modified Hornet by Front Modified Hornet. Position of Vehicles at Time of Impact

stroke and the center of the bumper contacted the second-stage bumper. The ends of the bumper were bent rearward giving the bumper an overall C shape in plan view.

Maximum dynamic crush of 12.2 inches occurred 49 msec after initial contact. Maximum static crush was 9.0 inches. Maximum static intrusion was 7.1 inches. Damage was confined mainly to the door and "B" post. The "B" post was displaced inward 5 inches at the level of the shoulder molding. Minor damage occurred in the quarter panel, rocker panel and front fender. The top and rear edges of the left rear window were sprung outward slightly.

The lateral crash pulse for the impacted vehicle, shown in Figure 6-30, had a peak amplitude of 13 g's. Rise time to an initial level of 6 g's was about 5 msec. Acceleration of 11 g's average amplitude was sustained for 14 msec, starting 22 msec after impact. This was followed by a 35 msec period with a 7 g average acceleration level.

System Test #10 may be compared with Baseline Test V (two unmodified vehicles), with System Test #12 (an unmodified vehicle impacted by a modified vehicle) and System Test #14 (a modified vehicle impacted by a 4170 lb unmodified vehicle).

Deflections of the "A" post and "B" post in System Test #10 were significantly less than in Baseline Test V. Maximum intrusion was 7.1 inches or 2.4 inches less than in the baseline test.

The lateral crash pulse for the impacted vehicle in System Test #10 has the same general form as that recorded in Baseline Test V. The major peaks occurred 10 to 15 msec earlier than in the baseline test. Major peaks were of comparable amplitude.

A summary of the results of System Test #10 and Baseline Test V is given in Table 6-11.

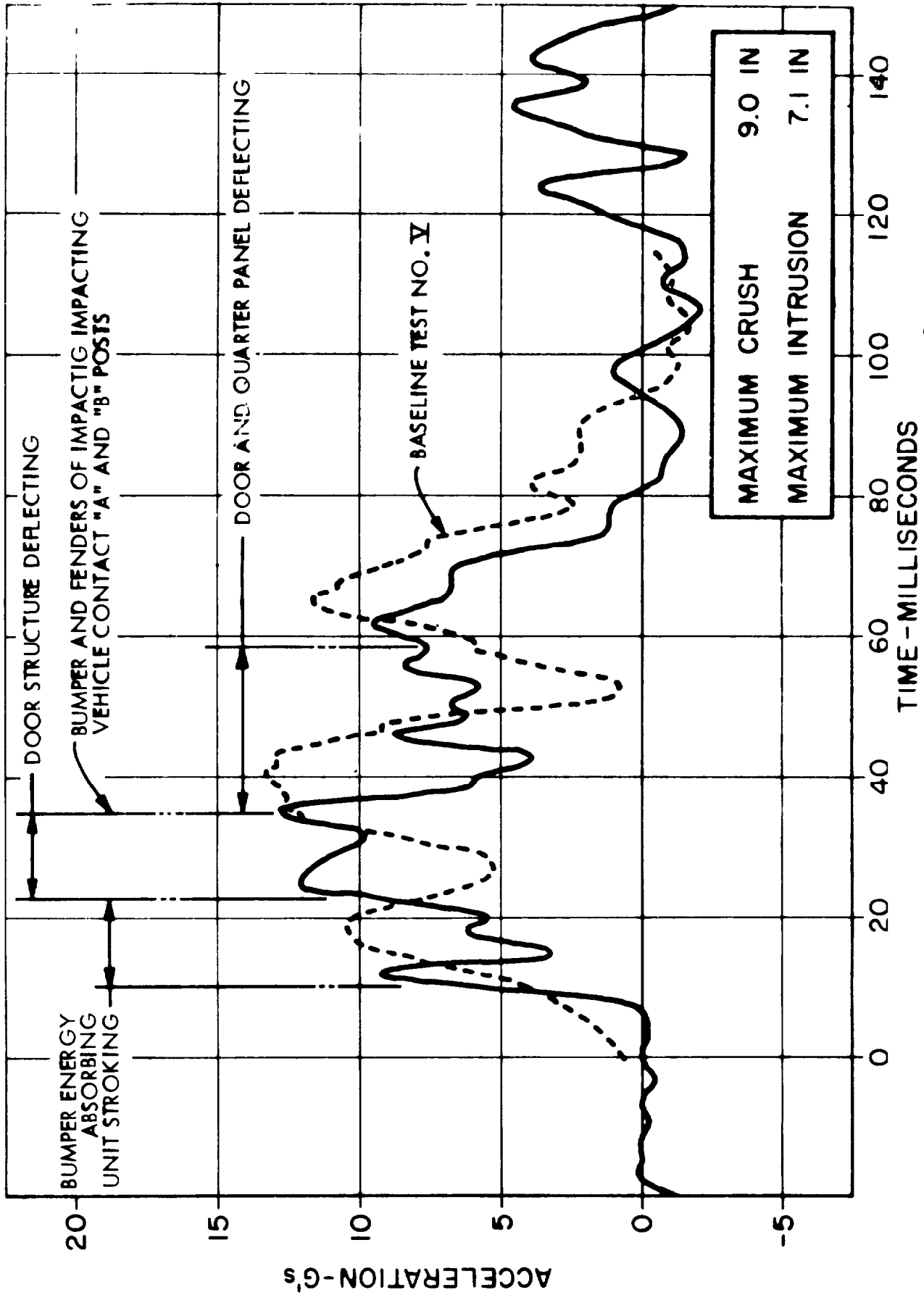


Figure 6-30. Test No. 10. 24.68 mph Vehicle -to-Vehicle Front/Side 270° Impact at Door Centerline. Impacting Vehicle No. 8 Front Modified Hornet. Impacted Vehicle No. 13 - Side Modified Hornet LATERAL CRASH PULSE VEHICLE NO. 13 (Modified)

Table 6-11

	System Test 10	Baseline Test V
Maximum crush	9"	13.5"
Maximum intrusion	7.1"	9.5"
Maximum acceleration	13 g	14 g

The design goal of 20 g maximum acceleration was met. The goal of 3.5 inches maximum intrusion was not met. Most of the intrusion resulted from deformation of the door between the rocker panel and the door beam. The door beam remained intact except for partial face sheet separation near the "B" post. The rocker panel was deformed inward 3.5 inches at the "A" post and 4.3 inches at the "B" post. Part of this deformation resulted from 1.1 inches of floor pan compression that occurred at the driveshaft tunnel. If further improvements are to be made in intrusion resistance, additional reinforcement of the floor pan structure will be required to anchor the "A" and "B" posts and to prevent compressive deformation.

System Test No. 11 - 24.33 mph, Vehicle-to-Vehicle, Front/Side 60°,
 Aiming Point Door Centerline, Impacting Vehicle #9
 Front Modified Hornet, Impacted Vehicle #13
 Side Modified Hornet

The relative position of the vehicles prior to impact is shown in Figure 6-31. The impacting vehicle suffered only superficial damage to the bumper and fender. Although the centerline of the impacting vehicle was aligned with the center of the door of the impacted vehicle, damage was confined primarily to the fender and "A" post of the impacted vehicle. The "A" post withstood the brunt of the crash with slight deformation. Intrusion was 0.5 inches. Compressive loads applied to the door caused delamination of the door beam and slight outward buckling of the door. The passenger compartment remained intact with no broken windows. There was no discernible distortion of the roof structure. The post-crash condition of the vehicle is shown in Figure 6-32.

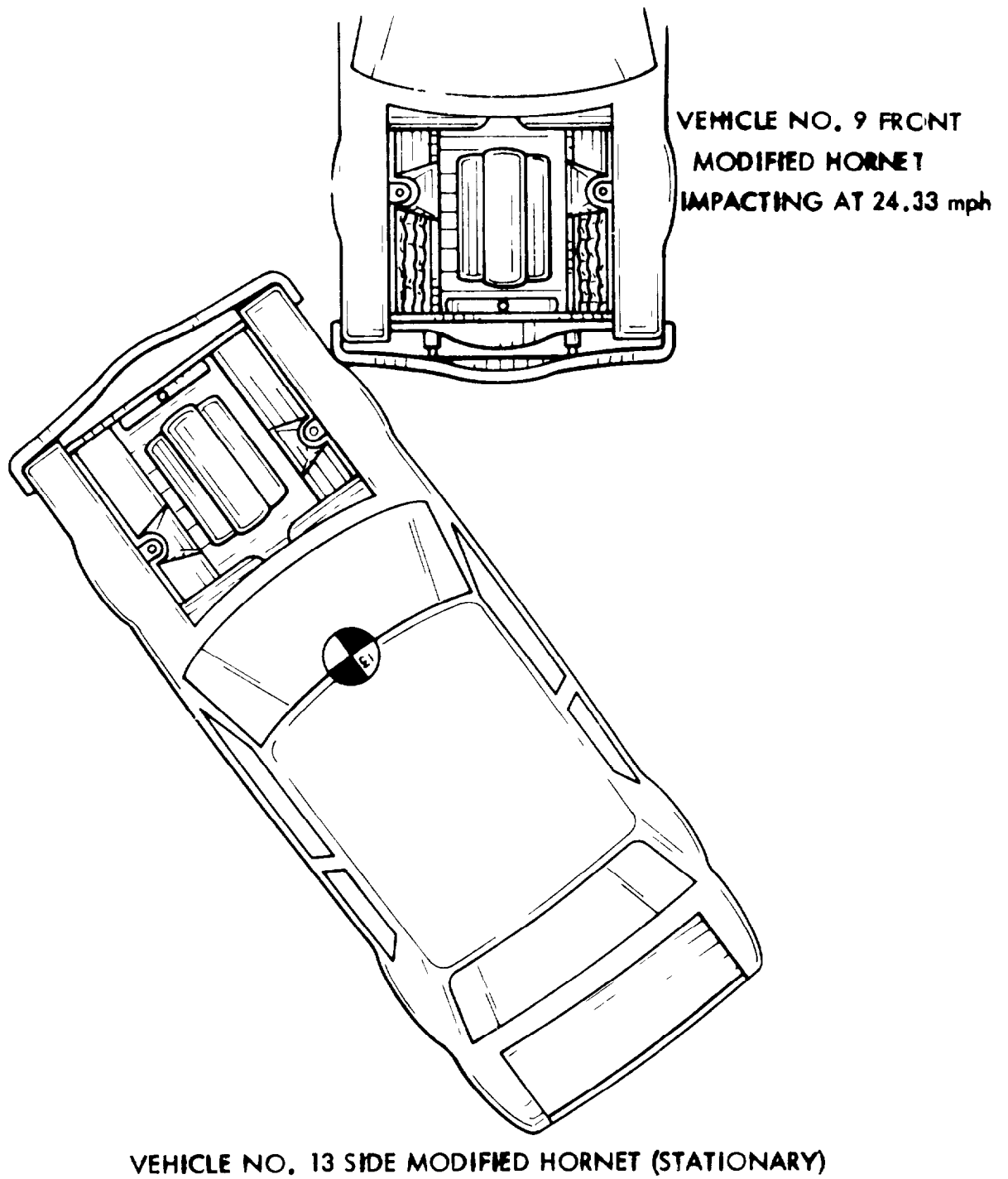


Figure 6-31. Test No. 11. Position of Vehicles at Time of Initial Contact

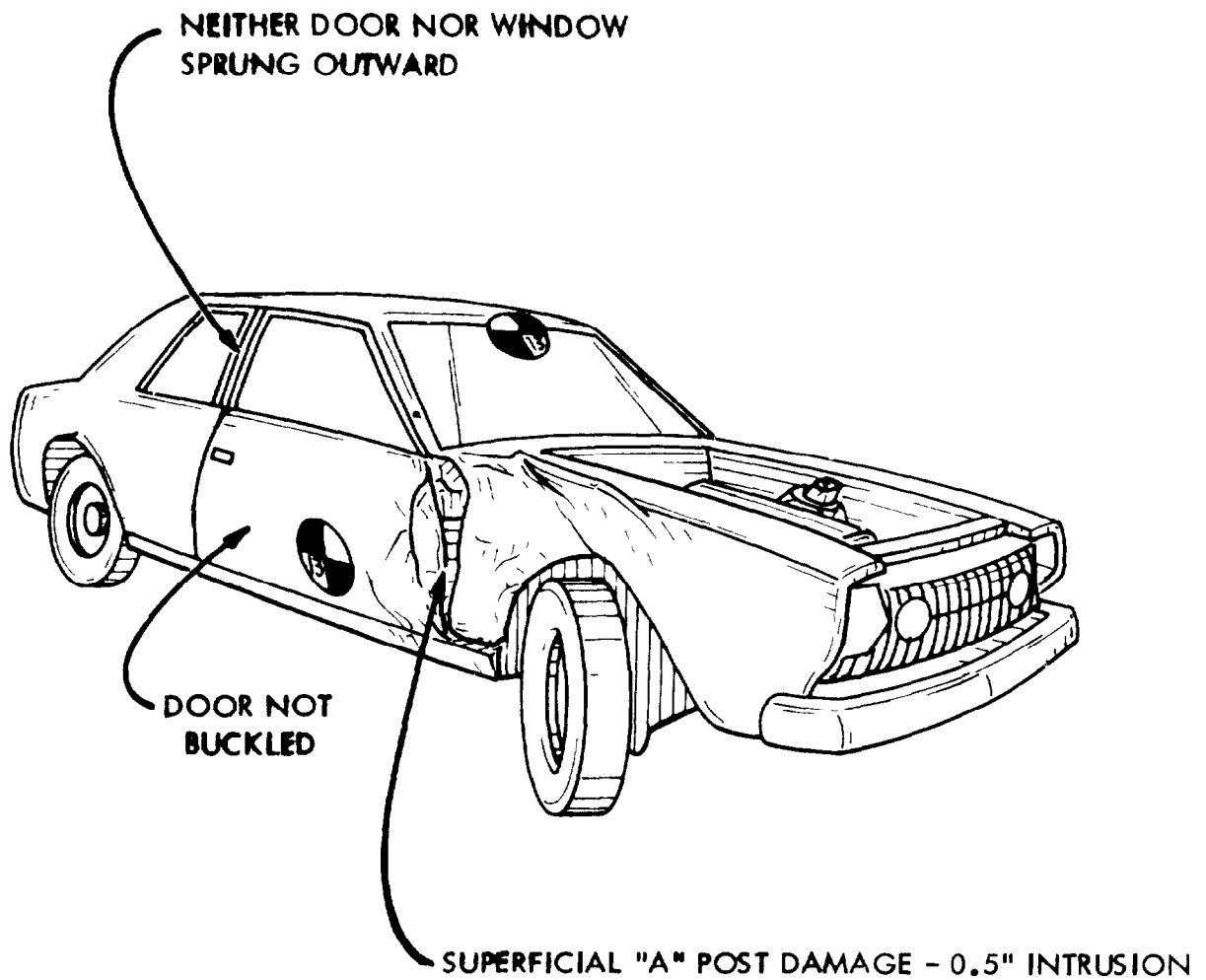


Figure 6-32. Test No. 11. Post Crash Condition of Vehicle No. 13 - Side Modified Hornet, After 24.33 mph 60° Impact by a Front-Modified Horn t

The lateral crash pulse for the impacted vehicle remained below 4 g's during the first 70 msec of the impact as the fender was deformed by the impacting bumper. A 10 msec pulse with 7 g's peak amplitude occurred at 70 msec as the impacting bumper contacted the "A" post. Then the acceleration fluctuated between 0 and 4 g's as the end of the impacting bumper slid past the "A" post and was bent around its own sill. The crash pulse is shown in Figure 6-33.

No baseline test is directly comparable to System Test #11. System Test #13 (an unmodified Hornet impacted by a modified Hornet) may be used for comparison. Intrusion in the unmodified vehicle in Test #13 was 5.1 inches, compared to 0.5 inches in the modified vehicle in Test #11.

The crash pulse and intrusion in Test #11 were well within the design criteria limits. The consequences of the crash can only be described as minor.

Results of the test are summarized in Table 6-12.

Table 6-12

	System Test 11
Maximum crush	7"
Maximum intrusion	.5"
Maximum acceleration	21 g

System Test No. 12 - 25.45 mph Front/Side 90°, Impacting Vehicle #8
 Front Modified Hornet, Impacted Vehicle #15
 Unmodified Hornet

The modified impacting vehicle severely compromised the door and quarter panel of the unmodified vehicle. Both vehicles jackknifed upward slightly at the point of impact. The impacting vehicle pushed the door past the rocker panel into the passenger compartment. Deformation of the impacting vehicle was limited to the bumper and the bumper energy absorbing units.

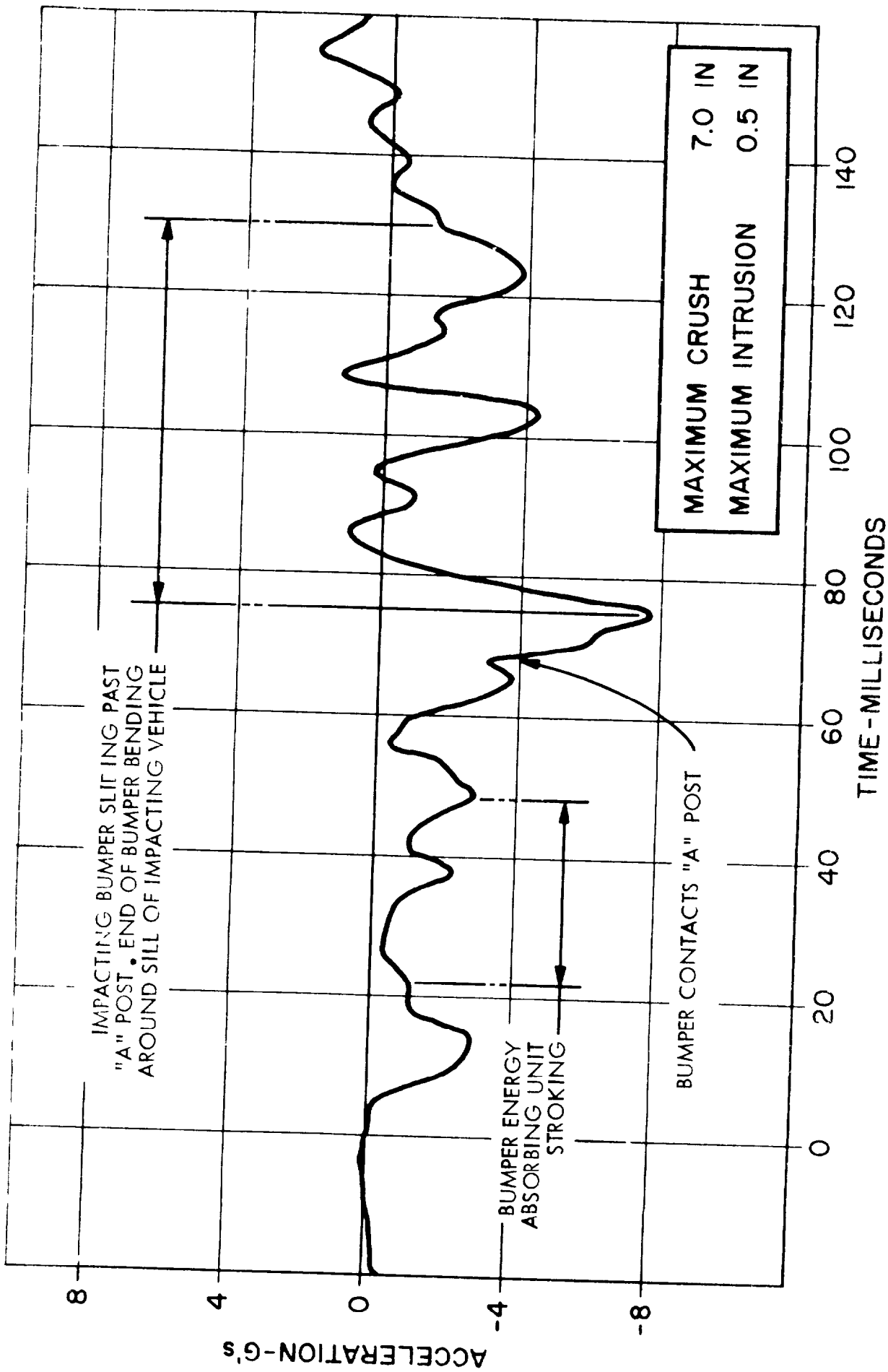


Figure 6-32 Test No. 11 24 33 mph Vehicle-to-Vehicle Front/Side 60° Impacting Vehicle No. 9
 Front Modified, on new Impact Vehicle No. 13 (Side Modified Hornet)
 LATERAL CRASH PULSE - VEHICLE NO. 13 (Modified)

... on the rocker panel resulting in 19.9 inch crush at the front. A maximum crush of 15.5 inches occurred in the front of the hood. Maximum intrusion was 7.8 inches at the center of the hood. Deformation of the "A" post caused the center of the dash panel to back down about 6 inches due to compressive loading.

The later load pulse for the impacted vehicle, shown in Figure 6-12, is a rectangular pulse of 60 msec. duration of 60 msec. Several peak accelerations of 14 g magnitude were recorded.

Results of System Test #12 are summarized in table 6-13.

Table 6-13

	System Test 12
Maximum	19.9"
Maximum intrusion	7.8"
Maximum acceleration	14g

... to the character vehicle in system test #12 resembles that of a modified Hornet. The modified Hornet does not appear to be more aggressive in a side impact than an unmodified Hornet. In fact, the maximum intrusion of test #12 was 7.8 inches compared to 9.5 inches in the modified Hornet.

... system test #12 may be compared with Baseline Test #4 (two unmodified Hornets) and Test #5 (two modified Hornets) with System Test #11 (two modified Hornets) and Test #12 (two modified Hornets).

... primarily due to the aggressivity of the modified Hornet. However, a comparison of the post strength of the modified Hornet with that of a modified vehicle...

... for all side impacts of two Hornets (Baseline Test #4) and Test #5) and Test #11 in a side impact magnitude.

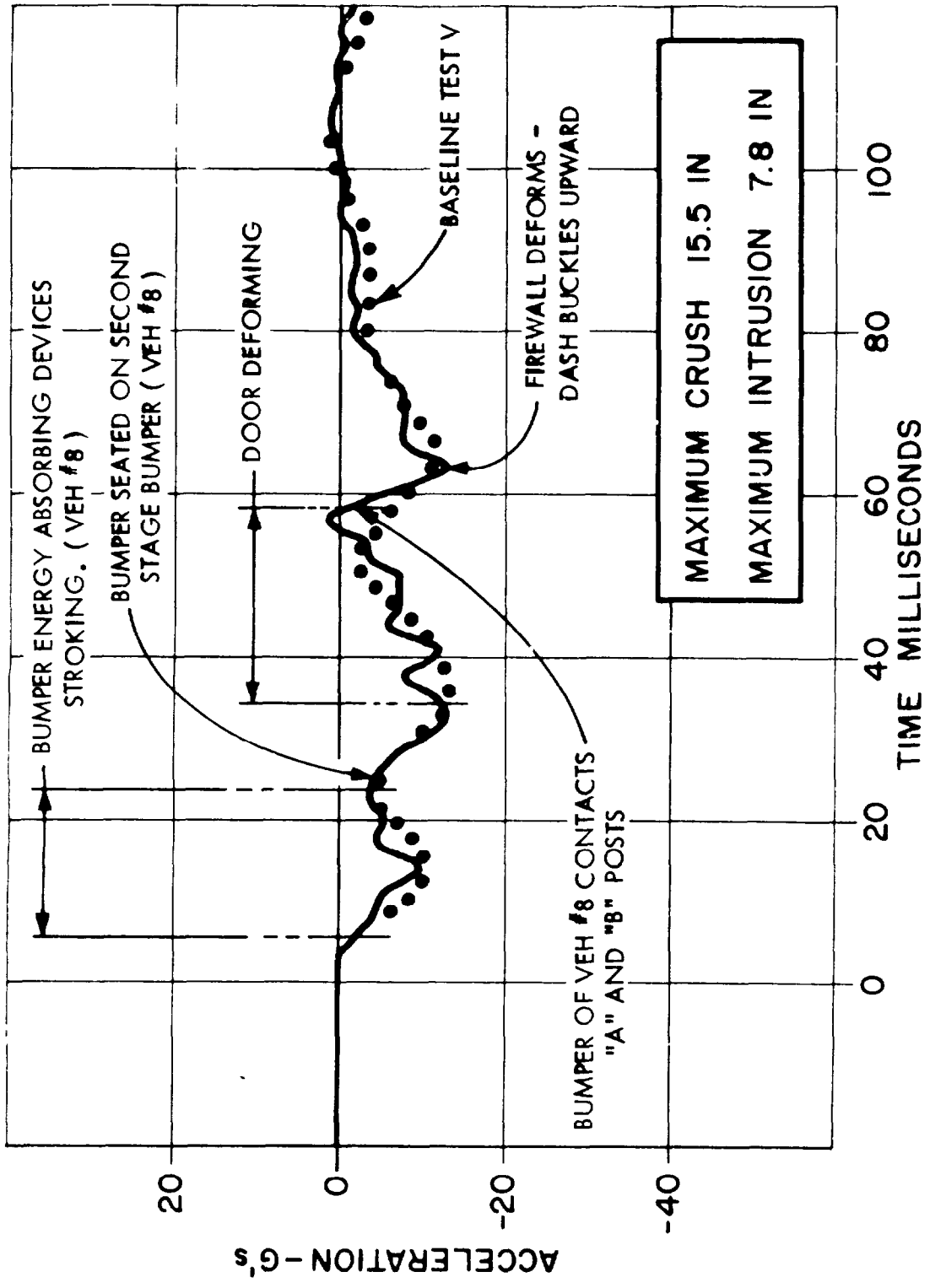


Figure 6-34. Test No. 12. 25.45 mph V hicle-to-V hicle Front/Sid 90°
 Impacting V hicle No. 8 (Front Modified Horn t)
 Impacted V hicle No. 15 (Unmodified Hornet)
 LATERAL CRASH PULSE - VEHICLE NO. 15 (Unmodified)

the door fell well within the design criteria limit of 20 inches maximum amplitude. The crash pulse resulted in a lower acceleration (System Test #14) had a more rapid rise time and higher amplitude but was still within the design criteria limit.

Significant improvement is apparent when comparing the side impact strength of a modified vehicle with that of an unmodified vehicle. The "B" post in the unmodified vehicle (Test #12) was severed from the rocker panel, resulting in total starting intrusion in the quarter panel area. Damage in the modified vehicle (Test #10) was confined almost entirely to the door. Intrusion in the quarter panel area was greatly reduced. While the figures for maximum intrusion do not vary greatly (modified vehicle 7.1 inches, unmodified vehicle 7.8 inches), intrusion in the unmodified vehicle was much more widespread. Maximum intrusion in the modified vehicle was confined to an area at the mid point of the door.

In summary, aggressivity of a modified vehicle in a side impact is no greater than that of an unmodified vehicle. In fact, the modified vehicle is slightly less aggressive. The impact strength of a modified vehicle is substantially improved over that of an unmodified vehicle.

System Test No. 12 - 24.95 mph vehicle-to-vehicle, front/side 90°
Impact Point above centerline, impacting vehicle #9
by Modified Hornet Impact to Vehicle #1
Unmodified Hornet

This test is comparable to Test #11 in which the impacted vehicle was a side-impact fault. Again, the front modified impacting vehicle received only superficial damage to the bumper and the front fender, similar to the impacted vehicle was more damaged than that of a 70 mph Test #11. Intrusion at the "A" bolt to the unmodified vehicle was 5.2 inches, in contrast to the 0.5 inch intrusion that occurred to the modified vehicle in Test #11. The lower portion of the door was buckled in a pleated fashion and the window frame was sprung outward several inches to the roof of the door. The door was damaged and could not be opened without substantial force. The post-crash condition of the vehicle is shown in Figure # 5.

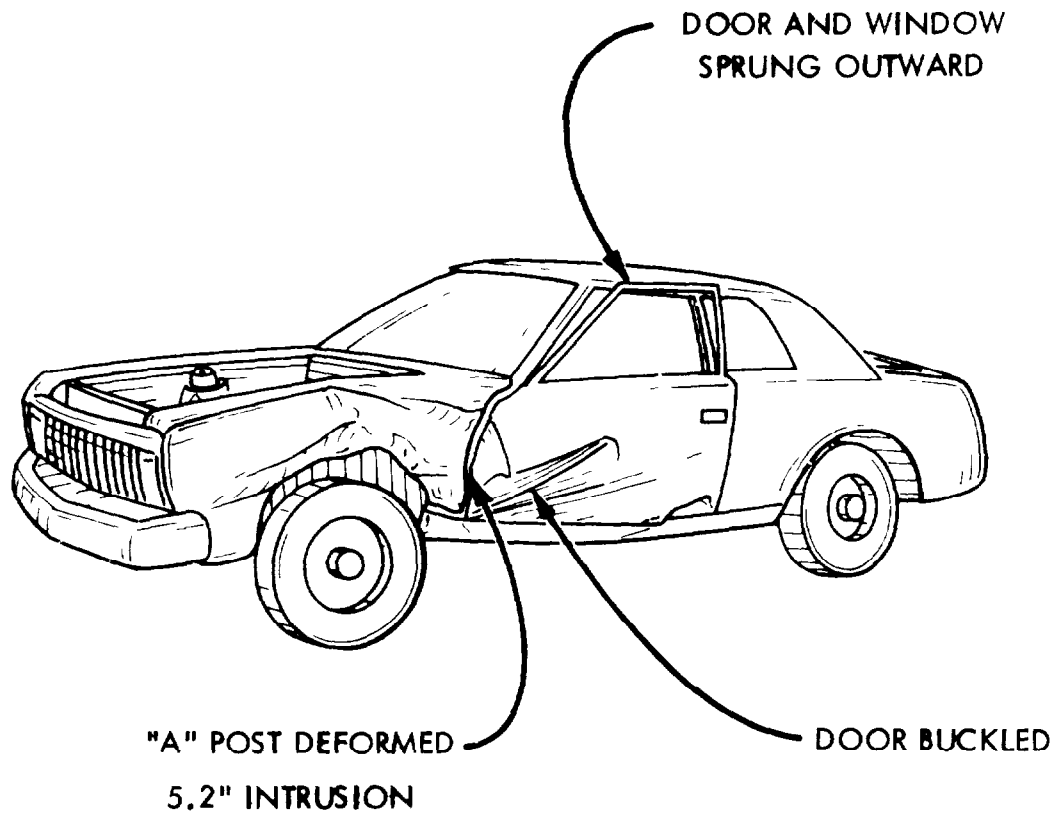


Figure 6-35. Test No. 13. Post Crash Condition of Vehicle No. 16 Unmodified Hornet
After 24.95 MPH 300° Impact by a Front-Modified Hornet.

During the first 80 msec after initial contact, the crash pulse for the impacted vehicle remained near zero amplitude. During this period, the impacting vehicle was deforming lightweight fender components. The impacting bumper contacted the "A" post 80 msec after impact, causing the average acceleration to increase to 6 g's for 20 msec. This was followed by 20 msec at near zero acceleration and then another period of acceleration at 4 g's and below. The crash pulse is shown in Figure 6-36.

No baseline test is directly comparable to System Test #13. System Test #11 may be used for reference. The crash pulse does not differ materially from that recorded for the modified vehicle in Test #11. The primary difference is a 4.7 inch reduction in intrusion for the modified vehicle.

A summary of results of System Test #13 is given in Table 6-14.

Table 6-14

	System Test 13
Maximum crush	12.6"
Maximum intrusion	5.2"
Maximum acceleration	11 g

System Test No. 14 - 24.08 mph, Vehicle-to-Vehicle, Front/Side 270°
 Impact Location Door Centerline, Impacting Vehicle
 #18 Standard 4170 lb Vehicle (Ford), Impacted
 Vehicle #12 Side Modified Hornet

The impacting 4170 lb vehicle was essentially undamaged. The side of the impacted vehicle was displaced inward from the rear quarter panel to the "A" post. Maximum static intrusion into the passenger compartment was 9.5 inches. The edge of the roof was deformed inward 2.1 inches. The rocker panel and the floor pan were deformed inward a maximum of 7.3 inches. The lower portion of the "A" post was deformed inward 3.4 inches. The sharp protruding fenders of the impacting vehicle caused two distinct indentations in the side of the impacted vehicle. One indentation was

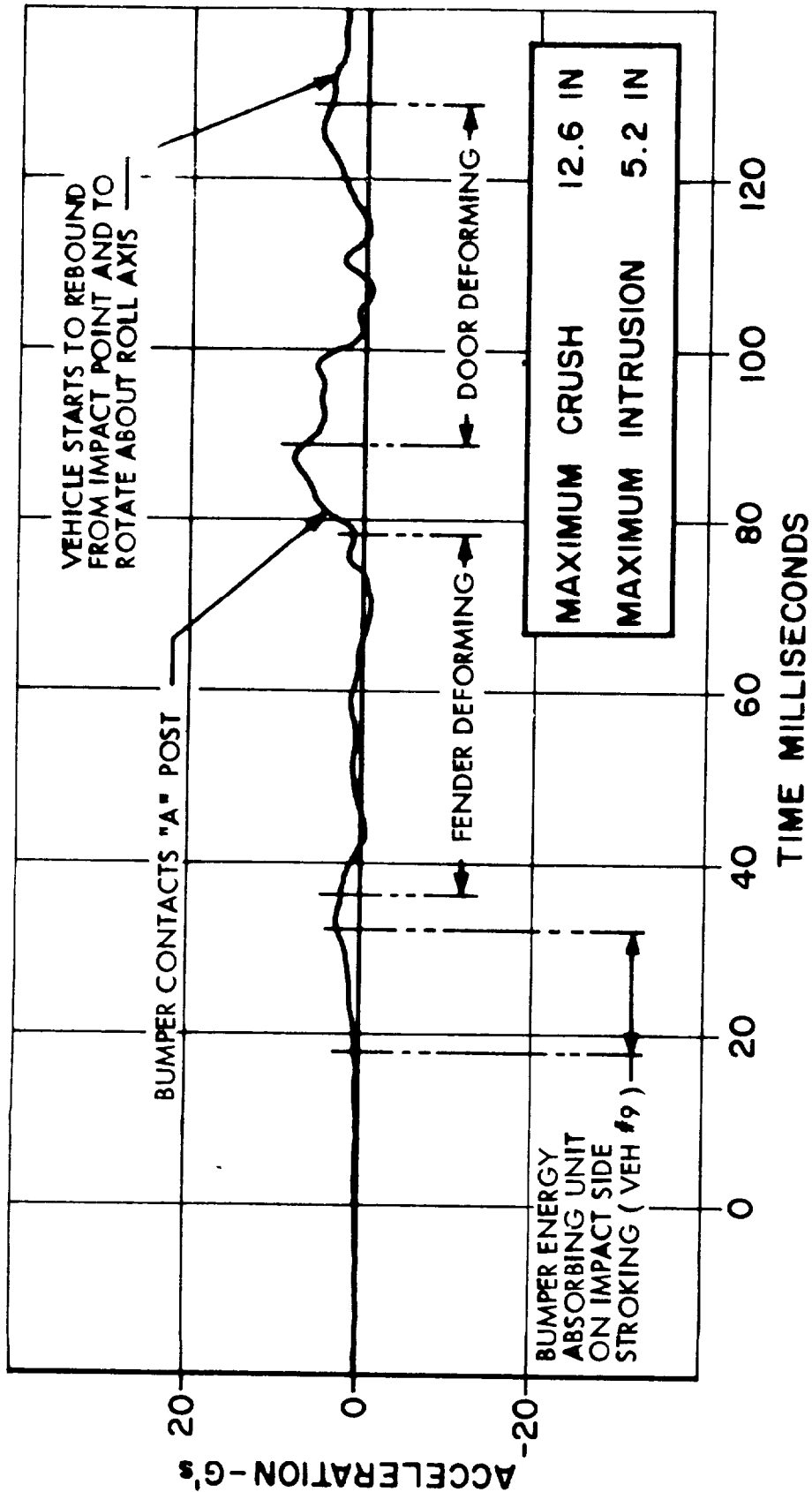


Figure 6-36. Test No. 13. 24.95 mph Vehicle-to-Vehicle Front/Side 300° Impacting Vehicle No. 9 (Front Modified Hornet)
 Impacted Vehicle No. 16 (Unmodified Hornet)
 LATERAL CRASH PULSE - VEHICLE NO. 16 (Unmodified)

located in the front fender of the impacted vehicle and was of little consequence. The other occurred in the center of the quarter panel and contributed to intrusion of the passenger compartment. The structural integrity of the side modified vehicle was maintained throughout the crash. The "A" post, door beam and "B" post performed well. The rocker panel and floor structure reinforcements were effective in limiting the deformation of the rocker panel and floor pan. The post-crash condition of the vehicles is shown in Figure 6-37 and the crash pulse is shown in Figure 6-38.

System Test #14 demonstrated the ability of the modified Hornet to resist side impacts by larger vehicles. No baseline test is directly comparable to System Test #14. Baseline Test V, System Tests #10 and #12 may be used for comparison.

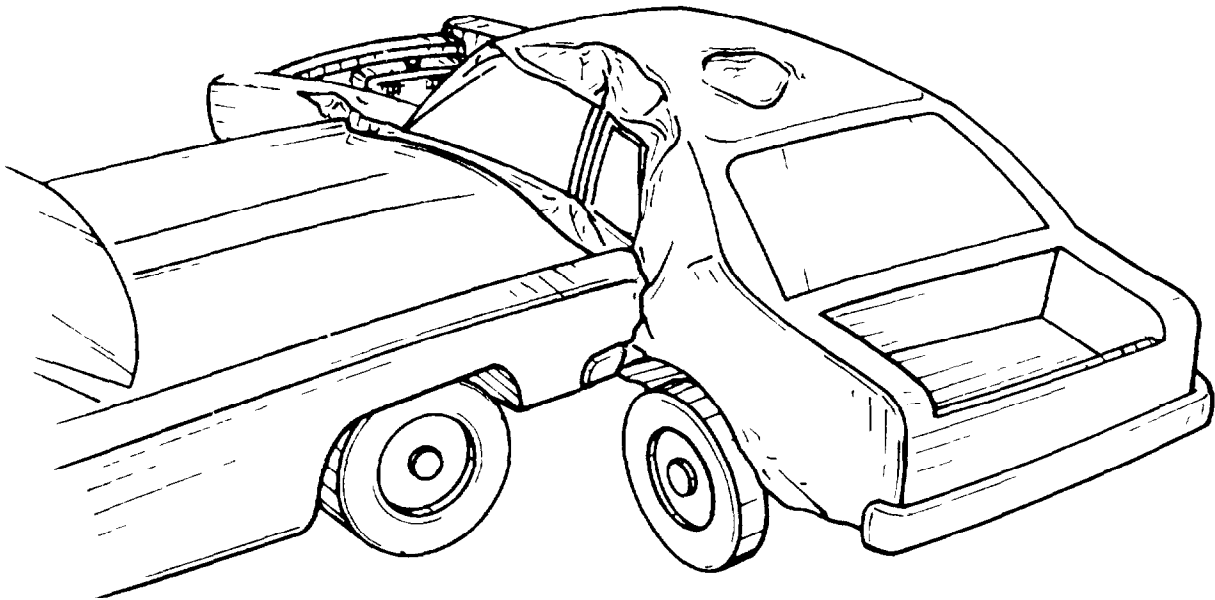
The maximum intrusion of 9.5 inches is the same as that received by an unmodified Hornet when it was impacted by another unmodified Hornet (Baseline Test V). No failure occurred in any of the side structural components. The "A" and "B" posts remained attached to the rocker panel and the door was not pushed past the rocker panel. The door beam continued to resist the impact loads throughout the crash.

A summary of results of System Test #14 is given in Table 6-15.

Table 6-15

	System Test 14
Maximum crush	11"
Maximum intrusion	9.5"
Maximum acceleration	22 g

VEHICLE NO. 12 SIDE MODIFIED HORNET



VEHICLE NO. 18 UNMODIFIED 4170 LB
FORD CUSTOM IMPACTING WITH 24.08 MPH
INITIAL VELOCITY

Figure 6-37. Test No. 14. 24.08 mph Side Impact of Side-Modified Hornet by 4170 lb Ford Custom. Condition of Vehicles 67 msec after Initial Contact Showing Maximum Dynamic Deformation of Hornet

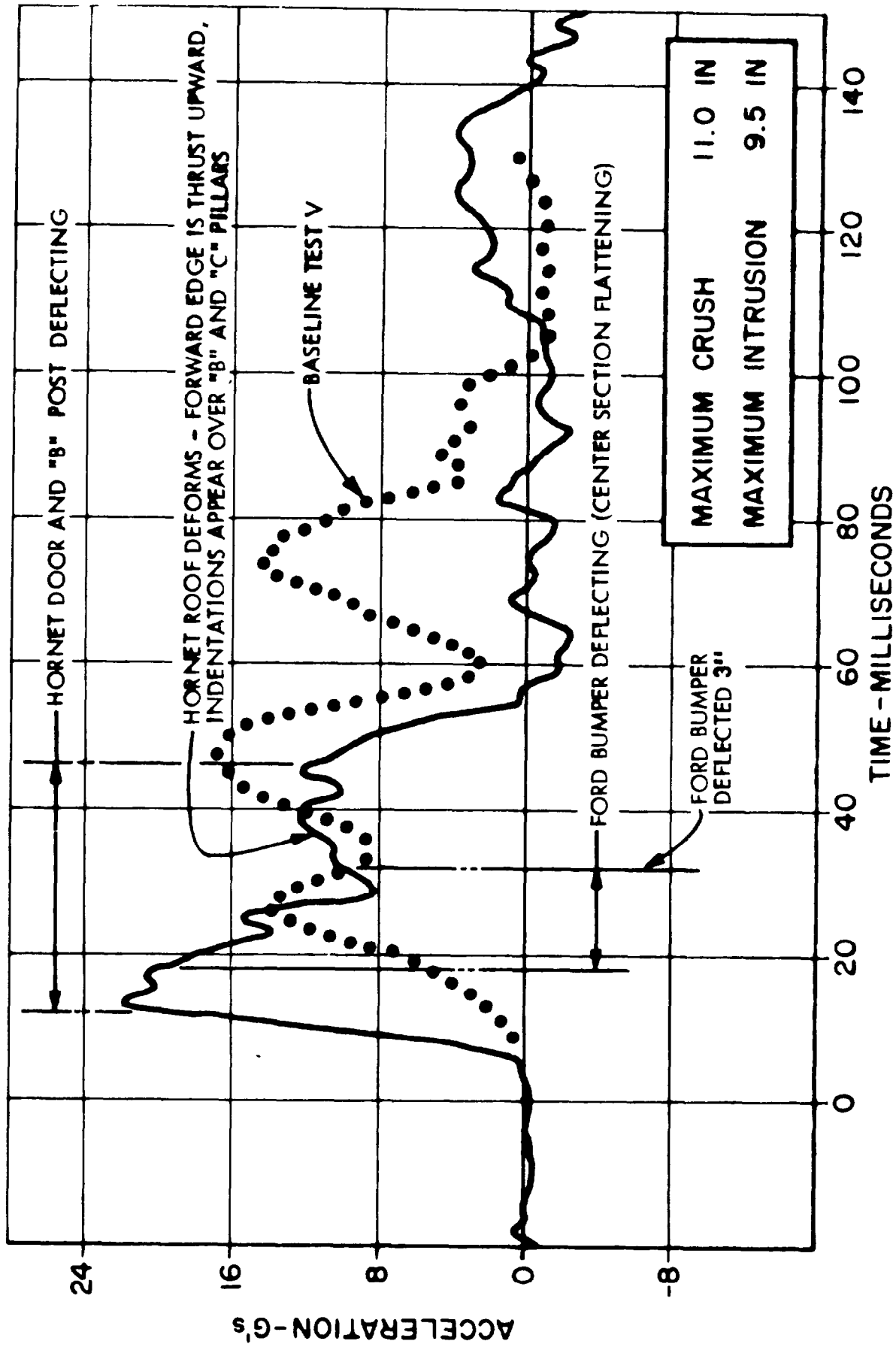


Figure 6-38. Test No. 14. 24.08 mph Vehicle-to-Vehicle Front/Side 270° Impact at Door Centerline. Impacting Vehicle No. 18 Unmodified 4170lb Ford Custom. Impacted Vehicle No. 12 - Side Modified Hornet LATERAL CRASH PULSE VEHICLE NO. 12 (Modified)

System Test No. 15 - 20.62 mph, Side Pole Impact 270^o, Impact Point
5 inches Forward of Door Centerline, Impacting
Vehicle #4 Integrated Vehicle (Front and Side
Modified)

Vehicle #4 was used previously in an offset frontal impact. The left side of the vehicle was left relatively undamaged allowing the vehicle to be re-used in Test #15.

The pole caused 14.5 inches static deformation of the rocker panel and 14.0 inches static deformation of the upper "A" pillar. Maximum static intrusion of the door was 14.2 inches and occurred slightly forward of the steering wheel. The door hinges and latch remained intact. The door beam remained attached at both ends. The inner door panel pushed the steering wheel to the right during the impact. The "A" post was displaced slightly inward accompanied by distortion of the firewall and the floor pan. The "B" post was displaced inward a maximum of 4.2 inches at the rocker panel. The floor pan accommodated the intrusion of the pole by localized crushing and by compression of flexible features such as the driveshaft tunnel. The upper "A" pillar was deformed by the pole and the windshield was crushed locally. The forward edge of the roof was displaced to the right by the pole. The quarter panel was undisturbed and the quarter window was not broken. The post-crash condition of the vehicle is shown in Figure 6-39.

The lateral crash pulse for Test #15 had a moderate 9 to 10 g average magnitude and a long duration of approximately 120 msec, as shown in Figure 6-40. A 26 g spike recorded 30 msec after initial contact was of too brief duration to have practical significance. The moderate crash pulse was obtained at the expense of significant intrusion at the driver's position. The crash pulse on the non-impacted (right hand) side of the vehicle was further moderated by compression in the driveshaft tunnel region of the floor pan assembly.

No baseline test is directly comparable to System Test #15. Baseline Test III and System Test #4 may be used for reference.

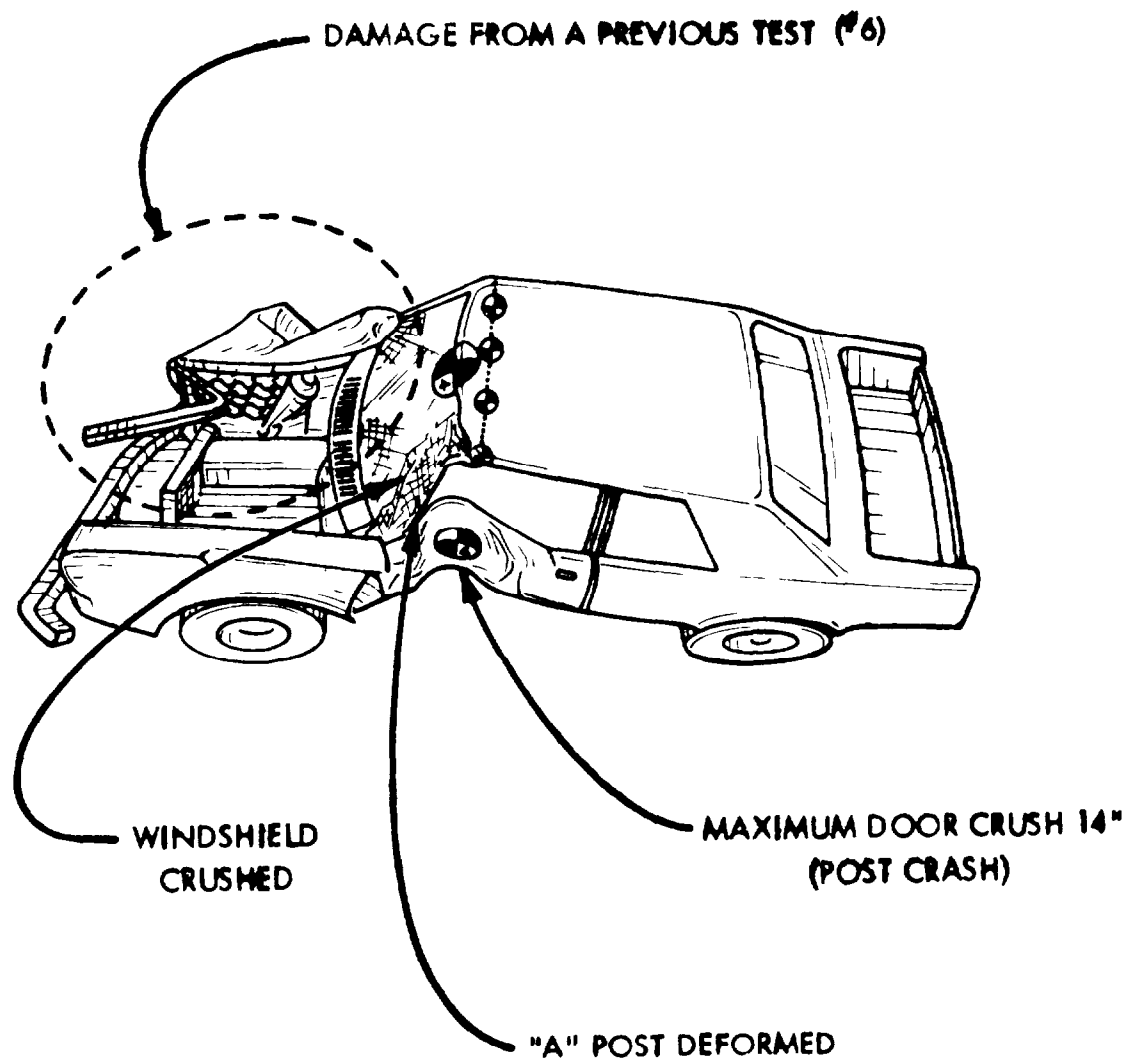
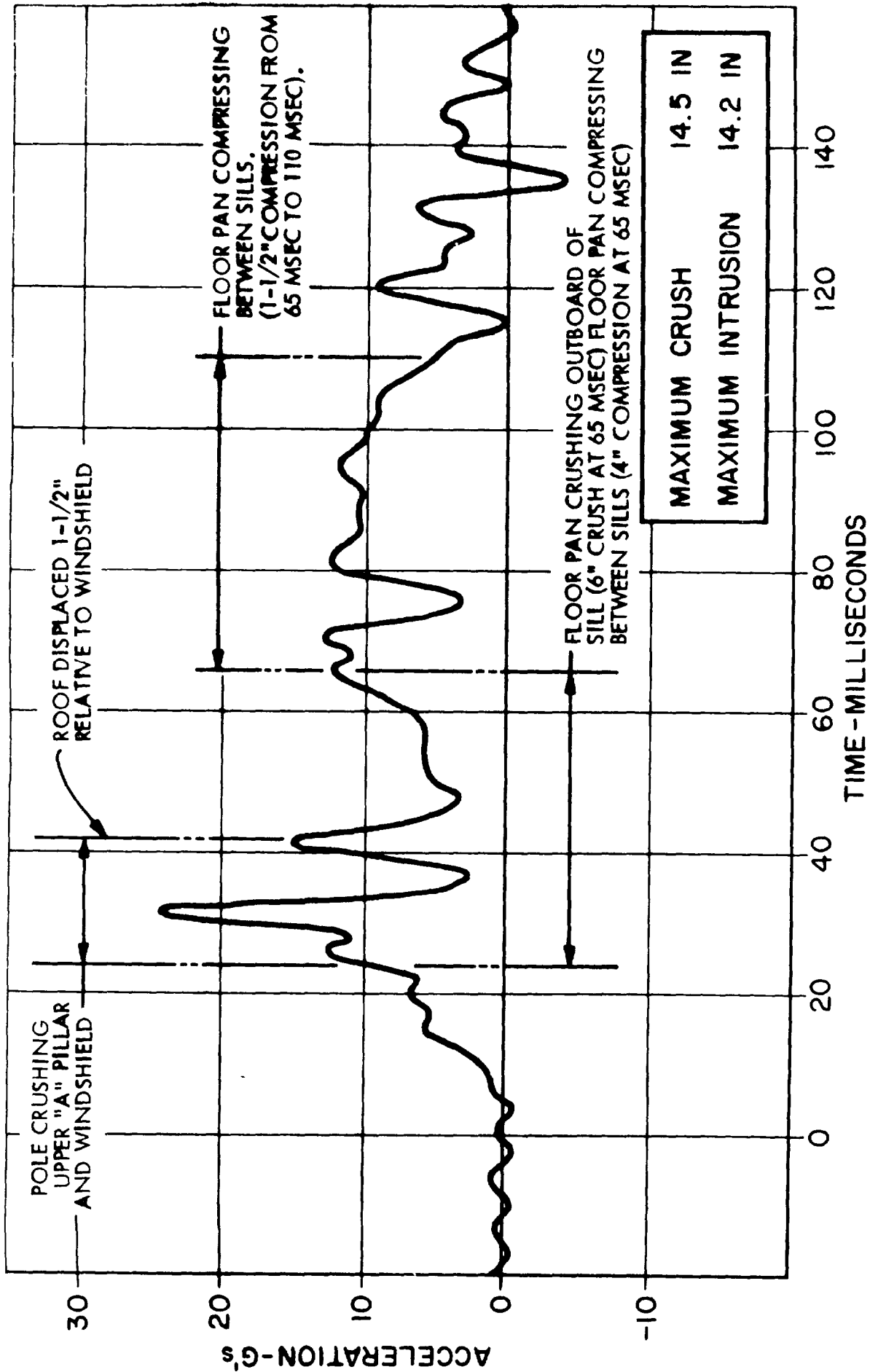


Figure 6-39. Test No. 15. Damage Resulting From 20.62 mph 90° Side Pole Impact.
Vehicle No. 4 Front and Side Modified Homet.
(Vehicle was Used Previously In Test No. 6).



Figur 6-40. Test No. 15. 20.62 mph 90° Side Pol Impact. Impact Pint 5 Inches Forward of Door Centerline
LATERAL CRASH PULSE - VEHICLE NO. 4 (Modified)

A summary of results of System Test #15 is given in Table 6-16.

Table 6-16

	System Test 15
Maximum crush	14"
Maximum intrusion near instrument panel	14.2"
Maximum occupant area intrusion	13.5"
Maximum acceleration	24 g

System Test #15 was run at twice the velocity of the previous pole impacts, and the impact was located 5 inches farther forward. The 20 mph side pole impact was not included in the design conditions for the modified vehicle.

System Test #15 demonstrated the basic structural integrity of the modified vehicle. Although large intrusion occurred, no major component failed. In particular, the door beam functioned throughout the test.

SECTION 7 EVALUATION OF SYSTEM PERFORMANCE

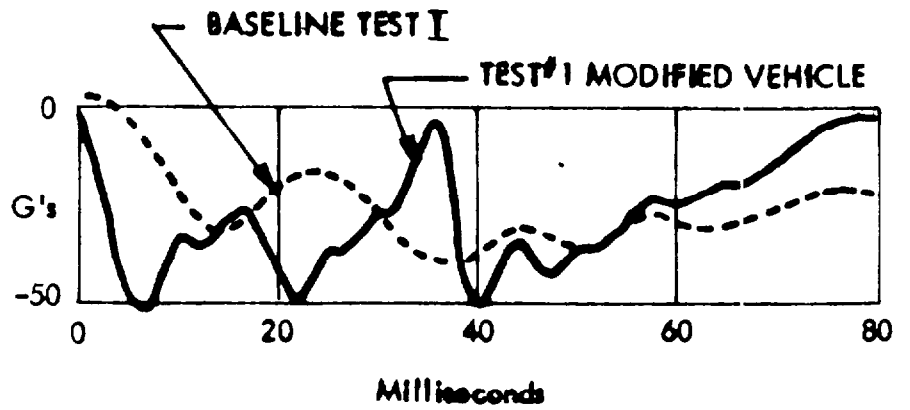
The objective of the Compact Car Crashworthiness program was to develop reliable techniques for the improvement in crashworthiness behavior of production vehicles without making the vehicle unduly aggressive when involved in impacts with other vehicles. This section describes the behavior of the various components and systems as they relate to vehicle crashworthiness and aggressivity. The basis of this evaluation is taken to be the magnitude and shape of the acceleration-time curves and the measurements of intrusion in the region of occupancy of the passenger compartment.

FRONT END SYSTEM CRASHWORTHINESS

The modified vehicles exhibited improvements in crashworthiness compared to unmodified vehicles. Intrusion was reduced in all cases. The onset of the crash pulse was faster and the acceleration was generally shifted to earlier regions of the crash. This may be observed in the crash pulses reproduced in Figure 7-1A, B, C and D. In the head-on crash with a 4170 lb vehicle (Figure 7-1F), the modified vehicle developed a reasonably "square" crash pulse and an acceptable 1.8 inches maximum intrusion. The modified vehicle in the offset head-on impact (Figure 7-1G) received a moderate crash pulse and an acceptable maximum intrusion of 1.2 inches.

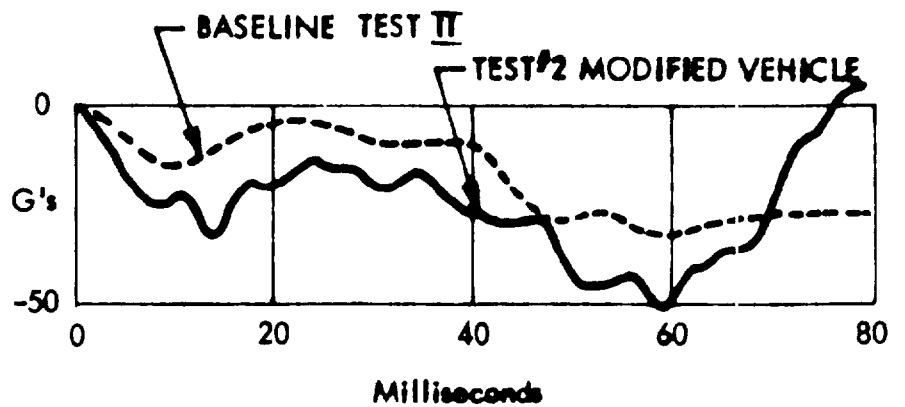
The modified vehicles exhibited favorable crash pulses and acceptable intrusion in the oblique tests. Since the baseline tests did not include an oblique impact, Figure 7-2 includes the head-on impact crash pulse for comparison with the 30° flat barrier crash pulse. Very moderate crash pulses resulted from the corner oblique impacts by modified vehicles. There is little difference in the crash pulse that resulted when a modified vehicle was impacted and that which resulted when an unmodified vehicle was impacted. The modified vehicle showed a substantial reduction in intrusion, however.

TEST	CRUSH INCHES	INTRUSION INCHES
I	33.0	10.8
1	27.7	7.0
NET CHANGE:	-5.3	-3.8



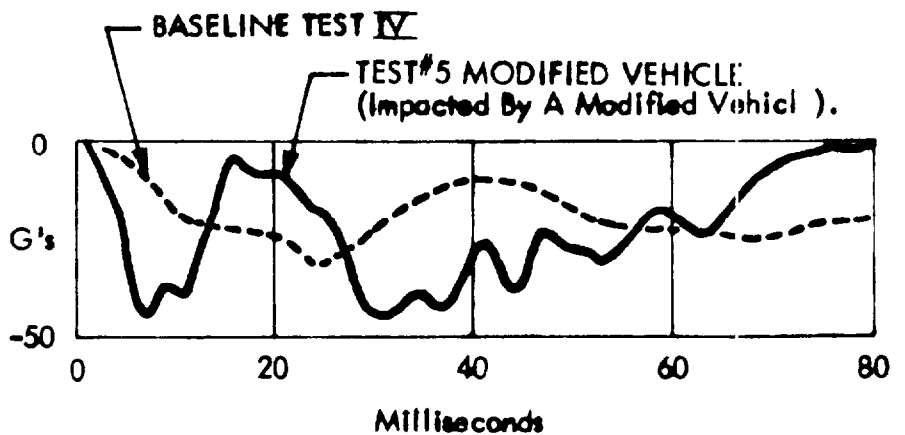
(A) Flat Barrier

II	39.5	7.8
2	27.9	2.3
	<u>-11.6</u>	<u>-5.5</u>



(B) Frontal Pole

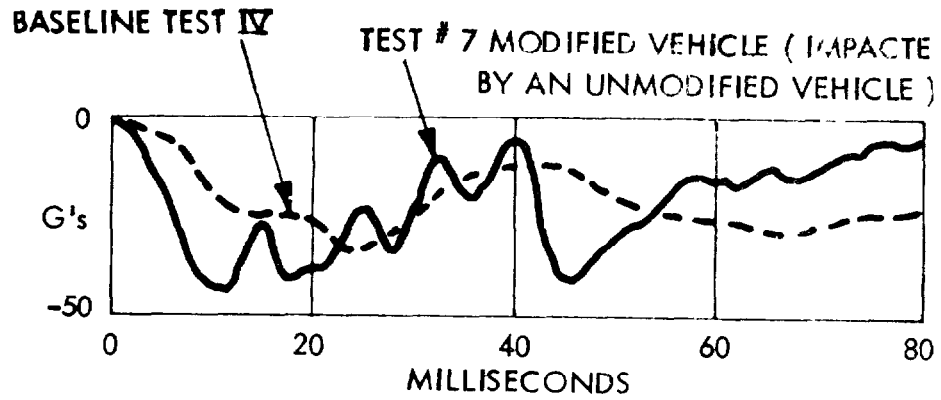
IV	25.0	5.0
5	25.7	2.3
	<u>+0.7</u>	<u>-2.7</u>



(C) Headon - 2 Vehicles

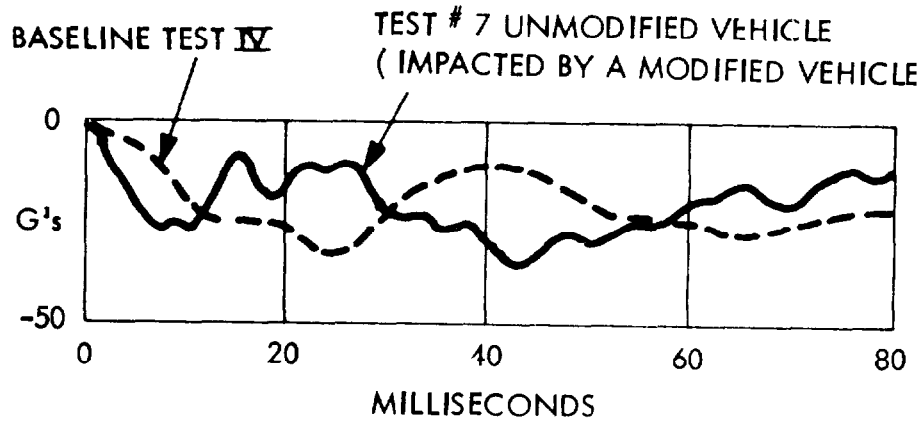
Figure 7-1. Comparison of Frontal Impacts

TEST	CRUSH INCHES	INTRUSION INCHES
IV	25.0	5.0
7-MODIFIED VEHICLE	14.4	1.5
NET CHANGE:	-10.6	-3.5



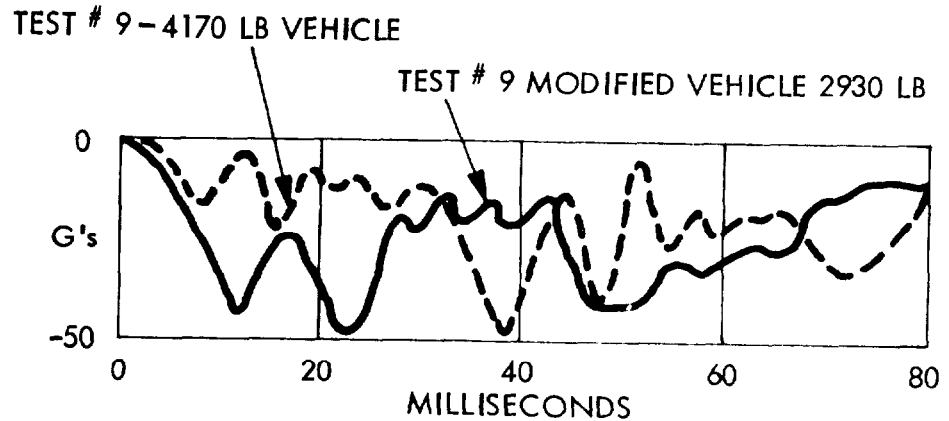
(D) HEADON - 2 VEHICLES - ALIGNED

IV	25.0	5.0
7-UNMODIFIED VEHICLE	26.3	4.5
	+1.3	-0.5



(E) HEADON - 2 VEHICLES - ALIGNED

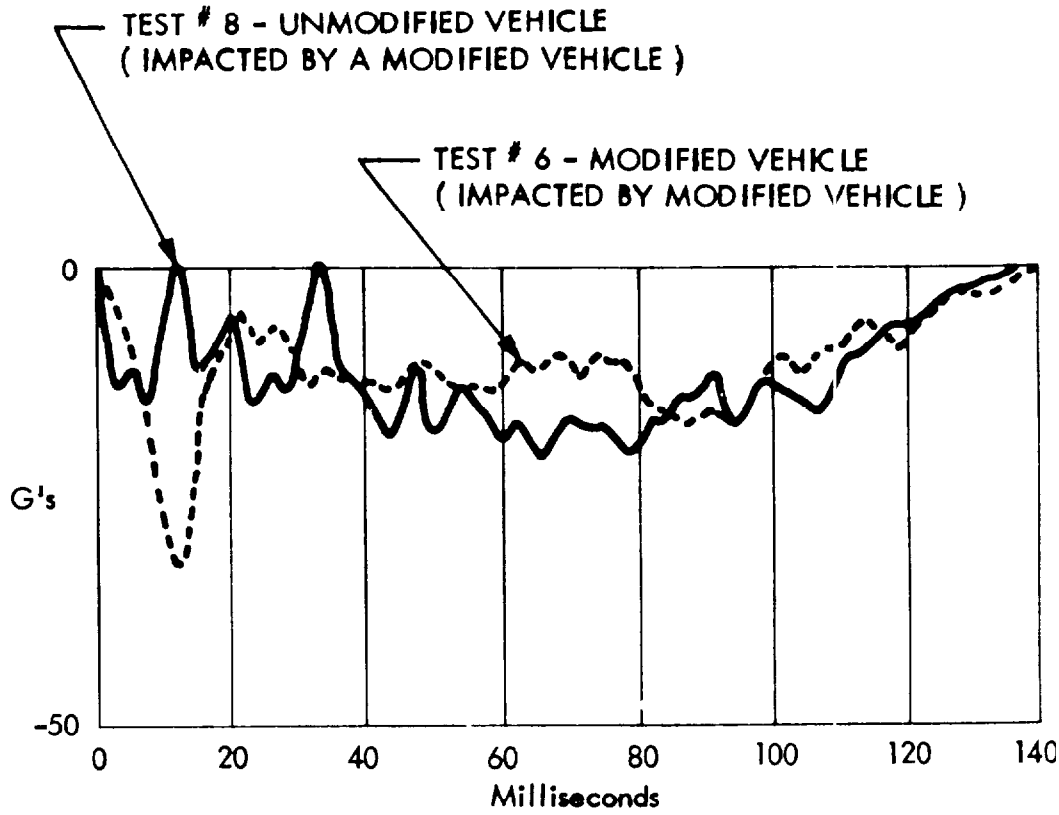
9-4170 LB UNMODIFIED	34.4	2.5
9-MODIFIED	22.3	1.8



(F) HEADON - 2 VEHICLES - ALIGNED

Figure 7-1 Continued. Comparison of Frontal Impacts

UNMODIFIED VEHICLE		
TEST	CRUSH INCHES	INTRUSION INCHES
6	34.8	5.5
8	56.0	6.0
NET CHANGE: -21.2		+0.5

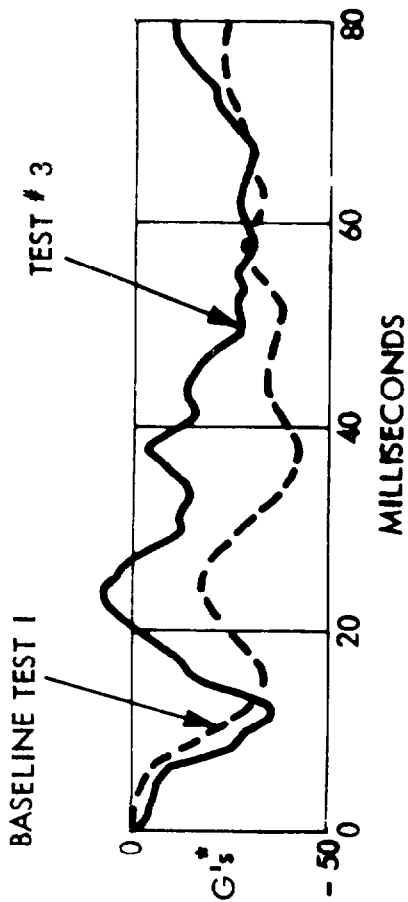


(G) HEADON - 2 VEHICLES - OFFSET 1/2 VEHICLE WIDTH

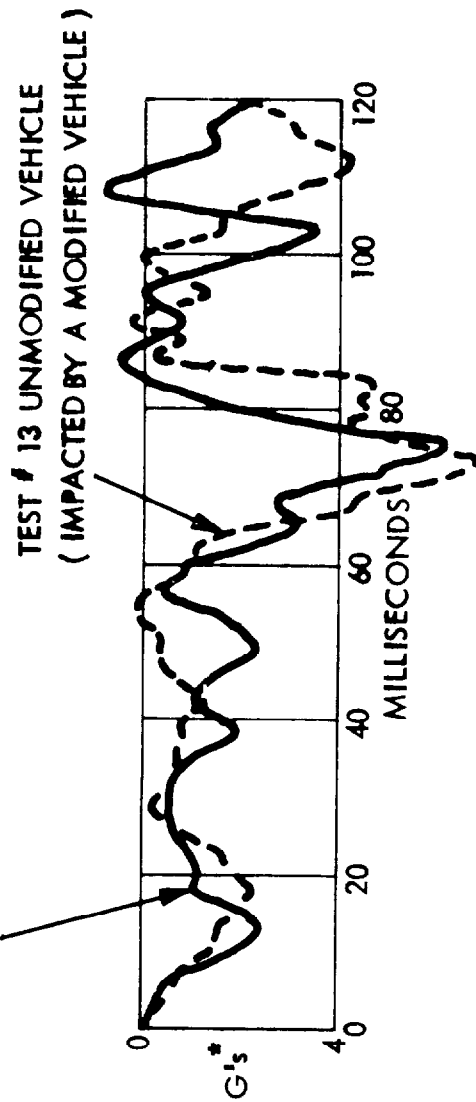
Figure 7-1 Continued . Comparison of Frontal Impacts

TEST	CRUSH INCHES	INTRUSION INCHES
I	33.0	10.8
3	30.0	6.7
NET CHANGE:	- 3.0	- 4.1

(A) 30° FLAT BARRIER



TEST # 11 MODIFIED VEHICLE (IMPACTED BY A MODIFIED VEHICLE)



(B) FRONT CORNER IMPACT BY ANOTHER VEHICLE

13	12.6	5.2
11	7.0	0.5
	- 5.6	- 4.7

* LATERAL ACCELERATION

Figure 7-2. Comparison of Obliqu Impacts

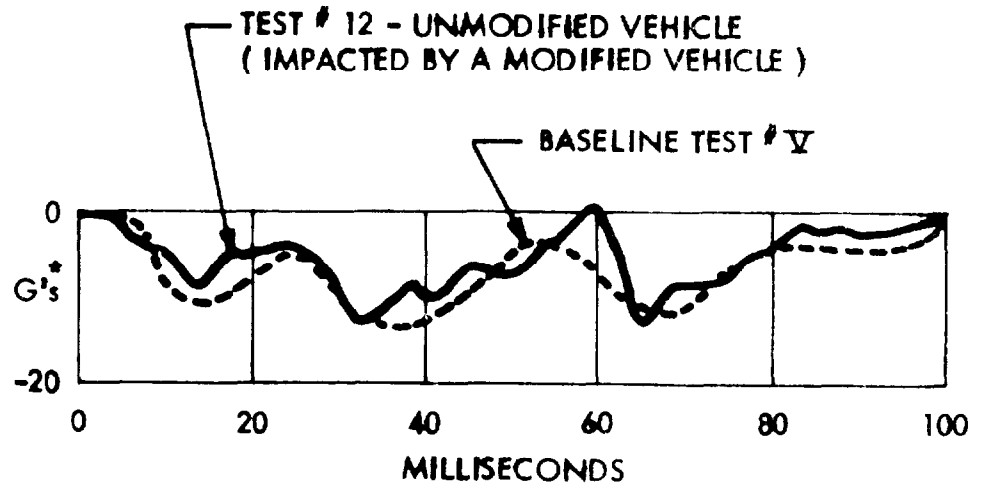
FRONT END SYSTEM AGGRESSIVITY

The modified vehicle is more aggressive than the unmodified vehicle. The modified vehicle in Figure 7-1D fared considerably better than the unmodified vehicle in Figure 7-1E. Yet the crash pulse and intrusion of the unmodified vehicle are equivalent to those of the baseline vehicles in Test IV. The design of the front end structure in the modified vehicle enabled both vehicles to develop crash pulses with fast rise times. As a result, the total crush (sum of both vehicles) was reduced 9.3 inches over that measured in the baseline test. The sum of the intrusion in both vehicles was reduced 4.0 inches over that measured in Baseline Test IV.

The modified vehicle proved somewhat aggressive in the head-on crash with a vehicle that was 42% heavier (4170 lbs). The heavier vehicle suffered slightly greater intrusion than the modified vehicle. The major peaks in the crash pulse for the heavier vehicle occurred quite late in the impact. Due to the greater bulk and weight of the heavier vehicle, neither the crash pulse nor the intrusion was unduly severe. In the offset frontal collisions, Figure 7-1G, the modified vehicle behaved aggressively toward the unmodified vehicle. Using the impact between two modified vehicles (test #6) as a baseline, the front end crush of the unmodified vehicle was 21.2 inches greater than that observed in the "baseline" test. Intrusion was 1.2 inches greater, bringing it to the barely acceptable level of 6.0 inches. The crash pulses are similar except for a single peak that removed energy early in the crash of the two modified vehicles.

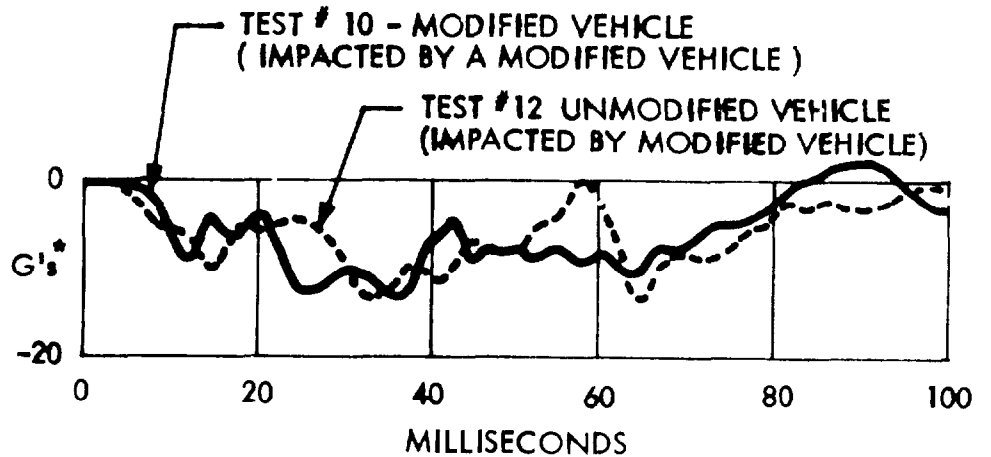
In the side impact tests, the aggressivity of the modified vehicle compares favorably with that of the unmodified vehicle (Figure 7-3A). The crash pulses are nearly identical. There is a slight increase in crush and decrease in intrusion in the impact involving the modified vehicle. A definite improvement in aggressivity appears when both vehicles are modified (Figure 7-3B). Again, there is no major difference in the crash pulses. Maximum crush was decreased 6.5 inches and maximum intrusion was

TEST	CRUSH INCHES	INTRUSION INCHES
∇	13.5	9.5
12	15.5	7.8
NET CHANGE:	+2.0	-1.7



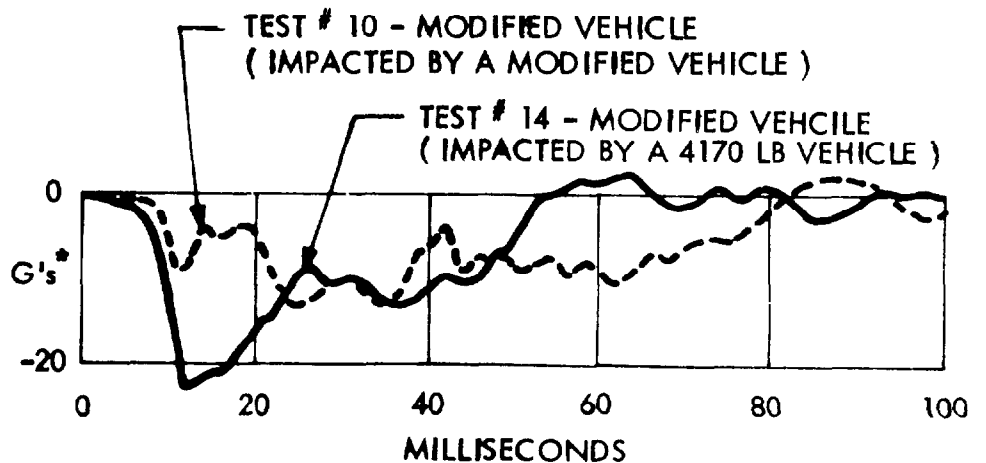
(A) SIDE IMPACT BY ANOTHER VEHICLE

12	15.5	7.8
10	9.0	7.1
	-6.5	-0.7



(B) SIDE IMPACT BY ANOTHER VEHICLE

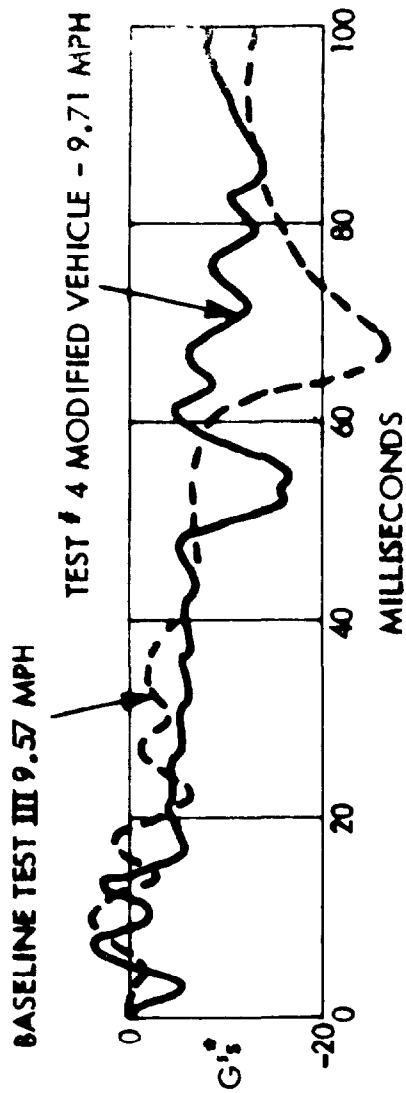
10	9.0	7.1
14	11.0	9.5
	+2.0	+2.4



(C) SIDE IMPACT BY ANOTHER VEHICLE

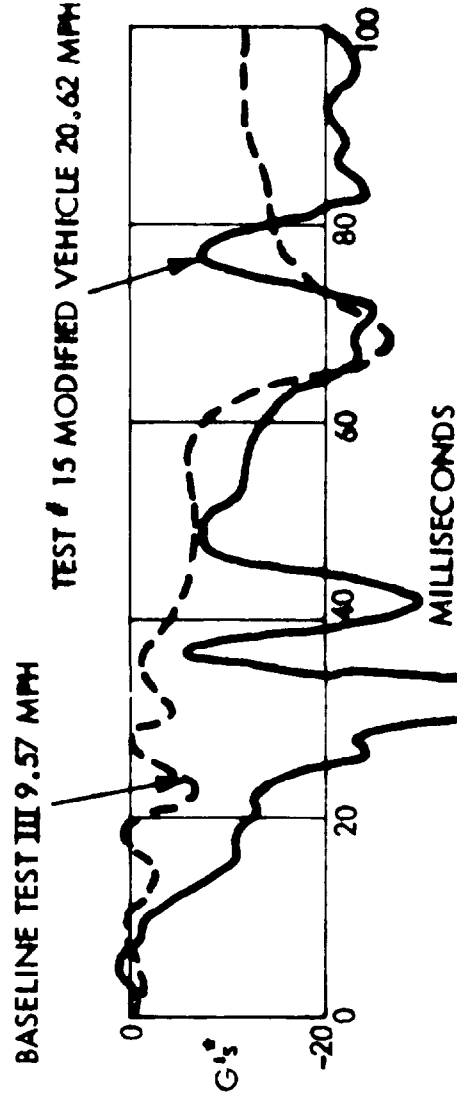
* LATERAL ACCELERATION

Figure 7-3. Comparison of Side Impacts



TEST	CRUSH INCHES	INTRUSION INCHES
III	10.0	6.0
4	7.0	3.5
NET CHANGE:	-3.0	-2.5

(D) SIDE POLE



TEST	CRUSH INCHES	INTRUSION INCHES
III	10.0	6.0
15	14.5	14.2
NET CHANGE:	+4.5	+8.2

(E) SIDE POLE

• LATERAL ACCELERATION

Figure 7-3 Continued. Comparison of Side Impacts

decreased 0.7 inches from those recorded in the crash of a modified vehicle and an unmodified vehicle. The net changes from baseline performance were a 4.5 inch decrease in crush and a 2.4 inch decrease in maximum intrusion.

FRONT END COMPONENTS

Energy Absorption Units. The energy absorption units support the bumper and protect the vehicle from damage in low velocity impacts - up to about 5 mph. In a high-speed impact, the hydraulic type units (Delco) furnished with the AMC Hornet vehicle burst and absorb little energy. One of the modifications performed in this program was to rework the standard energy absorption units to provide high-speed energy absorption capability. This was done by drilling a relief orifice through the piston to reduce pressure buildup in a high-speed impact. Of course, this eliminated the low-speed capability. Production units will require a relief valve or burst disc to close the orifice except when overpressure occurs in a high-speed impact.

The modified energy absorption units performed satisfactorily. None of the units burst. Correlation of the film records with accelerometer traces indicates that the modified energy absorption units are capable of providing useful energy absorption capacity.

Leading Edge Components. The second-stage bumper, ripple panel forward supports and the support brace form the leading edge of the energy management system (Figure 4-1). These components interact with an opposing vehicle or barrier, picking up concentrated loads and distributing them to energy absorbing components.

In most of the frontal impacts, major loads were received by the second-stage bumper and transmitted to the sills, causing the sills to crush. This was the primary load path in most of the frontal impacts. In asymmetrical impacts, the second-stage bumper and the support brace carried loads to the ripple panel on the non-impacted side of the vehicle. This was observed in the oblique barrier crash (test #3) and in the offset head-on crash (test #6).

In test #6, the support braces of both vehicles helped to capture the ripple panels on the impacted side allowing them to crush and absorb energy.

The ripple panel forward supports received minor loads in a number of tests and distributed them to the ripple panels. In test #5, the forward supports of vehicle #10 received a direct blow from the bumper and second-stage bumper of vehicle #11. The forward supports stabilized the front edges of the ripple panels allowing widespread crush to occur without buckling or collapse of the ripple panels.

Second-Stage Bumper. The second-stage bumper consists of a deep-section hollow beam. It is located behind the bumper and is attached to the ends of the sills. The primary purpose of the second-stage bumper is to prevent gross intrusion during a centered pole impact. The second-stage bumper was designed to transfer loads to the sills and to enable large amounts of sill crush to occur in flat barrier and vehicle-to-vehicle crashes as well as in pole impacts.

The second-stage bumper performed satisfactorily in the most severe case (test #2, centered pole impact). The deep-section tubular beam was deformed by the pole until it was almost flattened, yet it did not rupture. Although it was designed primarily as a load-carrying member, the second-stage bumper also served as an energy absorber in this and other tests. Often the trailing edge of the second-stage bumper was deformed by the engine, absorbing considerable energy.

The second-stage bumper was moderately aggressive in head-on impacts with unmodified vehicles (tests #7, #8, and #9). In lower-speed impacts, such as tests #10, #11, #12 and #13, aggressivity was less pronounced. The second-stage bumper and the sills supported the first-stage bumper, enabling it to distribute loads over a wide area of the impacted vehicle.

The design of the second-stage bumper is effective. No improvements appear to be needed.

Ripple Panels. The ripple panels performed very much as they were intended to perform. Large amounts of localized crush took place in many cases without buckling or gross failure of the ripple panels occurring. Examples of this may be seen in tests #1, #2, #5, #7 and #9. In the oblique flat barrier impact (test #3), a plastic hinge formed in the rear portion of the ripple panel on the impacted side of the vehicle, but did not compromise the overall strength of the panel. Forces transmitted to the non-impacted side of the vehicle in this test caused local deformation and crushing of the ripple panel.

The ripple panel upper support was partly responsible for the successful behavior of the ripple panels. It stiffens the upper edge of the ripple against buckling. The sill performs a similar function at the lower edge of the ripple panel.

Sills. The sills (and the ripple panel upper supports) contain dimples near their forward end to initiate the desired folding collapse mode and prevent the initial load spike that would otherwise occur. In general, crushing of the sills was observed to start at the dimples and progress rearward. When crushing occurred in the ripple panels, it also began at the forward edge and followed the collapse of the sills. In most tests, the primary loads were applied through the sills causing them to collapse. Loads applied through the upper structure were not large enough in any test to crush the ripple panel upper support. This behavior was especially apparent in the frontal pole test (test #2) and in the impacts with unmodified vehicles (tests #7 and #9). Crush resistance of the ripple panel upper support can be reduced by use of thinner gauge material, while increasing the external dimensions of the part by a proportionately lesser amount to maintain column stability.

The aft segments of the sills were designed to form plastic hinges in the event that forward components failed to provide adequate stroke. The aft segments were filled with plastic foam to prevent crippling of the tubular section during hinging. In most tests, the aft segments of the sills were not

called upon to provide additional stroke. Slight hinging took place at the "A" post in the 0° flat barrier impact (test #1). In the 30° flat barrier impact (test #3), the front end components rotated through a considerable angle, but no hinging took place in the sills aft of the front suspension. On the impacted side of the vehicle, the aft portion of the sill was curved in a gentle arc during the impact. The absence of hinging in the sills indicates a possible opportunity for weight reduction. The full energy absorbing capability of the foam-supported sills was not utilized in any of the tests.

Supporting Structure From "A" Post to Fender Support. The supporting components were designed to carry loads from the upper front end structure to the "A" post. They were not designed as energy absorbing members. The supporting structure performed without failure in all tests. Since the members were intended to be non-deforming, their design appears to be correct. Any appreciable reduction in the weight of the components would introduce a risk of failure.

SIDE CRASHWORTHINESS

The improvement in side crashworthiness of the modified vehicles shown in Figure 7-3B was described in Front End System Aggressivity. The side impact by a 4170 lb vehicle caused somewhat greater crush and intrusion than the impact by a modified vehicle of equal weight, Figure 7-3C. Intrusion exceeded the desired level by 3.5 inches. The crash pulse was within the desired limits and had a favorable shape.

The modified vehicle shows substantial improvement over the unmodified vehicle in the side pole impact, Figure 7-3D. Maximum crush was reduced to 3.0 inches and maximum intrusion was reduced to 2.5 inches. The major peaks of the crash pulse occurred 14 msec earlier and the maximum amplitude was reduced from 28 g's to 16 g's.

The side pole impact test was re-run at twice the velocity (Figure 7-3E). This demonstrated the ability of the side modifications to maintain their integrity at an impact speed of twice that for which they were designed.

SIDE COMPONENTS

Modifications to the "A" posts were designed to improve side impact crash resistance as well as front end crash resistance. A honeycomb door beam was installed inside the door structure. The "A" post and "B" post were modified to carry loads imposed by the door beam. Reinforcement consisted of die formed doublers welded to the existing structure. The reinforced sills extended rearward as far as the door centerline. Lateral braces made of formed hat sections joined the sills to the rocker panels.

"A" Post. The "A" posts were reinforced for several reasons. In a frontal impact, the "A" post transmits compressive loads to the door beam. In an oblique impact (tests #3, #11 and #13), the "A" post protects the passenger compartment from intrusion. In a side impact (tests #4, #10, #12, #14 and #15), the "A" post supports one end of the door beam enabling it to resist lateral forces and to develop longitudinal membrane tension. Damage to the reinforced "A" posts was negligible in the frontal impacts. In the offset frontal impact of two Hornets (test #6), the "A" post of vehicle #4 was contacted by the bumper of vehicle #3. Minor deformation of the "A" post occurred.

Effectiveness of the "A" post modifications in resisting intrusion may be seen by comparing the results of test #11 with those of test #13. Geometry of the tests was identical. In each test, a modified Hornet impacted the "A" post of a stationary vehicle at an angle of 60° . In test #11, a modified Hornet was impacted resulting in 0.5 inches intrusion. In test #13, an unmodified Hornet was impacted and the intrusion was 5.2 inches accompanied by widespread buckling of the door.

Effectiveness of the "A" post in supporting the door beam is best seen in the side pole impacts (tests #4 and #15). In test #4, the "A" post rotated through an angle of about 5° due to tension developed in the door beam. In test #15, the impact velocity was 20.62 mph, more than twice the impact speed for which the side modifications were designed. In this

test, the impact point was located 5 inches forward of the door centerline, bringing it 5 inches closer to the "A" post. In test #15, the "A" pillar rotated through an angle of about 20° , but some of this rotation was due to deformation of supporting structures such as the floor pan and rocker panel. The "A" post supported the door beam well in the vehicle-to-vehicle side impacts (tests #10 and #14).

"B" Post. The "B" post performs functions similar to those of the "A" post. It supports the end of the door beam and it acts as a vertical cantilever beam to directly resist intrusion. The "B" post resisted door beam tension loads more effectively than the "A" post. The quarter panel helps the "B" post to resist longitudinal tension loads. The "B" post benefits from having a T shape intersection with the rocker panel instead of an L shape intersection such as the "A" post has.

In test #10, and to a greater extent in test #14, the top of the "B" post was rotated slightly inward. Some deformation of a "B" post occurred above the reinforcing members but there was no deformation of the reinforced area. The "B" post appears to have more than adequate strength in relation to the strength of the surrounding structures. Improved performance would require considerable strengthening of the floor pan structure as a whole. Some weight reduction may be possible in the "B" post reinforcement itself without sacrificing performance.

Door Beam. The door beam functioned effectively in all tests. In the pole tests, the door beam continued to function as a membrane after failing as a beam. This was the intended behavior. There were no membrane failures of the door beam. Crush of the honeycomb core material in the pole tests was less than had been anticipated. Use of a lighter weight core material could yield as much as 1 inch additional energy absorbing stroke due to door beam crushing.

Door Beam Attachment Hardware (Hinge Bracket Reinforcement and Latch Reinforcement). An isolated door hinge failure occurred in test #1 due to hinge attachment bolts pulling loose. Aside from that, the door hinges and latches performed without failure in all tests. The door beam attachment hardware performed its function of passing loads along to the "A" post and "B" post without deflecting appreciably.

Lateral Braces. The lateral braces carried loads from the rocker panel to the sill in all side impacts. There were no failures of the lateral braces. In several tests, lateral loads in the floor pan were high enough to cause compression at the driveshaft tunnel. Additional reinforcement of the floor pan may be required to resist intrusion in the more severe side impact conditions.

SECTION 8 MATHEMATICAL MODELS

DYNAMIC RESPONSE MODELS

Mathematical models of automobiles in various crash situations were developed during the Compact Car Crashworthiness investigation. The purpose was to permit a study of dynamic response characteristics of vehicle configurations in crash situations through computer simulation. The models were used to determine desirable load deflection characteristics of structural elements during the design phase prior to fabrication and crash testing. They have been verified by comparing simulation results with crash test results.

The set of crash conditions modeled is as follows:

Single vehicle impacts

- Frontal flat barrier - normal impact
- Frontal flat barrier - angular impact
- Frontal pole
- Side pole

Two vehicle impacts

- Front to front vehicles aligned
- Front to front vehicles offset
- Front to side

The approach taken in the development of each of the models was to define the vehicle(s) in terms of a set of springs and lumped masses. Equations of motion for the system were then developed. Time-dependent solutions for the equations were then obtained by numerical integration. The particular tool chosen to perform the numerical integrations was a general purpose dynamic system simulation called DYSIM available on the G.E. Timeshare System.

DYSIM allows a user to set up a nonlinear dynamic problem on a digital machine using techniques similar to those used for analog computer simulations. This program is based on the program PACTOLUS which was presented by R.D. Brennan and H. Sano in the paper, "PACTOLUS - A Digital Analog Simulator Program for the IBM 1620", and published in the AFIPS Conference Proceedings, 1964 Fall Joint Computer Conference. DYSIM incorporates various improvements to the PACTOLUS program, such as the modified integration technique, expanded problem capability and on-line conversational features in order to take advantage of the G.E. Timesharing system. The fundamental building block in DYSIM is the integrator block which establishes the independent variable time. The operational algorithm for the integrator may be user-selected as either second order Runge-Kutta or fourth order Runge-Kutta with Gill coefficients. The dynamic model is described in DYSIM by the use of a configuration file which lists the various operations required to solve the equations of motion. The mathematical operations available in DYSIM include virtually all functions which are available in analog computer systems. Virtually any type of nonlinear dynamic system can be simulated using DYSIM as long as it can be adequately described mathematically by a lumped parameter system. The primary restriction on DYSIM is the size of the system to be evaluated. In general, a program of this type is best suited for systems with less than 10 degrees of freedom. Included in DYSIM is a plotting routine which is highly user-oriented. Time history plots of time-dependent parameters such as acceleration, velocity, displacement, and load can easily be obtained using the available plotting routine. The operator blocks and their description as they are used in DYSIM are shown on Table 8-1.

The set of structural elements which are used in the various models is given in Table 8-2. Specific load-deflection characteristics of these elements which are appropriate for the modified vehicles used in the system test series and which were used in verifying the models are tabulated in

Table 8-1. BLOCKS USED IN DYSIM

Legend			
e_1	= input from first input block	P_1	= initial condition or parameter 1
e_2	= input from second input block	P_2	= parameter 2
e_3	= input from third input block	P_3	= parameter 3
e_o	= output	t	= time
		Δt	= integration interval
NAME	TYPE	SYMBOL	DESCRIPTION
Arc Tangent	A		$e_o = \text{ArcTan}(e_1)$ e_1 is in radians
Bang Bang	B		$e_o = +1 (e_1 > 0)$ $e_o = 0 (e_1 = 0)$ $e_o = 1 (e_1 < 0)$
Cosine	C		$e_o = \text{Cos}(e_1)$ e_1 is in radians
Dead Space	D		$e_o = 0$ ($e_1 = 0$) $e_o = \text{MAX}(0, e_1, P_1)$ ($e_1 > 0$) $e_o = \text{MIN}(0, e_1, P_2)$ ($e_1 < 0$)
Exponential	F		$e_o = \text{Exp}(e_1)$
Function Generator	F		$e_o = f(e_1)$ Linear interpolation between 11 output points which are given at $e_1 = 0, 10, 20, 30, 40, 50, 60, 70, 80, 90$ and 100
Gain	G		$e_o = P_1 e_1$
Half Power	H		$e_o = \sqrt{e_1}$
Integrator	I		$e_o = P_1 + \int (e_1 + P_2 e_2 + P_3 e_3) dt$
Modulus (Remaindering)	I		$e_o = e_1 - \left[\frac{e_1}{P_1} \right] P_1$ Where $\left[\frac{e_1}{P_1} \right] = \text{integer of } e_1/P_1$

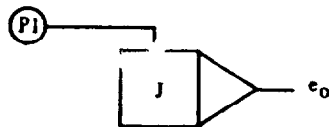
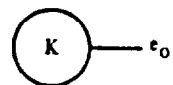
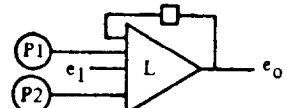
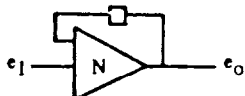
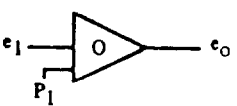
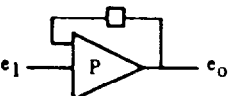
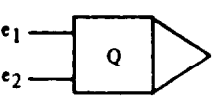
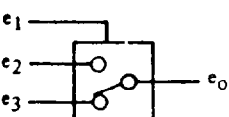
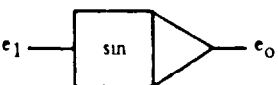
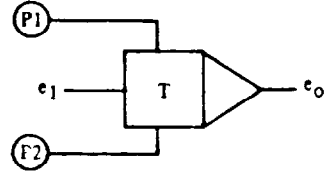
NAME	TYPE	SYMBOL	DESCRIPTION
Jitter	J		$P1 = 1$ Generates uniformly distributed random numbers between 0 and +1 or $P1 = 2$ Generates random numbers with a gaussian distribution of mean and sigma of 0.5
Constant	K		$e_0 = P_1$
Limiter	L		$e_0 = e_1$ ($P_2 \leq e_1 \leq P_1$) $e_0 = P_1$ ($e_1 > P_1$) $e_0 = P_2$ ($e_1 < P_2$)
Magnitude	M		$e_0 = \text{ABS}(e_1)$
Negative Clipper	N		$e_0 = 0$ ($e_1 \leq 0$) $e_0 = e_1$ ($e_1 > 0$)
Offset	O		$e_0 = e_1 + P_1$
Positive Clipper	P		$e_0 = 0$ ($e_1 \geq 0$) $e_0 = e_1$ ($e_1 < 0$)
Quit	Q		Terminates computation if $e_1 > e_2$. Control is subsequently at command 2 level
Relay	R		$e_0 = e_2$, ($e_1 \geq 0$) $e_0 = e_3$, ($e_1 < 0$)
Sine	S		$e_0 = \text{Sin}(e_1)$ e_1 is in radians
Time Pulse Generator	T		Generates pulse train with period equal to P_1 and with a pulse width equal to P_2 If P_2 is not specified the width is set to $\Delta t, 2$ First pulse occurs when $e_1 \geq 0$ Magnitude of pulse is equal to 1 $e_0 = 0$ when $e_1 < 0$ To restart pulse train after e_1 has been less than zero e_1 must be made equal to or greater than zero

Table 8-1. BLOCKS USED IN DYSIM - Continued

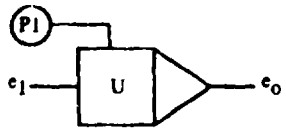
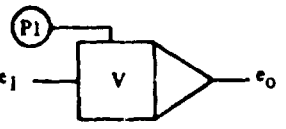
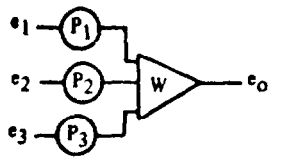
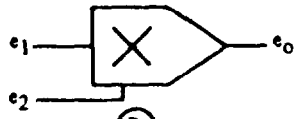
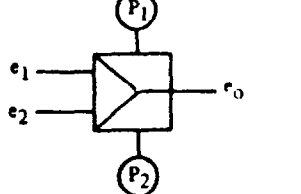
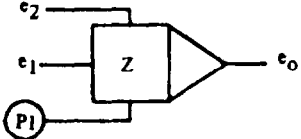
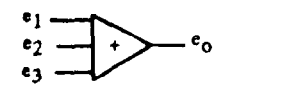
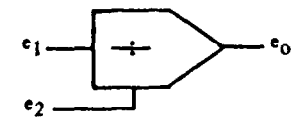
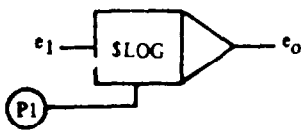
NAME	TYPE	SYMBOL	DESCRIPTION
Half Unit Delay	U		$e_0 = P_1$ when $t = 0$ $e_0 = e_1$ at $t = -(\Delta t/2)$ when $t > 0$
Vacuous	V		Used with WYE element
Weighted Summer	W		$e_0 = P_1 e_1 + P_2 e_2 + P_3 e_3$
Multiplier	X		$e_0 = e_1 e_2$
Wye	Y		Logical branch element $P_1 \neq 0$ $P_2 \neq 0$ $P_2 \neq 1$
Zero Order Hold	Z		$e_0 = 0$ ($e_2 < 0$) $e_0 = P_1$ ($e_2 = 0$) $e_0 = e_1$ ($e_2 > 0$) At $t = 0$, the value of P_1 is given by parameter 1. When $e_2 > 0$ the value of P_1 is made equal to e_1 . Therefore, each time e_2 is greater than zero, the value of P_1 is changed.
Summer	+		$e_0 = \pm e_1 \pm e_2 \pm e_3$
Divider	/		$e_0 = e_1 / e_2$
Sign Inverter	-		$e_0 = -e_1$
Log	SLOG		$e_0 = \text{Log}_e(e_1)$ ($P_1 = 0$) $e_0 = \text{Log}_{10}(e_1)$ ($P_1 = 1$)

Table 8-1. BLOCKS USED IN DYSIM - Continued

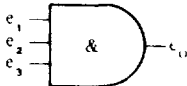
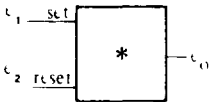
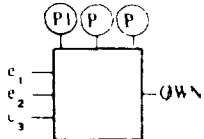
NAME	TYPE	SYMBOL	DESCRIPTION																																				
AND Gate	&		$e_0 = 1 \text{ when } e_1 > 0$ $e_2 \geq 0 \text{ and } e_3 \geq 0$ $e_0 = 0 \text{ otherwise}$ <p>Note: unused inputs are set at 1. This block is non-linear.</p>																																				
R-S Flip flop	*		<table border="1" data-bbox="916 587 1240 789"> <thead> <tr> <th>e_1</th> <th>e_2</th> <th>$e_0(t+\Delta t)$</th> <th>$e_0(t)$</th> </tr> </thead> <tbody> <tr> <td><0</td> <td><0</td> <td>1</td> <td>1</td> </tr> <tr> <td><0</td> <td>>0</td> <td>1</td> <td>1</td> </tr> <tr> <td>≥0</td> <td>0</td> <td>1</td> <td>+1</td> </tr> <tr> <td>≥0</td> <td>>0</td> <td>1</td> <td>+1</td> </tr> <tr> <td><0</td> <td><0</td> <td>+1</td> <td>+1</td> </tr> <tr> <td><0</td> <td>≥0</td> <td>+1</td> <td>1</td> </tr> <tr> <td>≥0</td> <td><0</td> <td>+1</td> <td>+1</td> </tr> <tr> <td>≥0</td> <td>≥0</td> <td>+1</td> <td>+1</td> </tr> </tbody> </table> <p>Note: Logic levels have been selected as +1 and -1 permitting direct use of the Sign Inverter block to obtain logical complements. This block is non-linear.</p>	e_1	e_2	$e_0(t+\Delta t)$	$e_0(t)$	<0	<0	1	1	<0	>0	1	1	≥0	0	1	+1	≥0	>0	1	+1	<0	<0	+1	+1	<0	≥0	+1	1	≥0	<0	+1	+1	≥0	≥0	+1	+1
e_1	e_2	$e_0(t+\Delta t)$	$e_0(t)$																																				
<0	<0	1	1																																				
<0	>0	1	1																																				
≥0	0	1	+1																																				
≥0	>0	1	+1																																				
<0	<0	+1	+1																																				
<0	≥0	+1	1																																				
≥0	<0	+1	+1																																				
≥0	≥0	+1	+1																																				
Arbitrary Block			<p>Operation defined by user-written FORTRAN function which must be named QWN.</p>																																				

Table 8-2. Structural Elements Used in Dynamic Response Models

R ₁	-	Fenders, partial ripple panel and upper support, left side
R ₂	-	Front sill, energy absorption units, partial ripple panel, left side
R ₃	-	Rear sill, left side
R ₄	-	Radiator, fan
R ₅	-	Engine mounts
R ₆	-	Firewall
R ₇	-	Passenger restraint system
R ₈	-	Bumper
R ₉	-	Driveline
R ₁₀	-	Lateral stiffness of R ₁ and R ₁₅
R ₁₁	-	Lateral stiffness of R ₂ and R ₁₆
R ₁₂	-	Lateral stiffness of R ₃ and R ₁₇
R ₁₃	-	Lateral stiffness of R ₅
R ₁₄	-	Lateral stiffness of R ₉
R ₁₅	-	Fenders, etc., right side
R ₁₆	-	Front sill, etc., right side
R ₁₇	-	Rear sill, right side
R ₁₈	-	Door beam
R ₁₉	-	"A" and "B" posts
R ₂₀	-	Rocker panel
R ₂₁	-	Roof rail
R ₂₂	-	Impacting vehicle front end, aligned impact
R ₂₃	-	Impacting vehicle front end, offset impact

Table 8-3 and plotted in Figure 8-1. These values were obtained either experimentally or by mathematical analysis. Analytical techniques employed to obtain calculated values are described later in this section.

MODELS

Frontal Flat Barrier - Normal Impact. This is a four-degree-of-freedom model with all degrees of freedom being movement along the longitudinal axis of the vehicle. The model, shown in Figure 8-2, assumes symmetrical structural elements on the right and left sides of the vehicle. The four lumped masses represent the following components:

1. Mass 1 (M_1): Total mass of the vehicle less the masses assigned to masses 2, 3 and 5.
2. Mass 2 (M_2): Mass of the engine, transmission and driveline.
3. Mass 3 (M_3): Mass of the crossmember, front suspension and front wheels.
4. Mass 5 (M_5): Mass of the passengers.

The degrees of freedom and their time derivatives are:

$X_1, \dot{X}_1, \ddot{X}_1$ - Displacement, velocity and deceleration of mass M_1 respectively.

$X_2, \dot{X}_2, \ddot{X}_2$ - Displacement, velocity and deceleration of mass M_2 respectively.

$X_3, \dot{X}_3, \ddot{X}_3$ - Displacement, velocity and deceleration of mass M_3 respectively.

$X_5, \dot{X}_5, \ddot{X}_5$ - Displacement, velocity and deceleration of mass M_5 respectively.

Table 8-3. Load-Deflection Characteritics of Modified Vehicle Structural Elements

1		2		3		4		5		6	
X	Force	X	Force	X	Force	X	Force	X	Force	X	Force
-50.	0.	-50.	0	-10.	-30000.	-50.	0.	-20.	-20000.	-10.	0.
6.	0.	0.	0.	-1.	-25000.	12.5	0.	-2.	-20000.	1.5	0.
7.	8500.	1.	20000.	0.	0.	14.5	2350.	-1.	-10000.	1.81	3970.
9.5	8500.	3.	25000.	1.	25000.	16.5	6180.	0.	0.	2.71	3970.
10.	3500.	3.5	33000.	4.	30000.	18.5	10760.	1.	10000.	5.15	9640.
190.	3500.	5.	30000.	10.	17500.	21.5	26460.	2.	20000.	6.36	9640.
		18.	25000.	11.	40000.	23.	62300.	20.	20000.	7.16	11080.
		19.	50000.	30.	40000.	23.1	120000.			8.76	11080.
		50.	50000.			28.5	500000.			10.12	15400.
										11.88	14700.
										17.5	16300.
										50.	16300.
7		8		9		10		11		12	
X	Force	X	Force	X	Force	X	Force	X	Force	X	Force
-10.	-3000.	-20.	0.	-10.	-5000.	-10.	0.	-10.	0.	-10.	0.
0.	0.	3.5	0.	0.	0.	0.	0.	0.	0.	0.	0.
4.	3800.	4.	28660.	1.95	12350.	.2	4350.	.2	18000.	.24	18000.
6.2	7750.	7.	59820.	7.02	15080.	5.	5000.	3.	25000.	5.	26000.
20.	0.	7.5	25730.	10.58	4700.	10.	5000.	10.	0.	15.	0.
50.	0	13.5	74870.	12.37	4700.	50.	0.	50.	0.	50.	0.
				13.42	0.						
				50.	0.						

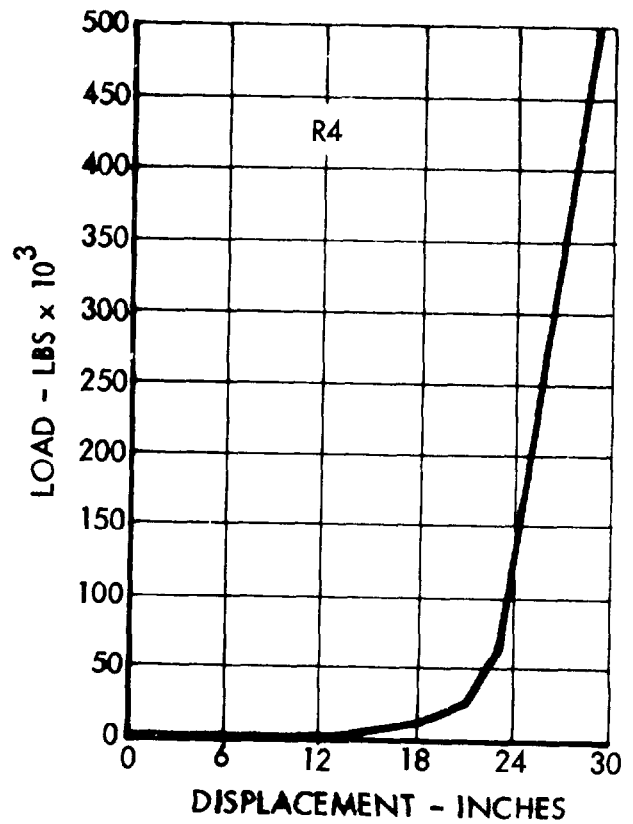
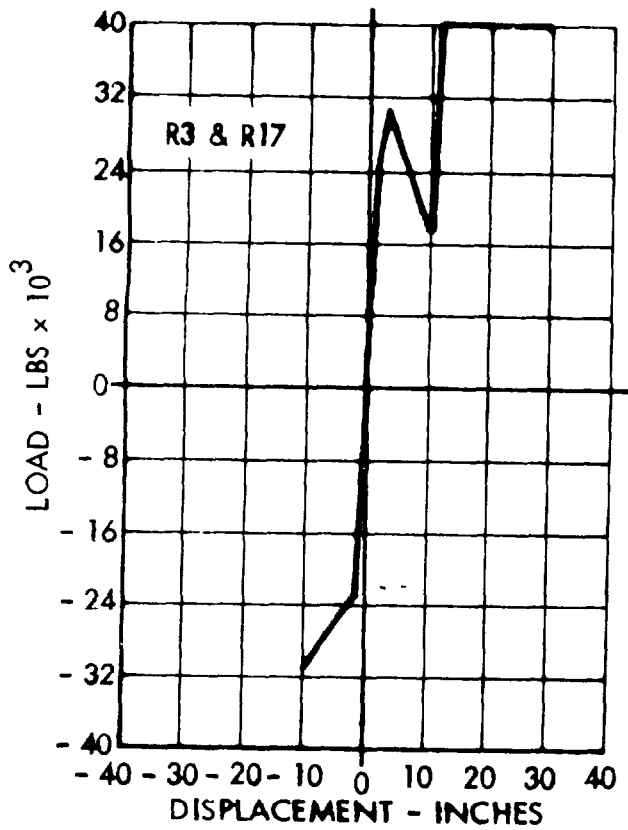
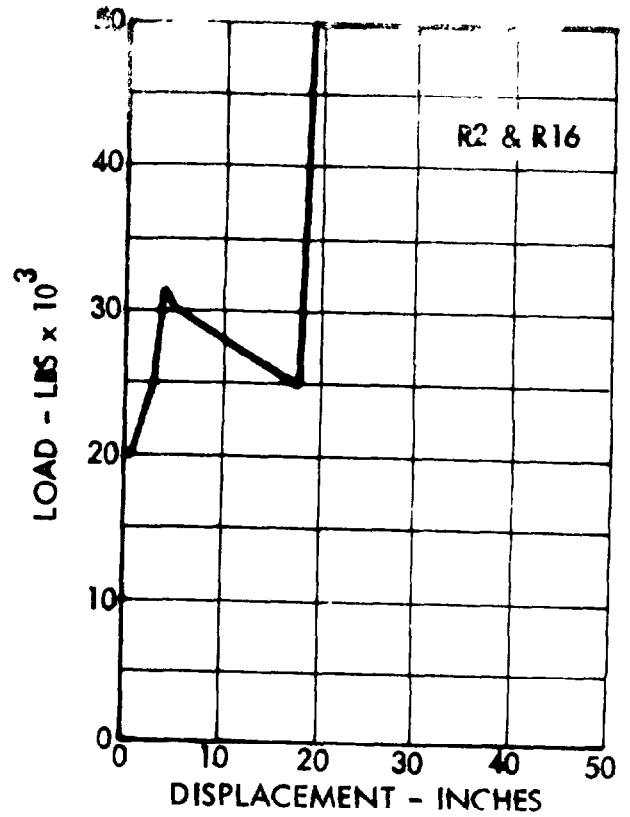
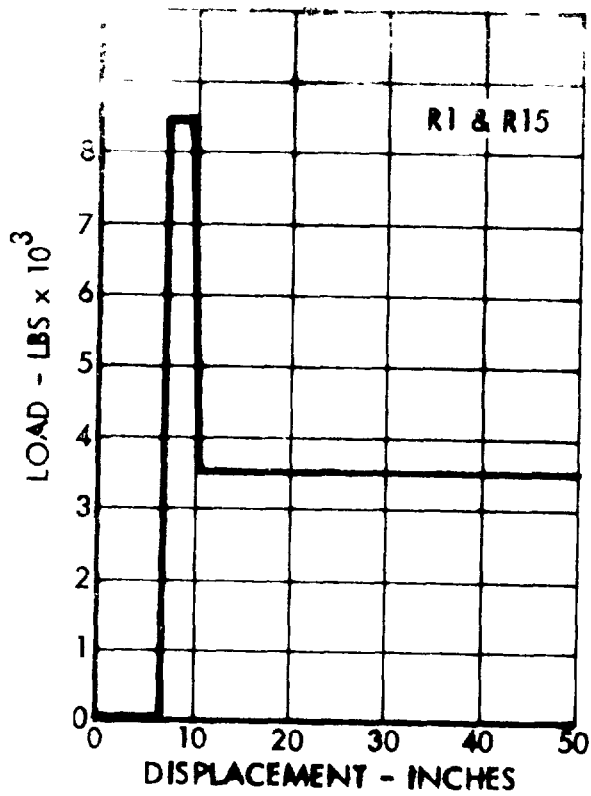


Figure 8-1(a). Load Deflection Characteristics Of Modified Vehicle Used In System Test Series.

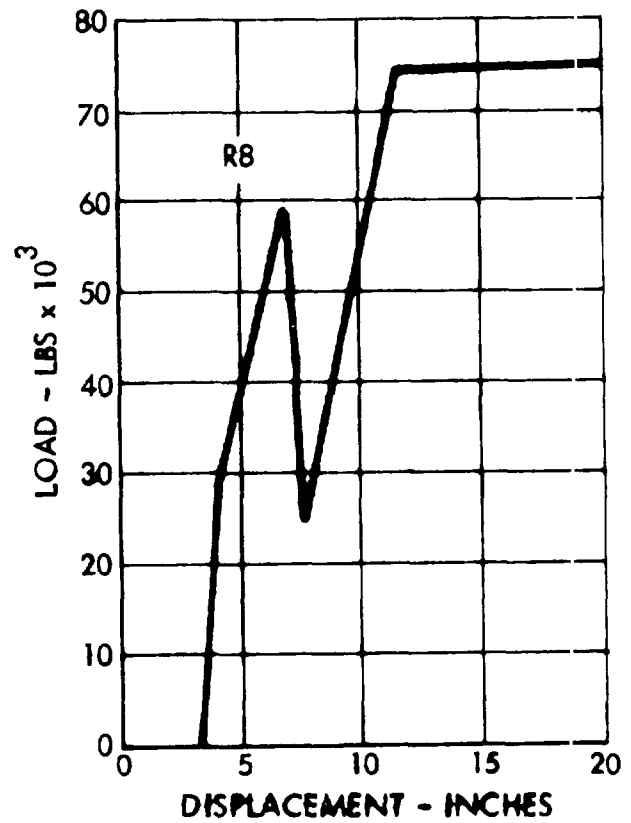
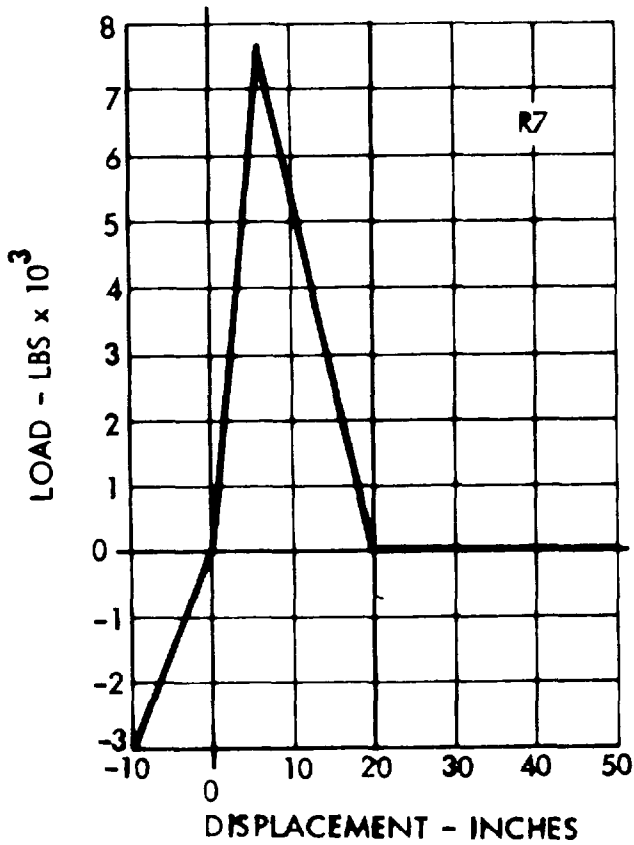
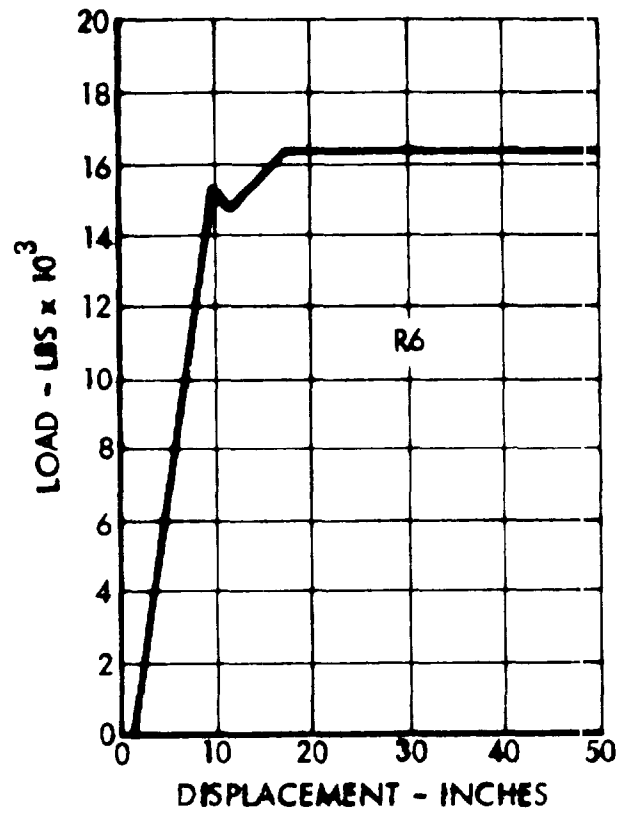
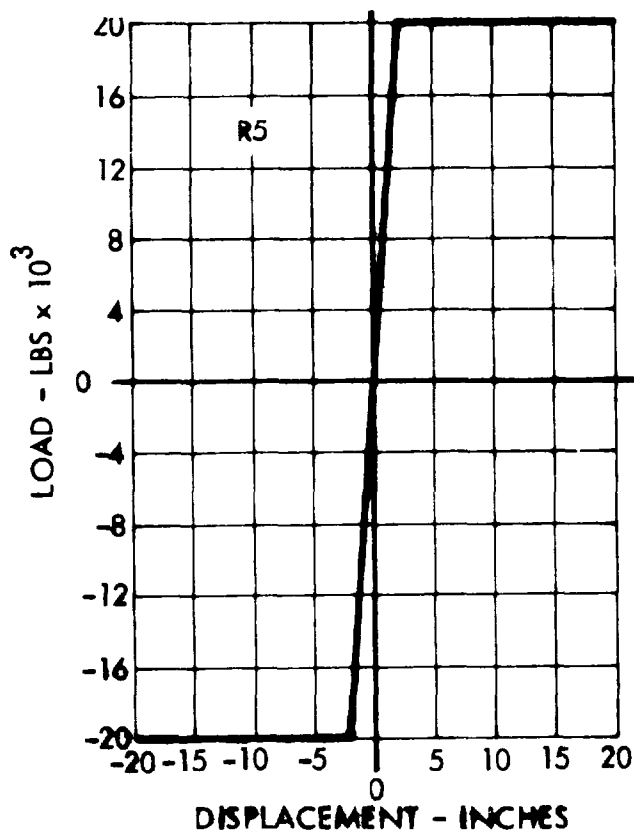


Figure 8-1(b). Load D flection Characteristics Of Modified Vehicle Used In System Test Series. (Continued)

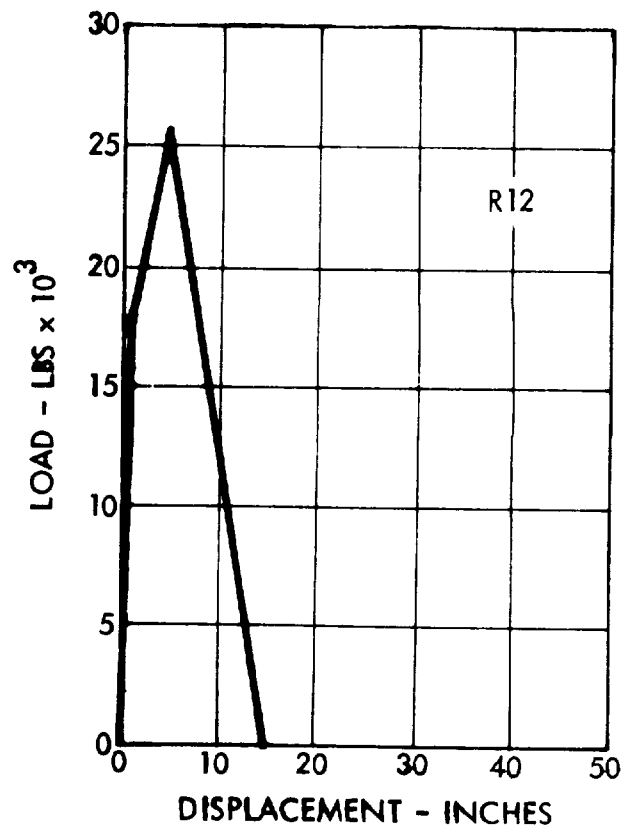
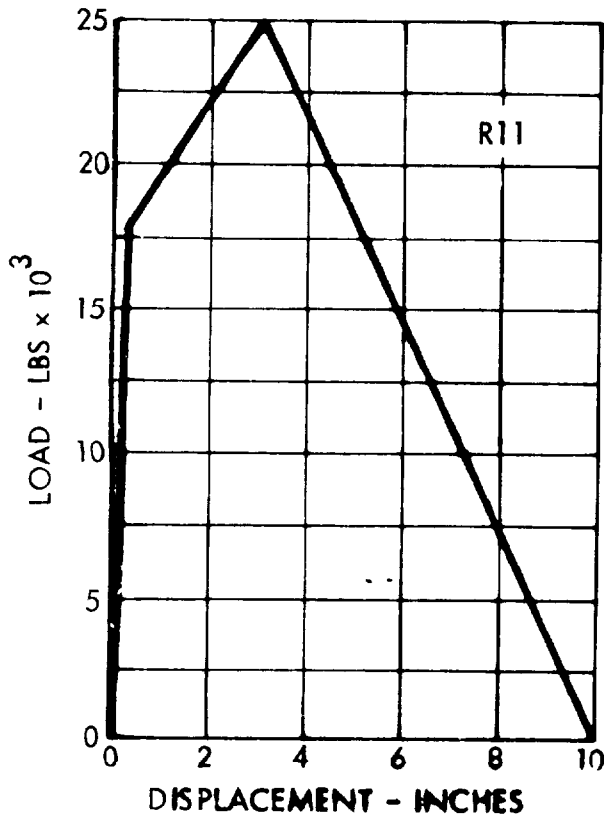
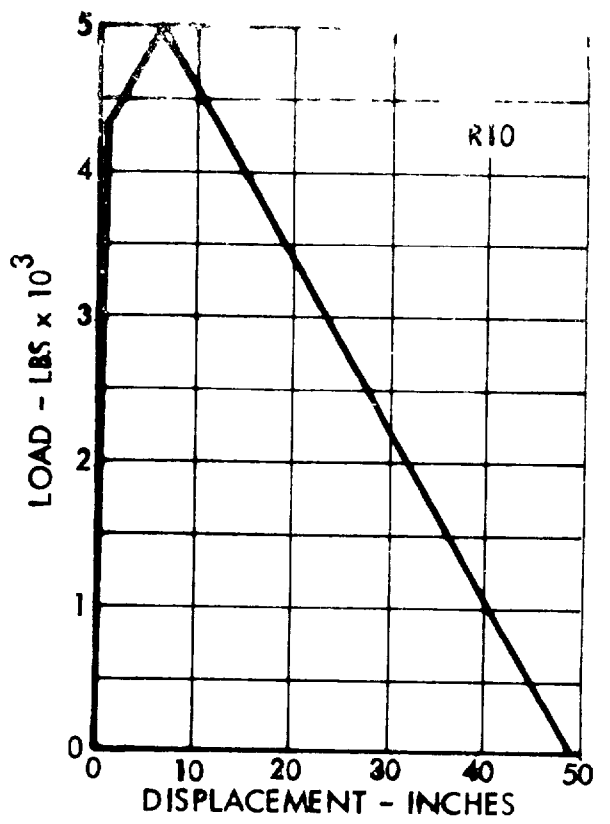
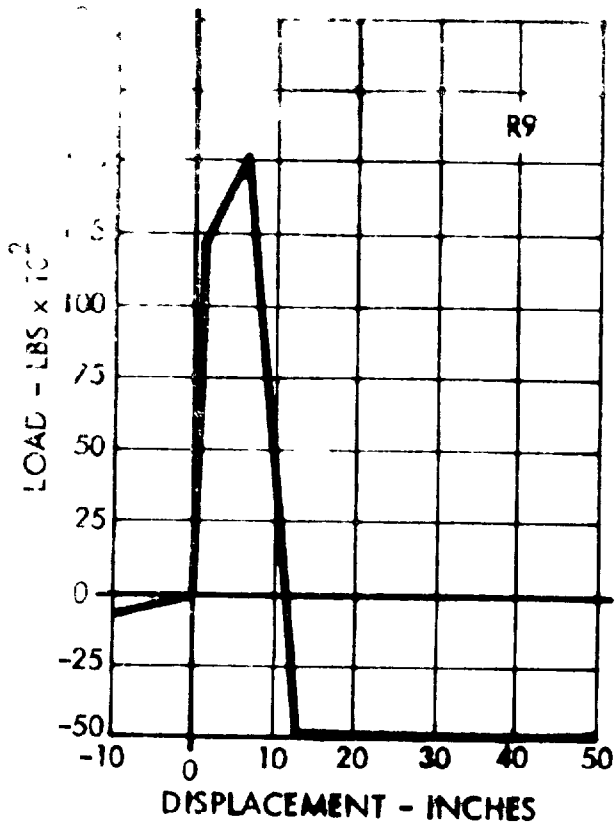


Figure 8-1(c). Load D flection Characteristics Of Modified V hicle Used In System Test Series. (Continued)

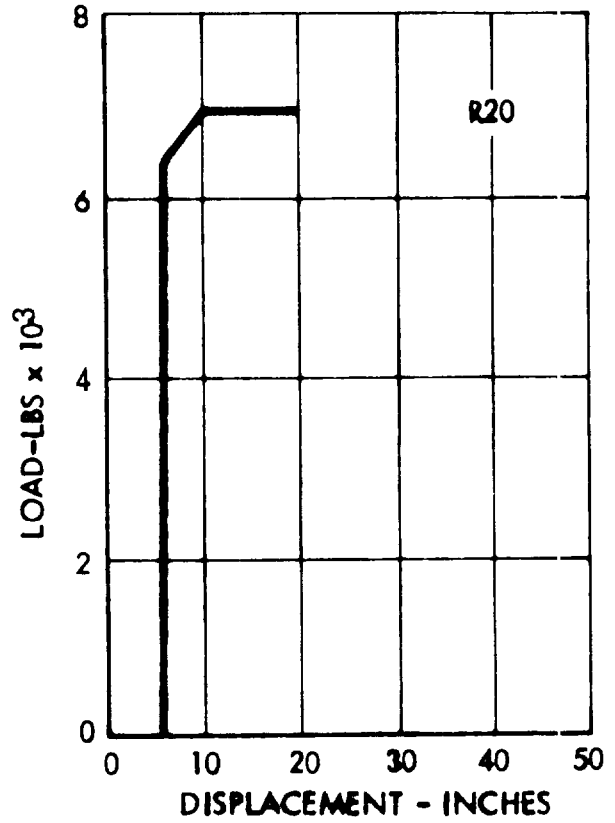
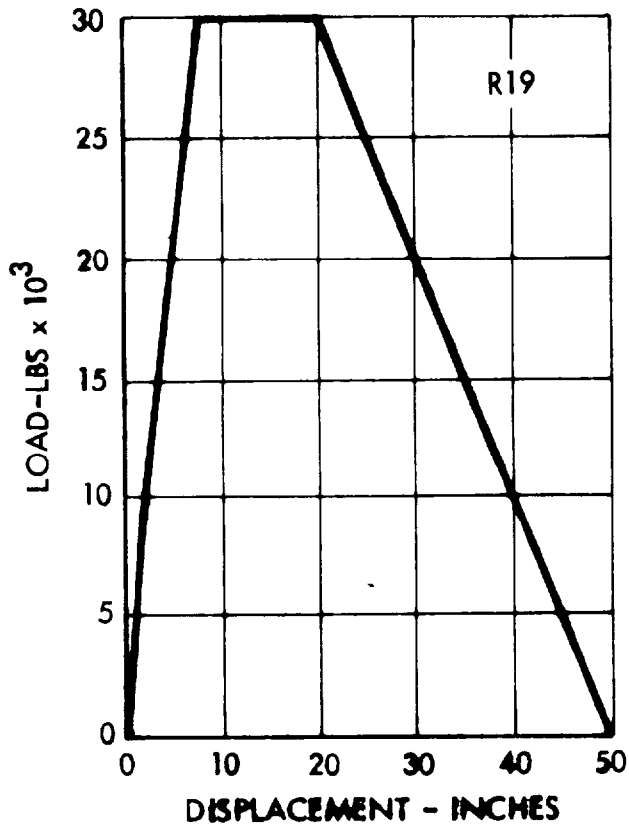
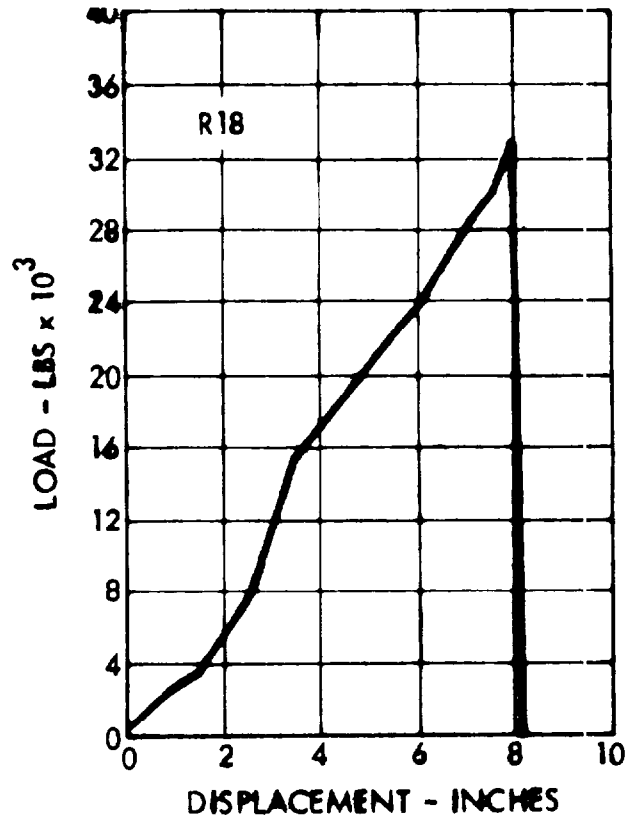
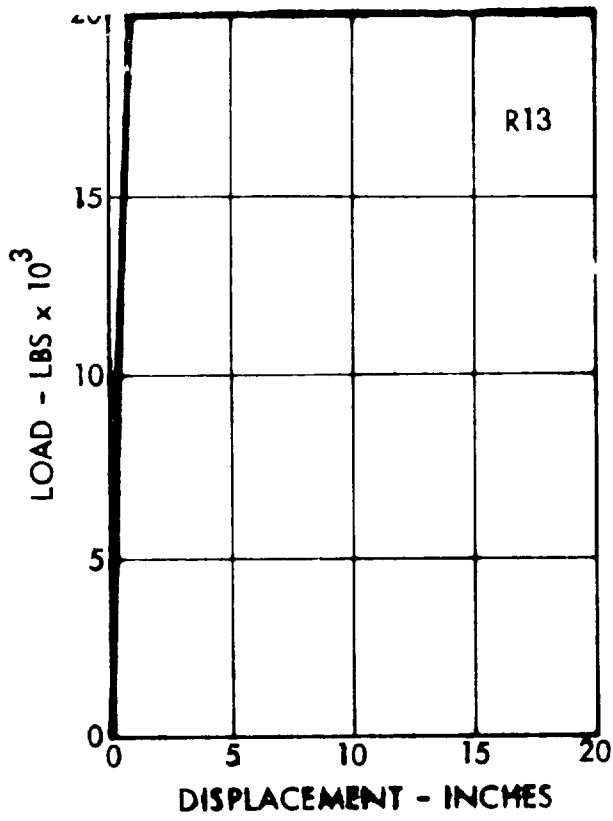


Figure 8-1(d). Load Deflection Characteristics Of Modified Vehicle Used In System Test Series. (Continued)

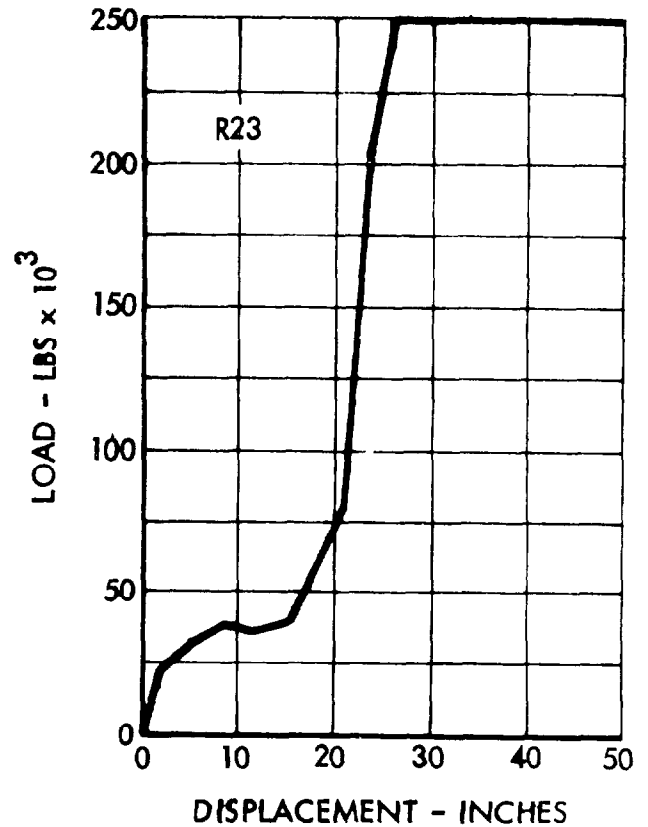
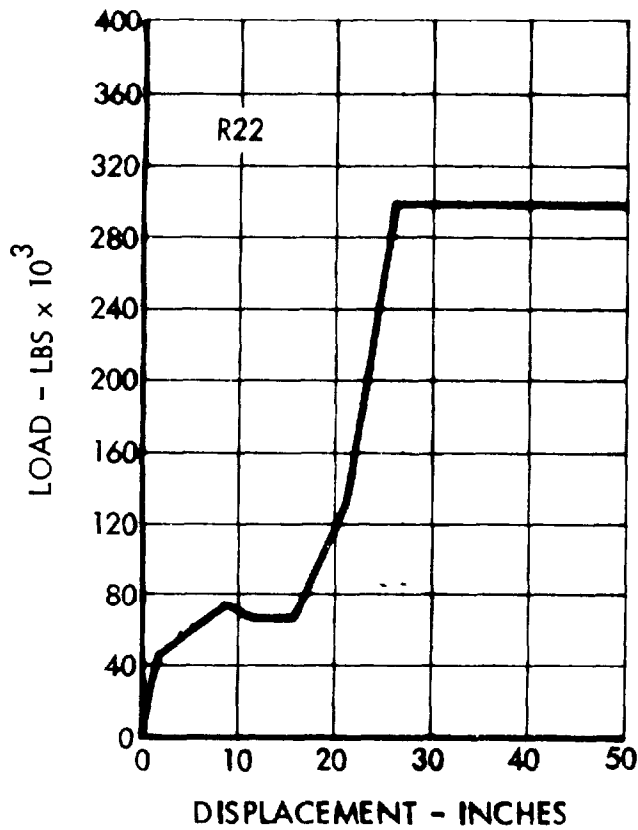
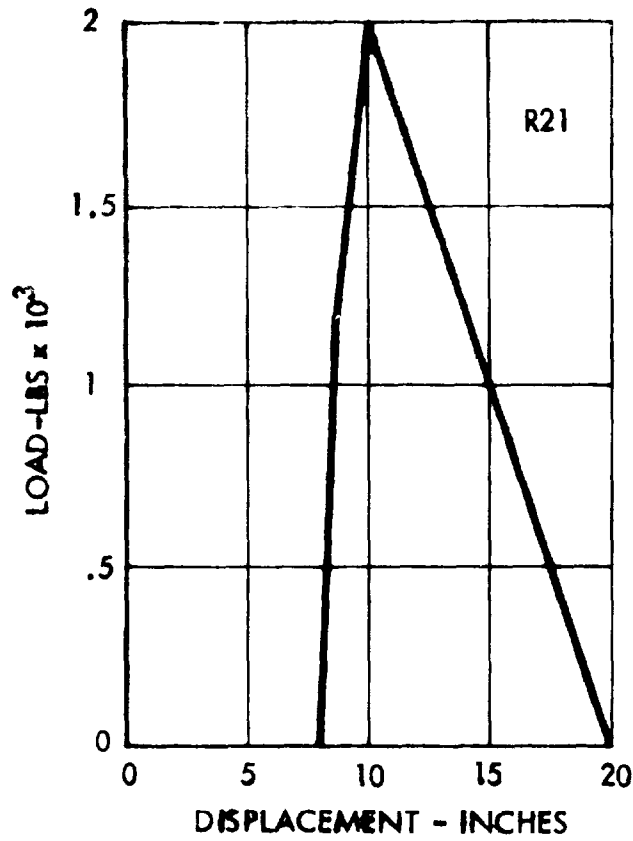


Figure 8-1(e). Load Deflection Characteristics Of Modified Vehicle Used In System Test Series. (Continued)

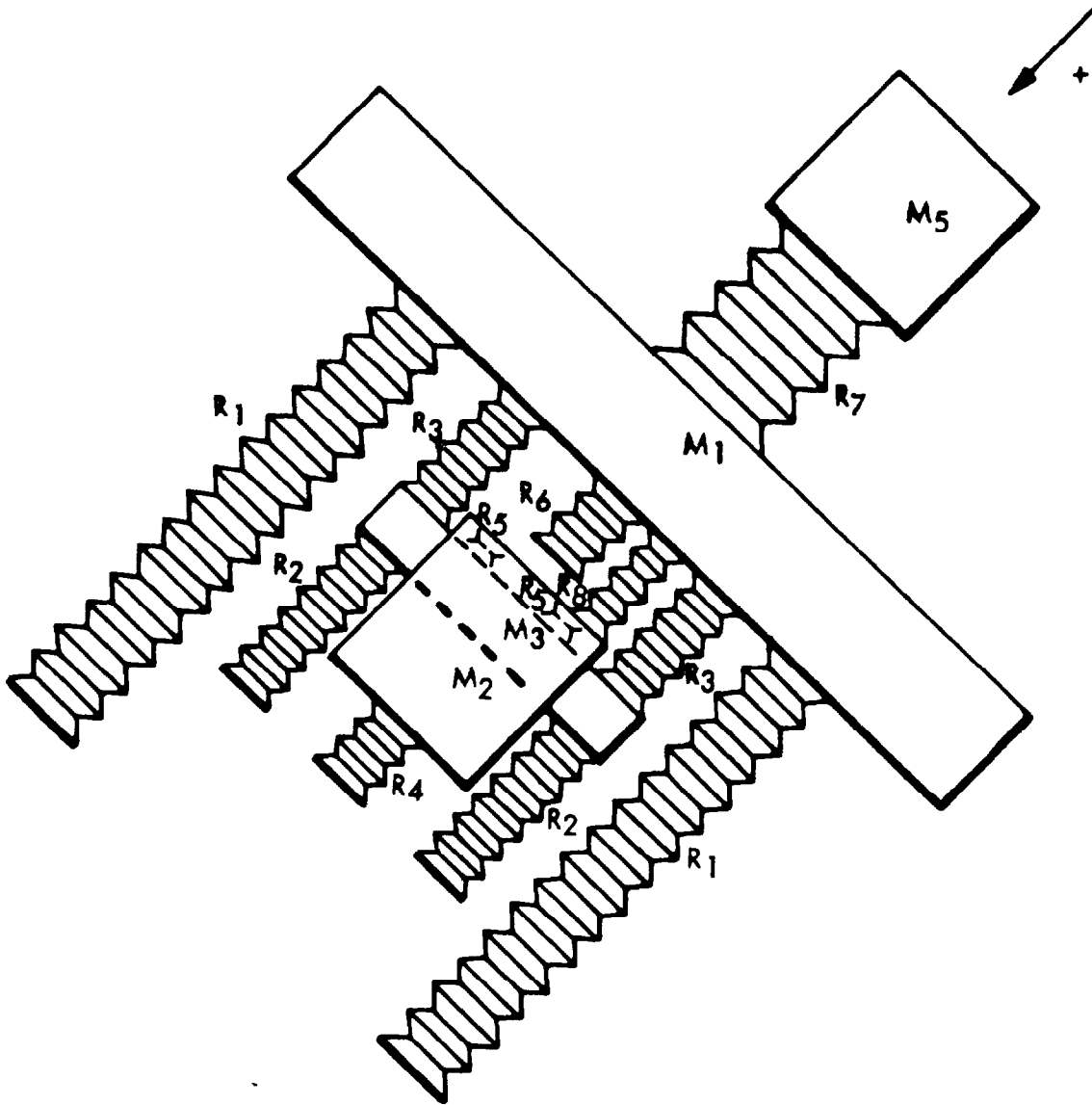


Figure 8-2. Frontal Norm I Barrier Impact Model

The equations of motion for this model are:

$$M_1 \ddot{X}_1 = -2F_1 - 2F_3 - F_6 - F_9 + F_7$$

$$M_2 \ddot{X}_2 = F_6 + F_9 - F_5 - F_4$$

$$M_3 \ddot{X}_3 = 2F_3 + F_5 - 2F_2$$

$$M_5 \ddot{X}_5 = -F_7$$

The forces (F) are defined as:

F_1 - Resistance offered by R_1 and function of (X_1) .

F_2 - Resistance offered by R_2 and function of (X_3) .

F_3 - Resistance offered by R_3 and function of $(X_1 - X_3)$.

F_4 - Resistance offered by R_4 and function of (X_2) .

F_5 - Resistance offered by R_5 and function of $(X_2 - X_3)$.

F_6 - Resistance offered by R_6 and function of $(X_1 - X_2)$.

F_7 - Resistance offered by R_7 and function of $(X_5 - X_1)$.

F_9 - Resistance offered by R_9 and function of $(X_1 - X_2)$.

The basic diagram for the frontal normal barrier model is described in Figure 8-3. Each block on the diagram is a standard DYSIM operator.

The results of a test case are given in Table 8-4 and are plotted in Figure 8-4 along with the results of a corresponding crash test.

Values used in this simulation were:

$$M_1 = 1832 \text{ lb/386.}$$

$$M_2 = 675 \text{ lb/386.}$$

$$M_3 = 423 \text{ lb/386.}$$

$$V_1 = 50 \text{ mph}$$

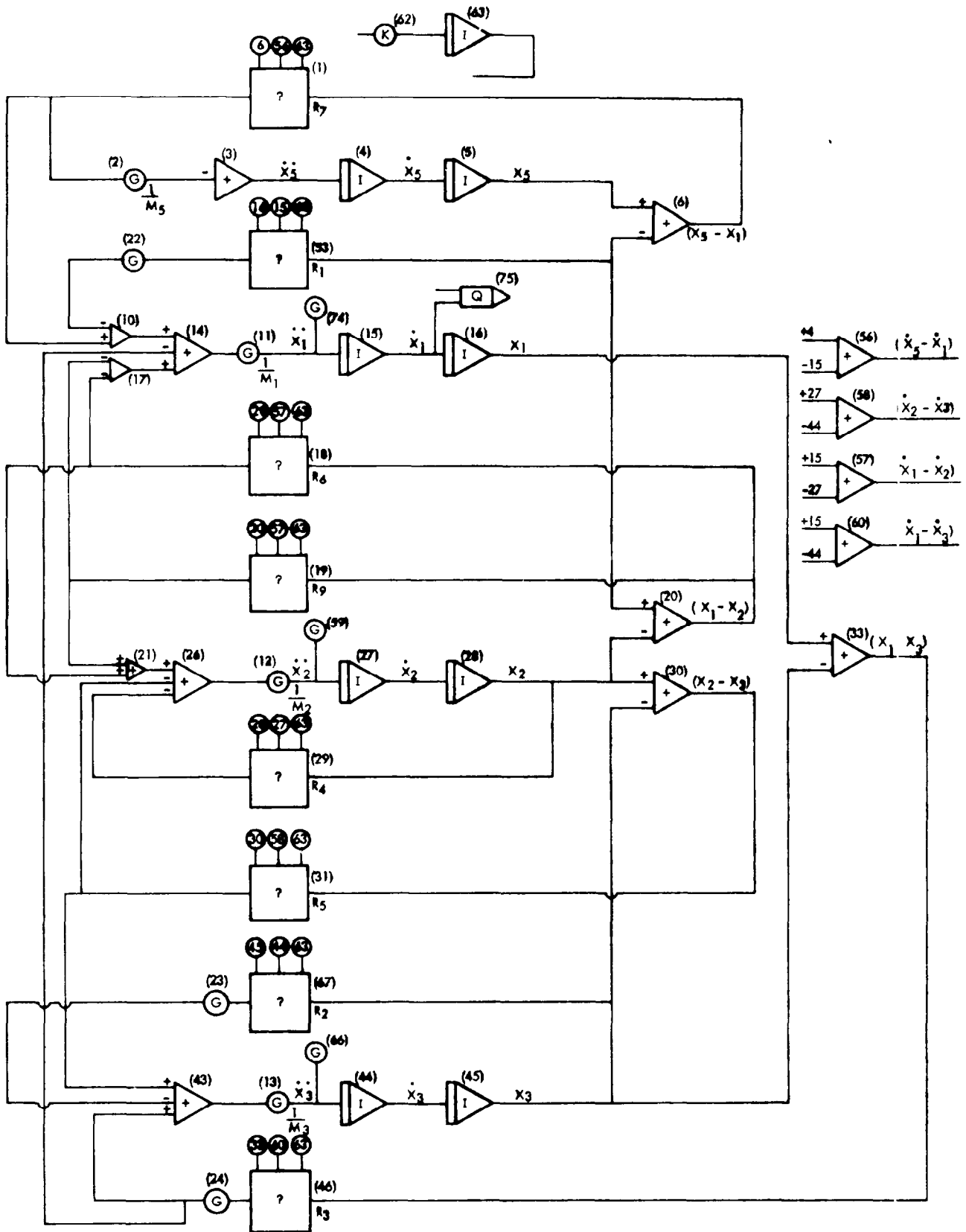


Figure 8-3. Logic Diagram For Frontal Normal Barrier Impact Model

Table 8-4. Frontal Normal Barrier Test Case

Time (sec)	\ddot{X}_1 (g)	X_1 (in)
0.	0.	0.
2.0000E-03	0.	1.7600000E+00
4.0000E-03	-9.3935940E+00	3.5200000E+00
6.0000E-03	-2.5369712E+01	5.2683301E+00
8.0000E-03	-4.5292992E+01	6.9795975E+00
1.0000E-02	-4.5642469E+01	8.6236659E+00
1.2000E-02	-3.7512350E+01	1.0196870E+01
1.4000E-02	-3.7246184E+01	1.1705976E+01
1.6000E-02	-3.6818177E+01	1.3157494E+01
1.8000E-02	-3.6254965E+01	1.4552093E+01
2.0000E-02	-3.5578166E+01	1.5890651E+01
2.2000E-02	-3.5003374E+01	1.7174219E+01
2.4000E-02	-3.2267112E+01	1.8402971E+01
2.6000E-02	-2.7720741E+01	1.9581106E+01
2.8000E-02	-2.2568502E+01	2.0715810E+01
3.0000E-02	-2.0125082E+01	2.1815532E+01
3.2000E-02	-3.0430419E+01	2.2886316E+01
3.4000E-02	-4.3545423E+01	2.3913582E+01
3.6000E-02	-4.9220691E+01	2.4872687E+01
3.8000E-02	-5.5504746E+01	2.5756426E+01
4.0000E-02	-5.7462196E+01	2.6554328E+01
4.2000E-02	-5.9686488E+01	2.7264278E+01
4.4000E-02	-5.7877483E+01	2.7881572E+01
4.6000E-02	-5.2681372E+01	2.8408635E+01
4.8000E-02	-4.8874190E+01	2.8854240E+01
5.0000E-02	-4.5464401E+01	2.9224828E+01
5.2000E-02	-4.1514496E+01	2.9524787E+01
5.4000E-02	-6.3274702E+01	2.9760849E+01
5.6000E-02	-6.0958394E+01	2.9895429E+01

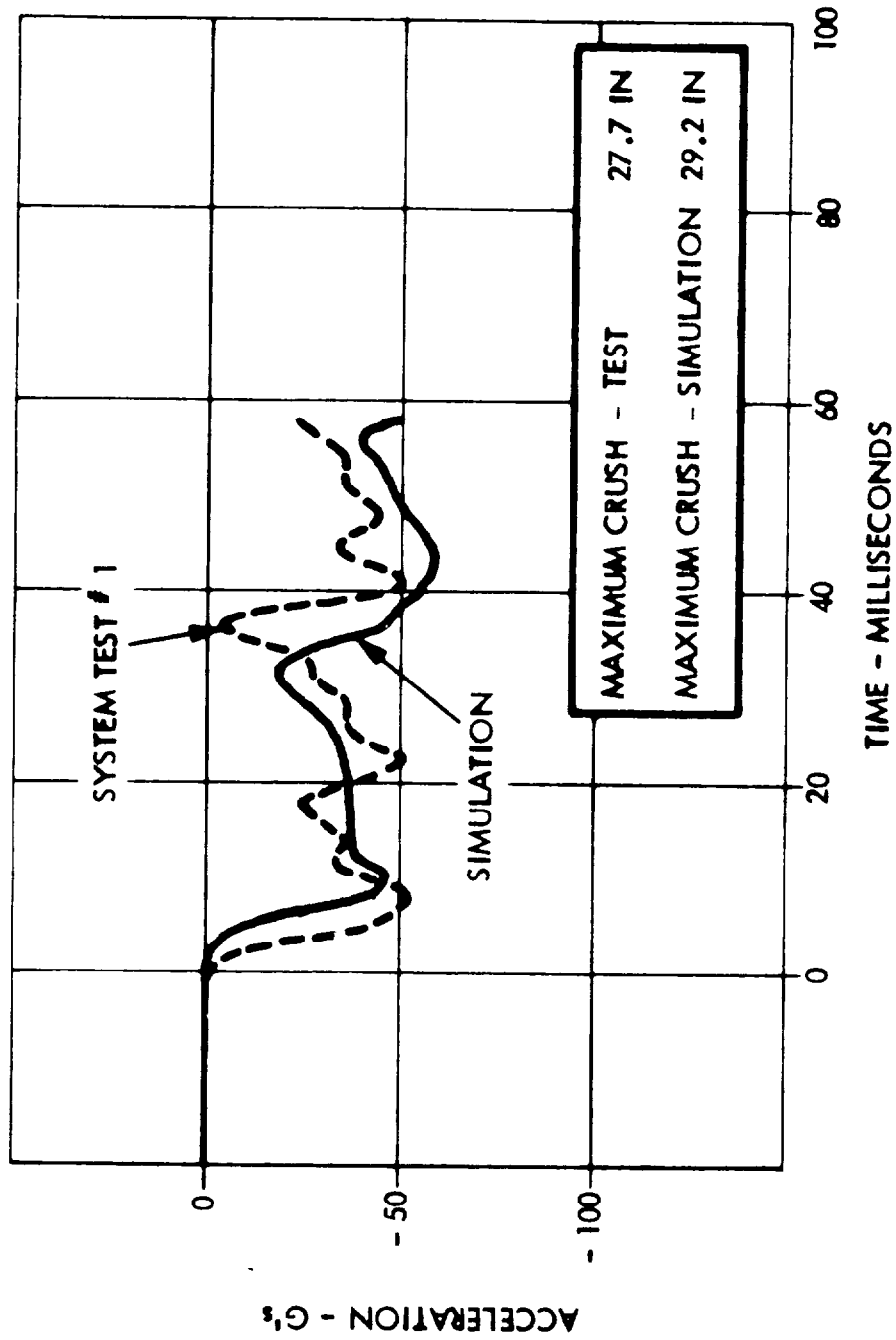


Figure 8-4. Front Normal Barrier Simulation (50 MPH)

Frontal Flat Barrier - Angular Impact. This is a 10-degree-of freedom model. There are three degrees along the vehicle longitudinal axis, four degrees perpendicular to the vehicle longitudinal axis and three degrees of rotation about the yaw or vertical axes. The model shown in Figure 8-1 permits asymmetrical modeling of the right and left sides of the vehicle. Transverse or shear stiffness of front end elements is also included. The model employs a total of four lumped masses and fifteen structural springs.

The four lumped masses are:

1. Mass 1 (M_1): Total mass of the vehicle less mass assigned to 2, 3 and 4.
2. Mass 2 (M_2): Mass of the engine, transmission and driveline.
3. Mass 3 (M_3): Mass of the crossbar, front suspension and front wheels.
4. Mass 4 (M_4): Mass of the bumper.

Degrees of freedom and their time derivatives are:

$X_1, \dot{X}_1, \ddot{X}_1$ - Displacement, velocity and deceleration of mass M_1 respectively of vehicle longitudinal axis prior to impact.

$X_2, \dot{X}_2, \ddot{X}_2$ - Displacement, velocity, deceleration or acceleration of mass M_2 respectively.

$X_3, \dot{X}_3, \ddot{X}_3$ - Displacement, velocity, deceleration or acceleration of mass M_3 respectively.

$Y_1, \dot{Y}_1, \ddot{Y}_1$ - Displacement, velocity and deceleration of mass M_1 respectively, in direction perpendicular to vehicle longitudinal axis.

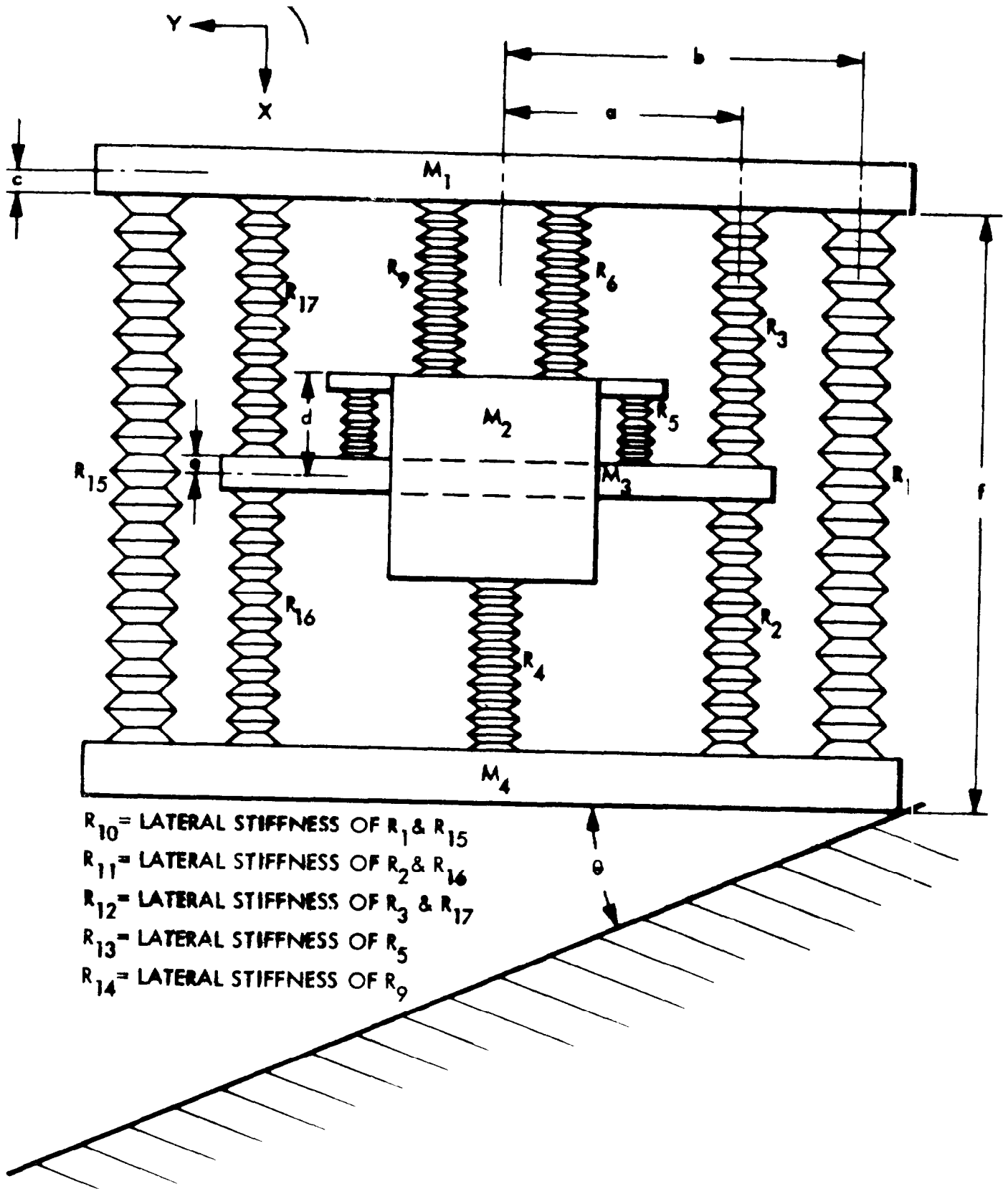


Figure 8-5. Angular Frontal Barrier Model

$Y_2, \dot{Y}_2, \ddot{Y}_2$ - Displacement, velocity, acceleration or deceleration of mass M_2 respectively.

$Y_3, \dot{Y}_3, \ddot{Y}_3$ - Displacement, velocity, acceleration or deceleration of mass M_3 respectively.

$Y_4, \dot{Y}_4, \ddot{Y}_4$ - Displacement, velocity, acceleration or deceleration of mass M_4 respectively.

$\theta_1, \dot{\theta}_1, \ddot{\theta}_1$ - Rotation, angular velocity, and angular acceleration of mass M_1 respectively.

$\theta_2, \dot{\theta}_2, \ddot{\theta}_2$ - Rotation, angular velocity, and angular acceleration of mass M_2 respectively.

$\theta_3, \dot{\theta}_3, \ddot{\theta}_3$ - Rotation, angular velocity, and angular acceleration of mass M_3 respectively.

The equations of motion are:

$$M_1 \ddot{X}_1 = (F_1 + F_3 + F_6 + F_9 + F_{15} + F_{17}) \cos\theta + F_7 - (F_{10} + F_{12}) \sin\theta$$

$$M_2 \ddot{X}_2 = (-F_4 - F_5 + F_6 + F_9) \cos\theta - (F_{13}) \sin\theta$$

$$M_3 \ddot{X}_3 = (-F_2 - F_{16} + F_3 + F_{17} + F_5) \cos\theta + (-F_{11} + F_{12} + F_{13}) \sin\theta$$

$$M_1 \ddot{Y}_1 = -(F_1 + F_3 + F_6 + F_9 + F_{15} + F_{17}) \sin\theta + (F_{10} + F_{12}) \cos\theta$$

$$M_2 \ddot{Y}_2 = (-F_4 - F_5 + F_6 + F_9) \sin\theta + (F_{13}) \cos\theta$$

$$M_3 \ddot{Y}_3 = (-F_2 - F_{16} + F_3 + F_{17} + F_5) \sin\theta - (-F_{11} + F_{12} + F_{13}) \cos\theta$$

$$M_4 \ddot{Y}_4 = [(F_1 + F_2 + F_4 + F_{15} + F_{16}) \cos \beta - (F_{10} + F_{11}) \sin \beta - \mu(F_1 + F_2 + F_4 + F_{15} + F_{16}) \sin \beta - \mu(F_{10} + F_{11}) \cos \beta] \cos \theta_0$$

$$I_1 \ddot{\theta}_1 = (F_1 - F_{15}) b + (F_3 - F_{17}) a - (F_{10} + F_{12}) c$$

$$I_2 \ddot{\theta}_2 = (F_{13}) d$$

$$I_3 \ddot{\theta}_3 = (F_2 + F_{17} - F_3 - F_{16}) b - (F_{11} + F_{12} + F_{13}) e$$

Terms are defined as follows:

F_1 - resistance offered by R_1 and function of $X_1 - b \theta_1 - Y_4 \sin \theta_0$

F_2 - resistance offered by R_2 and function of $X_3 - a \theta_3 - (b-a) \sin \theta_0 - Y_4 \sin \theta_0$

F_3 - resistance offered by R_3 and function of $X_1 - X_3 - a (\theta_1 - \theta_3)$

F_4 - resistance offered by R_4 and function of $X_2 - b \sin \theta_0 - Y_4 \sin \theta_0$

F_5 - resistance offered by R_5 and function of $X_2 - X_3$

F_6 - resistance offered by R_6 and function of $X_1 - X_2$

F_9 - resistance offered by R_9 and function of $X_1 - X_2$

F_{10} - resistance offered by R_{10} and function of $Y_4 - Y_1$

F_{11} - resistance offered by R_{11} and function of $Y_4 - Y_3$

F_{12} - resistance offered by R_{12} and function of $Y_3 - Y_1$

F_{13} - resistance offered by R_{13} and function of $Y_3 - Y_2$

F_{15} - resistance offered by R_{15} and function of $X_1 + b \theta_1 - 2 b \sin \theta_0 - Y_4 \sin \theta_0$

F_{16} - resistance offered by R_{16} and function of $X_3 + a \theta_3 - (b+a) \sin \theta_0 - Y_4 \sin \theta_0$

F_{17} - resistance offered by R_{17} and function of $X_1 - X_3 + a (\theta_1 - \theta_3)$

- a - Distance from longitudinal axis to sills
- b - Distance from longitudinal axis to fenders
- c - Distance from passenger compartment centroid to firewall
- d - Distance from engine centroid to engine mounts
- e - Distance from crossmember centroid to its edge
- f - Distance from firewall to front of vehicle
- μ - Coefficient of friction along barrier
- θ - Angle of distortion of front end - $(Y_4 - Y_1)/(Y_4 \text{ SIN}\theta_0 + f - X_1)$
- $\beta = (\pi - \theta - \theta_0)$

The logic diagram for the front angular barrier model is shown in Figure 8-6.

The results of a test case are given in Table 8-5 and plotted in Figure 8-7. Values used in the simulation were:

- $M_1 = 1832 \text{ lb}/386.$
- $M_2 = 675 \text{ lb}/386.$
- $M_3 = 373 \text{ lb}/386.$
- $M_4 = 50 \text{ lb}/386.$
- $I_1 = 11,350,000. \text{ lb.in}^2/386.$
- $I_2 = 154,000. \text{ lb.in}^2/386.$
- $I_3 = 193,000. \text{ lb.in}^2/386.$
- $\mu = .3$
- a = 15.43 in
- b = 20.35 in
- c = 64.75 in
- d = 2.13 in
- e = 1.13 in
- f = 53.5 in
- $\theta_0 = 30^\circ$
- V = 50 mph

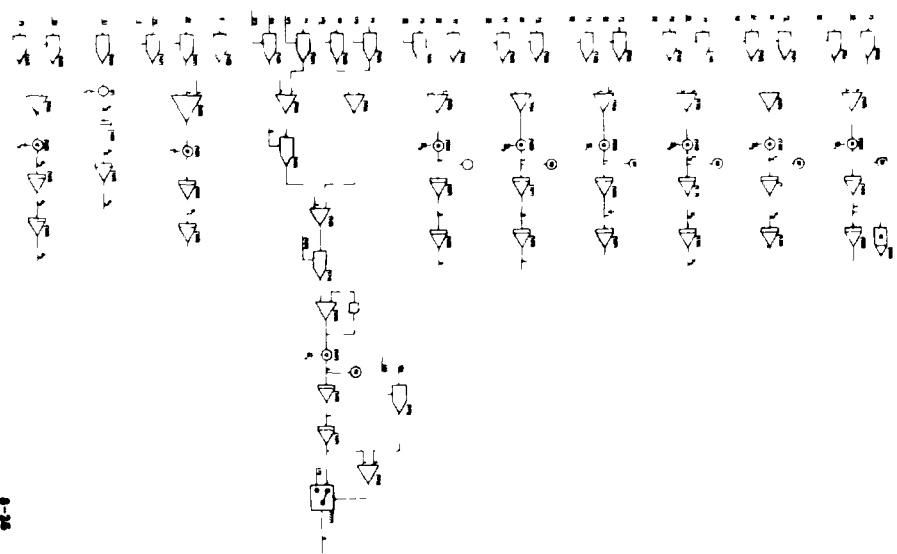
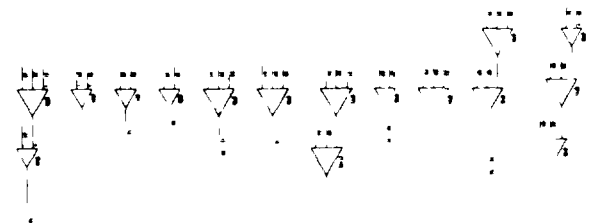
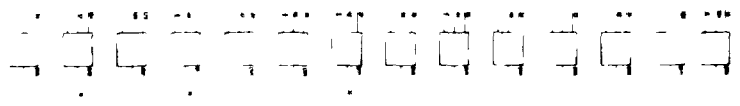
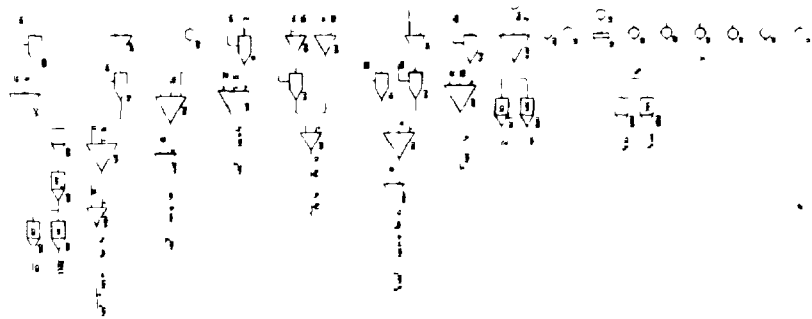


Figure 1-4 Light Diagram for Manual Assembly Inspection

Tab. 6.5 Input regular wave Test Case

Time (sec)	\ddot{X}_1 (g)	X_1 (in)
0.	-2.8649932E+00	0.
2.0000E-03	-2.8016147E+00	1.7577876E+00
4.0000E-03	-2.6235148E+00	3.5112014E+00
6.0000E-03	-4.3784913E+00	5.2605217E+00
8.0000E-03	-9.6449480E+00	7.0042524E+00
1.0000E-02	-1.7632820E+01	8.7343466E+00
1.2000E-02	-1.7511056E+01	1.0438021E+01
1.4000E-02	-1.7537313E+01	1.2114407E+01
1.6000E-02	-1.6759626E+01	1.3763445E+01
1.8000E-02	-1.5272191E+01	1.5386307E+01
2.0000E-02	-1.3314623E+01	1.6985321E+01
2.2000E-02	-1.1261403E+01	1.8563601E+01
2.4000E-02	-9.0282401E+00	2.0124467E+01
2.6000E-02	-7.2829892E+00	2.1671327E+01
2.8000E-02	-6.6203874E+00	2.3207240E+01
3.0000E-02	-7.1530590E+00	2.4733336E+01
3.2000E-02	-8.8401636E+00	2.6248832E+01
3.4000E-02	-1.1491636E+01	2.7751105E+01
3.6000E-02	-1.5141163E+01	2.9236002E+01
3.8000E-02	-1.9247897E+01	3.0697864E+01
4.0000E-02	-2.2843827E+01	3.2130106E+01
4.2000E-02	-7.5207314E+00	3.3526786E+01
4.4000E-02	-7.9136914E+00	3.4926095E+01
4.6000E-02	-1.0441918E+01	3.6312114E+01
4.8000E-02	-2.4243235E+01	3.7684726E+01
5.0000E-02	-2.6430863E+01	3.9015004E+01
5.2000E-02	-2.9223341E+01	4.0304627E+01
5.4000E-02	-3.1640538E+01	4.1549282E+01
5.6000E-02	-4.0190342E+01	4.2744833E+01
5.8000E-02	-3.0672698E+01	4.3883933E+01
6.0000E-02	-3.0227861E+01	4.4954678E+01
6.2000E-02	-2.6224158E+01	4.5978611E+01
6.4000E-02	-2.4831866E+01	4.6963933E+01
6.6000E-02	-2.4352471E+01	4.7910979E+01
6.8000E-02	-2.4233401E+01	4.8820503E+01
7.0000E-02	-2.6656738E+01	4.9692526E+01
7.2000E-02	-3.7439322E+01	5.0525414E+01
7.4000E-02	-3.6355283E+01	5.1302023E+01
7.6000E-02	-2.6744978E+01	5.2021729E+01
7.8000E-02	-1.8584005E+01	5.2701579E+01
8.0000E-02	-1.2210323E+01	5.3352154E+01
8.2000E-02	-1.1556729E+01	5.3985791E+01
8.4000E-02	-1.2157700E+01	5.4601463E+01
8.6000E-02	-1.2158977E+01	5.5199297E+01
8.8000E-02	-1.0209284E+01	5.5794658E+01
9.0000E-02	-9.5557644E+00	5.6375326E+01
9.2000E-02	-8.7058070E+00	5.6941200E+01
9.4000E-02	-7.7252627E+00	5.7493555E+01
9.6000E-02	-7.0494860E+00	5.8033931E+01
9.8000E-02	-6.4226800E+00	5.8563439E+01
1.0000E-01	-5.7769386E+00	5.9083017E+01

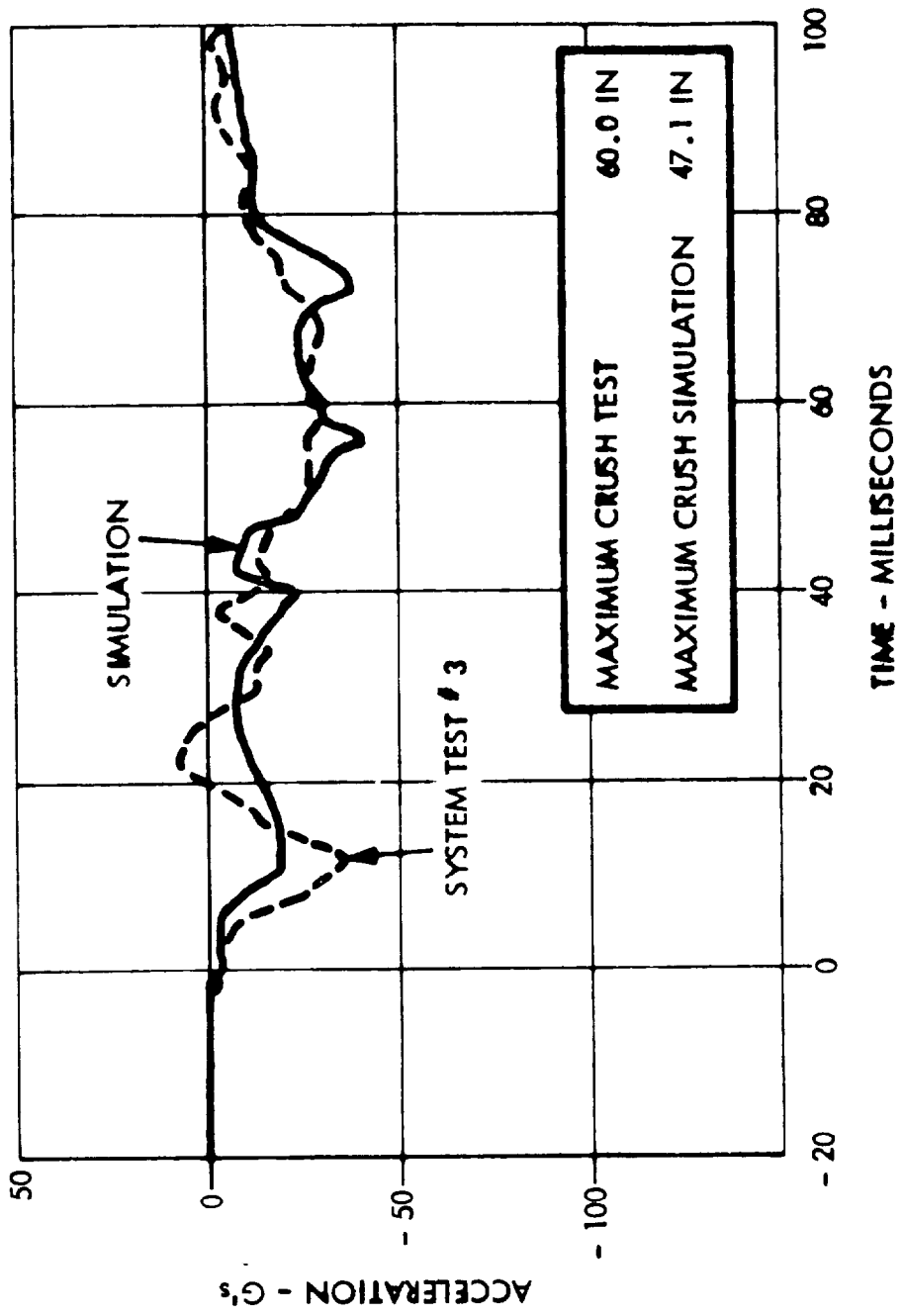


Figure 8-7. Front Angular Barrier Simulation (50 MPH)

Frontal Pole. This is a 5-degree-of-freedom model with all degrees of freedom being movement along the longitudinal axis of the vehicle. The model, shown in Figure 8-8, assumes symmetrical structural elements on the right and left sides of the vehicle. The five lumped masses are:

1. Mass 1 (M_1): Total mass of the vehicle less the masses assigned to masses 2, 3 and 4.
2. Mass 2 (M_2): Mass of the engine, transmission and the driveline.
3. Mass 3 (M_3): Mass of the crossmember, front suspension and front wheels.
4. Mass 4 (M_4): Mass of the bumper.
5. Mass 5 (M_5): Mass of the passengers.

The degrees of freedom and their time derivatives are:

$X_1, \dot{X}_1, \ddot{X}_1$ - Displacement, velocity and deceleration of mass M_1 respectively.

$X_2, \dot{X}_2, \ddot{X}_2$ - Displacement, velocity and deceleration of mass M_2 respectively.

$X_3, \dot{X}_3, \ddot{X}_3$ - Displacement, velocity and deceleration of mass M_3 respectively.

$X_4, \dot{X}_4, \ddot{X}_4$ - Displacement, velocity and deceleration of mass M_4 respectively.

$X_5, \dot{X}_5, \ddot{X}_5$ - Displacement, velocity and deceleration of mass M_5 respectively.

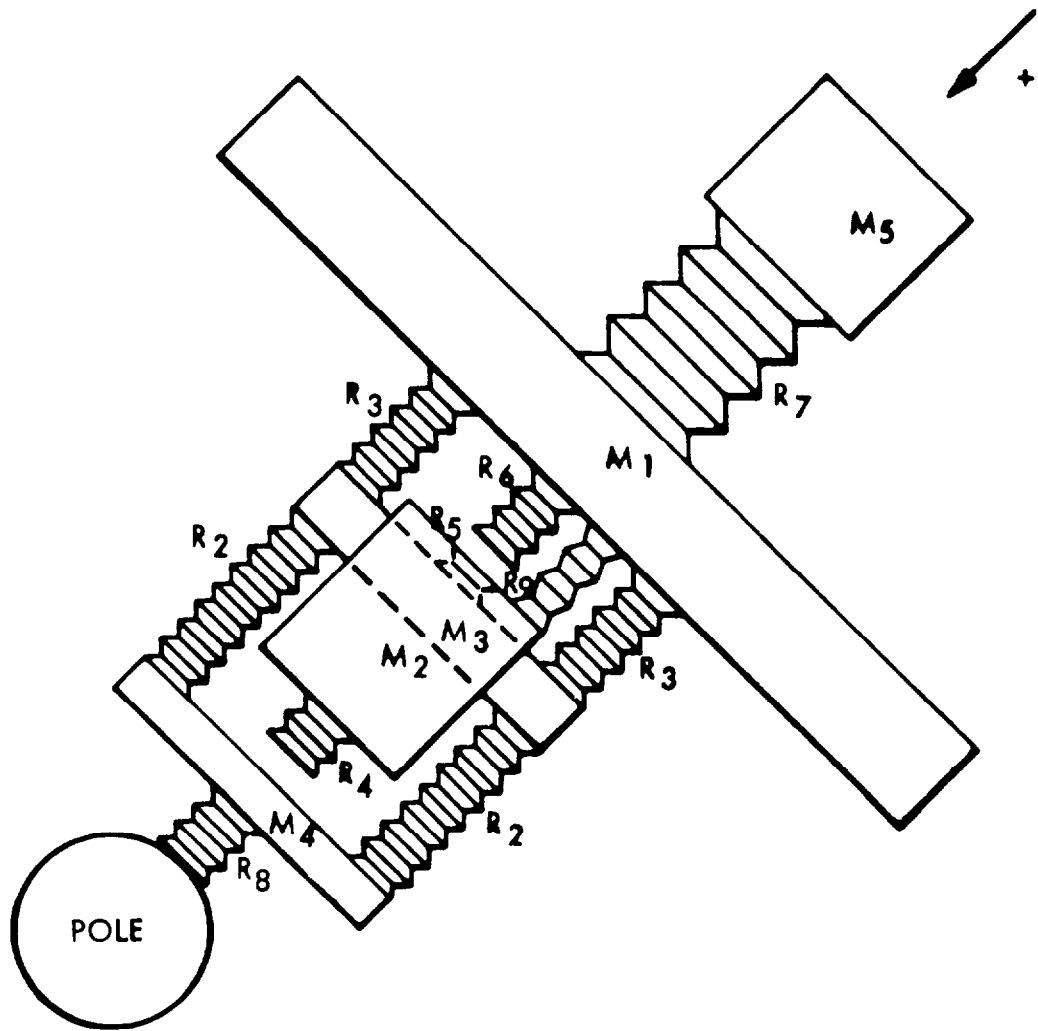


Figure 8-8. Frontal Pole Impact Model

The equations of motion are:

$$M_1 \ddot{X}_1 = -2F_3 - F_6 - F_9 + F_7$$

$$M_2 \dot{X}_2 = F_6 + F_9 - F_5 - F_4$$

$$M_3 \ddot{X}_3 = 2F_3 + F_5 - 2F_2$$

$$M_4 \ddot{X}_4 = -F_8 + 2F_2$$

$$M_5 \ddot{X}_5 = -F_7$$

Forces (F) are defined as:

F_2 - resistance offered by R_2 and function of $(X_3 - X_4)$

F_3 - resistance offered by R_3 and function of $(X_1 - X_3)$

F_4 - resistance offered by R_4 and function of (X_2)

F_5 - resistance offered by R_5 and function of $(X_2 - X_3)$

F_6 - resistance offered by R_6 and function of $(X_1 - X_2)$

F_7 - resistance offered by R_7 and function of $(X_5 - X_1)$

F_8 - resistance offered by R_8 and function of (X_4)

F_9 - resistance offered by R_9 and function of $(X_1 - X_2)$

The logic diagram for the frontal pole model is described in Figure 8-9. The results of a test case are tabulated in Table 8-6 and are plotted in Figure 8-10.

Values used in the simulation were:

$$M_1 = 1821 \text{ lb}/386.$$

$$M_2 = 670 \text{ lb}/386.$$

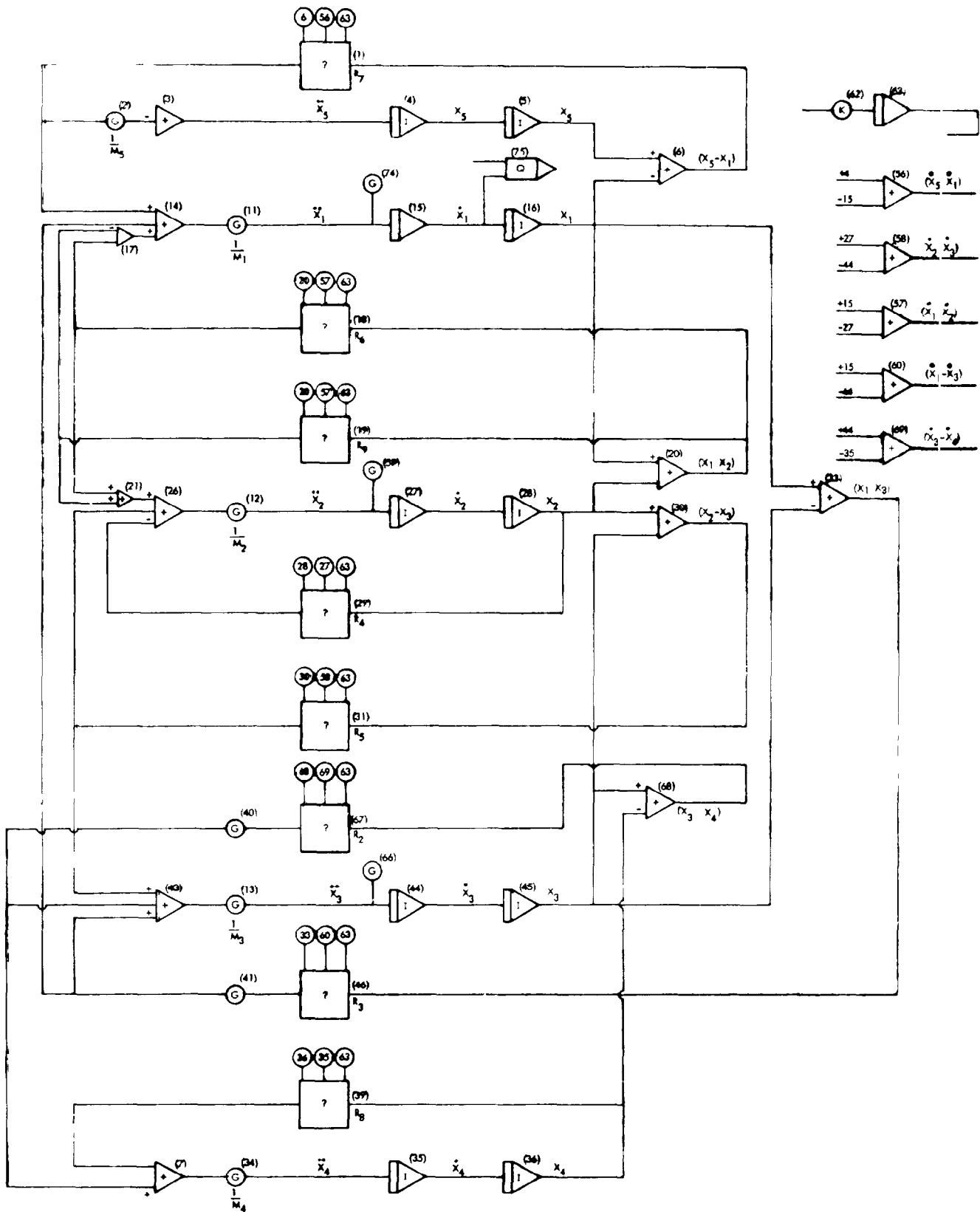


Figure 8-9. Logic Diagram for Front Pole Impact Model

Table 8-6. Front Pole Test Case

Time (sec)	\ddot{X}_1 (g)	X_1 (in)
0.	0.	0.
2.0000E-03	0.	1.4080000E+00
4.0000E-03	0.	2.8160000E+00
6.0000E-03	0.	4.2240000E+00
8.0000E-03	0.	5.6320000E+00
1.0000E-02	-2.3697916E+00	7.0400000E+00
1.2000E-02	-1.1584439E+01	8.4460710E+00
1.4000E-02	-2.3577569E+01	9.8362670E+00
1.6000E-02	-3.0181087E+01	1.1190856E+01
1.8000E-02	-3.0246929E+01	1.2495082E+01
2.0000E-02	-3.0020370E+01	1.3752557E+01
2.2000E-02	-2.9454487E+01	1.4963538E+01
2.4000E-02	-2.8888431E+01	1.6129040E+01
2.6000E-02	-2.4320110E+01	1.7250232E+01
2.8000E-02	-1.7152566E+01	1.8331331E+01
3.0000E-02	-1.1983412E+01	1.9384766E+01
3.2000E-02	-9.3261094E+00	2.0420271E+01
3.4000E-02	-1.1381068E+01	2.1442536E+01
3.6000E-02	-1.7768245E+01	2.2448875E+01
3.8000E-02	-2.7148965E+01	2.3429293E+01
4.0000E-02	-3.6839033E+01	2.4368777E+01
4.2000E-02	-4.2066327E+01	2.5251209E+01
4.4000E-02	-4.2998222E+01	2.6070724E+01
4.6000E-02	-4.6024658E+01	2.6823943E+01
4.8000E-02	-4.9547121E+01	2.7506334E+01
5.0000E-02	-5.0569724E+01	2.8112329E+01
5.2000E-02	-5.0171402E+01	2.8639923E+01
5.4000E-02	-4.7958339E+01	2.9088644E+01
5.6000E-02	-4.7252913E+01	2.9463475E+01
5.8000E-02	-4.6980550E+01	2.9765821E+01
6.0000E-02	-4.5938200E+01	2.9995567E+01
6.2000E-02	-4.5449983E+01	3.0153963E+01
6.4000E-02	-4.5074986E+01	3.0242929E+01

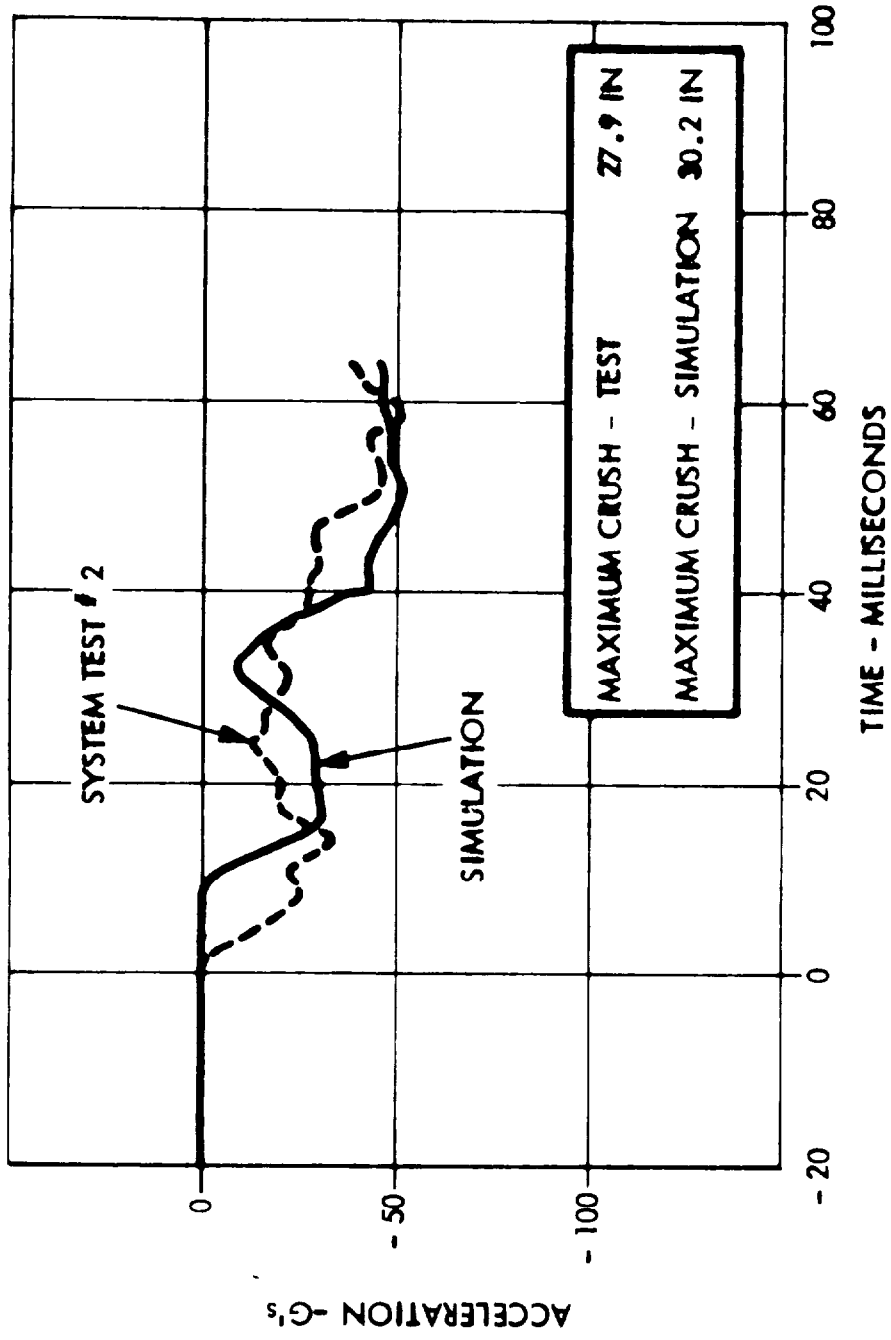


Figure 8-10. Front Pole Simulation (40 MPH)

$$M_3 = 420 \text{ lb}/386.$$

$$M_4 = 48 \text{ lb}/386.$$

$$V = 40 \text{ mph}$$

Side Pole. This is a 2-degree-of-freedom model with both degrees of freedom perpendicular to the longitudinal axis of the vehicle. The model is shown in Figure 8-11. The two lumped masses are:

1. Mass 1 (M_1): Mass of the doors and its accessories.
2. Mass 2 (M_2): Total mass of the vehicle less M_1 .

The degrees of freedom and their time derivatives are:

$X_1, \dot{X}_1, \ddot{X}_1$ - Displacement, velocity and acceleration of mass M_1 .

$X_2, \dot{X}_2, \ddot{X}_2$ - Displacement, velocity and acceleration of mass M_2 .

The equations of motion are:

$$M_1 \ddot{X}_1 = F_2 - F_1$$

$$M_2 \ddot{X}_2 = F_2 - F_3 - F_4$$

where

F_1 - resistance offered by R_1 and function of X_1

F_2 - resistance offered by R_2 and function of $X_2 - X_1$

F_3 - resistance offered by R_3 and function of X_2

F_4 - resistance offered by R_4 and function of X_2

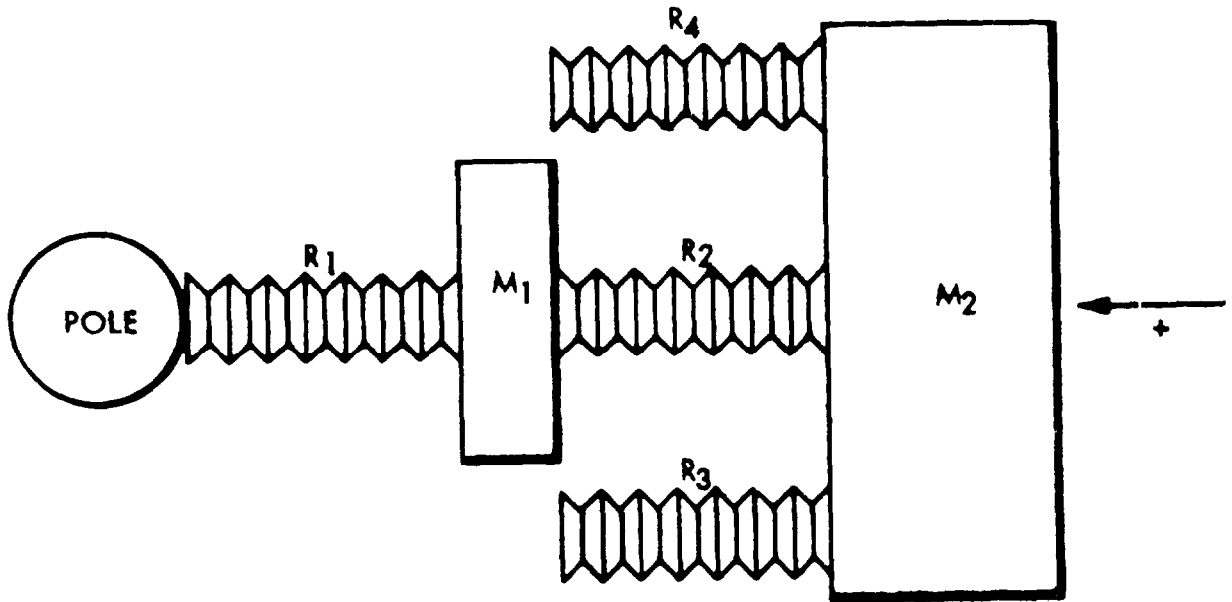


Figure 8-11. Side Pole Impact Mod I

A logic diagram of the side pole impact model is given in Figure 8-12. The results of a test case simulation are tabulated in Table 8-7 and plotted in Figure 8-13.

Values used in the test case are:

$$M_1 = 100 \text{ lb}/386.$$

$$M_2 = 2830 \text{ lb}/386.$$

$$V = 10 \text{ mph}$$

Front-to-Front Aligned. This is a 6-degree-of-freedom model with all degrees of freedom along the longitudinal axes of the impact vehicles. The model is shown in Figure 8-14.

The six lumped masses are:

1. Mass 1 (M_1): Total mass of the impacted vehicle less masses assigned to masses 2, 3, 4a and 5.
2. Mass 2 (M_2): Mass of the engine, transmission and driveline.
3. Mass 3 (M_3): Mass of the crossbar, front suspension and front wheels.
4. Mass 4 (M_4): Composed of mass 4a and mass 4b.
5. Mass 4a (M_{4a}): Mass of the impacted vehicle bumper.
6. Mass 4b (M_{4b}): Mass of the impacting vehicle bumper.

The common initial velocity (\dot{X}_4) of the bumpers is given by:

$$\dot{X}_4 = \frac{M_{4a} V_1 + M_{4b} V_2}{M_{4a} + M_{4b}}$$

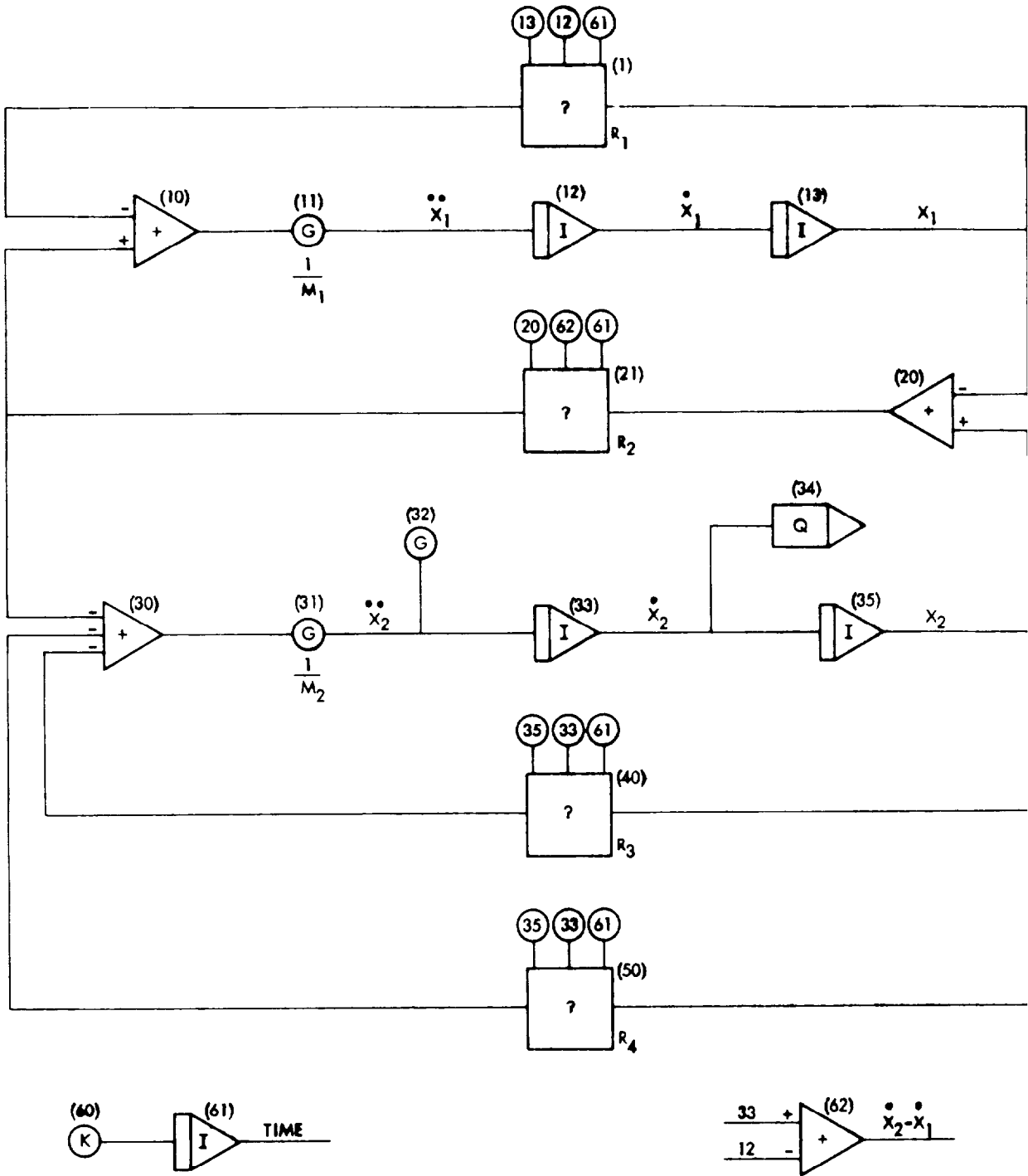


Figure 8-12. Logic Diagram For Side Pole Impact Model

Table 8-7. Side Pole Test Case

Time (sec)	\ddot{X}_1 (g)	X_1 (in)
0.	0.	0.
2.0000E-03	-1.7062374E-02	3.5200000E-01
4.0000E-03	-6.8171407E-02	7.0398682E-01
6.0000E-03	-1.5839077E-01	1.0558812E+00
8.0000E-03	-3.1585757E-01	1.4075483E+00
1.0000E-02	-5.6057429E-01	1.7587528E+00
1.2000E-02	-8.9872963E-01	2.1091240E+00
1.4000E-02	-1.3174493E+00	2.4581411E+00
1.6000E-02	-1.7876694E+00	2.8051520E+00
1.8000E-02	-2.2707779E+00	3.1494193E+00
2.0000E-02	-2.7321178E+00	3.4901834E+00
2.2000E-02	-3.1422395E+00	3.8267191E+00
2.4000E-02	-3.4099014E+00	4.1583830E+00
2.6000E-02	-3.5747092E+00	4.4847050E+00
2.8000E-02	-3.7421172E+00	4.8055000E+00
3.0000E-02	-3.9312490E+00	5.1205170E+00
3.2000E-02	-4.1579635E+00	5.4294711E+00
3.4000E-02	-4.4276224E+00	5.7320176E+00
3.6000E-02	-5.0730770E+00	6.0277413E+00
3.8000E-02	-7.4988264E+00	6.3159045E+00
4.0000E-02	-7.8204648E+00	6.5913633E+00
4.2000E-02	-8.1136883E+00	6.8547398E+00
4.4000E-02	-8.3649391E+00	7.1055747E+00
4.6000E-02	-8.5674567E+00	7.3434753E+00
4.8000E-02	-8.7213184E+00	7.5681266E+00
5.0000E-02	-8.8321939E+00	7.7792911E+00
5.2000E-02	-8.9093596E+00	7.9767997E+00
5.4000E-02	-9.0615580E+00	8.1605366E+00
5.6000E-02	-9.2013664E+00	8.3302778E+00
5.8000E-02	-9.3213240E+00	8.4857984E+00
6.0000E-02	-9.4274390E+00	8.6269157E+00
6.2000E-02	-9.5043125E+00	8.7534682E+00
6.4000E-02	-9.5528949E+00	8.8653233E+00
6.6000E-02	-9.6008388E+00	8.9624243E+00
6.8000E-02	-9.6473254E+00	9.0446974E+00
7.0000E-02	-9.6903917E+00	9.1120706E+00
7.2000E-02	-9.7273396E+00	9.1644764E+00
7.4000E-02	-9.7551582E+00	9.2018570E+00
7.6000E-02	-9.7714783E+00	9.2241681E+00

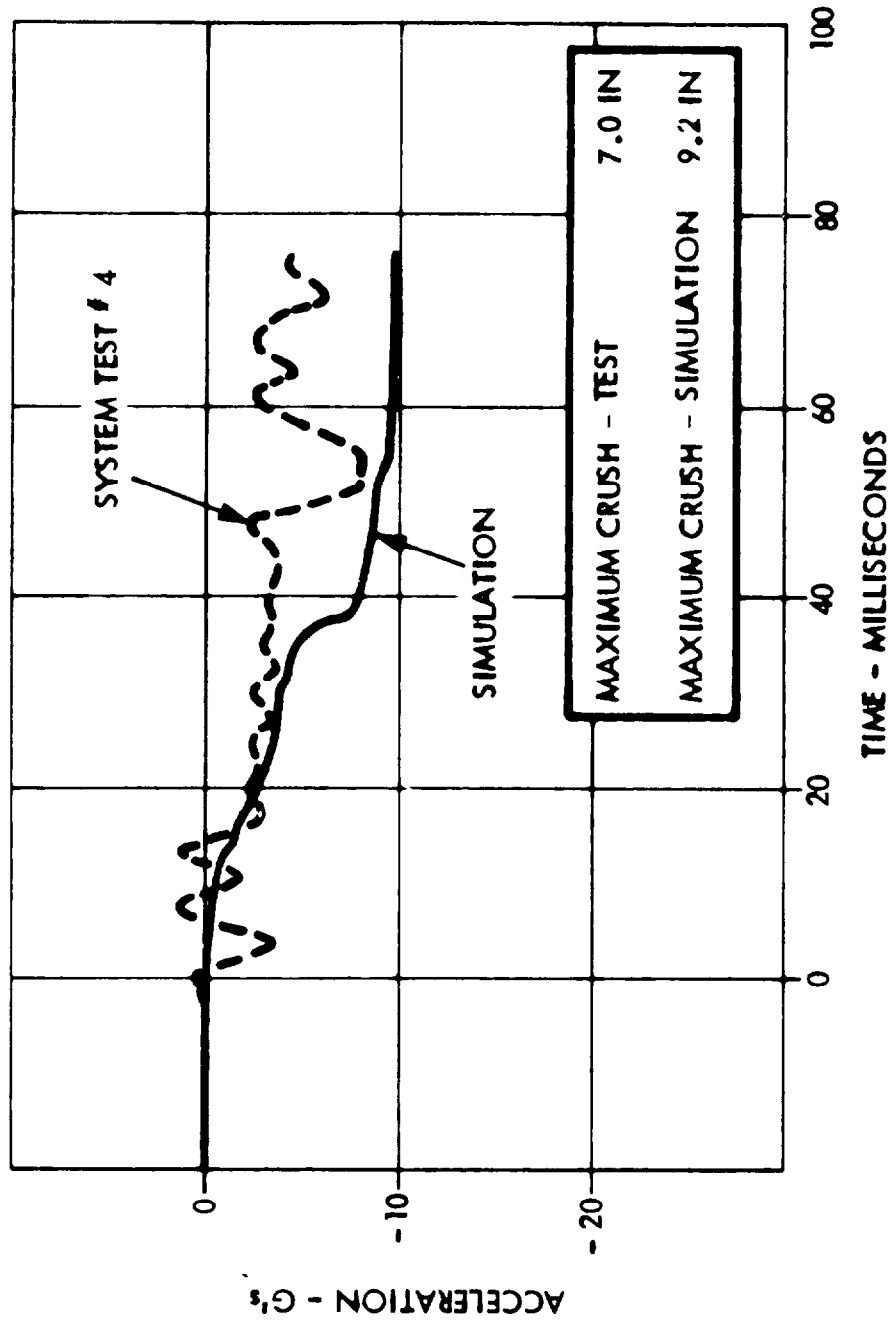


Figure 8-13. Side Pole Simulation (10 MPH)

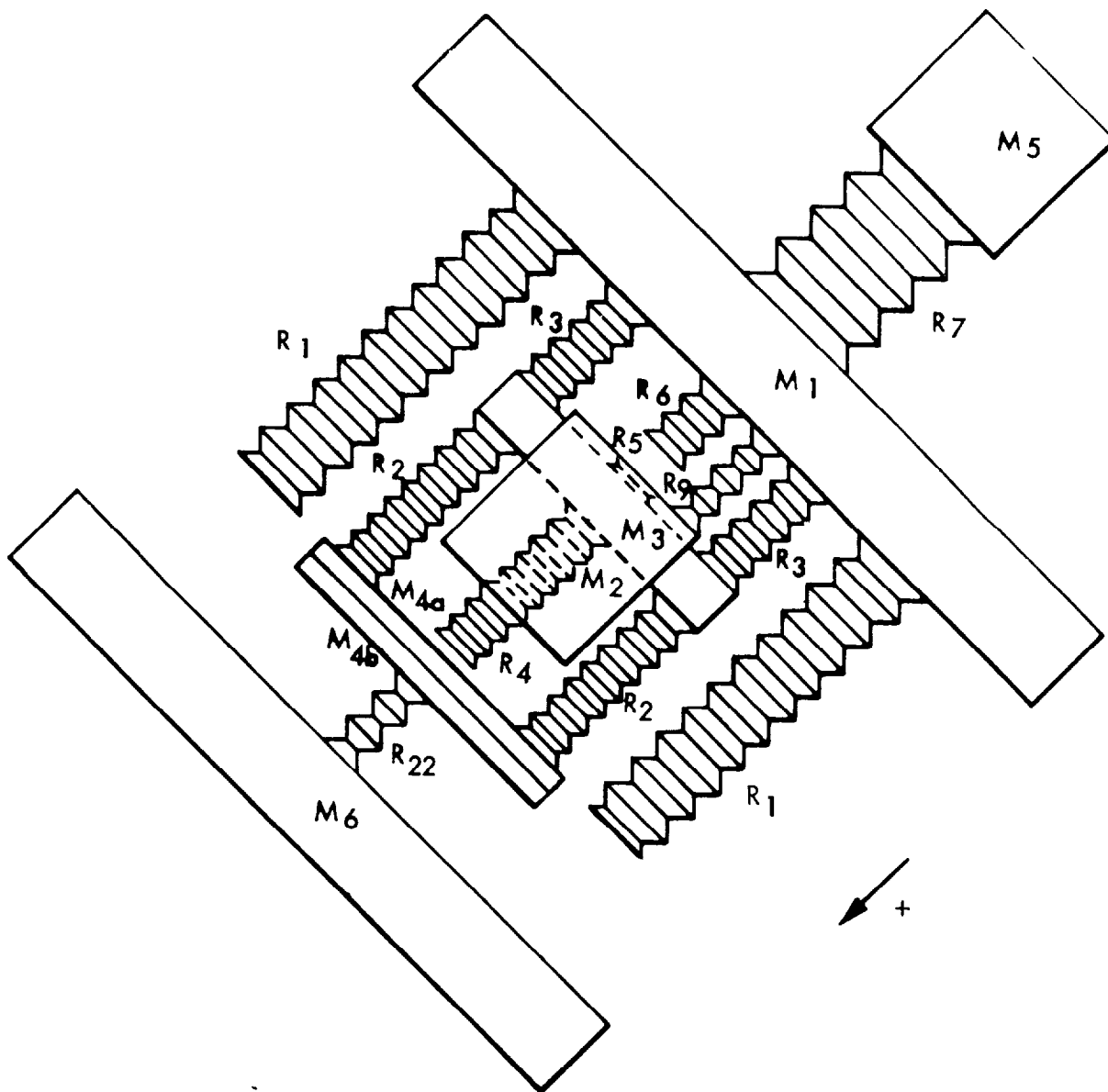


Figure 8-14. Front/Front Aligned Impact Mod I

where

V_1 is initial velocity of the impacted vehicle bumper

V_2 is initial velocity of the impacting vehicle bumper

7. Mass 5 (M_5): Mass of the passengers in the impacted vehicle.
8. Mass 6 (M_6): Total mass of the impacting vehicle less the masses assigned to 4b.

The degrees of freedom and their time derivatives are:

$X_1, \dot{X}_1, \ddot{X}_1$ - Displacement, velocity and deceleration of mass M_1 respectively.

$X_2, \dot{X}_2, \ddot{X}_2$ - Displacement, velocity and deceleration of mass M_2 respectively.

$X_3, \dot{X}_3, \ddot{X}_3$ - Displacement, velocity and deceleration of mass M_3 respectively.

$X_4, \dot{X}_4, \ddot{X}_4$ - Displacement, velocity and deceleration of mass M_4 respectively.

$X_5, \dot{X}_5, \ddot{X}_5$ - Displacement, velocity and deceleration of mass M_5 respectively.

$X_6, \dot{X}_6, \ddot{X}_6$ - Displacement, velocity and deceleration of mass M_6 respectively.

The equations of motion are:

$$M_1 \ddot{X}_1 = -2F_1 - 2F_3 - F_6 - F_9 + F_7$$

$$M_2 \ddot{X}_2 = F_6 + F_9 - F_5 - F_4$$

$$M_3 \ddot{X}_3 = 2F_3 + F_5 - 2F_2$$

$$M_4 \ddot{X}_4 = 2F_2 + F_4 - F_{22}$$

$$M_5 \ddot{X}_5 = -F_7$$

$$M_6 \ddot{X}_6 = F_{22} + 2F_1$$

where

F_1 - resistance offered by R_1 and function of $X_1 - X_4$

F_2 - resistance offered by R_2 and function of $X_3 - X_4$

F_3 - resistance offered by R_3 and function of $X_1 - X_3$

F_4 - resistance offered by R_4 and function of $X_2 - X_4$

F_5 - resistance offered by R_5 and function of $X_2 - X_3$

F_6 - resistance offered by R_6 and function of $X_1 - X_2$

F_7 - resistance offered by R_7 and function of $X_5 - X_1$

F_9 - resistance offered by R_9 and function of $X_1 - X_2$

F_{22} - resistance offered by R_{22} and function of $X_4 - X_6$

The logic diagram for the front-to-front aligned impact model is shown in Figure 8-15. The results of a test case are tabulated in Table 8-8 and plotted in Figure 8-16.

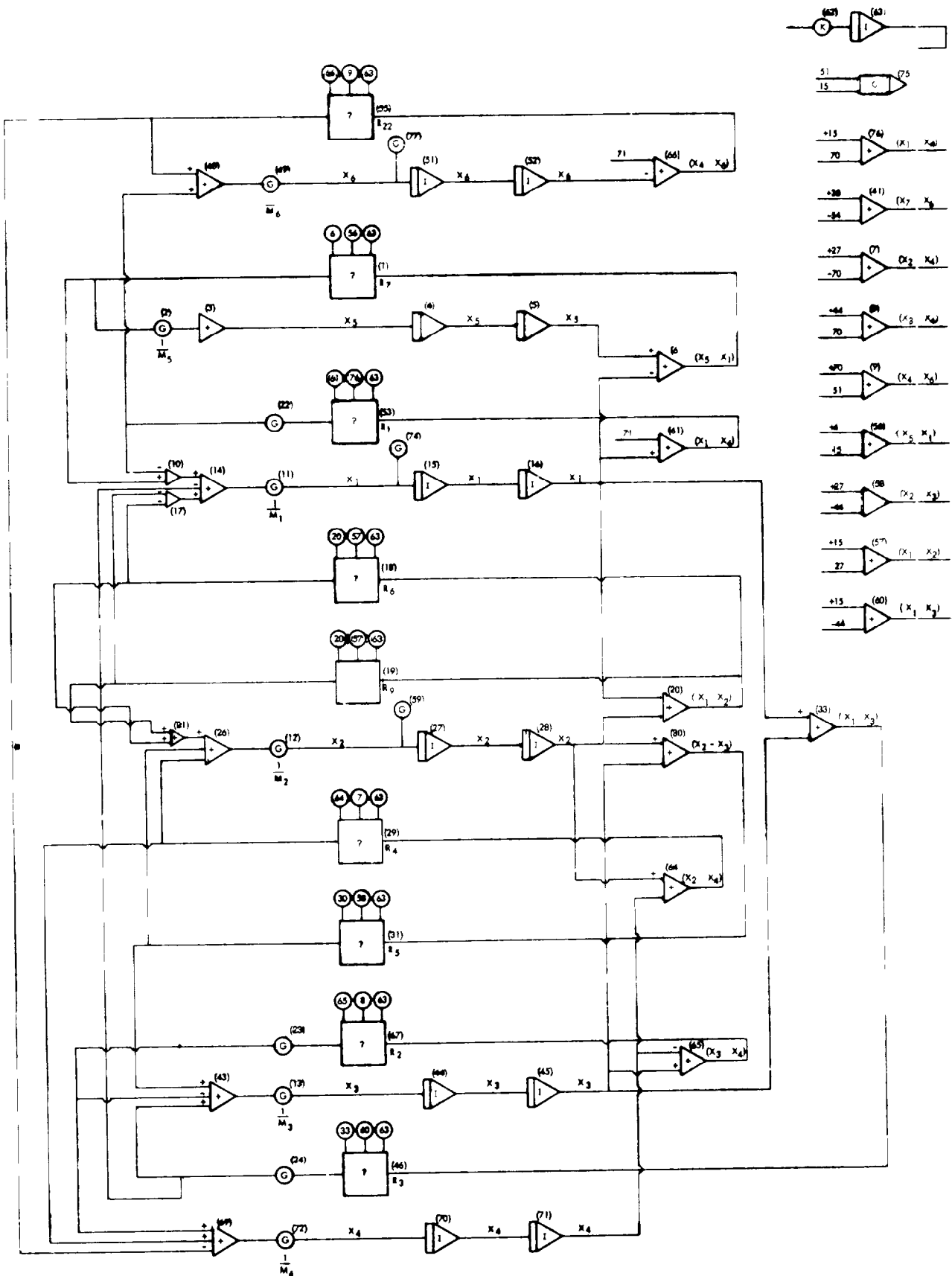


Figure 8-15. Logic Diagram for Front/Front Aligned Impact Model

Table 8-8. Front to Front Aligned Test Case

Time (sec)	\ddot{X}_1 (g)	X_1 (in)
0.	0.	0.
2.0000E-03	0.	1.3200000E+00
4.0000E-03	-7.0741186E+00	2.3812300E+00
6.0000E-03	-1.9524087E+01	3.7362108E+00
8.0000E-03	-3.1783513E+01	5.1924121E+00
1.0000E-02	-3.9794088E+01	6.5638762E+00
1.2000E-02	-4.5963567E+01	8.0322995E+00
1.4000E-02	-4.3723111E+01	9.6308612E+00
1.6000E-02	-3.7454153E+01	1.1213751E+01
1.8000E-02	-3.7035425E+01	1.2757229E+01
2.0000E-02	-3.6432603E+01	1.4227394E+01
2.2000E-02	-3.5838250E+01	1.5574101E+01
2.4000E-02	-3.4021375E+01	1.6759104E+01
2.6000E-02	-3.0111739E+01	1.7762970E+01
2.8000E-02	-2.4580773E+01	1.8580909E+01
3.0000E-02	-1.8702804E+01	1.9209381E+01
3.2000E-02	-1.4054327E+01	1.9698584E+01
3.4000E-02	-1.1830347E+01	2.0097436E+01
3.6000E-02	-1.4951038E+01	2.0101990E+01
3.8000E-02	-2.1943671E+01	1.9819847E+01
4.0000E-02	-3.1745489E+01	1.9614883E+01
4.2000E-02	-3.4823664E+01	2.0043607E+01
4.4000E-02	-3.4827084E+01	2.0732555E+01
4.6000E-02	-3.4222887E+01	2.0987361E+01
4.8000E-02	-3.6412656E+01	2.0841522E+01
5.0000E-02	-3.9045631E+01	2.0419722E+01
5.2000E-02	-3.8518328E+01	2.0666980E+01
5.4000E-02	-3.9950283E+01	2.1671760E+01
5.6000E-02	-4.1756233E+01	2.2252961E+01

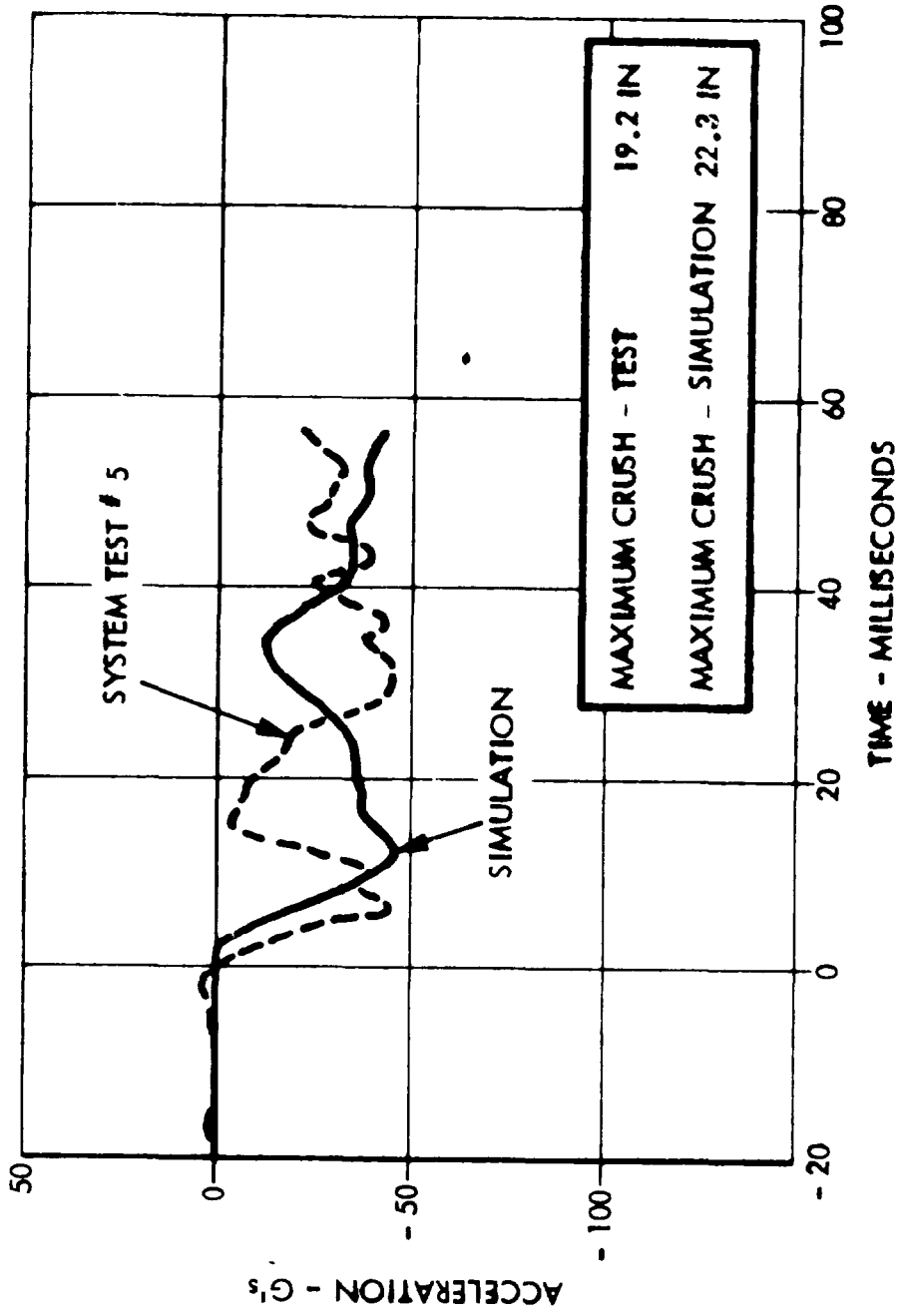


Figure 8-16. Front to Front Aligned Simulation (75 MPH)

Values used in the simulation were:

$$M_1 = 1778 \text{ lb}/386.$$

$$M_2 = 570 \text{ lb}/386.$$

$$M_3 = 420 \text{ lb}/386.$$

$$M_4 = 100 \text{ lb}/386.$$

$$M_6 = 2880 \text{ lb}/386.$$

$$V_1 = + 37.5 \text{ mph}$$

$$V_2 = - 37.5 \text{ mph}$$

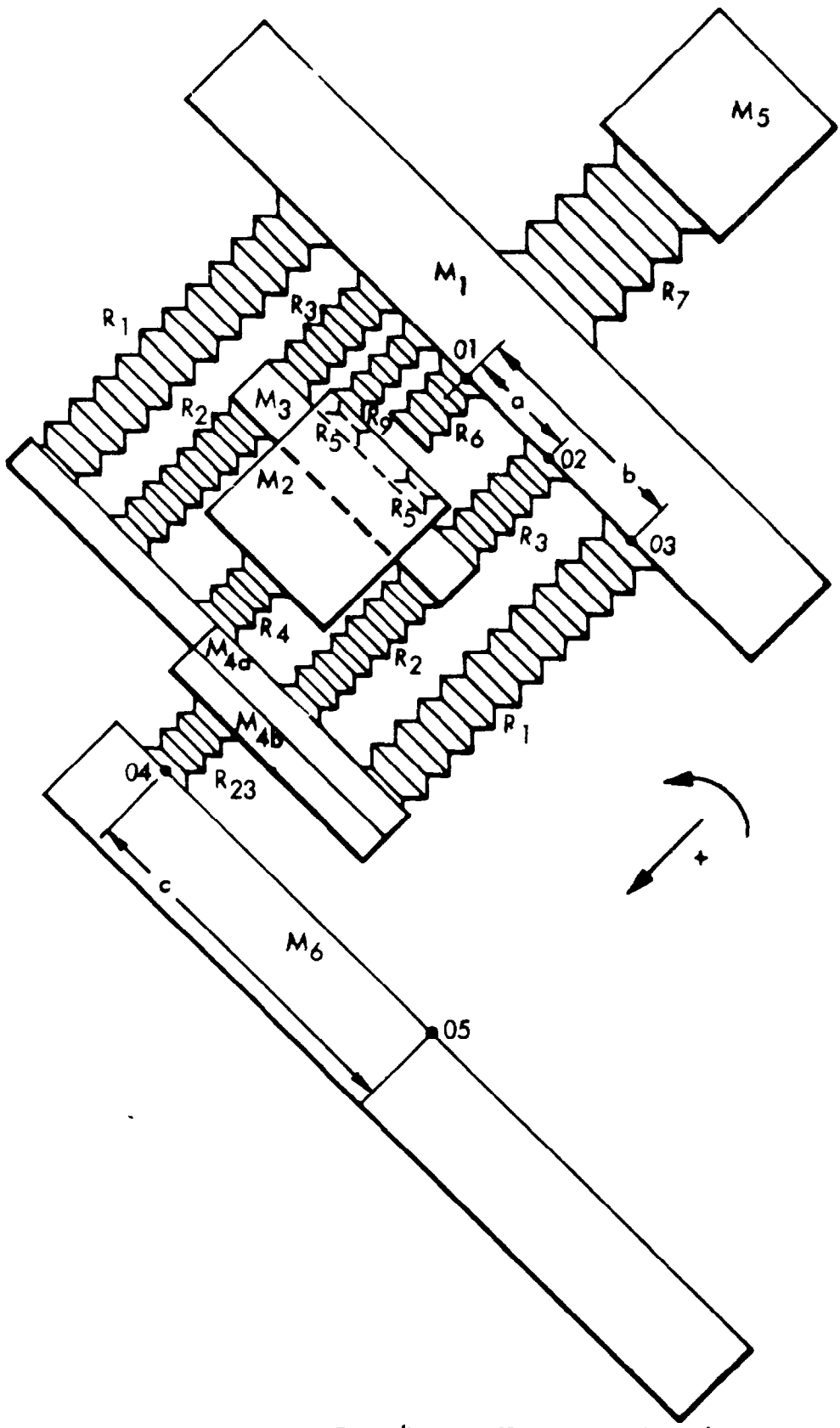
Front-to-Front Offset. This is a 9-degree-of-freedom system. Six degrees of freedom are parallel to the longitudinal axes of impacting vehicles and three degrees are rotating about yaw or vertical axes (Figure 8-17).

The lumped masses are:

1. Mass 1 (M_1): Total mass of the impacted vehicle less assigned to 2, 3, 4a and 5.
2. Mass 2 (M_2): Mass of the engine, transmission and driveline.
3. Mass 3 (M_3): Mass of the crossbar, front suspension and front wheels.
4. Mass 4 (M_4): Composed of mass 4a and mass 4b.
5. Mass 4a (M_{4a}): Mass of the impacted vehicle bumper.
6. Mass 4b (M_{4b}): Mass of the impacting vehicle bumper.

The common initial velocity (\dot{X}_4) of the bumpers is given by

$$\dot{X}_4 = \frac{M_{4a} V_1 + M_{4b} V_2}{M_{4a} + M_{4b}}$$



Figur 8-17. Front/Front Offset Impact Model

where

V_1 is initial velocity of the impacted vehicle bumper

V_2 is initial velocity of the impacting vehicle bumper

7. Mass 5 (M_5): Mass of the passengers in the impacted vehicle.

8. Mass 6 (M_6): Total mass of the impacting vehicle less the mass assigned to 4b.

Moments of inertia are:

1. Moment of inertia 1 (I_1): Moment of inertia of the passenger compartment of the impacted vehicle (mass M_1) about vertical axis passing through point "0"₁.

2. Moment of inertia 3 (I_3): Moment of inertia of crossbar (mass M_3) about vertical axis passing through centroid of crossbar.

3. Moment of inertia 6 (I_6): Moment of inertia of the impacting vehicle (mass M_6) about vertical axis passing through middle point of its bumper.

The degrees of freedom and their time derivatives are

$X_1, \dot{X}_1, \ddot{X}_1$ - Displacement, velocity and deceleration of mass M_1 respectively.

$X_2, \dot{X}_2, \ddot{X}_2$ - Displacement, velocity and deceleration or acceleration of mass M_2 respectively.

$X_3, \dot{X}_3, \ddot{X}_3$ - Displacement, velocity and acceleration or deceleration of mass M_3 respectively.

$X_4, \dot{X}_4, \ddot{X}_4$ - Displacement, velocity and deceleration or acceleration of mass M_4 respectively.

$X_5, \dot{X}_5, \ddot{X}_5$ - Displacement, velocity and deceleration of mass M_5 respectively.

$X_6, \dot{X}_6, \ddot{X}_6$ - Displacement, velocity and deceleration of mass M_6 respectively.

$\theta_1, \dot{\theta}_1, \ddot{\theta}_1$ - Rotation, angular velocity and angular retardation of mass M_1 respectively.

$\theta_3, \dot{\theta}_3, \ddot{\theta}_3$ - Rotation, angular velocity and angular retardation or acceleration of mass M_3 respectively.

$\theta_6, \dot{\theta}_6, \ddot{\theta}_6$ - Rotation, angular velocity and angular retardation of mass M_6 respectively.

The equations of motion are:

$$M_1 \ddot{X}_1 = -F_1 - F_3 - F_6 - F_9 + F_7$$

$$M_2 \ddot{X}_2 = F_6 + F_9 - F_5 - F_4$$

$$M_3 \ddot{X}_3 = F_3 + F_5 - F_2$$

$$M_4 \ddot{X}_4 = F_2 + F_4 + F_1 - F_{23}$$

$$M_5 \ddot{X}_5 = -F_7$$

$$M_6 X_6 = F_{23}$$

$$I_1 \theta_1 = F_1 b + F_3 a$$

$$I_3 \theta_3 = F_2 a - F_3 a$$

$$I_6 \theta_6 = F_{23} c$$

where

F_1 - resistance offered by R_1 and function of $(X_1 - b \theta_1) - X_4$

F_2 - resistance offered by R_2 and function of $(X_3 - a \sin \theta_3) - X_4$

F_3 - resistance offered by R_3 and function of $(X_1 - a \theta_1) - X_3 - a \sin \theta_3$

F_4 - resistance offered by R_4 and function of $(X_2 - X_4)$

F_5 - resistance offered by R_5 and function of $(X_2 - X_3)$

F_6 - resistance offered by R_6 and function of $(X_1 - X_2)$

F_7 - resistance offered by R_7 and function of $(X_5 - X_1)$

F_9 - resistance offered by R_9 and function of $(X_1 - X_2)$

F_{23} - resistance offered by R_{23} and function of $(X_4 - X_6 - c \theta_6)$

a - distance between 01 and 02

b - distance between 01 and 03

c - distance between 04 and 05

A logic diagram for the front-to-front offset impact model is given in Figure 8-18. The results of a test case simulation are tabulated in Table 8-9 and plotted in Figure 8-19.

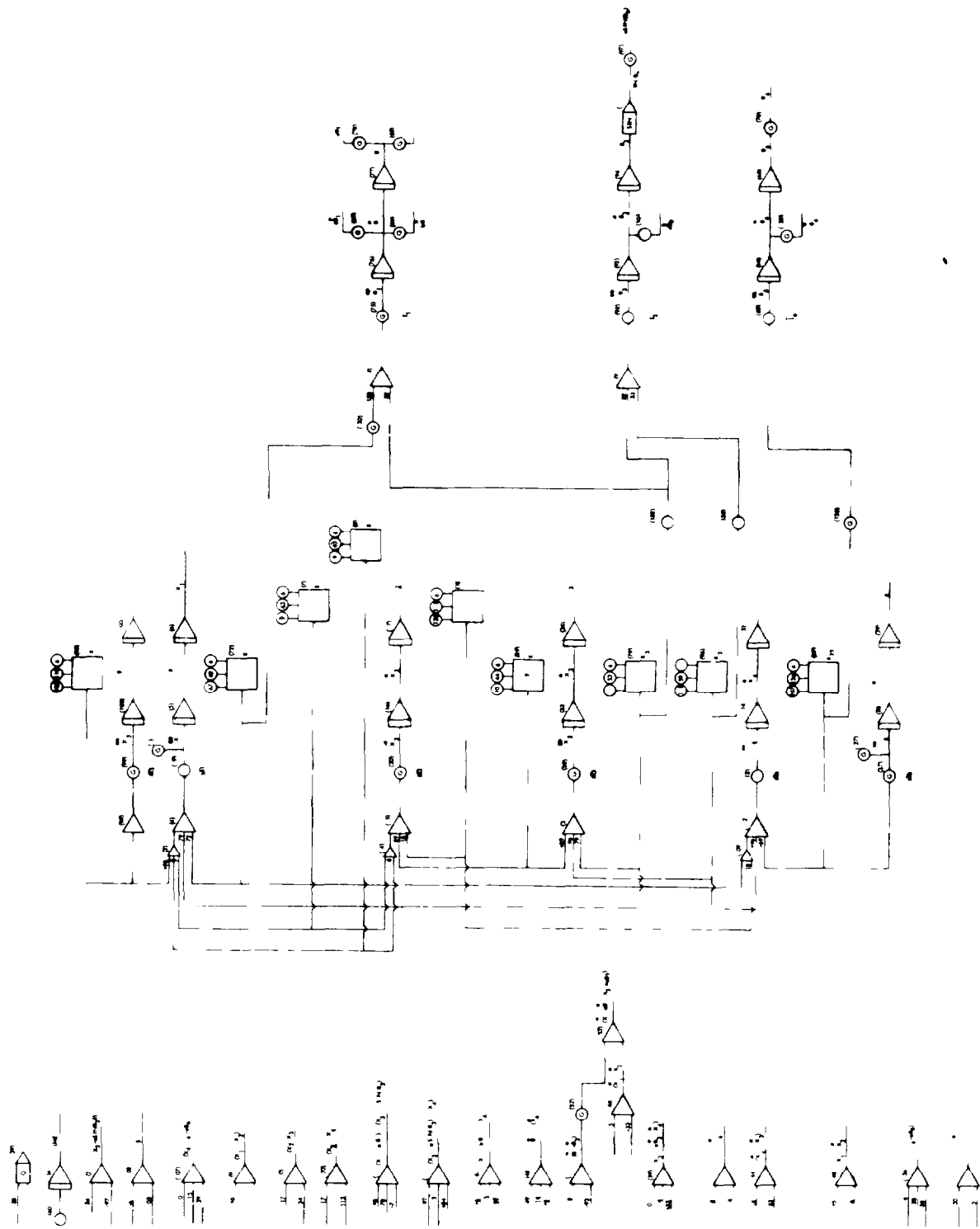


Figure 8-18. Logic Diagram for front/Innet Offset Impact Model

Table 8-9. Front to Front Offset Test Case

Time (sec)	\ddot{X}_1 (g)	X_1 (in)
0.	0.	0.
2.0000E-03	0.	1.3200000E+00
4.0000E-03	-4.8739470E+00	2.5042137E+00
6.0000E-03	-1.3336511E+01	3.8221460E+00
8.0000E-03	-1.6652877E+01	5.2248327E+00
1.0000E-02	-2.1336411E+01	6.6130267E+00
1.2000E-02	-2.4292865E+01	8.0371010E+00
1.4000E-02	-2.4503109E+01	9.3954246E+00
1.6000E-02	-2.0851733E+01	1.0676361E+01
1.8000E-02	-2.0967800E+01	1.2011500E+01
2.0000E-02	-2.0755742E+01	1.3297837E+01
2.2000E-02	-2.0131701E+01	1.4522838E+01
2.4000E-02	-1.9598603E+01	1.5668677E+01
2.6000E-02	-1.9144054E+01	1.6710442E+01
2.8000E-02	-1.8761816E+01	1.7634468E+01
3.0000E-02	-1.8456887E+01	1.8444690E+01
3.2000E-02	-1.8224460E+01	1.9146800E+01
3.4000E-02	-1.8066430E+01	1.9761470E+01
3.6000E-02	-1.8103376E+01	2.0315926E+01
3.8000E-02	-1.8476530E+01	2.1317804E+01
4.0000E-02	-1.8223329E+01	2.2586854E+01
4.2000E-02	-1.8445414E+01	2.2036520E+01
4.4000E-02	-2.4537676E+01	2.2855790E+01
4.6000E-02	-2.8747249E+01	2.5773131E+01
4.8000E-02	-3.3709681E+01	2.7098046E+01
5.0000E-02	-3.9510546E+01	2.5369457E+01
5.2000E-02	-3.5278426E+01	2.5994594E+01
5.4000E-02	-3.1224275E+01	3.0167324E+01

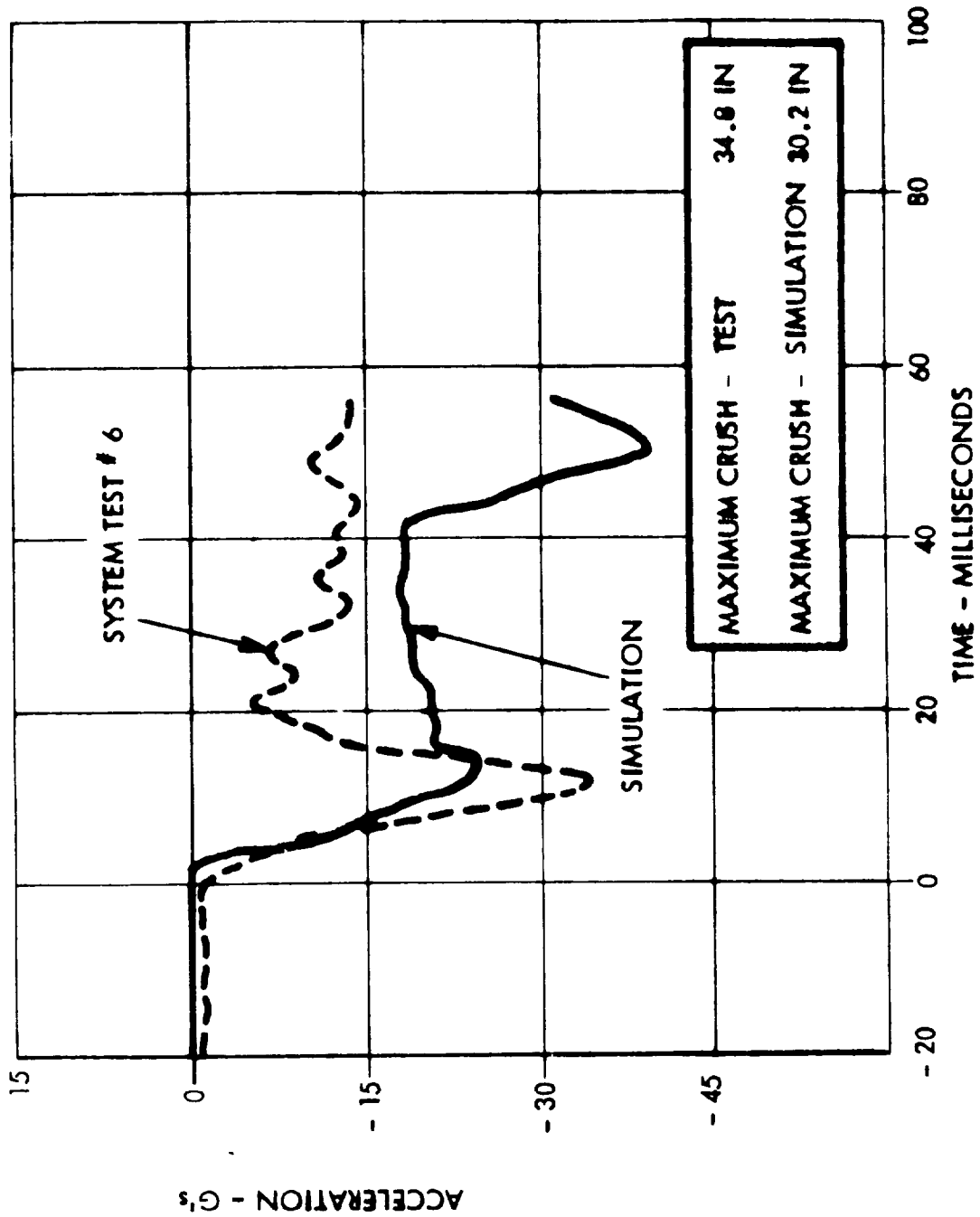


Figure 8-19. Front to Front Offset Simulation (75 MPH)

Values used in the simulation were:

$$M_1 = 1778 \text{ lb}/386.$$

$$M_2 = 670 \text{ lb}/386.$$

$$M_3 = 420 \text{ lb}/386.$$

$$M_4 = 100 \text{ lb}/386.$$

$$M_6 = 2880 \text{ lb}/386.$$

$$I_1 = 1,135,940 \text{ lb}\cdot\text{in}^2/386.$$

$$I_2 = 77,200 \text{ lb}\cdot\text{in}^2/386.$$

$$I_3 = 77,200 \text{ lb}\cdot\text{in}^2/386.$$

$$a = 17.5 \text{ in}$$

$$b = 27. \text{ in}$$

$$c = 17.5 \text{ in}$$

$$V_1 = + 37.5 \text{ mph}$$

$$V_2 = - 37.5 \text{ mph}$$

Front-Side. This is a 3-degree-of-freedom model. All degrees of freedom are in the direction of the longitudinal axis of the impacting vehicle. The model is shown in Figure 8-20.

The lumped masses are:

1. Mass 1 (M_1): Total mass of the impacted vehicle.
2. Mass 2 (M_2): Mass of the impacting vehicle bumper.
3. Mass 3 (M_3): Total mass of the impacting vehicle less the mass assigned to 2.

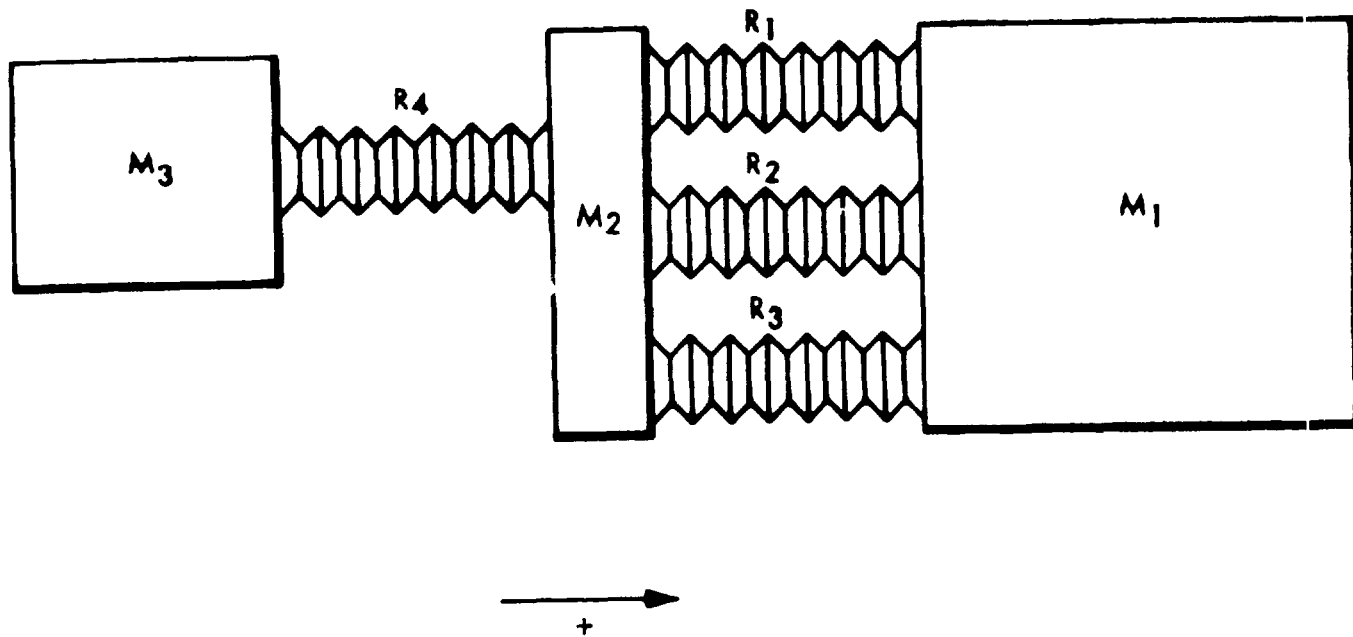


Figure 8-20. Front/Side Normal Impact Model

The degrees of freedom and their time derivatives are:

$X_1, \dot{X}_1, \ddot{X}_1$ - Displacement, velocity and acceleration of mass M_1 .

$X_2, \dot{X}_2, \ddot{X}_2$ - Displacement, velocity and acceleration of mass M_2 .

$X_3, \dot{X}_3, \ddot{X}_3$ - Displacement, velocity and acceleration of mass M_3 .

The equations of motion are:

$$M_1 \ddot{X}_1 = F_1 + F_2 + F_3$$

$$M_2 \ddot{X}_2 = -F_1 - F_2 - F_3 + F_4$$

$$M_3 \ddot{X}_3 = -F_4$$

where

F_1 - resistance offered by R_1 and function of $(X_2 - X_1)$

F_2 - resistance offered by R_2 and function of $(X_2 - X_1)$

F_3 - resistance offered by R_3 and function of $(X_2 - X_1)$

F_4 - resistance offered by R_4 and function of $(X_3 - X_2)$

A logic diagram for the front to side impact model is given in Figure 8-21.

The results of a test case simulation are tabulated in Table 8-10 and plotted in Figure 8-22.

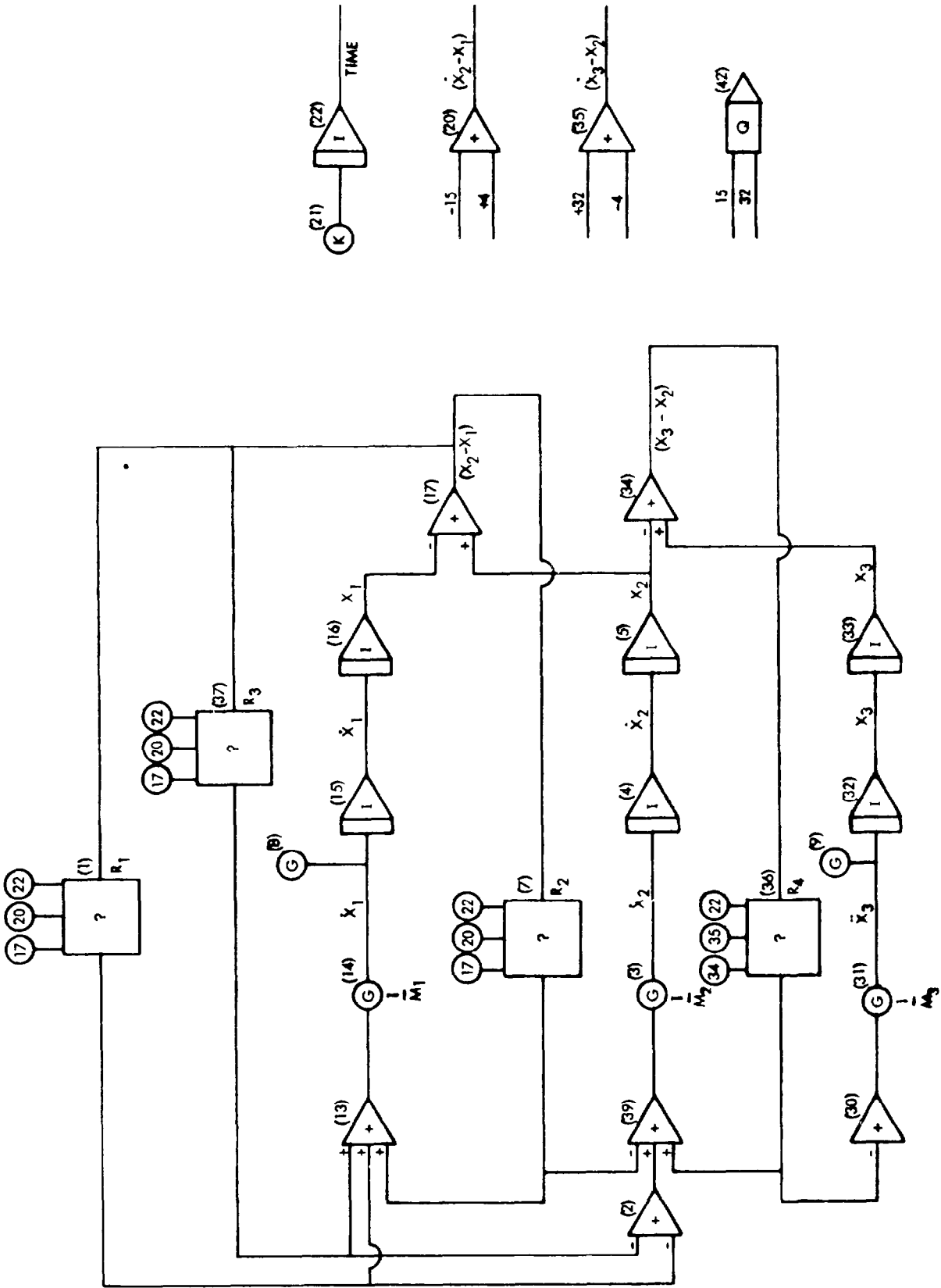


Figure 9-21 Logic Diagram For Three-Degree-of-Freedom Impulse Model

Table 8-10. Front to Side Test Case

Time (sec)	\ddot{X}_1 (g)	X_1 (in)
0.	4.0441902E-01	0.
2.0000E-03	2.9159786E+00	8.6142332E-01
4.0000E-03	4.8495026E+00	1.4737552E+00
6.0000E-03	5.6551847E+00	1.8011032E+00
8.0000E-03	7.5681406E+00	2.2846975E+00
1.0000E-02	1.1207730E+01	3.1056371E+00
1.2000E-02	1.3351182E+01	3.8646711E+00
1.4000E-02	1.3956485E+01	4.2679470E+00
1.6000E-02	1.5542554E+01	4.6501930E+00
1.8000E-02	1.6541415E+01	5.1456727E+00
2.0000E-02	1.7286745E+01	5.5686318E+00
2.2000E-02	1.7749305E+01	5.8984283E+00
2.4000E-02	1.9651424E+01	6.1513137E+00
2.6000E-02	1.9613893E+01	6.2406055E+00
2.8000E-02	1.9460138E+01	6.2309842E+00
3.0000E-02	1.9558863E+01	6.2325198E+00
3.2000E-02	1.9518919E+01	6.2470564E+00
3.4000E-02	1.9593676E+01	6.2428972E+00
3.6000E-02	1.9723121E+01	6.2079424E+00
3.8000E-02	1.8803051E+01	6.1246160E+00

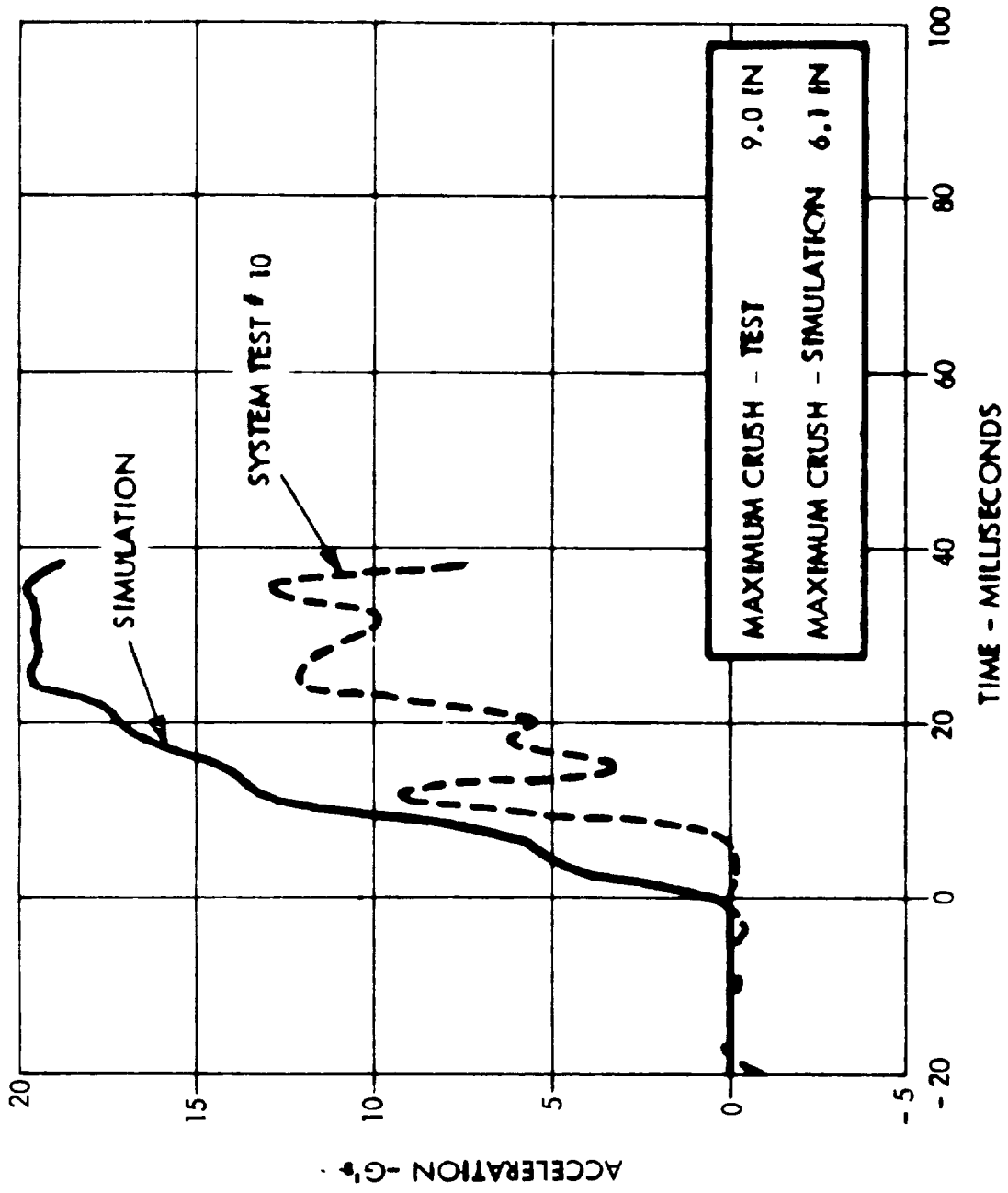


Figure 8-22. Front to Side Simulation (25 MPH)

Values used in the simulation were:

$$M_1 = 2930 \text{ lb}/386.$$

$$M_2 = 50 \text{ lb}/386.$$

$$M_3 = 2880 \text{ lb}/386.$$

$$V = 25 \text{ mph}$$

COMPUTER PROGRAMS

The seven model configurations were programmed and verified using the G.E. DYSIM simulation model. The program code names are:

<u>Model</u>	<u>Code Name</u>
Frontal Normal Barrier	FRBARN
Frontal Angular Barrier	FRBARA
Frontal Pole	FRPOLE
Side Pole	SIPOLE
Front/Front Aligned	FRFRA
Front/Front Offset	FRFRO
Front/Side	FRSI

All programs utilize the arbitrary block as a function generator for obtaining a structural element force for a given structural deformation. All structural data is stored in a program coded MODVEH. This program has provision for calculating the effects of velocity on structural load-deflection characteristics. The program also provides the capability for employing a structural hysteresis loop for structures which load and unload during an impact. The velocity sensitivity adjustment to a calculated force is

$$\text{Force}_{VS} = \text{Force} \left[1. + \text{Absolute} \left(\frac{\text{Relative velocity of structural deformation}}{1760 \text{ in/sec}} \right) \right]$$

The structural hysteresis loop employed is shown in Figure 8-23. The arbitrary block is accessed by identifying the following values

E_1 - structural deformation

E_2 - relative velocity of structural deformation

E_3 - time of structural deformation

P_1 - resistance number from Table 8-2

P_2 - unloading factor + 1 hysteresis loop
- 1 plastic loading & unloading

P_3 - velocity sensitivity + 1 sensitive
- 1 insensitive

OTHER MODELS

The dynamic response models previously discussed comprise the main mathematical modeling effort of the study. However, the dynamic response models required the support of other analyses both to determine the load-deflection characteristics of energy absorption elements and to ascertain the structural integrity of non-deforming elements.

The determination of load-deflection characteristics of energy absorption elements was made partly through experiment and partly through analysis. Load-deflection characteristics of elements currently used on the vehicle were obtained by tests. Examples of these elements are fenders, radiator, firewall and transmission mounts.

Energy absorption elements which were introduced to the vehicle during its modification received varied treatment.

The ripple panel which was used to replace the inner fender panel and which was intended to collapse in a controlled manner without buckling was designed primarily by experiment.

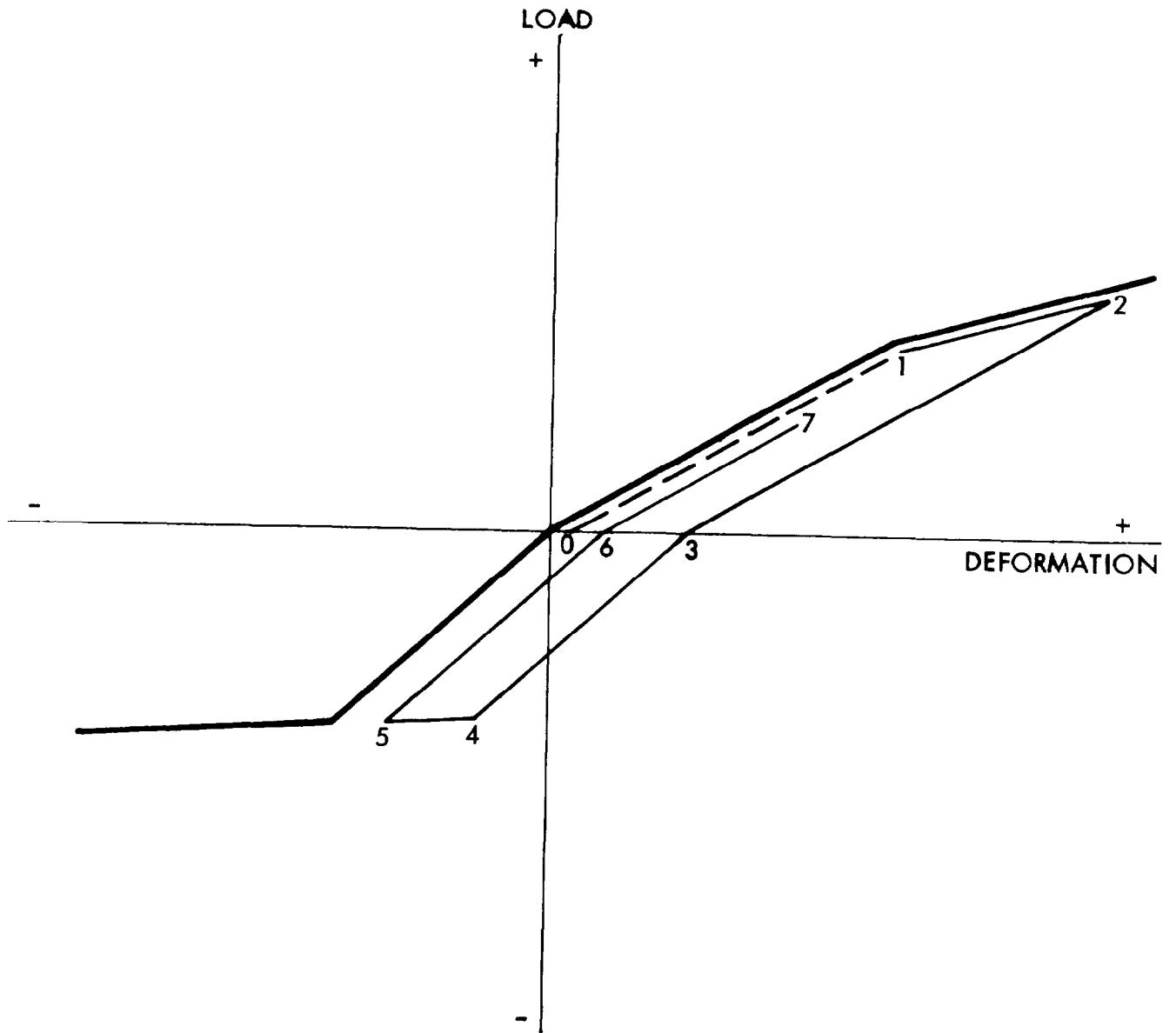


Figure 8-23. Structural Hysteresis Loop

The mechanism of collapse of this panel no doubt could be successfully modeled. However, it is a difficult problem. Satisfactory results for this program were achieved by fabricating a set of test panels and testing them under a variety of static and dynamic test conditions. The results of these tests were then extrapolated to arrive at the final design. Recommendations for utilizing this concept are:

- Design the pitch of the ripple to be compatible with the collapse pattern of surrounding structure. For example, the main support for the ripple panel used in the compact car project was the lower front sill which collapsed in convolutions repeating every three inches. Therefore, a three-inch pitch was selected for the ripple panel.
- Lateral stiffness is achieved by making the amplitude of the ripple transverse to the main load sufficient to give a moment of inertia large enough to prevent buckling as a simple column.
- The collapse of the panel can be estimated at one-fourth the compressive strength of the material for material thickness in the range of 30 to 60 mills.

Collapsing sills are similar to the ripple panel in that the physical behavior of the configuration is difficult to model. A series of specimens of varying dimensions was fabricated and tested under static and dynamic conditions and the final design determined by test results. Recommendations for design are:

- The pattern of collapse can be expected to occur at a length interval equal to the tube size.
- Moment of inertia should be made sufficient to prevent collapse as a simple column.

- Steady state load can be estimated at one-half the compressive strength of the material.
- The initial spike which occurs before the first convolution forms can be reduced and the point at which the convolution forms can be dictated by deforming the sill or by drilling holes at that point to weaken the section. Caution must be used, however, not to overly weaken the section against lateral bending.

Second-Stage Bumper and Intrusion-Resistant Door Panel. These two elements, although dissimilar in configuration, are similar in function. They were analyzed and designed using a model of a collapsed beam membrane. The model, shown in Figure 8-24, assumed hinged beam ends and pole loading at the beam center. The beam has a front and rear flange and a collapsing core. Initially, pole force is resisted by beam bending. As deflection increases, the beam is forced to stretch and begins to develop membrane resistance. Loads carried through the beam to the back flange are transmitted through the core. When this load reaches the collapse strength of the core, the beam begins to crush, losing its capacity for bending resistance. Energy is absorbed by core crush and by membrane stretching. The model progressively sets the deflection of the front flange and through an iterative process, calculates the deflection of the rear flange and the load required to maintain the deflection.

The objective of the analysis performed by the computer program MEMCRUSH is to determine the load-deflection characteristics of the structure. The results of the simulation of the second-stage bumper are given in Table 8-11.

Values used in the simulation were:

- Flange thickness - .2 in.
- Beam height - 3 in.
- Beam depth - 8 in.

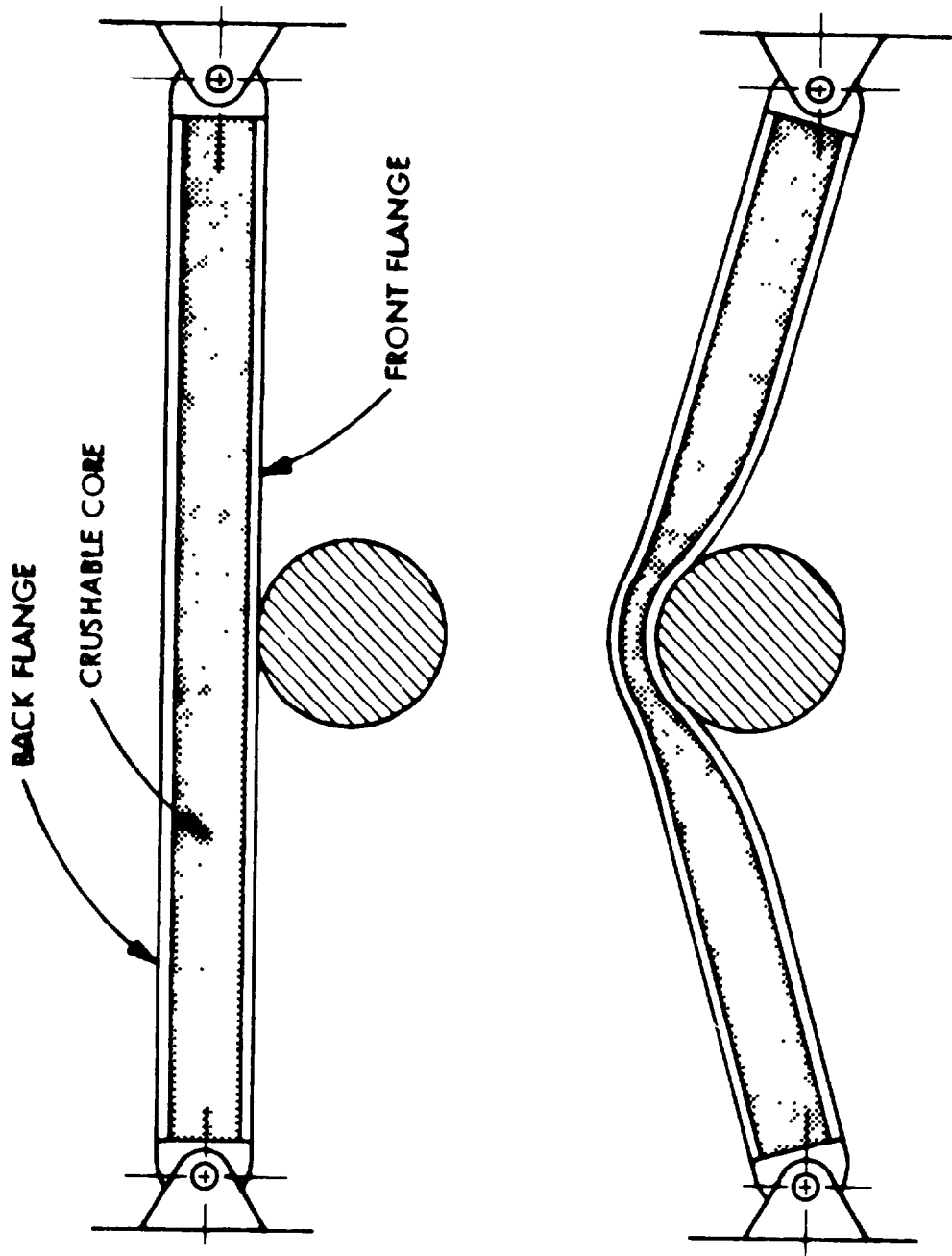


Figure 8-24. Crushable Beam Membrane Structure

Table 8-11. Second Stage Bumper Simulation

X (in)	P (1000 lb)
4.0000000E+00	2.8660000E+01
4.5000000E+00	3.4990000E+01
5.0000000E+00	3.9870000E+01
5.5000000E+00	4.4830000E+01
6.0000000E+00	4.9840000E+01
6.5000000E+00	5.4520000E+01
7.0000000E+00	5.9820000E+01
7.5000000E+00	2.5730000E+01
8.0000000E+00	2.9250000E+01
8.5000000E+00	3.2770000E+01
9.0000000E+00	3.6560000E+01
9.5000000E+00	4.0290000E+01
1.0000000E+01	4.4300000E+01
1.0500000E+01	4.8430000E+01
1.1000000E+01	5.2490000E+01
1.1500000E+01	5.6850000E+01
1.2000000E+01	6.1120000E+01
1.2500000E+01	6.5700000E+01
1.3000000E+01	7.0290000E+01
1.3500000E+01	7.4870000E+01

- Beam length - 28 in.
- Flange material - 1018 steel
- Flange material yield strength - 36,000 psi
- Flange material ultimate strength - 55,000 psi
- Core crush strength - 5,000 psi

The results of the simulation of the honeycomb sandwich door beam are given in Table 8-12.

Values used in the simulation were:

- Flange thickness - .04 in.
- Beam height - 8 in.
- Beam depth - 1.25 in.
- Beam length - 45.8 in.
- Flange material - 7075-T6 aluminum
- Flange material yield strength - 70,000 psi
- Flange material ultimate strength - 75,000 psi
- Core crush strength - 123 psi

Plastic Hinge in Rear Sill. A fairly common structural configuration found in automobiles is a hinge element which deforms plastically during impact. The rear sill of the modified vehicle employed a double hinge along the dash panel as shown in Figure 8-25.

The objective of the analysis is to determine the load at which yielding commences. The technique as shown in the figure is to first remove an area symmetrical about the neutral axis sufficient to provide the capacity to resist the compressive load. That is, the area removed times the compressive strength of the material is equal to the compressive load. The remaining material outboard of the neutral axis is loaded to yield stress in tension on one side and compression on the other. The resisting moment of the tensile and compressive loaded area about the neutral axis is set equal to the applied moment. The process is iterative until equality is achieved.

Table 8-12. Honeycomb Sandwich Door Beam Simulation

X (in)	P (1000 lb)
5.0000000E-01	4.9900000E-01
1.0000000E+00	9.9400000E-01
1.5000000E+00	1.4858750E+00
2.0000000E+00	1.9321250E+00
2.5000000E+00	2.3033750E+00
3.0000000E+00	2.6471250E+00
3.5000000E+00	2.9908749E+00
4.0000000E+00	3.3346249E+00
4.5000000E+00	3.6783749E+00
5.0000000E+00	4.0596249E+00
5.5000000E+00	4.5596249E+00
6.0000000E+00	5.0596249E+00
6.5000000E+00	5.5596249E+00
7.0000000E+00	6.0596249E+00
7.5000000E+00	6.5596249E+00
8.0000000E+00	7.0596249E+00
8.5000000E+00	7.5596249E+00
9.0000000E+00	8.0596248E+00
9.5000000E+00	8.5596248E+00
1.0000000E+01	9.0596248E+00
1.0500000E+01	9.5596248E+00
1.1000000E+01	1.0059625E+01

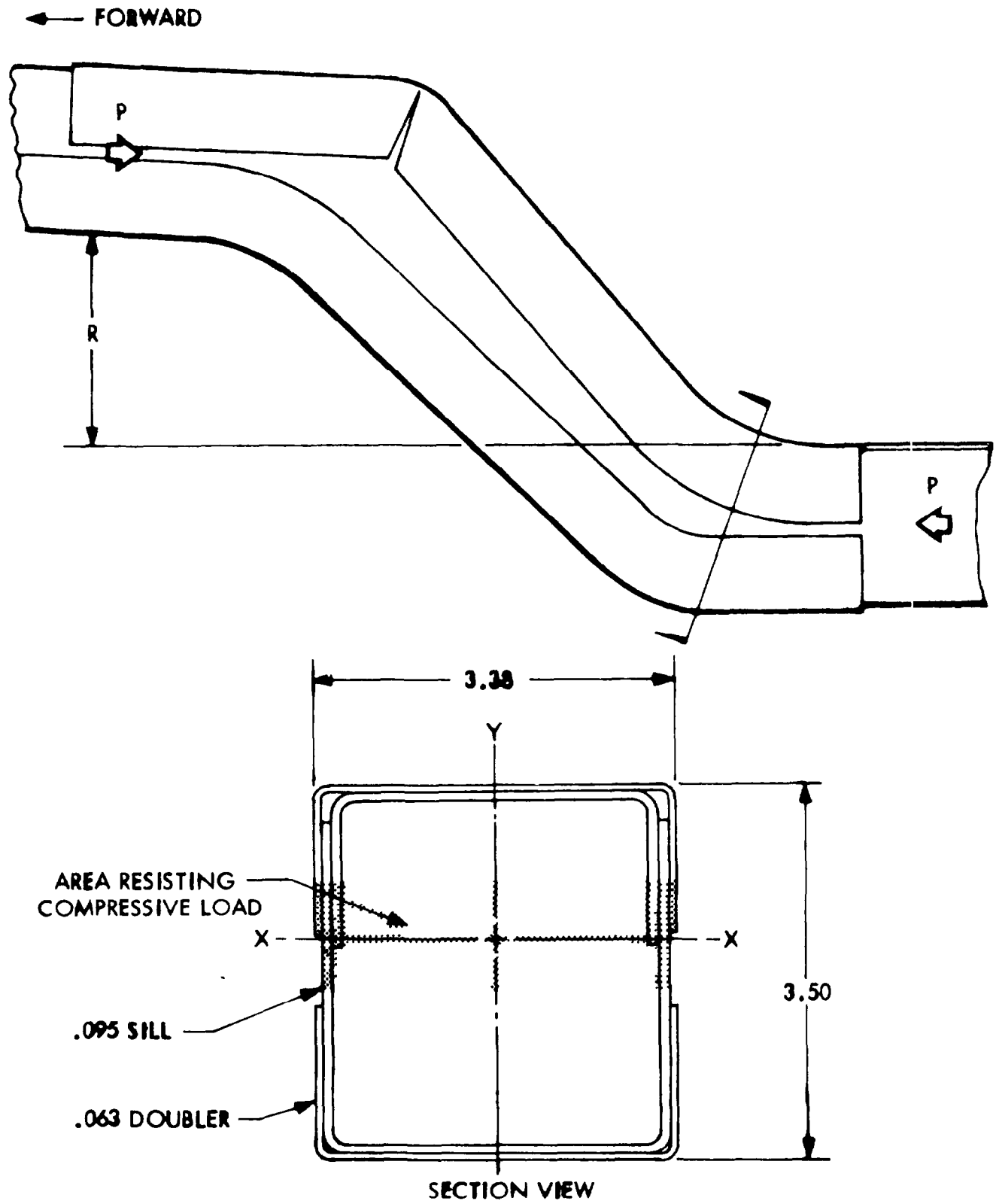


Figure 8-25. Rear Sill Plastic Hinge Structure

Results of the analysis have been compared to test results and found to be in good agreement. The configuration shown in the figure has been analyzed by the computer program called PLAHINGE and found to have a load-carrying capacity of 29,000 lbs.

A difficulty encountered in using plastic hinges as energy absorbers is that the section tends to collapse during bending resulting in a rapid loss of load-carrying capacity. During development of this component, studies were made of various filler materials to prevent section collapse. A plastic foam material was found to be effective. In addition to preventing collapse, the foam contributes to increased load-carrying capacity of the section. These results are discussed in the section on component development.

Non-Deforming Elements. There are numerous elements in the vehicle which contribute to the total structural integrity, but do not deform and absorb energy during impact. The design of these elements is not as sensitive as deforming elements in the sense that they only need to be strong enough to support the required load. These elements were analyzed in a conventional manner. Typical of these analyses was the study of the load-carrying capacity of the passenger compartment during frontal and side impact. For this purpose, the well-known program STRESS (Structural Engineering System Solver) was employed.

The STRESS system can perform the linear analysis of elastic, statically loaded, framed structures, that is, of structures composed of slender members which can be represented by their centroidal axis and analyzed with flexure theory. STRESS can analyze two- or three-dimensional structures whose members and joints may be pinned or rigidly connected. Using a general stiffness or displacement method of analysis, STRESS can determine the joint displacements, reactions, member end forces and member distortions for each specified loading condition. The program is available on most computer systems. Figures 8-26 and 8-27 show the way in which

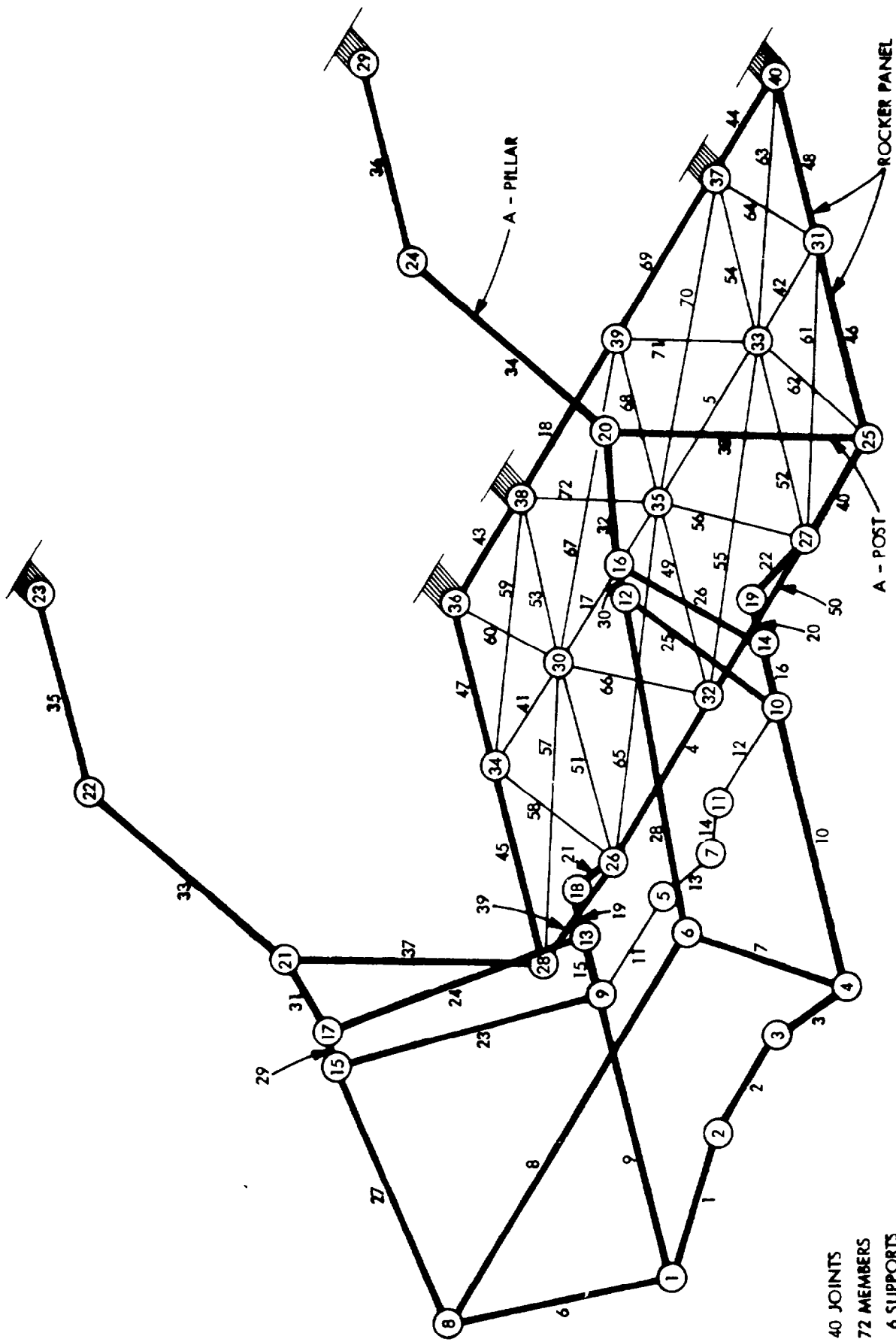
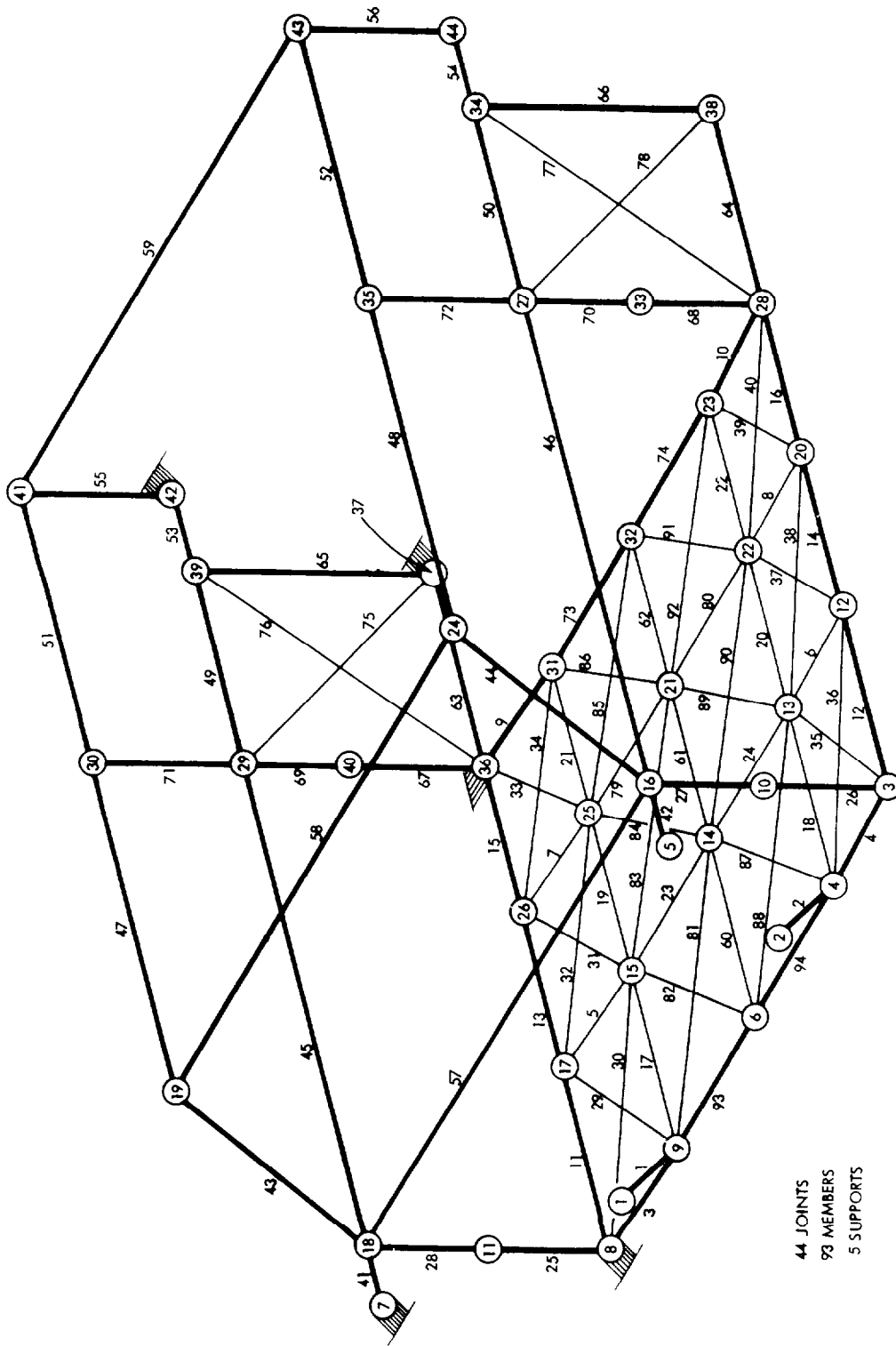


Figure 8-26. Frontal Structural Model Compact Car Stress Model



44 JOINTS
 93 MEMBERS
 5 SUPPORTS

Figure 8-27 Side Structure Model Compact Car Stress Model

STRESS was employed in the analysis of the passenger compartment in order to ascertain the structural capacity of all the defined elements. Elements which appeared weak were strengthened, but no attempt was made to reduce sections of elements which are stronger than required to survive crashes.

SECTION 9 CONCLUSIONS

The compact car modification program produced substantial improvements over baseline vehicle performance. In all cases, modified vehicle intrusion was less than baseline vehicle intrusion under identical crash conditions. This improvement was accomplished by a faster rising crash pulse.

In front impacts, the modified vehicle had a higher level of acceleration than the baseline. Performance goals were met with the exception that acceleration levels in front crashes reached 50 g for short durations and exceeded the target of 40 g. Intrusion in the region of passenger occupancy reached 7 inches in the front barrier impact and exceeded the goal of 5 inches. This was expected, as the available crush distance does not permit achieving a 40 g acceleration limit with a 5 inch intrusion limit for a 50 mph front barrier crash.

Since the modified vehicle is stiffer than the baseline vehicle, it is also somewhat more aggressive. This is as expected, but the increased aggressivity is relatively mild. The total weight increase for vehicle modifications was 104 pounds. This does not include any secondary weight effects such as might develop from a need for a larger suspension system or larger tires, etc.

Modifications to the bumper energy absorbing units prevented them from bursting during high-speed impacts and permitted them to stroke at a significant force level. This modification would require additional engineering for application to production vehicles.

The ripple panel replacing the fender inner panel has proven to be an effective energy absorbing element. It is considered to be currently production feasible and can be incorporated with a net reduction in weight.

The collapsing front sills in conjunction with the ripple panel provided a predictable well-controlled energy absorber which became effective early in the crash pulse. As designed, the sills adapt well to incorporation in front end designs. The sills as employed in crash tests were made from square tubing and welded to the rear sill. Typical mass production manufacturing technique is to fabricate the entire sill structure in two full-length pieces. These are then welded together. Further studies would be required to assure that the same predictable well-controlled collapse mode could be obtained with two-piece welded sills as was obtained with the square tubing.

The secondary high-strength bumper proved to be highly effective in front pole impacts and oblique impacts involving the front end. In pole impacts, the bumper crushed at a high load, absorbing substantial energy and transmitting load outward and rearward to the front sills which also collapsed, absorbing energy. In oblique impacts, the bumper provided a load transfer path between both sides of the front end so that the entire frontal structure collapsed in a parallelogram mode. This was effective in absorbing energy and in directing the vehicle away from the impact point. The bumper employed in the test series was drawn and fabricated from 1/8-inch thick mild steel. The adaptation of drawing such thick material and the welding of it to thinner sections is outside of normal automotive experience. Additional study would be required before this component design could be considered to be production feasible.

The rear sills, containing a pair of plastic hinges, were not required to deform at the impact speeds tested. That is, all of the available crush space was expended by involving only the front sills. However, the technique of design of effective plastic hinges which was developed in this program may be appropriate for other vehicles since the geometry which forms a plastic hinge is typical of automotive front ends. The fabrication technique developed includes the injection of plastic foam in the region where the hinge will form. This is necessary to stabilize the hinge against collapse of the section during bending. The production feasibility of the foam injection process has not been established and will require a development program.

The crushable beam membrane door panel which is aluminum honey-comb sandwich construction was effective in side impacts. The panel acted initially as a beam and under large deformations, acted as a stretching membrane absorbing a substantial amount of energy. The fabrication technique involved is typical of aircraft construction, but is not typical of automotive construction. This energy absorbing technique has proven to be highly effective, but may require some compromise in the design approach and a substantial development effort before it would be considered for adoption in mass production.

The "A" and "B" post structure and accessories were drawn from up to 1/8-inch thick material and welded to other thinner sections. This presents the same problem as discussed for the secondary bumper and will require some advances in normal production technique.

The mathematical modeling effort to simulate the dynamic response of automobiles in a wide variety of crash conditions is considered to be successful. Seven separate models were developed to simulate various front and side barrier and vehicle-to-vehicle crash situations. Peak accelerations and maximum crush results obtained from various simulations agree with crash test results generally within 10 to 15 percent which is within the range of expected deviations between tests. The shape of the crash pulse is in good agreement in most instances. In a few of the simulations, the timing of events differed somewhat. This can be attributed to random occurrences in the crash tests or in selection of structural deformation characteristics for the simulation which differ from the actual structural crash behavior. The models are simple to use and are appropriate for use on any production vehicle.

SECTION 10 RECOMMENDATIONS

The ultimate purpose of research in the field of vehicle crashworthiness is to provide a means of reducing injuries in the real crash environment. To this end, the results of this program are encouraging in the sense that various energy absorbing techniques have been conceived and developed to the point where they could be incorporated into the design of production vehicles. However, this program did not address the study of occupant response and interaction with vehicle structures.

It is recommended that the study be extended to incorporate the total occupant-vehicle system. Specifically, studies should be made to determine compatibility of structural performance with occupant restraint systems. For this study, structural performance goals were arbitrarily chosen to be consistent with performance goals specified in past DOT Experimental Safety Vehicle programs. With an expansion of the compact car study to include occupant response, optimum structural performance characteristics could be identified on the basis of compatibility with specified restraint systems. Vehicle performance characteristics could then be modified to achieve these performance goals. In the case of side crash when an occupant may impact the vehicle interior, occupant injury probability is highly dependent on the energy absorption characteristics of the vehicle interior. Studies of the total vehicle-occupant system should involve the vehicle interior in order to identify desirable interior crush characteristics and to develop a means of achieving these characteristics.

The problem of aggressivity was lightly addressed in this program in the sense that control of vehicle aggressivity was not a stated requirement. The vehicle selected for modification had limited front end crush space as is typical of any compact car. It was necessary to increase the stiffness of

the front end, particularly during the early part of the crash pulse, in order to meet performance goals at crash velocities of interest. This modification makes the vehicle more aggressive although care was taken to control the degree of increased aggression. It is recommended that further study be undertaken to address the problem of incompatibility of the need of an efficient front end and the need to minimize vehicle aggressivity. Specifically, a study should address the possibility of development of an adaptive front end which is production feasible at a reasonable cost. An adaptive front end is one which changes its performance characteristics to be compatible with the crash situation, such as the hybrid structural-hydraulic system employed on the AMF Optimized ESV.

The vehicle selected for modification was equipped with a 6-cylinder in-line engine because this is typical of vehicles in use. The characteristics of this engine are that it is relatively long and narrow which leaves little crush space in the front end. Furthermore, the engine sits high in the compartment and close to the dash panel so that there is no possibility of deflecting the engine downward during impact to provide more crush space. It is recommended that a study be undertaken to develop a means of achieving additional crush space by rotating the engine, during impact, about a yaw or vertical axis. It would appear that there is enough time to accomplish a 90° engine rotation, which in the case of the Hornet, would provide approximately 15 more inches of crush space and would also absorb some energy.

Several of the concepts employed in this program exhibit very good potential for application to crashworthy vehicles, but the production feasibility remains in question. These concepts are the plastic hinge and the crushable beam membrane door panel. The foam injection which is required to prevent collapse during bending of the plastic hinge is not a normal automotive production process nor is the fabrication of the honeycomb sandwich which forms the door panel. It is recommended that a further study be undertaken to either establish production feasibility of these concepts as they were developed, or to devise alternate means of achieving the performance provided by these energy absorption concepts.